Friedrich-Schiller-Universität Jena

Chemisch-Geowissenschaftliche Fakultät

Design and application of functional polymers: From self-healing materials *via* hard tissue composites to methacrylate tougheners

Dissertation

(kumulativ)

zur Erlangung des akademischen Grades

doctor rerum naturalium (Dr. rer. nat.)

vorgelegt dem Rat der Chemisch-Geowissenschaftlichen Fakultät

der Friedrich-Schiller-Universität Jena

von Diplom-Ingenieur (FH) Benedict Sandmann

geboren am 14.07.1985 in Straubing

Gutachter:

1. …….
2. …….

(3. …….)

Tag der öffentlichen Verteidigung: ……..

Table of contents

Documentation of authorship

This section contains a list of individual authors' contributions to the publications reprinted in this thesis.

P1) "Metallopolymers as an emerging class of self-healing materials" B. Sandmann,[1,#] S. Bode,[2,#] M. D. Hager,[3] U. S. Schubert,[4] *Adv. Polym. Sci.* **2013**, *262*, 239-257. [#]Both authors contributed equally				
Autor	1	2	3	4
Conception of the manuscript	X	X		
Preparation of the manuscript	X	X		
Correction of the manuscript	X	X	X	X
Supervision of B. Sandmann			X	X
Proposal for crediting publication equivalents	0.5			

P2) "The self-healing potential of triazole-pyridine-based metallopolymers" B. Sandmann,[1] B. Happ,[2] F. H. Schacher,[3] M. D. Hager,[4] U. S. Schubert,[5] *Macromol. Rapid Comm.* **2015**, *36*, 604-609.					
Autor	1	2	3	4	5
Conception	X				
Monomer and polymer synthesis	X				
Polymer characterization	X		X		
Conception and preparation of the manuscript	X	X			
Correction of the manuscript		X	X	X	X
Supervision of B. Sandmann				X	X
Proposal for crediting publication equivalents	1.0				

P3) "Efficient Cu(I) acetate-catalyzed cycloaddition of multifunctional alkynes and azides: From solution to bulk polymerization"

B. Sandmann,[1] B. Happ,[2] M. D. Hager,[3] J. Vitz,[4] E. Rettler,[5] P. Burtscher,[6] N. Moszner,[7] U. S. Schubert,[8] *J. Polym. Sci., Part A: Polym. Chem.* **2014**, *52*, 239–247.

	1	2	3	4	5	6	7	8
Conception			X			X	X	
Synthesis of monomers and polymers	X	X						
Polymer characterization	X	X						
Mechanical investigations				X	X			
Preparation of the manuscript	X	X		X	X			
Correction of the manuscript	X	X	X	X	X	X	X	X
Supervision of B. Sandmann			X					X
Proposal for crediting publication equivalents	1.0							

P4) "Photoinduced polyaddition of multifunctional azides and alkynes"

B. Sandmann,[1] B. Happ,[2] J. Vitz,[3] M. D. Hager,[4] P. Burtscher,[5] N. Moszner,[6] U. S. Schubert,[7] *Polym. Chem.* **2013**, *4*, 3938-3942.

	1	2	3	4	5	6	7
Conception				X	X	X	
Synthesis of monomers and polymers	X	X					
Polymer characterization	X	X					
Mechanical investigations			X				
Preparation of the manuscript	X	X	X				
Correction of the manuscript	X	X	X	X	X	X	X
Supervision of B. Sandmann				X			X
Proposal for crediting publication equivalents	1.0						

P5) "Metal-free cycloaddition of internal alkynes and multifunctional azides under solvent-free conditions"

B. Sandmann,[1] B. Happ,[2] J. Vitz,[3] R. M. Paulus,[4] M. D. Hager,[5] P. Burtscher,[6] N. Moszner,[7] U. S. Schubert,[8] *Macromol. Chem. Phys.* **2014**, *215*, 1603-1608.

	1	2	3	4	5	6	7	8
Conception					X	X	X	
Synthesis of monomers and polymers	X	X						
Polymer characterization	X	X		X				
Mechanical investigations			X					
Preparation of the manuscript	X	X						
Correction of the manuscript	X	X	X	X	X	X	X	X
Supervision of B. Sandmann					X			X
Proposal for crediting publication equivalents	1.0							

P6) "Biological evaluation of 1,2,3-triazole-based polymers for potential applications as hard tissue material"

D. Pretzel,[1] B. Sandmann,[2] M. Hartlieb,[3] J. Vitz,[4] S. Hölzer,[5] N. Fritz,[6] N. Moszner,[7] U. S. Schubert,[8] *J. Polym. Sci., Part A: Polym. Chem.* **2015**, in press (DOI: 10.1002/pola.27676).

	1	2	3	4	5	6	7	8
Conception	X	X	X					
Synthesis of monomers and polymers		X						
Polymer characterization		X	X	X	X	X		
Biological studies	X							
Preparation of the manuscript	X	X	X					
Correction of the manuscript	X	X	X	X	X	X	X	X
Supervision of B. Sandmann								X
Proposal for crediting publication equivalents		0.5						

P7) "Incorporation of core-shell particles in methacrylate based composites for an improvement of the mechanical properties"

B. Sandmann,[1] B. Happ,[2] I. Perevyazko,[3] T. Rudolph,[4] F. H. Schacher,[5] S. Hoeppener,[6] U. Mansfeld,[7] M. D. Hager,[8] U. Fischer,[9] P. Burtscher,[10] N. Moszner,[11] U. S. Schubert,[12] *Polym. Chem.* **2015**, in press (DOI: 10.1039/C4PY01544D).

	1	2	3	4	5	6	7	8	9	10	11	12
Conception								X		X	X	
Synthesis of polymer particles	X	X										
Particle characterization			X	X		X	X					
Mechanical investigations									X			
Preparation of the manuscript	X		X	X								
Correction of the manuscript	X	X	X	X	X	X		X			X	X
Supervision of B. Sandmann								X				X
Proposal for crediting publication equivalents	1.0											

Erklärung zu den Eigenanteilen des Promovenden/der Promovendin sowie der weiteren Doktoranden/Doktorandinnen als Koautoren an den Publikationen und Zweitpublikationsrechten bei einer kumulativen Dissertation

Für alle in dieser kumulativen Dissertation verwendeten Manuskripte liegen die notwendigen Genehmigungen der Verlage („Reprint permissions“) für die Zweitpublikation vor.

Die Co-Autoren der in dieser kumulativen Dissertation verwendeten Manuskripte sind sowohl über die Nutzung, als auch über die oben angegebenen Eigenanteile informiert und stimmen dem zu (es wird empfohlen, diese grundsätzliche Zustimmung bereits mit Einreichung der Veröffentlichung einzuholen bzw. die Gewichtung der Anteile parallel zur Einreichung zu klären).

Die Anteile der Co-Autoren an den Publikationen sind in den vorausgehenden Tabellen aufgeführt.

Ich bin mit der Abfassung der Dissertation als publikationsbasiert, d.h. kumulativ, einverstanden und bestätige die vorstehenden Angaben. Eine entsprechend begründete Befürwortung mit Angabe des wissenschaftlichen Anteils des Doktoranden/der Doktorandin an den verwendeten Publikationen werde ich parallel an den Rat der Fakultät der Chemisch-Geowissenschaftlichen Fakultät richten.

Name Doktorand	Datum	Ort	Unterschrift
Name Erstbetreuer(in)	Datum	Ort	Unterschrift

1. Introduction

In the year 2012, the worldwide plastic production reached a maximum of 288 million tons the year. Thereby Europe ranks second in the global plastics production with an output of 57 million tons.[1] Polymers and polymer composites are used in a variety of applications of transportation vessels (*e.g.*, cars, aircrafts, ships, and spacecrafts), sport articles, civil engineering, and electronics.[2] Though, these materials are prone to damage induced by mechanical, chemical, thermal, UV radiation, or a combination of these factors. With polymers and composites being increasingly used in a wide range of applications, a number of techniques have been developed and applied by industries for mending visible or detectable defects on the polymeric structures. Nevertheless, these conventional repair methods are not effective for mending invisible microcracks within the structure during its service lifetime. Consequently, the concept of self-healing polymeric materials was proposed in the 1980s[3] as a way of healing invisible microcracks for extending the working life and safety of the polymeric components. The publications of Dry and Sottos[4] in 1993 and subsequently of White *et al.*[5] in 2001 further attracted worldwide interest in these special materials.[6] Conceptually, the self-healing ability of a material leads to the (partial) recovery of the mechanical properties after a damage. A distinction between autonomously or non-autonomously self-healing is made. In the latter case, self-healing is activated after an application of a specific stimulus (*e.g.*, heat, radiation). The conceptual inspiration from nature for self-healing is not new and many engineering approaches, in particular for polymeric materials, have been inspired by observing natural systems, *e.g.*, in wound healing.[7-10] As a closer look into the supramolecular chemistry of self-healing polymers, various interactions[11] in polymers like ionic interactions,[12] π-π stacking,[13] hydrogen-bonding,[14-15] and metal-ligand interactions[16-17] have been shown to impart the self-healing ability into the respective materials. In the last decades, metallopolymers gained more and more attention as attractive self-healing materials.[18] These materials combine the features of polymers and metal complexes enabling the design of new systems with outstanding properties whereupon the structural properties of the respective complexes are of decisive importance for the self-healing properties.[19] For the self-healing process it is important that specific properties can be changed upon application of an external stimulus such as light, heat, or changes in the pH

value. These stimuli-responsive metallopolymers could be affected in many different ways, *e.g.*, by redox processes. The group of Peng provided a significant scientific contribution to the field of metallopolymers.[20] In a redox reaction, iron(II) was formed from iron(III) by using the external stimulus light in order to convert the phase change of an iron metallopolymer. By the reversible change of the charged states from iron(III) to iron(II), the material was converted into a liquid polymer by simply reducing the iron ions. Zhou and coworkers reported a ruthenium-containing polymer with two distinct glass transition temperatures. These transitions induced a kind of mobility that is necessary for the self-healing.[21-22] **Chapter 2** provides a detailed insight into the latest research results of self-healing metallopolymers.

Many different stimuli can affect a metallopolymer to result in the desired properties. In particular, the dynamics of the metal–ligand interaction and the chain mobility in the polymer represent key factors for the generation of artificial self-healing metallopolymers.[8, 23] Hence, polymers with low glass transition temperatures, bearing triazole-pyridine and *bis*(terpyridine) moieties, were synthesized, characterized and at least utilized as coatings with self-healing properties (**Chapter 3**).

Next to the application areas mentioned above, many synthetic polymers are presently used with success in medicine, *e.g.*, surgery, dentistry and prosthesis.[24] They offer distinct advantages of biocompatibility, versatility of chemistry, and the biological properties that are significant in the application of tissue engineering.[25] Synthetic polymers are often cheaper than biologic scaffolds as they can be produced in large uniform quantities and have a long shelftime. Many synthetic polymers show physicochemical and mechanical properties comparable to those of biological tissues. They exhibit in general predictable and reproducible mechanical as well as physical properties such as tensile strength, fracture toughness, elastic modulus, and degradation rate.[26] Mechanical properties like elastic modulus, compression modulus, fracture toughness and bending stress are important characteristics to determine their use in the body, for example for bone implants, prosthesis materials or dental composites. Hence, potential biomaterials have to be evaluated in terms of their biocompatibility, mechanical properties and biodegradation to determine if they are suitable for specific medical applications.[27]

The copper(I)-catalyzed azide–alkyne cycloaddition (CuAAC), also known in literature as a type of "click" reaction, represents a powerful tool in modern synthesis chemistry. This cycloaddition of terminal alkynes and organic azides is inert to a wide range of reactive moieties and functional groups. Among the "click"-type reactions (*e.g.*, Diels–Alder[28], thiole-ene reaction[29]), the CuAAC is the most appealing since it proceeds in most cases in high yields, regioselective and without undesirable side reactions.[30-31] Due to its high tolerance to a wide range of building blocks and, generally, with the generation of minor (or conveniently separable) by-products it has found a wide range of applications ranging from drug discovery over polymer chemistry to materials science.[31-37] Thus, click-chemistry represents an important and powerful synthetic tool in chemistry that enables a variety of synthetic polymeric materials, *e.g.*, functional and biocompatible polymers. Hence, within this thesis the CuAAC was utilized to synthesize new polymeric materials with outstanding mechanical and biocompatible features under solvent-free conditions (**Chapter 4**). As a part of this work, different copper salts were evaluated as potential catalysts for thermal- and photo-induced polymerization. The mechanical properties of the resulting polymers have been investigated. In addition, the polymerization kinetics of the CuAAC in solution were examined.

The CuAAC often generates very high reaction enthalpies in a short time period. That can result in a spontaneous release of reaction heat and an uncontrolled reaction progress[38] which causes problems, in particular, for biomedical applications of these materials. Due to the cytotoxic properties of the copper catalysts it is important to remove the copper residues from the resulting polymer.[31] A way to solve these problems is to perform the click-reaction without any catalyst. In the last years, significant efforts have been devoted to the development of metal-free click reactions.[39-52] Generally, the reactivity of alkynes for the click reaction is rather low due to its high electron density at the alkyne functionality. One pathway to increase the reactivity of internal alkynes is to reduce its electron density by implementing vicinal electron-withdrawing groups, *e.g.*, carbonyl moieties.[53-55] For that purpose internal alkynes bearing electron-withdrawing carbonyl moieties have been synthesized and utilized for the metal-free click-reaction. On this occasion the exothermicity of the catalyst-free click reaction was studied. The mechanical properties and biocompatibility

of the resulting polymers were examined in detail, as they represent key factors for a potential biomedical use of materials.

Polyester compounds, such as polymethacrylates, are very promising materials for biomedical applications. However, their reliability, strength and fracture toughness excludes their application as single material for implants or dental composites due to their weak mechanical properties, unless these properties are modified by controlling the stages of syntheses or by using additives.[56] There are various additives like hyperbranched polymers,[57-58] fibers,[59] or core-shell nanoparticles[60] that can increase the mechanical properties. All these mentioned additives cause an enhancement of fracture toughness, however, accompanied by a loss of mechanical resistance (*i.e.* E-modulus). Up to now there is no report in literature about the implementation of latex particles into polymer composites that leads to an increase of fracture toughness and mechanical resistance at the same time. To overcome that drawback, the synthesis of PBA/PMMA core-shell particles and their utilization as tougheners for TEGDMA/UDMA polymer blends (**Chapter 5**) is discussed. Thereby an improvement of fracture properties accompanied with an improvement in resistance (E-modulus) was achieved.

Besides this approach, another promising way to influence the mechanical properties is the polymerization-induced phase separation (PIPS). The PIPS is characterized by the formation of two incompatible phases during the polymerization (i.e. monomer and soluble polymer become two incompatible polymer phases). The PIPS method was extensively studied on epoxy resins.[61-64] Though the minor addition of rubbers results in an enhancement of fracture toughness, however, accompanied by a drop of the E-modulus. In contrast, the addition of thermoplastic polymers (*e.g.*, polyetherimides, polyphenylene oxides) leads to an improvement of fracture properties without a loss in E-modulus.[62-63] The PIPS was applied for methacrylates only scarcely in literature.[65-68] The present examples focus on the investigation of polymerization shrinkage and not the effect on the mechanical properties.

Hence, the PIPS was utilized for improving the mechanical properties of methacrylate based composites. **Chapter 6** describes the current research approach and outlook for the attempt towards an enhancement of mechanical properties of methacrylate composites by PIPS.

2. Metallopolymers as an emerging class of self-healing materials

Parts of this chapter have been published in **P1**) B. Sandmann, S. Bode, M. D. Hager, U. S. Schubert, *Adv. Polym. Sci.* **2013**, *262*, 239-257.

The material properties described in **Chapter 1** are the key factors for the generation of a self-healing behavior in metallopolymers. Examples of self-healing materials based on metal–ligand interactions can be observed in nature, *e.g.*, in mussel byssus threads. In 2001, Vaccaro and Waite studied the ability of mussel byssus threads to heal after an inflicted damage.[69] This research enabled a more detailed insight into the healing mechanism and the parameters that influence this natural system. The authors described the self-healing behavior which is based on an interaction between iron(III) ions and 3,4-dihydroxyphenylalanine (dopa).[70] Thereby, the iron center is able to bind one, two or three catechol-based ligands that are attached to the polymer backbone. The number of bond ligands depends on the pH value.[71-73] At a pH value below 5, the *mono*-dopa iron(III) complex is formed leading to non-crosslinked polymer chains. The resulting polymer exhibits ductile material properties. By increasing the pH value above 5, *bis*- and *tris*-dopa iron(III) complexes are preferably formed, leading gradually to a crosslinked polymer. During that process the material properties of the polymer change from a soft, linear polymer to a network with hard mechanical characteristics.[70, 74-77] This principle occuring in nature could, in principal, be mimicked by synthetic polymers. Up to now there is only a limited set of synthetic metallopolymers that have been successfully utilized for self-healing purposes based on metal–ligand interactions. The structural moieties of metal complexes within self-healing metallopolymers can be distinguished into main-chain and side-chain attached systems. Holten-Andersen and coworkers functionalized PEG with catechol units at the ends of the polymer chains. In this way the authors were able to show a dynamic reversibility of the metal–ligand interaction.[71-72] Besides the iron–dopa interaction, also a zinc-histidine system was proven to allow a self-healing behavior in mussel byssus threads.[78-80] The hierarchical structured natural material contains collagen fibers as middle block flanked by histidine-rich domains; in the presence of zinc ions a reversible crosslinking will be triggered.[80-81] The restoration of mechanical properties was demonstrated (**Figure 2.1**) and it was possible to construct a model system, based on a PEG star functionalized polymer with histidine moieties as a metal-containing hydrogel.[82-83]

In 2005, the group of Varghese developed an acryloyl-6-amino caproic acid (A6ACA) based hydrogel with self-healing properties.[84] By dipping the polymer into an aqueous copper(II) chloride solution it was possible to heal scratches. However, the detailed mechanism and the influence of the metal-ligand interactions, potential hydrogen bonds of the solvent medium and the mobility of the gel to the healing effect is still unclear. Yuan and coworkers developed a self-healing material bearing ligands within the main chain.[17]

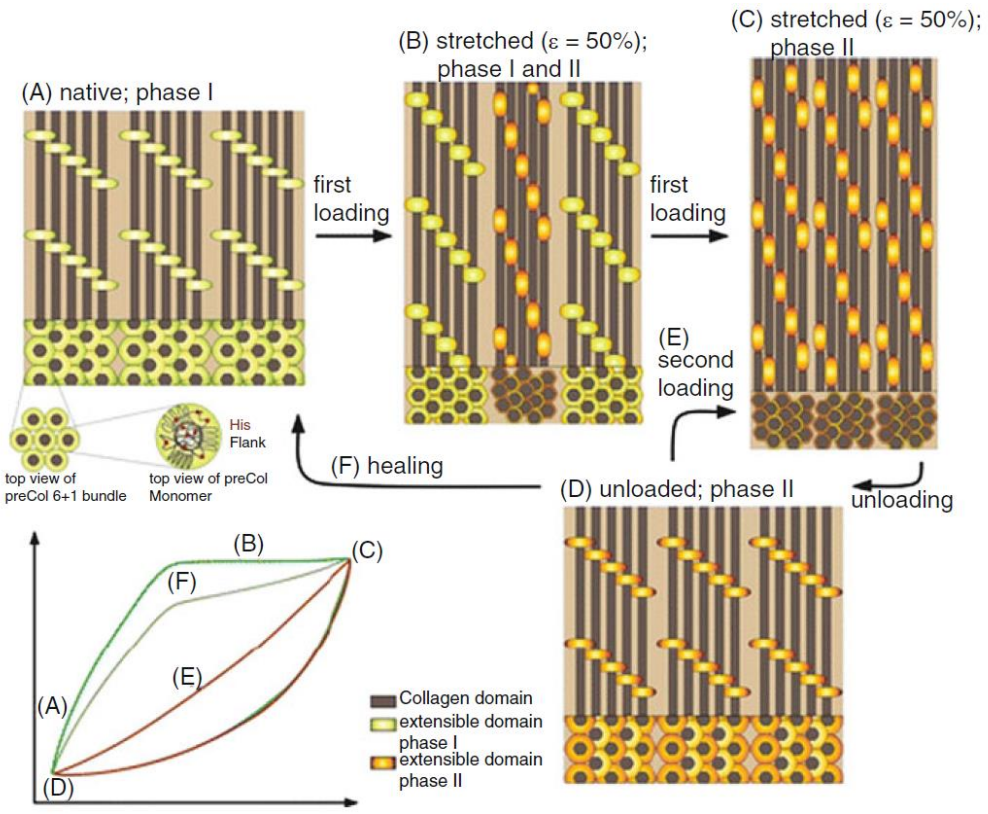

Figure 2.1 Molecular model of the reversible deformation behavior in mussel byssal threads (reproduced with permission ref. [88], Copyright 2014 Springer).

The polymer was based on polyurethane analogue macromolecules bearing *bis*(1,2,3-trizol-4-yl) pyridine units. The complexation of the ligands was performed with zinc(II) and europium(III) ions leading to a metallopolymer with self-healing properties. A simplified healing mechanism was proposed by an exchange of the ligand macromolecules between two adjacent blocks. Although the material allows the formation of hydrogen bonds, their effect to the self-healing process as well as a quantification of the self-healing efficiency was not investigated and discussed in the publication.

Beside that example, the group of Terech developed a self-healing metallopolymer gel which contains diterpyridyl moeties. The polymerization was performed by the addition of nickel ions and subsequent complexation of the diterpyridyl units.[85] The resulting linear polymer exhibited soft mechanical properties and showed a good healing efficiency that can be related to the high flexibility of the polymer itself.

In 2011, Rowan and Weder described the self-healing behavior of a linear metallopolymer, triggered by UV light.[86] The polymer consists of poly(ethylene-*co*-butylene) with two 2,6-*bis*(1'-methylbenzimidazolyl)pyridine units at both ends of each polymer chain. The addition of zinc di[*bis*(trifluoromethylsulfonyl)imide] or lanthanum tri[*bis*(trifluoromethyl-sulfonyl)imide] leads to a linear metallopolymer. Self-healing within the metallopolymer occurs by UV light illumination at a wavelength corresponding to the absorption band of the polymer. Due to the energy transfer the temperature within the polymer rose up to 220 °C. The supposed mechanism of the self-healing process is based on the reversibility of the metal-ligand interaction as well as the breakage and recombination of metal-complex clusters (**Figure 2.2**).

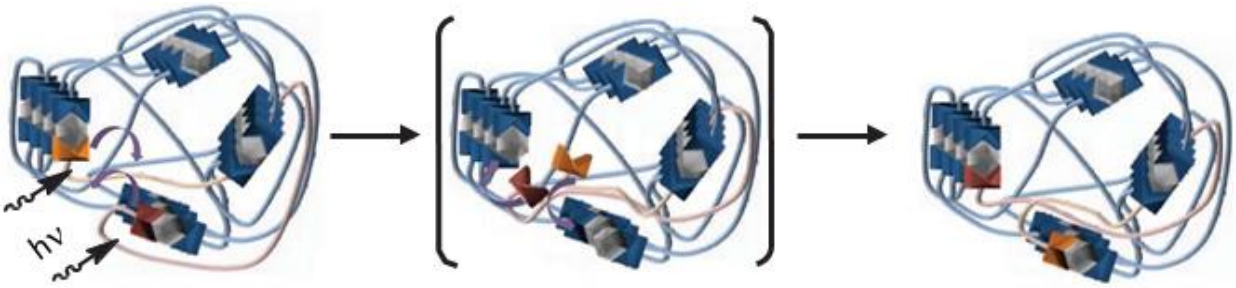

Figure 2.2 Proposed optical self-healing mechanism of metallosupramolecular, phase-separated network (reproduced with permission from ref. [90], Copyright 2014 Springer).

Upon cleavage of the metal complexes the mobility within the polymer increases, leading to a dynamic motion of the polymers and to self-healing of the inflicted damage.

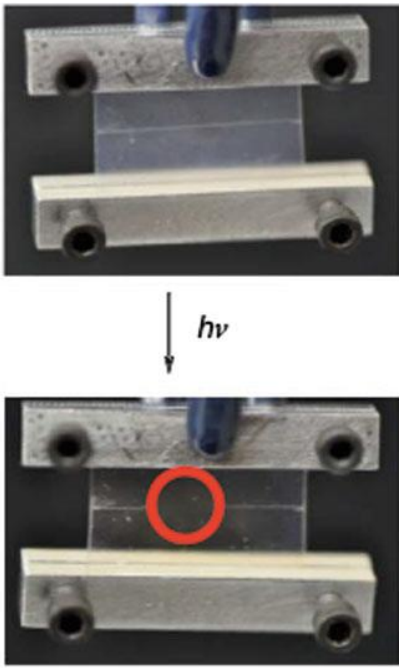

Figure 2.3 Demonstration of the optical healing of a linear Zn-based metallopolymer (reproduced with permission from ref. [90], Copyright 2014 Springer).

After cooling the polymer, the complexes (and clusters) will be reformed resulting in an immobilization of the mobile phase and the (complete) healing of the scratch (**Figure 2.3**). Recently the group of Schubert published an example of a self-healing metallopolymer coating.[87] A poly(alkyl methacrylate) polymer bearing terpyridine units was crosslinked with several iron(II) salts, resulting in insoluble and hard polymer films that show self-healing properties. Mechanistic investigations revealed that the decomplexation is not the main mechanism. Most likely the self-healing is based on the ionic interactions between the charged complexes and the counter-ions (*i.e.* sulfate). A similar self-healing principle, including clusters, is already known for self-healing ionomers.[12]

Even if several basic principles of self-healing metallopolymers have been described in literature, a detailed understanding of the process and its prediction is still complicated due to the different key factors that play a role (properties of the polymer, binding strength, ionic interactions, etc.). The phenomena of reversibility and switchability of metal-ligand bonds in solution are well investigated. However, the behavior in the solid state has not been investigated thoroughly up to now.[88-91] Therefore, the development of suitable methods for understanding the conditions of metal–ligand interactions in bulk represent a challenging task for the prospective research, performed within this thesis.

3. The development of self-healing metallopolymers (selected examples)

Parts of this chapter have been published in **P2**) B. Sandmann, B. Happ, F. H. Schacher, M. D. Hager, U. S. Schubert, *Macromol. Rapid Comm.* **2015**, *36*, 604-609.

Beside the examples of self-healing discussed in **Chapter 2**, the development of novel metallopolymers with self-healing properties is an ambitious and still challenging field in science. For this purpose, polymers bearing triazole-pyridine complex units in the side chain were employed for the development of self-healing materials. The utilization of these materials for self-healing applications will be discussed in the following chapters.

3.1. The self-healing potential of triazole-pyridine-based metallopolymers

As already discussed in **Chapter 2**, kinetic- and thermodynamic properties of the metal-ligand bond are the key factors for the generation of self-healing properties in synthetic metallopolymers. Recently published polymethacrylates with terpyridine moieties were the first examples for side-chain functionalized metallopolymers with self-healing abilities. These materials were crosslinked with iron(II) sulfate, respectively.[87] It was hypothesized that the bidentate triazole-pyridine can exhibit comparable complex properties and, therefore, represent a potential system for the application in self-healing materials. Happ *et al.* already investigated the complexation properties of 4-(pyridin-2-yl)-1H-1,2,3-triazole with iron(II) chloride tetrahydrate and cobalt(II) tetrafluoroborate hexahydrate.[92]

In a follow-up study a novel triazole-pyridine based polymer (**P1**) was synthesized, characterized and successfully utilized to create a self-healing polymer coating. For this purpose, the polymer was crosslinked with several divalent metal salts. The self-healing efficiency of the metallopolymer-films at different temperatures was investigated by light microscopy. For mechanistic studies, SAXS and UV-Vis spectroscopic investigations were performed. The T_g of the polymers was determined by DSC measurements. Monomers **1** and **2** were polymerized using the RAFT polymerization procedure (**Scheme 3.1**). Effective self-healing systems in general feature a low glass transition temperature, a high flexibility and network mobility.[87, 93] Therefore, laurylmethacrylate was utilized as comonomer. The

aliphatic environment of the alkyl chain decreases the glass transition temperature and enhances the flexibility of the polymer backbone as well as the network mobility.

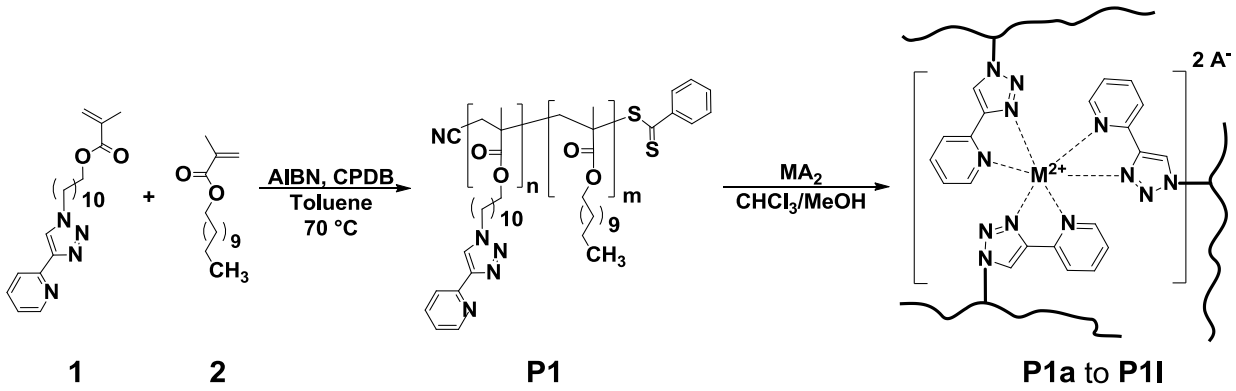

Scheme 3.1 Schematic representation of the synthesis of copolymer **P1** and the subsequent crosslinking using different metal salts into copolymer networks **P1a** to **P1l**.

Sufficient network mobility in the metallopolymer was ensured by a ligand content of 9% (confirmed by ^{1}H NMR spectroscopy) and a T_g of –85 °C of copolymer **P1** (determined by DSC). The influence of different divalent cations and anions on the glass transition temperature and the self-healing behavior of the crosslinked copolymers were investigated. The crosslinking of copolymer **P1** with several transition metal salts led to an increase of the T_g for copolymers **P1a** to **P1l** to –40 °C. Due to the relative strong complex bond of Fe(II) and Co(II) triazole pyridine complexes we mainly focused on the investigation of the metallocopolymers formed by these salts.

Subsequently, the self-healing ability of differently crosslinked copolymers was studied (**Table 3.1**). The crosslinking of copolymer films **P1a** and **P1h** was confirmed by means of UV-Vis spectroscopy *via* the increase of the absorption feature of the $[FeL_3]^{2+}$ species at 433 nm and the $[CoL_3]^{2+}$ species at 320 nm. Hence, UV-Vis spectroscopy represents an appropriate tool to monitor the crosslinking of the copolymers. Two scratches with different widths and the same length (**Table 3.1**) were induced on a film with a scalpel (**Figure 3.1**).

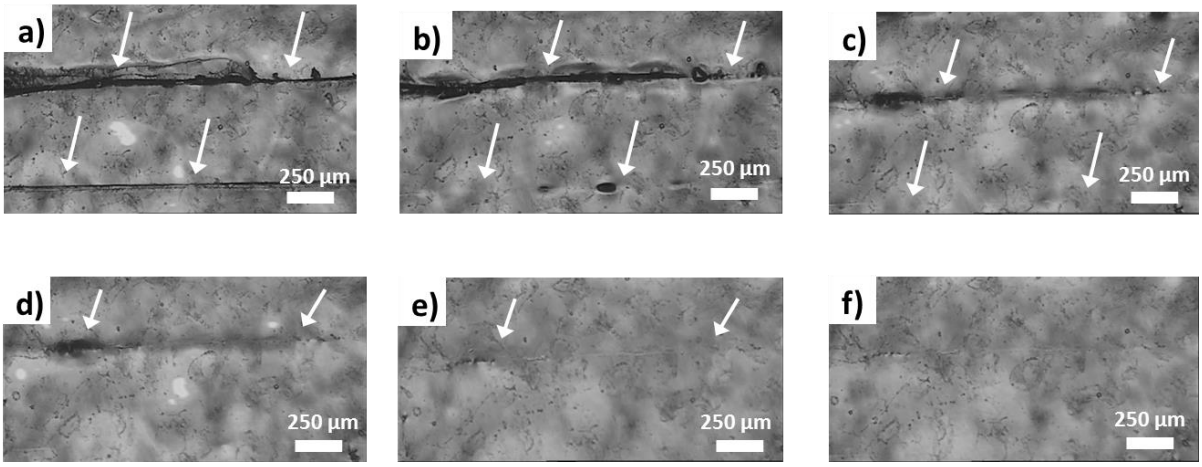

Figure 3.1 Self-healing of the $FeCl_2$-crosslinked copolymer **P1a** at 75 °C; a) t = 0 h, b) t = 2 h, c) t = 5.5 h, d) t = 8.5 h, e) t = 26.5 h and f) t = 50.5 h (white arrows indicate the scratch).

Preliminary assessments of copolymer **P1a** showed already a certain self-healing tendency at 50 °C. Though only small scratches of 96 µm length and 10 µm width were healed at 50 to 65 °C. Due to the higher healing performance, the temperature was increased to 75 °C. After 5.5 hours of annealing the smaller scratch was healed completely. By increasing the healing time to 26.5 hours, the larger scratch (length: 1880 µm; width: 55 µm) was also completely restored. The relatively low healing temperature and high healing efficiency can be explained by the high mobility and flexibility in the copolymer network **P1a**. By using $FeBr_2$ as crosslinking agent, copolymer **P1b** showed an efficient self-healing behavior at 100 °C. There is only a small effect of the bromine anion to the self-healing efficiency. Detailed information is provided in the publication.[94] In case of $Fe(OTf)_2$-crosslinked copolymer **P1d**, efficient self-healing occurred at 75 to 100 °C already within 12 hours (**Figure 3.2**).

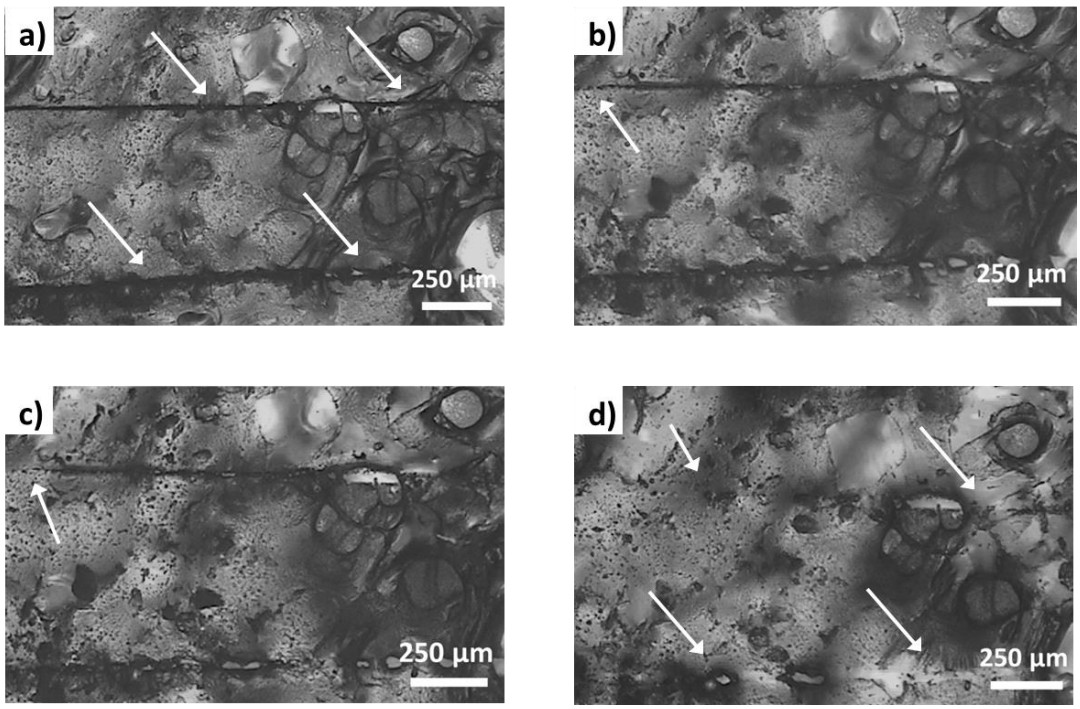

Figure 3.2 Self-healing of the $Fe(OTf)_2$-crosslinked copolymer **P1d** (annealing temperature 75 to 100 °C). a) t = 0 h, b) t = 3.5 h (75 °C), c) t = 9 h (75 °C) and d) t = 12 h (100 °C) (white arrows indicate the scratch).

The optimal healing temperature of 100 °C is higher in comparison to copolymer **P1a**. The ability of triflate to act as additional ligand is in general lower than in case of chloride, resulting in a less flexible and more rigid network. Due to the higher rigidity of the copolymer network **P1e** the material was not able to selfheal even at elevated temperatures of 130 °C that was attributed to the presence of the sulfate anion.

Besides Fe(II)-salts, four different Co(II)-salts, *i.e.* $CoCl_2$, $CoBr_2$ $Co(BF_4)_2$, and $Co(OAc)_2$, were chosen as crosslinker to investigate the influence of the cation on the healing behavior in comparison to the Fe(II) salts. Due to the analogy to $FeCl_2$ and $FeBr_2$, we started with $CoCl_2$ and $CoBr_2$. Both copolymers **P1f** and **P1g** revealed a self-healing behavior, however, not below 100 °C. Besides, $Co(BF_4)_2$ crosslinked copolymer **P1h** was able to self-heal at 100 °C (**Figure 3.3**).

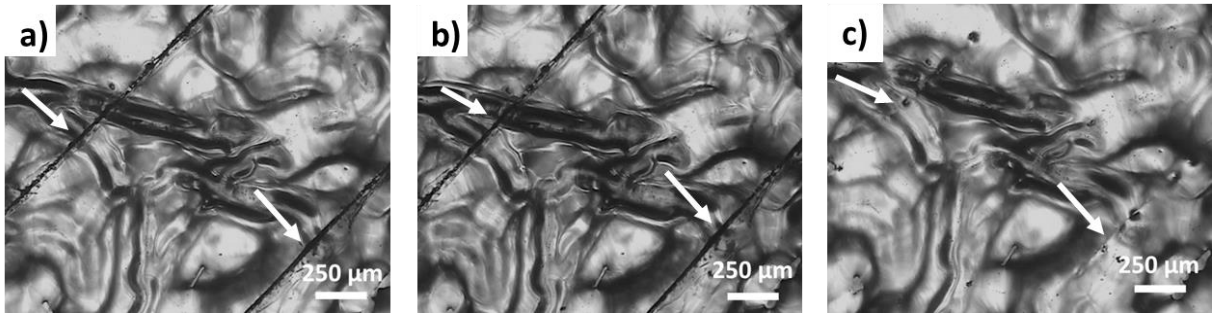

Figure 3.3 Self-healing of the $Co(BF_4)_2$-crosslinked copolymer **P1h**. a) t = 0 h, b) t = 48 h (room temperature) and c) t = 16.5 h (100 °C) (white arrows indicate the scratch).

Copolymers **P1i** to **P1l** revealed rather weak crosslinking, resulting in a rubbery material like the pristine copolymer **P1**. In case of the $Co(OAc)_2$ crosslinked copolymer **P1i**, the presence of the acetate counter ions led to weaker network formation, probably caused by the presence of competing ligands, triazole as well as acetate and, consequently, to inappropriate material properties. Cu(II) and Mn(II) were chosen as cations with different complex formation properties compared to Co(II) and Fe(II). In both cases chloride was chosen as anion. The most promising self-healing results were found for the respective Fe(II) and Co(II) crosslinked networks. Copolymer **P1l** did not reveal any healing behavior below 75 °C. In addition, it seems that the metallopolymer irreversibly decomplexes at 100 °C. Also copolymer **P1k** did not show any significant self-healing properties within a temperature range of 75 to 100 °C.

For structural investigations of the copolymers **P1** and **P1a** to **P1l**, SAXS investigations were performed. Binder already described the formation of clusters as a necessary prerequisite for an efficient self-healing behavior of supramolecular materials based on hydrogen bonding.[11] Bode *et al.* reported on characteristic domain sizes of 6.3 nm ($2\Theta = 1.44°$) of presumably ionic clusters, consisting of iron(II)-terpyridine units as well as the corresponding counter ions. In case of $CdCl_2$ crosslinked terpyridine-containing copolymers, 2Θ values of 1.40° and a corresponding domain size of 6.3 nm had been reported.[93]

Table 3.1 Overview of the investigated copolymers, crosslinking agents, glass transition temperatures, self-healing temperatures (SH), reflections observed in X-ray investigations, and crack dimensions (^{S}= data shown in publication; *= data not shown).

Polymer	Crosslinking agent	Glass transition temperature [°C]	SH temperatures [°C]	Healed crack dimensions (length/ width) [μm]	2 theta [°] (SAXS)	d [nm] (SAXS)
P1	-	– 85^{S}	-	-	-^{S}	-
P1a	$FeCl_2$	– 40^{S}	50 to 100	1880/34 and 55	1.51^{S}	5.8
P1b	$FeBr_2$	– 40^{S}	75	1660/18	1.52^{S}	5.8
P1c	$Fe(OAc)_2$	– 40*	no SH	-	-^{S}	-
P1d	$Fe(OTf)_2$	– 40^{S}	75 to 100	2170/42	1.51^{S}	5.8
P1e	$FeSO_4$	– 40*	no SH	-	1.13*	7.8
P1f	$CoCl_2$	– 40^{S}	75 to 100	1370/20	1.51*	5.8
P1g	$CoBr_2$	– 40^{S}	75 to 100	627/18	1.53^{S}	5.8
P1h	$Co(BF_4)_2$	– 40^{S}	100	1470/23	1.58*	5.6
P1i	$Co(OAc)_2$	– 40^{S}	no SH	-	1.12*	7.9
P1k	$MnCl_2$	– 40^{S}	no SH	-	1.47*	6.0
P1l	$CuCl_2$	– 40^{S}	no SH	-	1.41*	6.3

Regarding the triazole-pyridine metallocopolymers **P1a** to **P1l**, domain sizes from 5.8 to 7.9 nm were observed (**Table 3.1**). All materials showing self-healing behavior (**P1a**, **P1b**, **P1d**, **P1f**, **P1g**, and **P1h**) exhibited distinct broad reflections at 2Θ values of 1.51 to 1.58°. These signals correspond to domain sizes of 5.6 to 5.8 nm. For 2Θ <1.51° no self-healing behavior was observed. These findings are in accordance with the previously investigated terpyridine polymers. A SAXS-signal, *i.e.* an ordered structure (presumably ionic clusters), seems to be a prerequisite for successful self-healing.

In summary, a statistical copolymer of triazole-pyridine methacrylate with lauryl methacrylate was synthesized by RAFT polymerization. The copolymer was crosslinked with several transition metal salts. Fe(II) and Co(II) crosslinked metallocopolymers was utilized for self-

healing studies. UV-Vis spectroscopy was applied as a straight-forward method for the confirmation of successful crosslinking within $FeCl_2$- and $Co(BF_4)_2$-based metallopolymer films. X-ray investigations revealed characteristic domain sizes of 5.8 to 7.9 nm. A relation between the presence of presumably ionic clusters and a self-healing tendency of the respective materials could be established. Moreover the influence of the anion on the self-healing behavior was evaluated. For Fe(II) and Co(II) crosslinked polymers, chloride salts revealed the most promising self-healing behavior. The required healing temperature depends on the salt used for crosslinking and was found to be between 50 and 100 °C, (with healing times between 5.5 and 26.5 hours). The facile and efficient monomer and polymer synthesis enables this class of metallopolymers for a wide field of applications in the area of self-healing materials.

4. Click-chemistry as a tool towards functional- and biocompatible polymers

Part of this chapter have been published in **P3**) B. Sandmann, B. Happ, M. D. Hager, J. Vitz, E. Rettler, P. Burtscher, N. Moszner, U. S. Schubert, *J. Polym. Sci., Part A: Polym. Chem.* **2014**, *52*, 239–247. **P4**) B. Sandmann, B. Happ, J. Vitz, M. D. Hager, P. Burtscher, N. Moszner, U. S. Schubert, *Polym. Chem.* **2013**, *4*, 3938-3942. **P5**) B. Sandmann, B. Happ, J. Vitz, R. M. Paulus, M. D. Hager, P. Burtscher, N. Moszner, U. S. Schubert, *Macromol. Chem. Phys.* **2014**, *215*, 1603-1608. **P6**) D. Pretzel, B. Sandmann, M. Hartlieb, J. Vitz, S. Hölzer, N. Fritz, N. Moszner, U. S. Schubert, *J. Polym. Sci., Part A: Polym. Chem.* **2015**, in press (DOI: 10.1002/pola.27676).

4.1. Efficient Cu(I) acetate-catalyzed cycloaddition of multifunctional alkynes and azides: From solution to bulk polymerization

Solvent-free click reactions of polymeric compounds and polymerizations by CuAAC, respectively, were rarely studied.[44] The following section describes the neat bulk CuAAC polymerization of multifunctional azides and alkynes (depicted in **Scheme 4.1**).

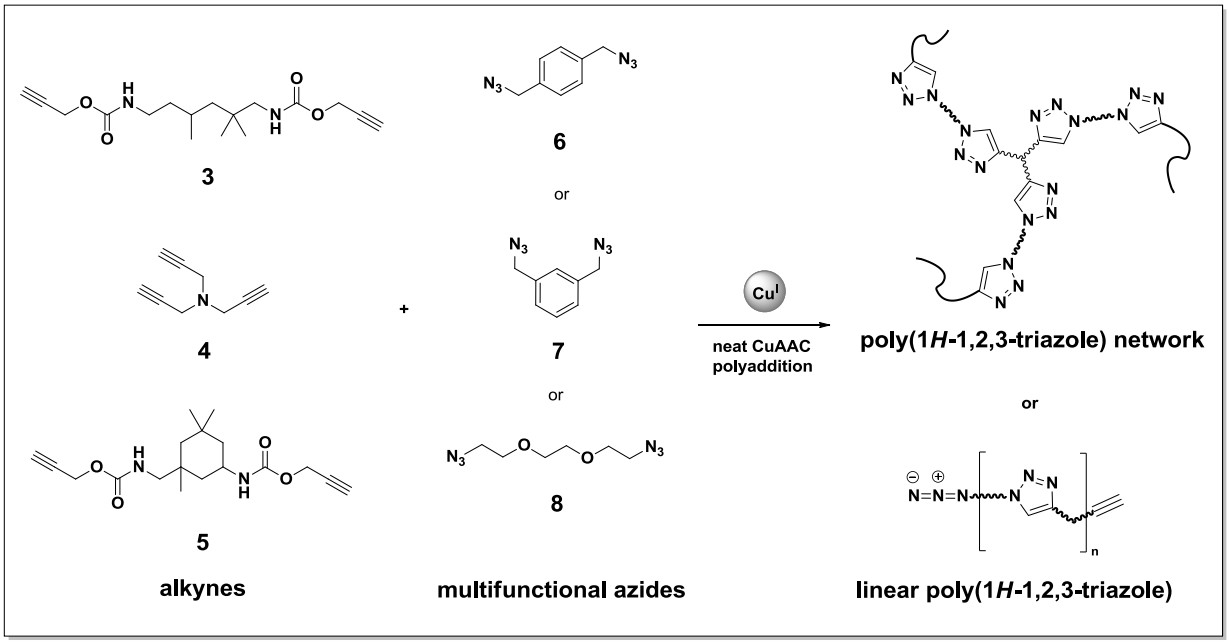

Scheme 4.1 Schematic representation of the CuAAC of alkynes and multifunctional azides.

In a study of different copper(I) salts as potential catalyst systems, the "simple" copper(I) acetate showed unexpectedly the highest reactivity. The kinetics of the CuAAC polymerization was investigated by size exclusion chromatography in solution. Additionally polymerization kinetics were investigated by ^{1}H NMR spectroscopy. For further details, the reader is referred to the publication. Moreover, the click-polymerization was also investigated in bulk. The mechanical properties of the resulting polymers were studied by nano-indentation. First, different Cu(I) sources have been studied in order to identify a highly efficient catalyst for the solvent-free cycloaddition (**Scheme 4.1**). For the screening of different copper salts monomers **3** and **8** were chosen as model system. The amount of catalyst was varied from 0.5 to 2 mol%. The catalyst efficiency was correlated with the temperature shift of the exothermic click reaction, whereby the non-catalyzed reaction served as a reference (temperature onset at 70 °C). It was assumed that in case of a larger shift of the DSC curve to lower temperatures, the catalyst contribution to the reaction is higher. The higher contribution to the reaction results at least in a higher copper catalyst efficiency. The integration of the individual peaks provides the reaction heat ΔH, generated during the reaction. The reaction heat ΔH of the polyaddition was in the range of 560 kJ·mol^{-1}. In case of the CuAAC polyaddition of tetraethylene glycol diyne and *bis*phenol A *bis*azide as well as tetraethylene glycol diyne/*bis*phenol E *bis*azide the reaction heat is in the range of 396 to 419 kJ·mol^{-1} by applying different catalysts.[95] The commonly used copper salt Cu(TBTA)BF_4 and $Cu(CH_3CN)_4BF_4$ revealed a relatively low-temperature shift. Hence, the reaction mainly proceeds uncatalyzed and shows only a minor contribution of the catalyst. In case of $Cu(PPh_3)_3Br$, there is a significant shift of the onset temperature from 95 °C (no catalyst) to 75 °C with a catalyst concentration of 1.0 mol%. When a concentration of 1.0 mol% is used, the reaction seems to be mainly driven by the catalyst. However, there is still a copper-free contribution to the reaction that is depicted in a small shoulder next to the main peak. The amount of added catalyst has a remarkable effect on the initiation temperature. The non-catalyzed reaction starts at 90 °C and can be lowered to at least 45 °C (2.0 mol% CuOAc). This catalytic system showed the highest efficiency and may lead to carbonization at room temperature.

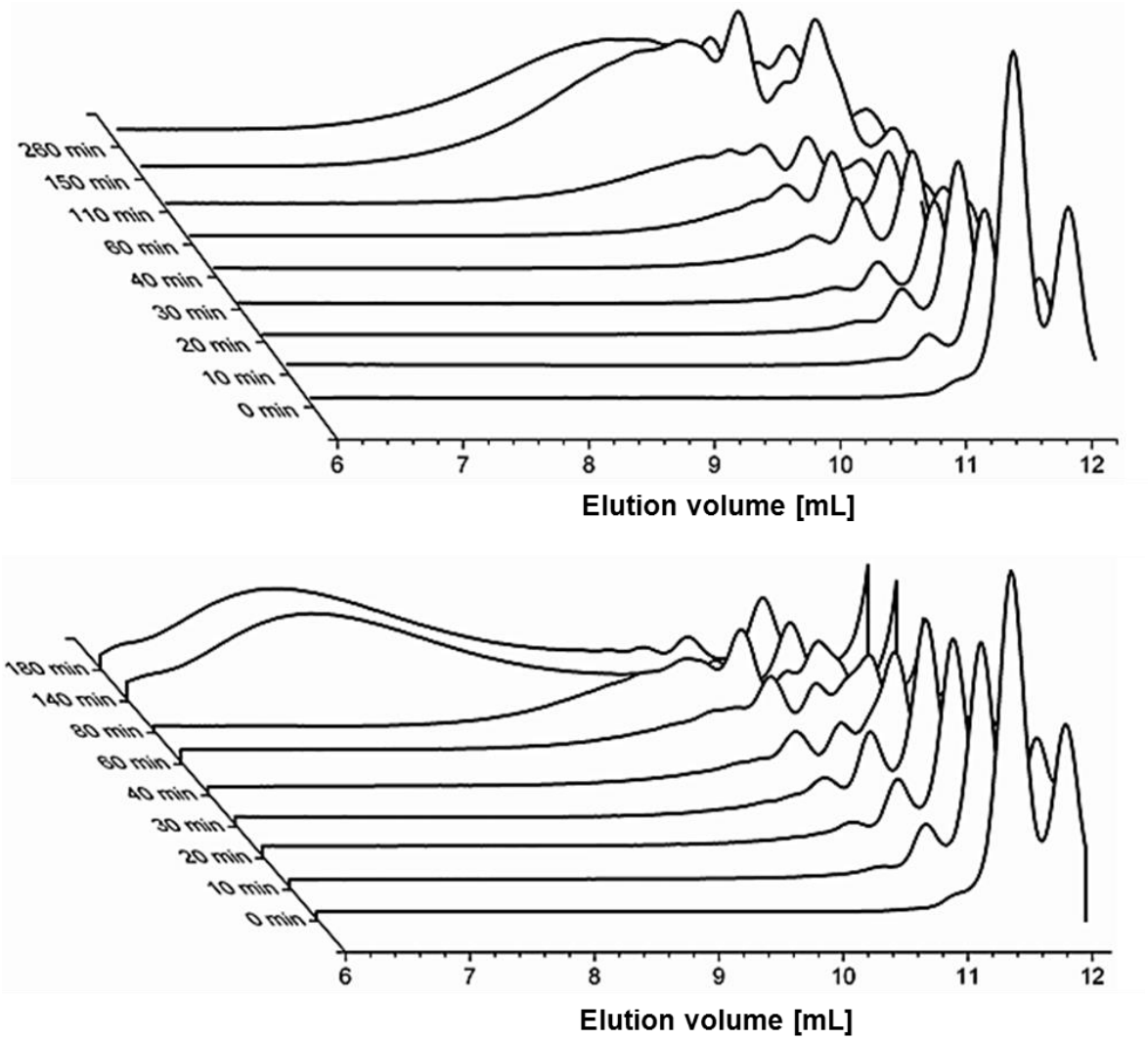

Figure 4.1 SEC analyses of the polymerization processes (DMSO-D_6, DMF-D_7, 1.5 mol% CuOAc, 32 °C) of the TEG-$(N_3)_2$ and the urethane-*bis*alkyne monomers. a) deuterated dimethyl sulfoxide and b) deuterated DMF as solvents.

In order to obtain information on the kinetics and the achievable molar masses of the CuAAC, SEC studies were performed using DMSO-d_6 and DMF-d_7 as solvent. The reaction of bifunctional monomers **3** and **8** (**Scheme 4.1**) served as a model system, whereby an equimolar monomer ratio was used. The molar monomer ratio was 1:1. The reactions were performed at 32 °C with a CuOAc concentration of 1.5 mol% in each solvent. In deuterated dimethylformamide, the reaction progress did not significantly change after 180 min and in deuterated methanol after 260 min (**Figure 4.1**), respectively. After 10 min reaction time, a slight increase of oligomeric reaction products is noticeable in case of DMF (**Figure 4.1**) correlating with a decrease of monomer concentration (elution volume of 11.4 mL). After a reaction time of 80 min (DMF) polymers are formed. In case of DMSO as solvent, the reaction

tends to the formation of oligomers after a reaction time of 5 min. After 300 min, the molar masses did not increase further. In DMF molar masses (M_n) of 17,000 g mol^{-1} (Đ = 1.76) can be observed corresponding to a degree of polymerization (DP) of 33. In contrast to DMF molar masses of 166,000 g·mol^{-1} (Đ = 2.40) were obtained with a DP of 318 in DMSO. The relative high molar masses achieved in DMSO in comparison to DMF can be explained by the higher solubility of the polymer and catalyst in DMSO.

Table 4.1 Composition of polymers, catalyst concentrations, and corresponding E-Moduli.

Polymer	Monomer I	Monomer II	Monomer III	CuOAc concentration [mol%]	Indentation modulus [GPa]
P2a	**4**	**8**	**5**	0.25	6.25 ± 0.4
P2b	**4**	**6**	-	0.25	5.78 ± 0.14
P2c	**4**	**7**	-	0.25	5.6 ± 0.5

For the polymerization, alkyne **4** was activated by stirring with 0.25 mol% CuOAc for several hours. Afterwards, the azide was added to the monomer/catalyst mixture. The CuAAC reactions were performed under inert conditions for 24 h at room temperature and subsequently heated to 50 °C on a heating plate to maximize the conversion rate. The mechanical properties of the polymers were correlated with the azide conversion of the monomer by ATR-IR. The reaction progress was followed by the change of the azide absorption band at 2100 cm^{-1} and azide conversions rates of >95% could be achieved in all cases. With a quantitative azide conversion polymer **P2b** exhibited an E-modulus of 5.78 ± 0.14 GPa (**Table 4.1**). Unexpectedly, choosing a more flexible monomer **7** leads to an indentation modulus of 5.6 ± 0.5 GPa (**P2c**). With polymer **P2a**, the network density is believed to be increased and a maximum of 6.25 ± 0.4 GPa could be achieved.

The polymerization of tripropargylamine, 3-(2-methyl-3-(prop-2-yn-1-yloxy)-2-((prop-2-yn-1-yloxy)methyl)propoxy)prop-1-yne, and 3-(3-(prop-2-yn-1-yloxy)-2,2-bis((prop-2-yn-1-yloxy) methyl)propoxy)prop-1-yne with 1,2-bis(2-azidoethoxy)ethane resulted in soft materials with a low E-modulus. The reader is referred to the publication for further details.[38]

By applying different Cu(I)-salts for the solvent-free click-polyaddition, CuOAc was identified as the most efficient catalyst. The achievable molar masses by using the CuAAC strongly depended on the solvents and the solubility of the polymers. For DMSO-d_6, molar masses (M_n) of 166,000 g mol^{-1} could be achieved in comparison to DMF-d_7 where only molar masses of 17,000 g mol^{-1} were obtained. The obtained elevated indentation moduli make these polymers interesting for a variety of applications.

4.2. Photoinduced polyaddition of multifunctional azides and alkynes

The photoinduced CuAAC requires a Cu-(I) catalyst that can be generated by several approaches. A common method includes the *in situ* photoreduction of Cu^{II} to Cu^{I}. Photoinduced reduction of copper(II) sources can be performed by either direct or indirect photolysis. The main drawback of the direct photolysis, in comparison to the indirect photolysis, are undesired side-reactions and byproducts.[96-98] In this work, several copper(II) salts were tested towards facilitating a photoinduced polymerization of multifunctional azides and alkynes by CuAAC without using a radical-generating photoinitiator. The E-modulus of the materials was determined by nano-indentation measurements. The aim was to reduce copper(II) to copper(I) ions by light excitation and, consequently, to gain control over the initiation of the polyaddition.

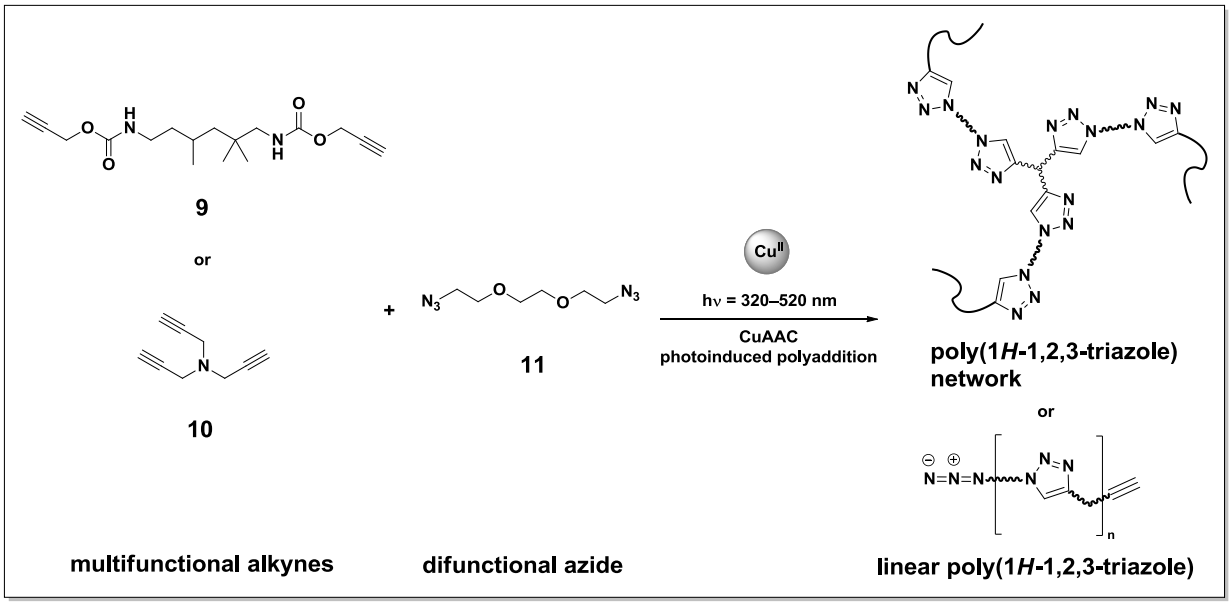

Scheme 4.2 Schematic representation of the photo-induced CuAAC of alkynes **9** and **10** with azide **11**.

The monomers depicted in **Scheme 4.2** were used to engineer different model systems with an average functionality equal or greater than two. The bifunctional system consisting of 1,2-*bis*(2-azidoethoxy)-ethane and di(prop-2-yn-1-yl) (2,2,4-trimethylhexane-1,6-diyl)-dicarbamate served as a model system in order to study the solubility of different copper(II) salts in a neat reaction regime. Di-μ-hydroxo-*bis*[(*N,N,N',N*'-tetramethylethylenediamine)-copper(II)] chloride (Cu[TMEDA]Cl_2) and copper(II) triflate have emerged to be soluble in the neat bifunctional system. However, these salts were unable to launch the copper-catalyzed polyaddition when irradiated with light. The only copper(II) salt being photocatalytically active without additional photoinitiator was copper(II) acetate. However, a solvent e.g. methanol or DMF has to be present (weight fraction greater than 15%). The curing of the polymer was optimized by an appropriate adjustment of the photocatalysis conditions in the Kulzer device (catalyst and solvent content). A copper(II) acetate content of 2.5 mol% had to be used in order to successfully polymerize at an irradiation time of 180 s. Concentrations exceeding 5 mol% led to carbonization of the reaction mixture. The photopolymerization usually yielded yellow-brownish polymers, which were insoluble in common organic solvents. Hence, the obtained materials could not be studied by NMR spectroscopy or size exclusion chromatography. ATR-IR provided the monomer conversion by using the asymmetric azide vibration at 2101 cm^{-1}. The monomer conversion exceeded 95% at a catalyst concentration of 2.5 mol%. The mechanical properties of the photo-polymerized specimens with the monomers **9** and **11** were correlated with the monomer conversions obtained by ATR-IR spectroscopy. If the monomer conversion fell below 90% (catalyst concentration <2.5 mol%) the specimens were too soft for indentation measurements. The polymerization resulted in a hard, homogeneous material (E-modulus: 1.6 GPa ± 0.1 GPa) with a monomer conversion of 95%. Thereby, a small amount of MeOH as solvent was used. A commercial polycarbonate polymer (Hysitron PC standard 5-218, E_r = 2.95 GPa) was used a reference system and an average indentation modulus of 3.1 ± 0.2 GPa was determined. The photo-induced polymerization of the difunctional azide **11** and tripropargylamine can only be carried out in solution using at least 15 wt% of methanol; otherwise precipitation of the catalyst occurred. Similar observations for the catalyst behavior (solubility and catalytic activity) were retrieved as for the bifunctional system. However, the threshold limit value of the catalyst concentration for almost quantitative monomer conversion dropped to 0.7 mol%; the trifunctional alkyne turned out to be more reactive than the bifunctional one. Uncontrollable reaction rates and

carbonization has been already observed at copper(II) acetate concentrations of 2.5 mol%. When stirring a methanolic solution of the monomer mixture **10** and **11** with $Cu(OAc)_2$ (0.7 to 2.5 mol%) a color change from turquoise to colorless takes place within a few minutes. The catalyst activity highly depends on the color status and reaches its maximum at the colorless state. The polymerization proceeds quantitatively and resulted in a colorless polymer with an average indentation modulus of 0.17 ± 0.03 GPa. Furthermore, an overall decrease of the indentation modulus with the increasing depth of indentation was observed revealing an increase in softness of the material.

Among several copper(II) salts only copper(II) acetate is capable of facilitating the photo-induced copper(I)-catalyzed polymerization of multifunctional azides and alkynes by the photo-reduction of copper(II) to copper(I) ions without any additional photoinitiator. The copper(I)-catalyzed azide–alkyne polyaddition can only be carried out in solution using at least 15 wt% of a solvent. Depending on the catalyst concentration in the different reaction regimes (bifunctional azide/bifunctional alkyne, bifunctional azide/trifunctional alkyne, bifunctional azide/tetrafunctional alkyne) quantitative monomer conversions can be achieved whereby the controllability of the polymerization decreases with higher functionality. A quantitative conversion allowed the determination of the E-modulus by nano-indentation. The bifunctional system consisting of a *bis*-azide and *bis*-alkyne revealed the highest value of 1.6 GPa. In future the development of hybrid-systems including a polymerizable solvent and the azide–alkyne photosystems will be in the focus.

4.3. Metal-free cycloaddition of internal alkynes and multifunctional azides under solvent-free conditions

Two different classes of electron-deficient internal alkynes have been chosen to study the influence of the substitution pattern of the alkynes, namely acetylene dicarboxylates as well as an alkyne-based ketone. At least bifunctional monomers are required for the polyaddition with the corresponding azides. Therefore, oligoesters based on the acetylene dicarboxylate and glycol as well as hexanediol have been synthesized. These materials were prepared *via* a transesterification of diethylene dicarboxylate with the corresponding diol (**Scheme 4.3**).

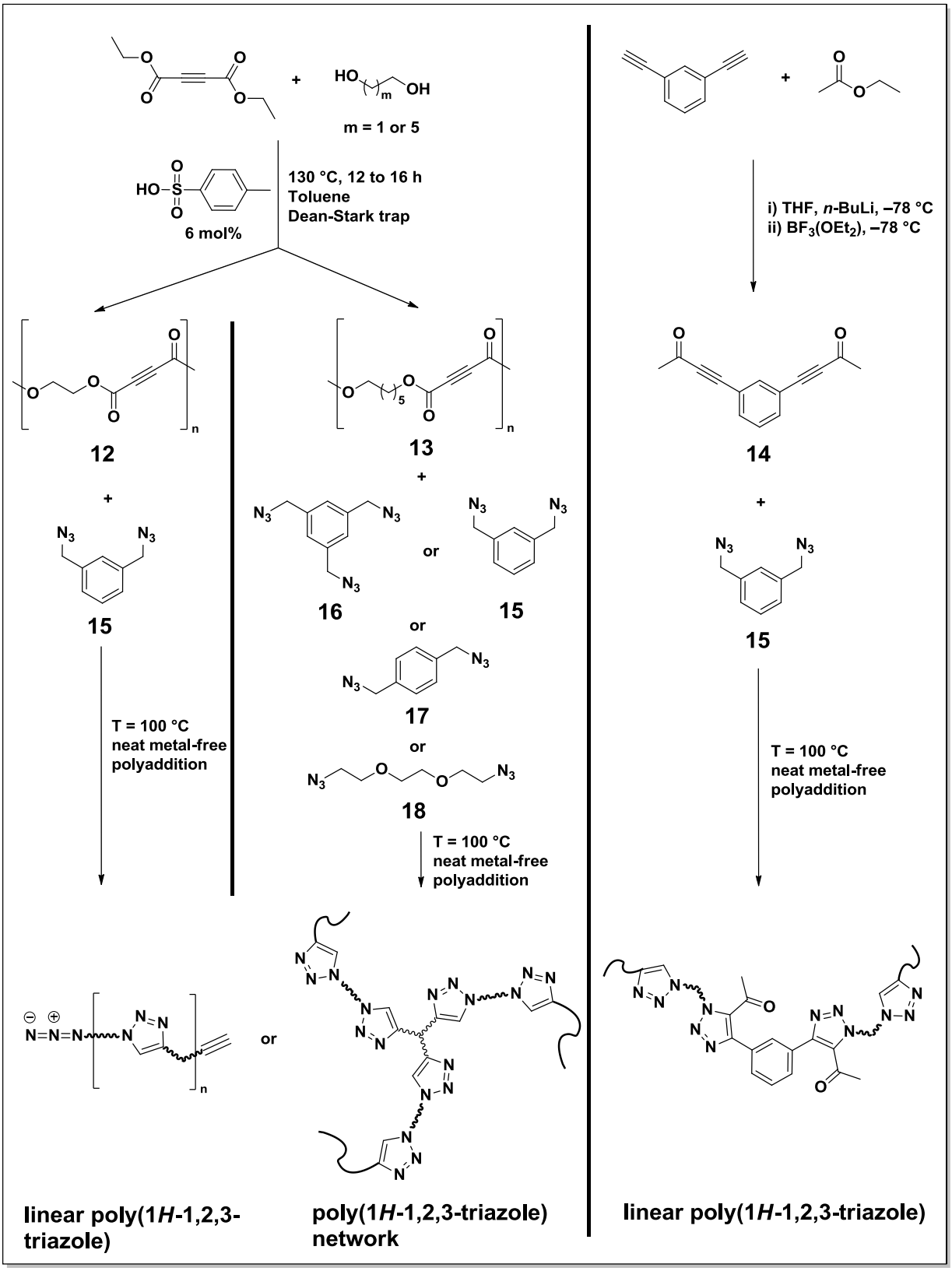

Scheme 4.3 Schematic representation of the metal-free click reaction of alkynes and multifunctional azides.

The acetylene dicarboxylate was used in a slight excess (1.22:1). As a consequence, only oligomers were obtained and the end-group of the resulting oligoesters were ethylesters. The theoretical DP was 10; the SEC measurements revealed for both oligomers DPs of around 10. The alkyne ketone **14** was synthesized in a reaction of diethynylbenzene and ethyl acetate (**Scheme 4.3**). The reaction temperature and the reaction enthalpies of the metal-free polyadditions of the internal alkynes **12** to **14** and the corresponding azides were investigated via DSC.

Table 4.2 Composition and E-modulus of the polymer networks and reaction enthalpies of the metal-free polyadditions.

Polymer	Monomer I	Monomer II	ΔH [kJ·mol^{-1}]	Indentation modulus [GPa]
P3	**12**	**15**	-	2.5 ± 0.20
P4	**13**	**17**	-	1.54 ± 0.17
P5	**13**	**16**	-	1.58 ± 0.24
P6	**13**	**18**	– 278	material too soft
P7	**14**	**15**	– 284	-

The integration of the individual peaks provided the reaction heat ΔH generated during the reaction. For the polymerization of monomers **13** and **18**, a reaction heat of –278 kJ·mol^{-1} was measured and the polymerization already initiated at a temperature of 5 °C. In contrast, the reaction of the *bis*-alkyne **14** with azide **15** started at a temperature of 40 °C. An enthalpy of –284 kJ·mol^{-1} was generated during the polymerization. In contrast, the reaction heat of the Cu(I)-catalyzed click reaction of 1,2-*bis*(2-azidoethoxy)-ethane and di(prop-2-yn-1-yl)(2,2,4-trimethylhexane-1,6-diyl)dicarbamate with different copper(I) salts is in a range of –315 to –526 kJ·mol^{-1}.[38] The reactivity and the required reaction temperature of the used monomers can be tuned by the substitution pattern. Reasonable temperatures (75 to 130 °C), particularly for the oligoesters, can be used for the polyaddition in bulk materials in order to harden these materials. The alkyne monomers **12** to **14** and the corresponding azides **15** to **18** have been utilized for the polyaddition (**Scheme 4.3**). The DSC measurements revealed that both alkyne monomers showed sufficient reactivity at 100 °C. Therefore, the click reactions were performed for 24 h at this temperature in order to achieve a quantitative azide conversion. The

reaction progress was followed by ATR-FT-IR spectroscopy. The change of the azide absorption band at 2100 cm^{-1} correlates to the monomer conversion. For all of the investigated monomer pairs, a conversion between 80% and 100% of the azide moieties was achieved under the applied reaction conditions. The mechanical properties of the synthesized polymer networks were investigated *via* depth-sensing indentation. The E-moduli of the resulting polymers are depicted in **Table 4.2**. Polymer **P3** exhibited an E-modulus of 2.5 ± 0.20 GPa. The indentation moduli of the polymers **P4** (1.54 ± 0.17 GPa), **P5** (1.58 ± 0.24 GPa) and **P7** were lower than for polymer **P3** due to the more flexible monomer **13** and a lower azide conversion of about 80%. The aliphatic monomer **18** decreases the network density as well as rigidity in contrast to the aromatic azides. Consequently, a softer and more flexible material was obtained. Due to the softness of polymer **P6** indentation measurements were not possible.

By attaching electron-withdrawing carbonyl moieties to the adjacent alkyne functionalities, it was possible to increase the reactivity of the alkyne monomers for the metal-free azide‑alkyne cycloaddition under solvent-free conditions. Thereby, the reaction temperature of the polymerization of the alkynes **13** and **14** with the azides **18** and **15** could be lowered to at least 5 and 40 °C. For the CuAAC, highly efficient catalysts are used which often leads to a release of high reaction enthalpies in a short time period.[38] By performing the click reaction with electron-poor internal alkynes, the exothermicity was reduced to a value of –278 and –284 $kJ \cdot mol^{-1}$, respectively. The polyaddition reaction of oligomers **12** and **13** with the *bis*-alkynes **15**, **16**, and **17** results in hard polymer resins with a maximum E-modulus of 2.5 ± 0.20 GPa. These moderate mechanical properties and the absence of catalyst make these polymers especially interesting for biomedical applications.

4.4. Biological evaluation of 1,2,3-triazole based polymers for potential applications as hard tissue material

In the **Chapter 4.3**, the synthesis of cross-linked 1,2,3-triazole based polymers and their resulting mechanical characteristics showed excellent properties for the production of hard scaffolds for biomedical applications, including prosthetic materials, scaffolds for tissue engineering, bone cements as well as parts of medical devices and disposable supplies.[99] In

the development of new synthetic hard polymer materials, cell culture based test are the first step to determine the biocompatibility. Hence, *in vitro* tests were conducted investigating the toxicity of monomers, polymeric bulk material as well as extracts from polymerized samples using L929 mouse fibroblasts, representing a standard cell line for named tests. The materials described in this chapter consist of oligomeric alkynes, multifunctional azide cross-linkers, as well as their resulting polymers, respectively (**Scheme 4.4**). In order to investigate the influence of the length of this building block, two oligoesters with different molar masses (M_n) and dispersities (Đ) were synthesized (**19** (M_n = 1058 g mol^{-1}; Đ = 2.68), **20** (M_n = 1850 g·mol^{-1}; Đ = 1.66). Besides the influence of the substitution pattern (**21** *vs.* **24**) and the number of azide groups per monomeric unit (**21** *vs.* **22**), the role of the hydrophilicity of the monomer was investigated by using triethylene glycole *bis*-azide (TEG-N_3) (**23**).

For the production of scaffolds by metal-free cycloaddition, both, alkyne and azide were mixed at room temperature using an equimolar ratio of both functional moieties and subsequently polymerized at 100 °C for 24 h.[99] The azide conversion was followed by ATR-IR spectroscopy, monitoring the change of the absorption band at 2100 cm^{-1}. Conversions between 60 and 80% were achieved for all of the investigated monomer pairs under the applied reaction conditions. **Table 4.3** displays the used component combinations and the resulting analytical data. For all investigations **P16** (a commercial cross-linked dimethacrylate duromer) was used as a reference. The mechanical properties of the synthesized polymer networks were investigated *via* depth sensing indentation (DSI). Unexpectedly, the influence of the length of the alkyne oligomer is negligible, as expressed by the comparison of **P8** to **P11** that were polymerized using **19** with their corresponding **20** adduct (**P12** to **P13**). However, the substitution pattern has an impact, as scaffolds produced using **21** have a significantly increased E-modulus compared to **24**. As expected, the utilization of **23** (TEG-N_3), yields networks with an E-modulus three orders of magnitude lower than all other substrates according to literature reports.[99]

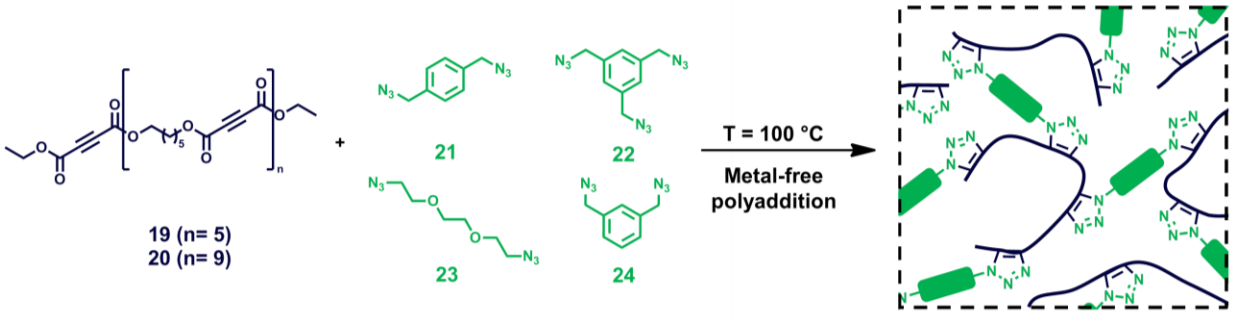

Scheme 4.4 Schematic representation of the metal-free click reaction of alkynes **19** and **20** with multifunctional azides **21** to **24**.

Table 4.3 Composition and analytical data of the polymer networks.

Polymer	Alkyne	Azide	Azide conversion [%]	Indentation modulus [GPa]	Cellular growth density [%, referring to P16]
P8	**19**	**21**	78	2.41 ± 0.32	45
P9	**19**	**22**	60	3.09 ± 0.27	114
P10	**19**	**23**	72	0.008 ± 0.002	87
P11	**19**	**24**	71	1.95 ± 0.07	33
P12	**20**	**21**	66	2.51 ± 0.09	68
P13	**20**	**22**	62	2.58 ± 0.12	26
P14	**20**	**23**	67	0.01 ± 0.006	78
P15	**20**	**24**	80	1.19 ± 0.10	108
P16	-	-	-	3.74 ± 0.23	100

The *in vitro* cytotoxicity experiments were performed on the basis of the well-known XTT assay using L929 mouse fibroblasts, according to DIN ISO 10993-5. First, the cytotoxic potential of the monomers used for the polymerization was tested in order to determine a possible undesired biological side effect of residual (non-reacted) monomers remaining in the polymerized samples (**Figure 4.2A**). After 24 h of incubation with different concentrations of the educts (**19** to **24**), the metabolic activity of cells was found to be drastically reduced in the case of the alkynes **19** and **20** as well as for the aromatic azides **21**, **22** and **23** displaying a concentration dependent inhibition of the cell metabolism. Alkyne **20** and azides **21**, **22** and **24** resulted in a reduction of the cell viability under the defined border to cytotoxicity of 70% in a

concentration from 3 to 0.3 mg mL^{-1}, lower substance concentration around 0.06 mg mL^{-1} were tolerated by the cells. In contrast, alkyne **19** showed cytotoxic potential at all analyzed concentrations. Exclusively cells treated with azide **23** displayed a metabolic activity on the level of the untreated controls that proves the absence of a toxic effect mediated by the TEG *bis*-azide (**23**). These results indicate that a significant amount of unbound monomer within the final scaffolds would lead to materials incompatible with biological systems. However, as the viability of cells treated with **23** shows the presence of azide groups does not necessarily lead to a significant cytotoxic effect. While salts such as sodium azide display potent toxins *via* the inhibition of the cytochrome C oxidase[100] by the azide anion, covalently bond azides cannot dissociate within a biological environment.

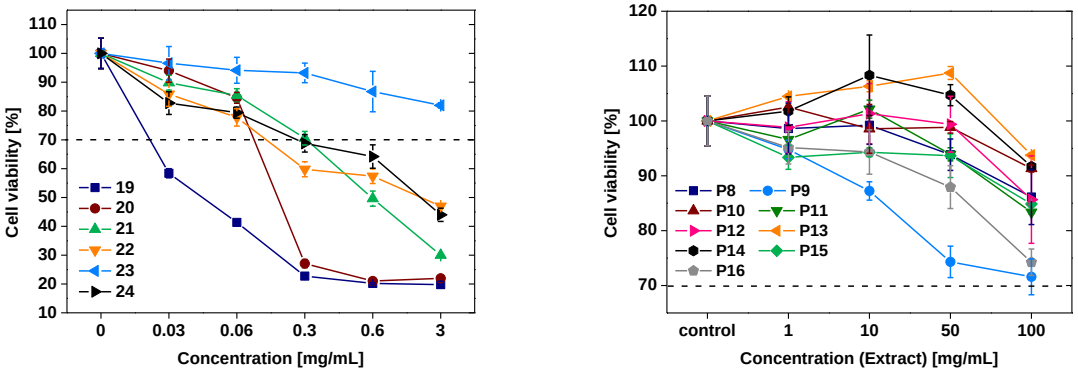

Figure 4.2 Cell viability of L929 mouse fibroblasts after 24 h incubation with different concentrations of the monomers **19** to **24** (A); extracts of fine grinded polymer powders **P8** to **P16** (B). Cells incubated with pure culture medium served as control. Data are expressed as mean ± SD of six determinations.

It is rather likely that the chemical structure of the azide containing molecules plays an important role in their cell biological behavior. In particular, the hydrophobic nature of the aromatic hydrocarbons in **21**, **22** and **24** presumable provoke a harmful interaction with cellular membranes as indicated by the drastic reduction of the cell viability. A similar reason might be responsible for the cytotoxic effects of the alkynes **19** and **20**, which are highly hydrophobic due to their nonpolar character. Interpreting these results, the monomers by themselves (except **23**) are of potential harmful character and need to be absent in their unreacted form in the final polymeric material. Otherwise a reduced biocompatibility can be expected. In order to examine this assumption the resulting materials **P8** to **P15** including the reference material **P16** were screened for their impact on cellular integrity. First investigations were conducted using aqueous extracts of grinded polymers. The extracts were directly

incubated with L929 mouse fibroblasts for 24 h followed by performance of the XTT viability assay. This approach enables the efficient extraction and effect-detection of potentially remaining educts within the polymerized samples. As depicted in **Figure 4.2B** all extracts resulted in an acceptable viability rate above 70% in the case of undiluted extract samples, approaching the level of the untreated control with increasing dilution steps. Interestingly, the resulting viability rates after incubation with the polymerized samples **P8** to **P15** showed a similar profile like the reference material **P16** thus proving the good biocompatibility of the extracts derived from the newly polymeric materials. It has to be noted, that the concentrations generated by the extraction method are far above the values which can be expected by simple exposure of substrates to water, rendering the cytotoxicity results highly promising.

To confirm the general biocompatibility of the click scaffolds, a live/dead microscopy study of cells that were seeded onto films consisting of the materials **P8** to **P16** was performed. 24 h after cell seeding, the materials were washed to remove non-adherent cell bodies and analyzed microscopically. The transparent character of the samples enabled capture of phase contrast micrographs, which showed that L929 mouse fibroblast cells attach onto the polymeric surfaces and display morphologies of adherent viable cells. The cell viability was further investigated using Hoechst/Fluorescein diacetate (FDA)/propidium iodide (PI) live/dead staining, which gave information about the cell-membrane integrity (exclusion of red fluorescent PI from cell nuclei that were additionally tagged by Hoechst dye) and the viability (strong green fluorescence of FDA in cytoplasm) (**Figure 4.3**).

The absence of the red fluorescence of PI in all pictures and the successful FDA staining prove the excellent cytocompatibility of used click scaffolds. The bright field images also give an indication about the surface roughness of click substrates which is pronounced for **P13** to **P16**.

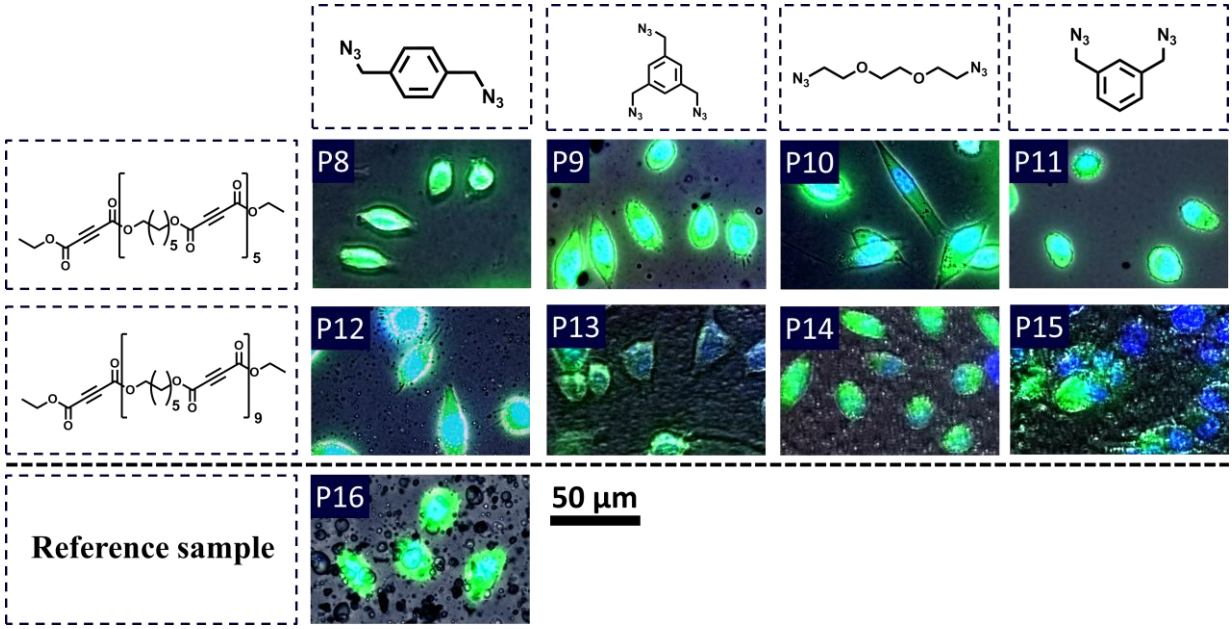

Figure 4.3 The panels display the viability and morphology of L929 cells after incubation on polymer films for 24 h. An overlay of representative bright field and fluorescence microscopy images of cells on the scaffolds **P8** to **P16** is depicted. Blue fluorescent Hoechst dye labels nuclei of all cells present, green fluorescence from FDA tags viable cells while red fluorescent PI signals originates from nuclei of dead cells. Bright field images also give an indication about the surface roughness of the click substrates, as well as **P16**.

To assess quantitative information of the cellular growth on distinct materials, representative sections of micrographs were subjected to cell counting. The results were referred to the growth density obtained from **P16** (**Table 4.3**). No clear trend is visible comparing the results to the elastic moduli, conversions or the use of distinct monomer combinations. However, **P8** and **P13,** which show a significantly reduced growth density also have an increased surface hydrophilicity compared to the other substrates. Hydrophilic surfaces are known to repel microorganism due to a prevention of attachment.[101] The growth density on the substrates **P9** and **P15** exceeds the value obtained for the reference material **P16** rendering these substrates particularly suitable for the productions of hard tissue replacements. The observed biocompatibility of the 1,2,3-triazole based polymers **P8** to **P15** is in accordance with literature values, stating a non-toxicity of many poly(triazole) containing structures, mainly designed in the pharmaceutical field, e.g., as a tool for drug discovery for cancer treatment.[102-103] Due to its chemical composition, the triazole units are not subject to metabolic degradation and are stable in typical biological conditions, which are usually of aqueous and mildly reducing nature.[104-105]

In summary, the cell study on the click monomers clearly revealed a cytotoxic potential of the alkynes and aromatic azides used in this study, exceptionally the TEG like *bis*-azide turned out to be cytocompatible at all applied concentrations. Further investigations on the final polymer samples neglected the hazardous character of the educts and presented a polymeric material which exhibits highly biocompatible character in its bulk format as well as in the contact of cells with aqueous polymer extracts. Cells grown on the scaffolds were analyzed regarding their viability and growth density. All polymers show good biocompatibility with various growth densities of L929 fibroplasts. Nevertheless, in view of the development of new synthetic hard polymer materials, the *in vitro* assays based on cell culture models described in this chapter display only the first step to determine the biocompatibility of a material. Before a potential clinical application of the described materials, additional tests have to be performed, including mainly *in vivo* animal models for the determination of acute and (sub-) chronic toxicity, genotoxicity, carcinogenicity, reproductive/developmental problems, neurotoxicity, immunotoxicity as well as the presence of endotoxins in the final product.

5. Core-shell nanoparticles as tougheners for methacrylate based composites

Part of this chapter have been / will be published in **P7**) B. Sandmann, B. Happ, I. Perevyazko, T. Rudolph, F. H. Schacher, S. Hoeppener, U. Mansfeld, M. D. Hager, U. Fischer, P. Burtscher, N. Moszner, U. S. Schubert, *Polym. Chem.* **2015**, in press (DOI: 10.1039/C4PY01544D).

This chapter reports the synthesis of core-shell nanoparticles consisting of an ethylene glycol dimethacrylate (EGDMA) crosslinked soft poly(butyl acrylate) PBA core and a hard poly(methyl methacrylate) PMMA shell in a three step emulsion polymerization. In some cases the shell was additionally crosslinked with triethylene glycol dimethacrylate (TEGDMA). The particle sizes and morphologies were investigated by dynamic light scattering (DLS), cryogenic-transmission electron microscopy (cryo-TEM) and analytical ultracentrifugation (AUC) experiments. Particles were dispersed in a resin mixture of TEGDMA and urethane dimethacrylate (UDMA) and were subsequently photo-polymerized (**Scheme 5.1**). The mechanical properties of the resulting polymers were investigated in three-point bending tests. The compositions and types of lattices are shown in **Table 5.1**.

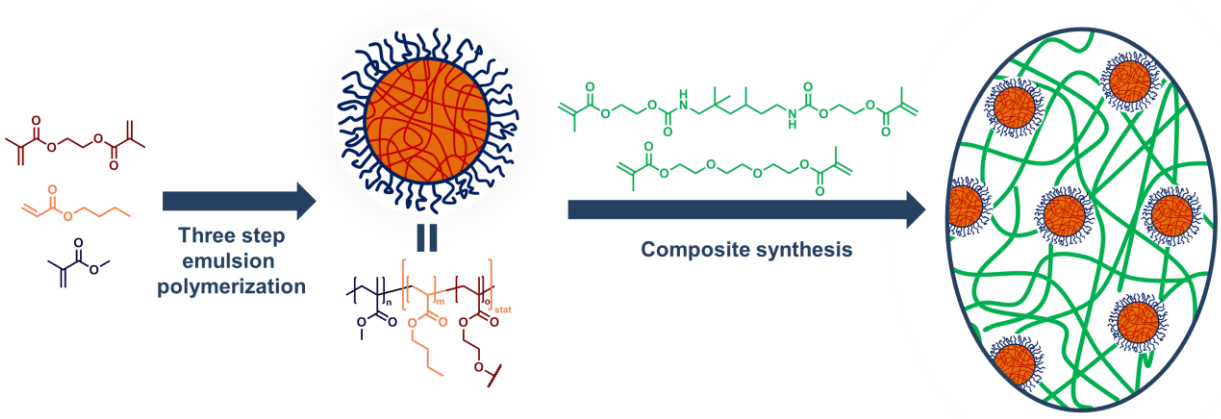

Scheme 5.1 Schematic representation of the core-shell nanoparticle synthesis and their incorporation into a TEGDMA/UDMA based composite.

In the first step, EGDMA crosslinked polymer seeds (latex **L1**) with an average particle size of 70 nm (determined by AUC) and 86 nm (determined by DLS), respectively, were synthesized. Subsequently, seed particles were used for the synthesis of the polymer cores. The sizes of the

resulting particles revealed an increase in size up to 114 nm for latex **L3**. For latex **L2** there is only a minor size increase concluded from the DLS (106 nm) and, in particular from the AUC (89 nm) results. In the last synthesis step, crosslinked and non-crosslinked polymer shells were attached to the polymer cores, resulting in the lattices **L4** to **L9**. Thereby, particle sizes of 144 to 234 nm (determined by DLS) or 115 to 220 nm (determined by AUC), respectively, were achieved. Different crosslinked and non-crosslinked core-shell particles with particle sizes between 160 and 220 nm (acc. to AUC) were synthesized in a three step emulsion polymerization. Particle sizes and shapes were investigated by cryo-TEM and were discussed in detail in the attached publication. The average values of the sizes and corresponding densities are summarized in **Table 5.1**. The corresponding average sizes of lattices obtained by AUC and DLS are in good agreement. The largest particles with a size of 220 nm were observed for sample **L8** (core/shell ratio: 10/90). Moreover, the value of the density has as well reached its maximum of 1.19 $g \cdot cm^{-3}$ for the sample **L8**. As a second method, DLS was used to investigate the different particles concerning their sizes.

Table 5.1 Latex particle composition, average hydrodynamic diameter of latex particle (determined by DLS (d^{DLS}) and analytical ultracentrifugation (d^{AUC})) and concentration of core-shell particles in test specimens.

Latex	Core/Shell Ratio	Crosslinker content of polymer shell [%]	d^{DLS} [nm]	d^{AUC} [nm]	Test specimen	Latex conc. in test specimens [wt%]
L1	–	–	86	70	**–**	
L2	–	–	106	89	**–**	
L3	–	–	114	115	**–**	
L4	(30/70)	–	160	180	**TS1**	9
L5	(30/70)	2	166	170	**TS2**	3
L5	(30/70)	2	166	170	**TS3**	6
L5	(30/70)	2	166	170	**TS4**	9
L6	(30/70)	4	166	160	**TS5**	9
L7	(30/70)	8	164	160	**TS6**	9
L8	(10/90)	**–**	234	220	**TS7**	9
L9	(50/50)	4	144	140	**TS8**	9
–	**–**	**–**	–	–	**TS9**	0

The apparent hydrodynamic diameter ($<d_{h,app}>$) determined *via* DLS revealed a size of 86 nm for the seeds (**L1**), while for the first core (**L2**) a size increase up to 106 nm could be observed *via* DLS (**Table 5.1**). However, AUC showed a smaller increase in diameter up to 89 nm. For core **L3,** the results were in good agreement for both methods (DLS and AUC) and a significant shift to higher hydrodynamic diameter from 70 to 115 nm confirmed the successful formation of an additional PBA layer. In further steps different compositions/ratios of 30/70 and 50/50 were applied to the cores (**L2** and **L3**). The size distributions (determined by DLS) showed an increase of the hydrodynamic diameter, after attaching the polymer shell to core **L3**, of 52 nm (**L5** and **L6**), 50 nm (**L7**) and 30 nm (**L9**), respectively. For core **L2** size increases up to 54 nm (**L4**) and 128 nm (**L8**) were observed. In direct comparison of core-shell lattices **L5**, **L6** and **L7** there is no significant influence of the TEGDMA crosslinker to the

sizes of the resulting core-shell lattices. The increasing size after shell-attachment can be correlated to the amount of MMA added and at least to the different core/shell ratios for all core-shell particles.

The morphology of polymer particles was investigated by means of cryo-TEM, because the nanoparticles can be investigated close to their state in solution and to reduce artefacts from the preparation (*e.g.*, loss of solvent, drying effects, etc.). **Figure 5.1** depicts representative examples of synthesized polymer particles **L1** to **L8**. cryo-TEM revealed a spherical shape for seed particles (**L1**). **Figure 5.1** displays the seed particles after the core formation, resulting in latex **L2** and **L3** while the spherical shape of particles is preserved. Though the same synthesis conditions were applied to obtain **L2** and **L3**, different seed-core sizes were observed according to DLS and AUC results. For the subsequent studies the seed-core nanoparticles **L2** and **L3** were utilized. In the following synthesis step the non-crosslinked PMMA shell was synthesized on the core particles resulting in lattices **L4** and **L8**. For core-shell particle **L4** cryo-TEM picture revealed a contrast distinction. This potentially stems from the polymer core with a darker contrast and the attached shell with a weaker contrast. This distinguishing feature was only clearly observable for sample **L4**. The particle shapes of **L4** and **L8** did not remain clearly spherical and became uniform. Gutiérrez-Mejía *et al.* synthesized PBA/PMMA nanoparticles similar to our latex, with a core-shell ratio of 30/70. In their study the clear spherical shape remained after shell formation.[60] This observation is not in accordance with our results as non-uniform particles were observed. The polymer shell of lattices **L5**, **L6**, **L7** and **L9** was crosslinked (up to 8%) with TEGDMA in order to improve the particle stability, the dispersability in TEGDMA monomer and to evaluate the effects on the mechanical properties. As already observed for particles **L4** and **L8**, a change of the nanoparticle morphology was observed when the PMMA shell was attached. The resulting core-shell nanoparticles (**L5**, **L6**, **L7** and **L9**) were not homogeneously spherical anymore. This irregular particle shape was attributed to the incompatibility of both constituting polymers and the polymerization sequence.[106-108]

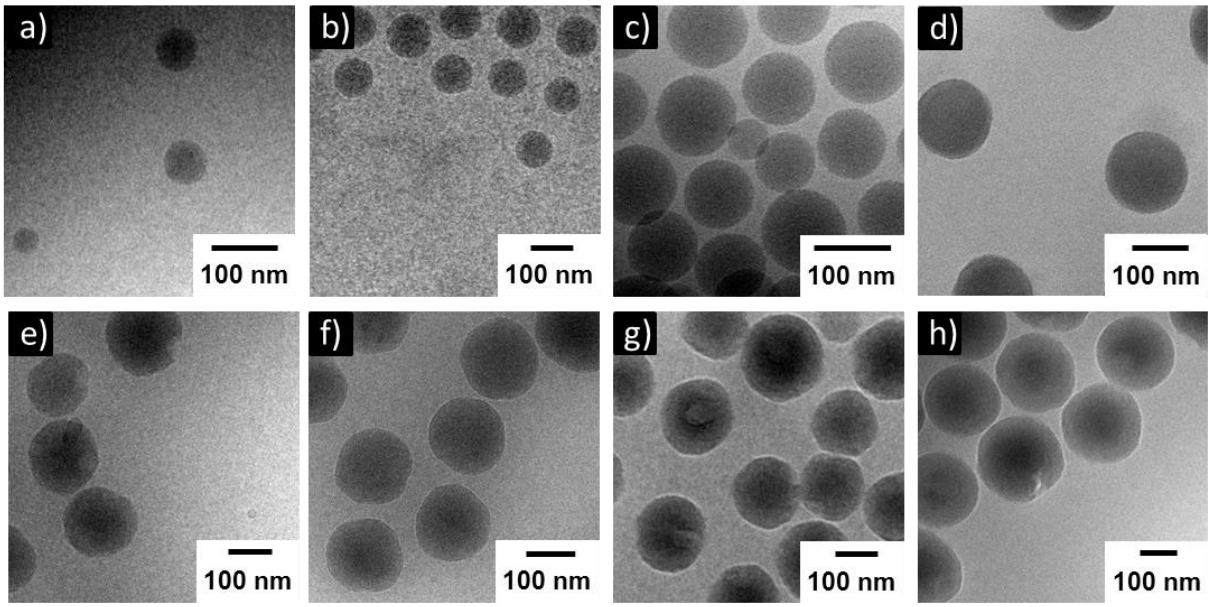

Figure 5.1 Cryo-TEM images of latex particles **L1** to **L8**; a) **L1**, b) **L2**, c) **L3**, d) **L4**, e) **L5**, f) **L6**, g) **L7** and h) **L8**.

The preparation of test specimens was performed by mixing and homogenising the initial components with the particle dispersions. Pre-examinations revealed that the dispersability of the non-crosslinked core-shell particles (**L4** and **L8**) in TEGDMA was inferior to the crosslinked ones (**L5** to **L7** and **L9**). The monomer formulations were photo-polymerized. Experimental data of E-modulus and stress intensity factor (K_{1c}) of samples of the test specimens **TS1** to **TS9** are displayed in **Table 5.2**. Sample **TS9** was used as a reference sample and therefore not enriched with latex particles. The composition of **TS9** was adapted so that there are equal monomer concentrations in all test specimens (**TS1** to **TS9**). Polymer lattices **L5**, **L6**, **L7** and **L9** were crosslinked with TEGDMA to improve the dispersability and to investigate its effect on the mechanical features.

To investigate the influence of different core/shell ratios on the mechanical properties, polymer particles were synthesized with core-shell ratios of 10/90, 30/70 and 50/50 (**TS1**, **TS7** and **TS8**). The implementation of latex particles with a core-shell ratio of 50/50 (**L9**) in a composite (**TS8**) led to a drop of E-modulus (1.77 GPa) and K_{1c} (0.763 MPa·m$^{1/2}$). Thus, only by applying particles with a core shell ratio of at least 30/70, corresponding to test specimen **TS1**, showed an elevated E-modulus (1.72 GPa) and K_{1c} (1.139 MPa·m$^{1/2}$). By increasing the shell content up to a ratio of 10/90 (**TS7**), the E-modulus and K_{1c} (1.186 MPa·m$^{1/2}$) reached a maximum of 1.90 GPa.

In order to obtain information about the influence of different shell crosslinker ratios on the mechanical properties, the polymer particles were crosslinked with 2, 4 and 8% TEGDMA and utilized for test specimens. A crosslinker content of 2% (**TS4**) provided the highest K_{1c} value (1.206 MPa·$m^{1/2}$) and an increased E-modulus (1.78 GPa). With a linker content of 4% (**TS5**) a considerable enhancement of the mechanics (E-modulus: 1.89 GPa, K_{1c}: 1.116 MPa·$m^{1/2}$) was obtained. A further increase of the crosslinker content up to 8% (**TS6**) did not result in an enhancing effect of the mechanical properties. With an E-modulus of 1.87 GPa and K_{1c} of 0.835 MPa·$m^{1/2}$ the TEGDMA linker softens the material.

Table 5.2 Mechanical properties of test specimens.

Test specimen	E-modulus (standard deviation) [GPa]	K_{1c} (standard deviation) [MPa·$m^{1/2}$]
TS1	1.72 (0.05)	1.139 (0.059)
TS2	1.55 (0.09)	0.752 (0.065)
TS3	1.86 (0.10)	0.850 (0.038)
TS4	1.78 (0.07)	1.206 (0.055)
TS5	1.89 (0.05)	1.116 (0.056)
TS6	1.87 (0.07)	0.835 (0.273)
TS7	1.90 (0.10)	1.186 (0.070)
TS8	1.77 (0.07)	0.763 (0.062)
TS9	1.61 (0.07)	0.733 (0.071)

Additionally, the influence of various particle concentrations within the test specimens and their effect to the mechanical properties was studied. For that purpose a series of samples filled with 3, 6 and 9 wt% of polymer particles (**L5**) were investigated (**TS2** to **TS4**). With a particle concentration of 3 wt% (**TS2**), there is a slightly decreasing influence to the E-modulus (1.55 GPa) and K_{1c} (0.752 MPa·$m^{1/2}$). By increasing the particle concentration to 6 wt%, (**TS3**) an extensive enhancement of E-modulus (1.86 GPa) and K_{1c} (0.850 MPa·$m^{1/2}$) was observed. When the particle concentration was further increased up to 9 wt% (**TS4**) the

mechanical properties show a lower E-modulus (1.61 GPa), however, with a maximum of K_{1c} (1.206 MPa·$m^{1/2}$).

By incorporation of core-shell nanoparticles into a matrix, consisting of TEGDMA / UDMA and consequently photo-polymerizing the monomer mixture, it was possible to improve the E-modulus and K_{1c} values of the unfilled polymer composition. Particles with sizes of 70 to 220 nm in diameter (determined by AUC) were achieved. cryo-TEM investigations showed that all core-shell particles (**L4** to **L9**) revealed irregular particle geometries, differing from the clear spherical shape of the polymer seed (**L1**) and the cores (**L1** and **L2**). By crosslinking the polymer shell with a TEGMDA concentration up to 4% it was possible to enhance the dispersability of particles in the monomer (TEGDMA) together with an improvement of the mechanical properties. The best mechanical properties were achieved with the test specimens **TS5** and **TS7** (see **Table 5.2**) that refers to lattices **L6** (core-shell ratio: 30/70) and **L8** (core-shell ratio: 10/90). Particles with a lower shell content (core-shell ratio: 50/50) have a decreasing effect to the E-modulus and K_{1c}. In a concentration dependent study of polymer particles within the test specimens, optimal E-modulus values were achieved at a particle concentration of 6% (**TS3**). However, for a test sample filled with 9% polymer particles (**TS4**), the highest K_{1c} (1.206 MPa·$m^{1/2}$) value was obtained of all investigated samples. These improvements of mechanical properties of TEGDMA/UDMA composites make them attractive as a potential toughening additive.

5.1. Preliminary results of polymerization-induced phase separation (PIPS) experiments

Besides the approach discussed in the previous section (**Chapter 5**), the polymerization-induced phased separation (PIPS) represents another promising way to enhance the fracture properties of polymer composites. This chapter describes the current research approach towards an enhancement of the mechanical properties of methacrylate based composites by PIPS.

The theory of polymerization induced phase separation (PIPS) was first proposed by Inoue *et al.* in the 1980s.[109] At the PIPS, a precursor monomer (*e.g.*, alkyl methacrylates, epoxides) is polymerized in the presence of a modifier that is initially miscible, such as an oligomer, a

polymer, or a small molecule.[110] During the polymerization process, the miscibility between precursor monomer and pre-polymer decreases as the molar mass of the thermoset resin is growing. As a result a phase separation occurs and different types of morphologies arise. The respective morphologies strongly affect the final properties and applications of these materials are largely dependent on the thermodynamics of the phase separation.[111-116] The PIPS method was intensively studied on epoxy resins as a way to improve mechanical properties like the tensile strength[61, 117] or the tensile toughness[61] of polymer composites. Besides it is possible to enhance the fracture properties of polymeric thermosets by the PIPS. The addition of small amounts of rubber additives leads to an improvement of the fracture toughness, however, generally accompanied by a drop of the mechanical resistance (Young's modulus). In contrast the addition of thermoplastic polymers (*e.g.*, poly(ether imides), poly(phenylene oxides)) may result in an enhancement of the fracture properties, devoiding a loss in E-modulus.[64] The PIPS applied for methacrylates were only rarely studied. At the copolymerization of *bis*-methacrylates with alkyl methacrylates (*e.g.*, *Bis*GMA with LMA) a phase separation takes place.[65, 118] The PIPS of different poly(methacrylates) in TEGDMA[68] was investigated whereupon an increase in E-modulus was obtained in comparison to the reference material.[67] These examples are mainly focused on the investigation of the polymerization shrinkage. Detailed investigations about the effect of PIPS on the fracture toughness of methacrylate based composites have not been performed up to now to the best of my knowledge.

Therefore this study attempts towards the utilization of PIPS for an enhancement of fracture properties and E-modulus of methacrylate based polymer composites. For that purpose a bulk homopolymer matrix consisting of TEGDMA was modified with a PLMA pre-polymer. The heterogeneous mixture was subsequently photo-polymerized. Both the molar masses of the pre-polymers as well as the additive concentrations in the matrix were varied to investigate their effect on the phase separation process.

To ensure a sufficient toughening effect within the final composite, PLMA was chosen as pre-polymer as the T_g of the homopolymer with –65 °C is relatively low. To investigate various molar masses of PLMA pre-polymers on the PIPS, polymers with M_n values between 10,000 g/mol and 68,000 g/mol were synthesized using the RAFT polymerization procedure. The polymerization conditions as well as the characterization data of the resulting polymers are

summarized in **Table 5.3**. The absence of residual monomer was confirmed by ^{1}H NMR measurements (**Figure 5.2**).

Table 5.3 Characterization data of statistical PLMA prepolymers (**P20** to **P23**).

Polymer type	M_n[e] [g·mol^{-1}]	M_w[e] [g·mol^{-1}]	Conversion[f] [%]	Đ
P17[a]	11,000	13,000	49	1.10
P18[b]	25,000	28,000	51	1.12
P19[c]	33,000	45,000	77	1.08
P20[d]	68,000	74,000	85	1.34

a [LMA]$_{total}$:[CTA]:[AIBN] = 100:1:0.1 in bulk; T = 65 °C; t = 8 h;
b [LMA]$_{total}$:[CTA]:[AIBN] = 200:1:0.14 [M]$_{total}$ = 3.4 mol·L^{-1} in THF; T = 65 °C; t = 16 h;
c [LMA]$_{total}$:[CTA]:[AIBN] = 100:0.33:0.25. [M]$_{total}$ = 3.4 mol·L^{-1} in THF; T = 70 °C; t = 19 h;
d [LMA]$_{total}$:[CTA]:[AIBN] = 100:0.22:0.25. [M]$_{total}$ = 3.4 mol·L^{-1} in THF; T = 70 °C; t = 19 h;
f obtained from SEC ($CHCl_3$, RI detection, PMMA calibration);
g monomer conversions obtained gravimetrically.

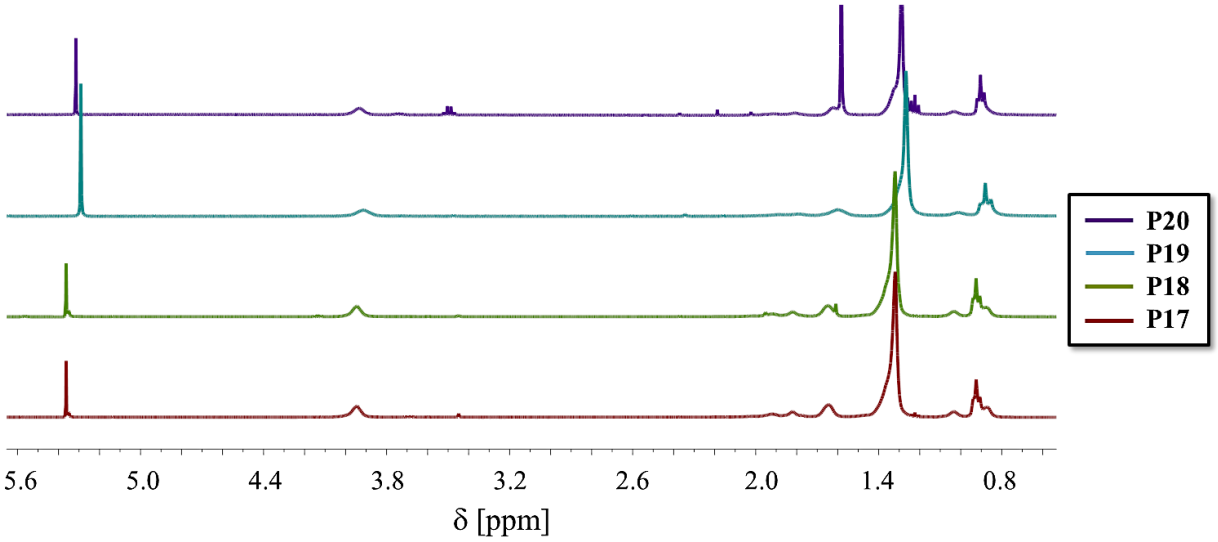

Figure 5.2 ^{1}H NMR spectra (400 MHz) of the PLMA homopolymers **P17** to **P20** in $CDCl_3$.

6. Summary

The interdisciplinary interplay of macromolecular chemistry, organic chemistry and supramolecular chemistry within this thesis enabled the development of a range of functional polymers ranging from self-healing materials to hard scaffold (biocompatible) polymers and up to polymer particles as toughness modifiers (**Scheme 6.1**).

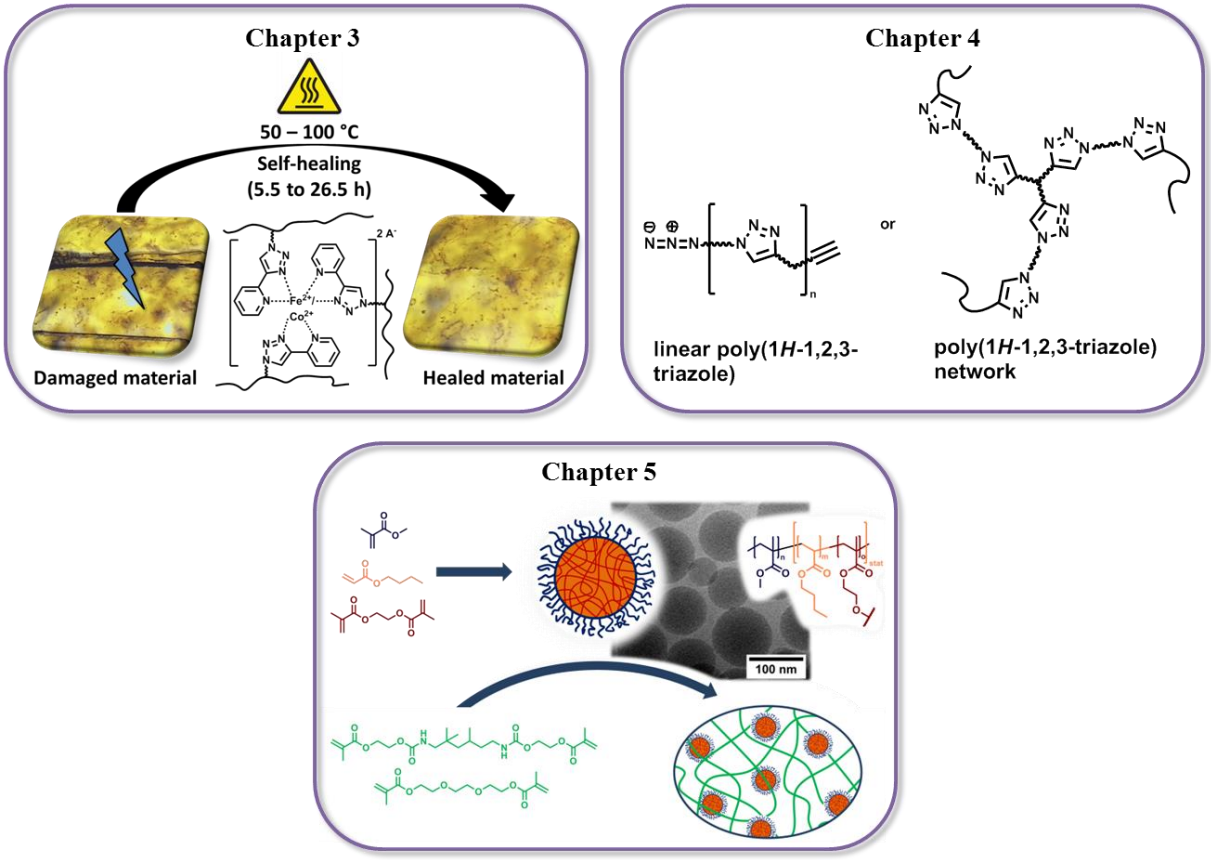

Scheme 6.1 Graphical overview of the content of **Chapters 3** to **5**.

Attaching triazole-pyridine ligands in the side chain of a PLMA based polymer and the subsequent complexation with appropriate iron(II), cobalt(II), copper(II) and manganese(II) metal salts enabled the fabrication of metallocopolymer networks. The appropriate interplay between glass transition temperature and complexation properties resulted in a utilization of this type of metallopolymer as a coating with self-healing properties by crosslinking with designated iron(II) and cobalt(II) salts ($FeCl_2$, $FeBr_2$, $Fe(OTf)_2$, $CoCl_2$, $CoBr_2$ and $Co(BF_4)_2$). The obtained materials showed pronounced self-healing performances within time intervals of

5.5 to 26.5 hours at moderate temperatures of 50 to 100 °C. The characterization of the metallopolymers by DSC, SAXS, UV-Vis spectroscopy and light microscopy provided insights into the interrelation of glass transition temperature, cluster size and complexation interplay of the metal center and the anions that represent the decisive factors for the self-healing abilities.

The regioselective copper(I)-catalyzed 1,3-dipolar cycloaddition between multifunctional azides and terminal alkynes (CuAAC) represents the key step for the preparation of thermosets within the scope of this thesis. In a DSC study, different copper(I) sources such as CuOAc, $Cu^{I}(TBTA)BF_4$, $Cu^{I}(CH_3CN)_4BF_4$, and $Cu^{I}(PPh_3)_3Br$ were evaluated under solvent-free conditions as catalysts. CuOAc was proven to be the most efficient one for the click-reaction. The molar masses (M_n) of the resulting linear poly(1H-1,2,3-triazoles) could be adjusted to 17,000 (DMF) and 166,000 g/mol (DMSO) by applying different polar solvents. Among the various combinations of alkynes and azides for the CuAAC, the polymerization of tripropargylamine with xylene and mesitylene *bis*azides as well as the combination of tripropargylamine and di(prop-2-yn-1-yl)isophorone-dicarbamate with 1,2-*bis*(2-azidoethoxy)ethane resulted in hard materials with elevated indentation moduli accessing these materials for potential biomedical applications. Besides the direct copper(I) catalysis of the CuAAC, it is possible to generate the required Cu(I) species by *in-situ* photo-reduction of Cu^{II} to Cu^{I}. Within this thesis, an evaluation of several copper(II) salts, facilitating a photo-induced polymerization, was performed. The photo-reduction of copper(II) acetate generating copper(I) ions without using any additional photo-initiator enabled the polymerization that can only be carried out in solution using at least 15 wt% of methanol. Depending on the catalyst concentration quantitative monomer conversions were achieved, allowing the determination of the elevated mechanical properties (1.6 GPa). Towards the biomedical application of CuAAC polymerized 1,2,3-polytriazoles, it is of great importance to substantially reduce the copper residues within the resulting polymer to avoid toxic effects. A convenient way to circumvent this issue represents the metal-free 1,3-dipolar cycloaddition of electron-poor alkynes. Within this dissertation, the synthesis of electron-deficient internal alkynes and, subsequently, the metal-free click-reaction with multifunctional alkynes under mild conditions coped the way for poly(1H-1,2,3-triazole) networks with interesting mechanical properties. The elevated E-moduli of 2.5 GPa and the absence of cytotoxic copper species paved the way of these

materials as potential biomaterials. Within the scope of the executed biomedical investigations, cell biological studies were performed on the alkyne and azide monomers as well as on the resulting polymers. The cell study on the click monomers clearly revealed a cytotoxic potential for all applied alkynes and azides, except the TEG-$(N_3)_2$ that turned out to be cytocompatible at all investigated concentrations. Additional investigations on the final poly(1H-1,2,3-triazole) networks showed a highly biocompatible character of the materials in its bulk format. Cells grown elevations on the scaffolds revealed various growth densities of L929 fibroplasts confirming the biocompatible character of the represented poly(1H-1,2,3-triazole) networks.

The application of polymer composites as advanced materials is restricted due to their limited mechanical properties *i.e.* the fracture toughness. Several modifiers like hyperbranched polymers[57-58] or fibers[59] overcome that limitation and lead to an increase in fracture toughness however mostly at cost of the mechanical resistance (E-modulus). Within the scope of this thesis core-shell particles consisting of an EGDMA crosslinked soft PBA core and a hard PMMA shell that was crosslinked in some cases with TEGDMA. The obtained polymer particles were analyzed (particle size, morphology and distribution) by means of DLS, AUC and cryo-TEM investigations as they represent established characterization methods for polymer nanoparticles. The incorporation of the lattices into a TEGDMA/UDMA matrix and subsequently photo-polymerization of the monomer mixture caused an enhancement of fracture toughness and E-modulus of the resulting thermosets in comparison to the reference material. Therefore this study represents the first report about the improvement of fracture toughness and E-modulus (within the same time) of polymer composites.

Beside the core-shell particles, the polymerization induced-phase separation represents an additional promising technique to improve the fracture- and resistance properties of polymer composites, as a soft, toughening phase can be generated within this polymerization method.[67] Within this thesis PLMA pre-polymers with different molar masses were synthesized. The pre-polymers were embedded into a TEGDMA monomer matrix and subsequent photo-polymerized. While polymerization, a second, PLMA rich phase arises resulting in an increased toughening of the resulting composite.

Within this thesis various structural modified polymers were synthesized and characterized. Thereby their potential field of applications as self-healing metallopolymers, (biocompatible) hard tissue materials and toughener for methacrylate based composites was proven. The results described in this thesis represent an important contribution to the chemical understanding of structure-property relationships of polymeric materials and their material properties. Thus, the presented compounds within this thesis might be promising materials for a potential future application as self-healing polymeric coating-system and mechanically tunable polymer composites.

7. Zusammenfassung

Im Rahmen dieser Dissertation konnten durch die interdisziplinäre Interaktion von makromolekularer-, organischer- und supramolekularer Chemie, selbstheilende (Metallo-) Polymere, biokompatible Hartgewebematerialien und Kern-Schale Nanopartikel als Zähigkeitsvermittler hergestellt werden.

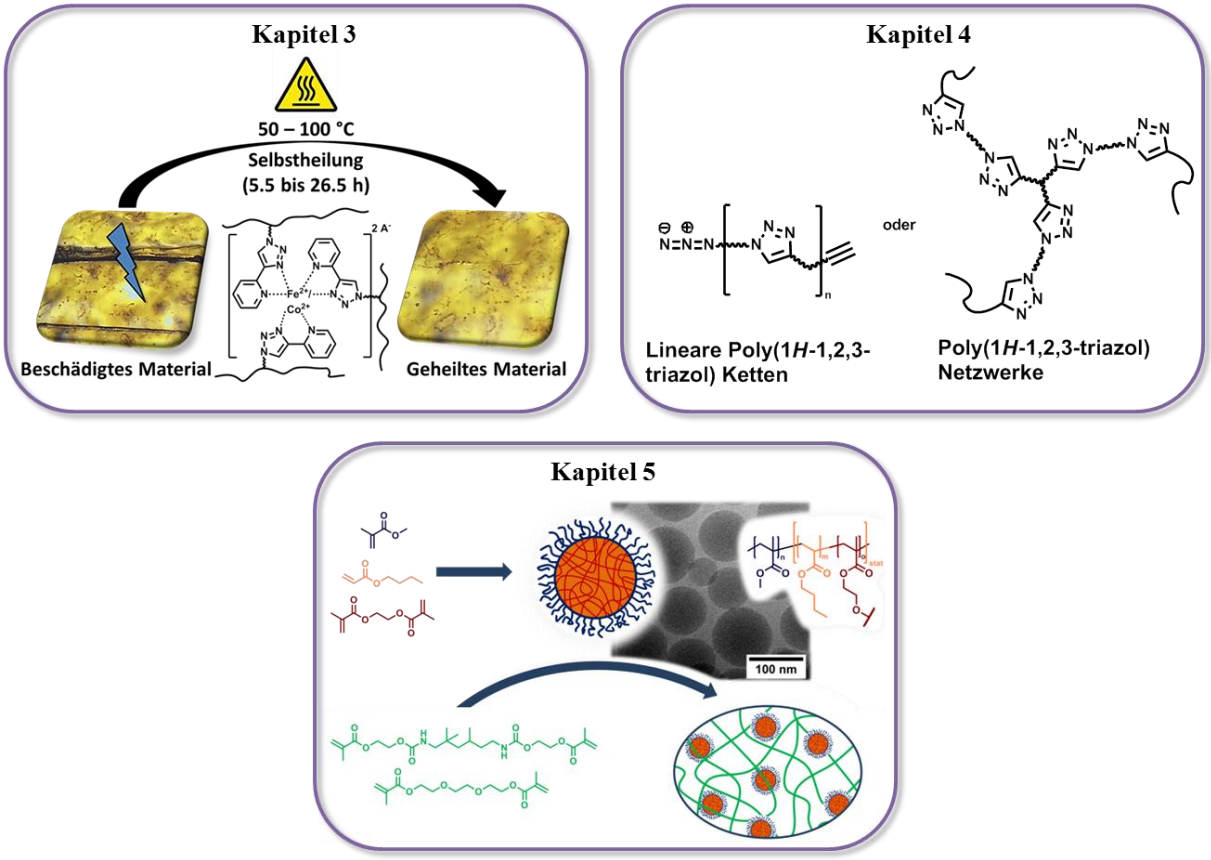

Scheme 7.1 Grafische Zusammenfassung der Inhalte aus den **Kapiteln 3** bis **5**.

Im Rahmen dieser Arbeit wurde ein zweizähniger, methacrylat-funktionalisierter Triazolpyridin-Ligand mit Laurylmethacrylat copolymerisiert. Durch die anschließende Zugabe von geeigneten Eisen(II)-, Kobalt(II)-, Kupfer(II)- und Mangan(II)-Salzen konnten Metallopolymer-Netzwerke aufgebaut werden. Die Abstimmung von Glasübergangstemperatur und Komplexierungseigenschaften ermöglichte es, diese Metallopolymer-Typen durch Vernetzen mit geeigneten Eisen(II)- und Kobalt(II)-Salzen ($FeCl_2$, $FeBr_2$, $Fe(OTf)_2$, $CoCl_2$, $CoBr_2$ und $Co(BF_4)_2$) als Beschichtungen mit Selbstheilungseigenschaften nutzbar zu machen. Diese Materialien zeigten ein ausgeprägtes

Selbstheilungsverhalten innerhalb von 5,5 bis 26,5 Stunden bei milden Temperaturen von 50 bis 100 °C. Die Charakterisierung der Metallopolymere durch dynamische Differenzkalorimetrie, Röntgenbeugung, UV-Vis Spektroskopie und Lichtmikroskopie geben dabei einen Einblick in die Wechselbeziehung von Glastemperatur, Clustergröße und Komplexierungsverhalten von Metallzentrum und Gegenionen, welche die ausschlaggebenden Faktoren für die Selbstheilung dieses Systems darstellen. Um ein besseres Verständnis für den Heilungsmechanismus dieses Systems zu bekommen, wird im Fokus zukünftiger Forschung die Untersuchung von mechanischen Eigenschaften und mechanistische Studien, welche die Selbstheilung beeinflussten, stehen.

Die regioselektive Kupfer(I)-katalysierte 1,3-dipolare Cycloaddition zwischen multifunktionellen Aziden und terminalen Alkinen (CuAAC) stellt im Rahmen dieser Arbeit den entscheidenden Schritt für die Herstellung von duroplastischen Werkstoffen dar. In einer DSC Studie konnten verschiedene Kupfer(I)-Salze wie $Cu^{I}OAc$, $Cu^{I}(TBTA)BF_4$, $Cu^{I}(CH_3CN)_4BF_4$ und $Cu^{I}(PPh_3)_3Br$ auf ihre Eigenschaften hin, die CuAAC zu katalysieren, in lösemittelfreier Umgebung untersucht werden. Dabei hat sich CuOAc als effizientester Katalysator für diese Click-Reaktion erwiesen. Die molaren Massen (M_n) der linearen 1,2,3-Polytriazole konnten durch die Wahl von unterschiedlich polaren Lösungsmitteln auf 17.000 g/mol (DMF) und 166.000 g/mol (DSMO) eingestellt werden. Innerhalb der verschiedenen Kombinationen von Alkinen und Aziden für die CuAAC führte die Kombination von Tripropargylamin mit Xylen- und Mesitylen-*Bis*aziden als auch die Verknüpfung von Tripropargylamin, Di(prop-2-yn-1-yl)isophoron-dicarbamat mit 1,2-*Bis*(2-azidoethoxy)ethan zu polymeren Materialien mit harten mechanischen Eigenschaften. Die erhöhten E-Moduli dieser Polymere ermöglichen dabei deren Verwendung als potentielle biomedizinische Materialien. Neben der direkten Kupfer(I)-Katalyse ist es möglich, die für die CuAAC benötigte Kupfer(I)-Spezies durch *in-situ* Reduktion von Cu^{II} zu Cu^{I} zu generieren. Im Rahmen dieser Arbeit wurden verschiedene Kupfer(II)-Salze hinsichtlich ihrer Eigenschaft, eine photoinduzierte Kupfer(I)-katalysierte Click-Reaktion zu ermöglichen, untersucht. Durch die Photoreduktion von $Cu(OAc)_2$ in einer Lösung aus 15 Gewichts% MeOH konnten Cu^{I}-Ionen generiert werden, welche die Polyadditionsreaktion ermöglicht hat. Abhängig von der Katalysatorkonzentration konnten quantitative Monomerumsätze und erhöhte mechanische Festigkeiten (1,6 GPa) erzielt werden. Im Hinblick auf die biomedizinische Verwendung von

1,2,3-Polytriazolverbindungen, welche durch die CuAAC hergestellt werden ist es von entscheidender Wichtigkeit, die Kupferrückstände im auspolymerisierten Material auf ein Minimum zu reduzieren. Die metallfreie 1,3-dipolare Cycloaddition von elektronenarmen Alkinen stellt dabei eine geeignete Methode dar, dieses Problem zu umgehen. Im Rahmen dieser Arbeit wurden elektronenarme interne Alkine synthetisiert, welche anschließend in einer katalysatorfreien Click-Reaktion mit multifunktionalen Aziden umgesetzt wurden. Durch diese Reaktion konnten Polytriazol-Netzwerke aufgebaut werden, die erhöhte E-Moduli (2,5 GPa) aufwiesen, was sie zusätzlich als metallfreie Systeme besonders interessant für biomedizinische Anwendungen macht. Im Rahmen von biomedizinischen Untersuchungen wurden zellbiologische Studien sowohl an den Ausgangsverbindungen für die Click-Reaktion (Alkine und Azide) als auch an den entsprechenden Polymeren durchgeführt. Die Zellstudie der Click-Monomere zeigte ein deutlich zytotoxisches Verhalten für alle untersuchten Verbindungen auf. Nur TEG-$(N_3)_2$ war bei allen untersuchten Konzentrationen zytokompatibel. Bei den korrespondierenden Polymernetzwerken konnte ein durchweg zytokompatibles Verhalten der Materialien nachgewiesen werden. Anhand von Zellwachstumsstudien wurde durch mannigfaltige Wachstumsdichten von L929 Fibroplasten auf den Polymeren der biokompatible Charakter dieser Werkstoffe bestätigt.

Die Verwendung von Polymerkompositen als hochentwickelte Werkstoffe ist beschränkt durch ihre limitierten mechanischen Eigenschaften, wie der Bruchzähigkeit. Diverse Additive wie hyperverzweigte Polymere[57-58] oder Fasern[59] lösen diese Maßgabe und führen zu einer Steigerung der Bruchzähigkeit. Jedoch geschieht dies meistens auf Kosten der mechanischen Festigkeit (E-Modul). Im Rahmen dieser Arbeit wurden polymere Kern-Schale-Partikel, bestehend aus einem EGDMA vernetzten weichen PBA-Kern und einer harten PMMA-Schale (in einigen Fällen mit TEGDMA zusätzlich vernetzt), synthetisiert. Die Charakterisierung der Polymerpartikel (Partikelgröße, Morphologie und Verteilung) erfolgte dabei mittels DLS, AUC und cryo-TEM, welche etablierte Charakterisierungsmethoden für Polymernanopartikel darstellen. Dabei wurden die Kern-Schale Partikel in eine TEGDMA/UDMA Matrix eingebettet und anschließend photo-polymerisiert. Das resultierende duroplastische Material wies dabei im Vergleich zu dem ungefüllten Referenzmaterial eine verbesserte Bruchzähigkeit und mechanische Festigkeit (E-Modul) auf. Diese Ergebnisse repräsentieren den ersten

wissenschaftlichen Bericht für eine gleichzeitige Verbesserung von Bruchzähigkeit und E-Modul in Polymerkompositen.

Neben den Kern-Schale-Partikeln stellt die polymerisationsinduzierte Phasenseparation eine weitere vielversprechende Methode dar, gezielt die Brucheigenschaft und Festigkeit von Polymerkompositen durch die Bildung einer weichen, zähigkeitssteigernden Phase innerhalb dieser Polymerisationstechnik, zu verbessern.[67] Im Rahmen dieser Arbeit wurden PLMA Präpolymere mit unterschiedlichen Molmassen hergestellt. Dabei wurden die Präpolymere in eine TEGDMA Matrix eingebettet und anschließend photo-polymerisiert. Während der Polymerisation bildete sich eine zweite PLMA-reiche Phase, die innerhalb des Komposites zu einer Zähigkeitssteigerung führt.

Im Rahmen dieser Arbeit konnten verschiedene, strukturell abgestimmte Polymere hergestellt und charakterisiert werden. Dabei konnte deren Einsatzmöglichkeit als selbstheilende Metallopolymere, (biokompatible) Hartgewebematerialien und Kern-Schale Nanopartikel als Zähigkeitsvermittler für methacrylat-basierte Komposite, belegt werden. Die Ergebnisse dieser Arbeit leisten einen wichtigen Beitrag zum chemischen Verständnis der Struktur-Eigenschafts-Beziehung polymerer Werkstoffe und deren Materialeigenschaften. Die innerhalb dieser Arbeit neu dargestellten Verbindungen stellen somit vielversprechende Materialien für zukünftige Anwendungen im Bereich selbstheilender polymerer Beschichtungssysteme und mechanisch modifizierbarer Polymerkomposite, dar.

8. References

[1] www.plasticseurope.org [last accessed 6/2/2015]
[2] D. Y. Wu, S. Meure, D. Solomon, *Prog. Polym. Sci.* **2008**, *33*, 479-522.
[3] K. Jud, H. H. Kausch, J. G. Williams, *J. Mater. Sci.* **1981**, *16*, 204-210.
[4] C. M. Dry, N. R. Sottos, in *Proc. Recent Advances in Adaptive and Sensory Materials and their Applications*, Technomic, Virginia, **1992**, pp. 438-444.
[5] S. R. White, N. R. Sottos, P. H. Geubelle, J. S. Moore, M. R. Kessler, S. R. Sriram, E. N. Brown, S. Viswanathan, *Nature* **2001**, *409*, 794-797.
[6] A. J. M. Schmets, S. Van der Zwaag, in *First International Conference on Self Healing Materials, Vol. 100*, Springer, Noordwijk, Netherlands, **2007**.
[7] B. J. Blaiszik, S. L. B. Kramer, S. C. Olugebefola, J. S. Moore, N. R. Sottos, S. R. White, *Annu. Rev. Mater. Res.* **2010**, *40*, 179-211.
[8] E. B. Murphy, F. Wudl, *Prog. Polym. Sci.* **2010**, *35*, 223-251.
[9] J. A. Syrett, C. R. Becer, D. M. Haddleton, *Polym. Chem.* **2010**, *1*, 978-987.
[10] S. Burattini, B. W. Greenland, D. Chappell, H. M. Colquhoun, W. Hayes, *Chem. Soc. Rev.* **2010**, *39*, 1973-1985.
[11] F. Herbst, D. Dohler, P. Michael, W. H. Binder, *Macromol. Rapid Commun.* **2013**, *34*, 203-220.
[12] S. J. Kalista, *Mech. Adv. Mater. Struc.* **2007**, *14*, 391-397.
[13] S. Burattini, H. M. Colquhoun, J. D. Fox, D. Friedmann, B. W. Greenland, P. J. F. Harris, W. Hayes, M. E. Mackay, S. J. Rowan, *Chem. Commun.* **2009**, 6717-6719.
[14] G. M. L. van Gemert, J. W. Peeters, S. H. M. Sontjens, H. M. Janssen, A. W. Bosman, *Macromol. Chem. Phys.* **2012**, *213*, 234-242.
[15] P. Cordier, F. Tournilhac, C. Soulie-Ziakovic, L. Leibler, *Nature* **2008**, *451*, 977-980.
[16] Z. H. Wang, M. W. Urban, *Polym. Chem.* **2013**, *4*, 4897-4901.
[17] J. C. Yuan, X. L. Fang, L. X. Zhang, G. N. Hong, Y. J. Lin, Q. F. Zheng, Y. Z. Xu, Y. H. Ruan, W. G. Weng, H. P. Xia, G. H. Chen, *J. Mater. Chem.* **2012**, *22*, 11515-11522.
[18] B. Sandmann, S. Bode, M. D. Hager, U. S. Schubert, in *Hierarchical Macromolecular Structures: 60 Years after the Staudinger Nobel Prize Ii, Vol. 262* (Ed.: V. Percec), **2013**, pp. 239-257.
[19] G. R. Whittell, M. D. Hager, U. S. Schubert, I. Manners, *Nat. Mater.* **2011**, *10*, 176-188.
[20] F. Peng, G. Z. Li, X. X. Liu, S. Z. Wu, Z. Tong, *J. Am. Chem. Soc.* **2008**, *130*, 16166-16167.
[21] G. C. Zhou, I. I. Harruna, C. W. Ingram, *Polymer* **2005**, *46*, 10672-10677.
[22] R. P. Wool, *Soft Matter* **2008**, *4*, 400-418.
[23] F. Wang, J. Q. Zhang, X. Ding, S. Y. Dong, M. Liu, B. Zheng, S. J. Li, L. Wu, Y. H. Yu, H. W. Gibson, F. H. Huang, *Angew. Chem. Int. Ed.* **2010**, *49*, 1090-1094.
[24] M. I. Shtilman, in *New Concepts in Polymer Science* Taylor & Francis Ltd., Zeist, The Netherlands, **2003**, p. 294.
[25] E. Tamariz, A. Rios-Ramírez, *Biodegradation of Medical Purpose Polymeric Materials and Their Impact on Biocompatibility*, **2013**.
[26] P. Gunatillake, R. Mayadunne, R. Adhikari, *Biotechnol. Annu. Rev.* **2006**, *12*, 301-347.
[27] M. N. Helmus, D. F. Gibbons, D. Cebon, *Toxicol. Pathol.* **2008**, *36*, 70-80.
[28] M. A. Tasdelen, *Polym. Chem.* **2011**, *2*, 2133-2145.

[29] A. B. Lowe, *Polym. Chem.* **2010**, *1*, 17-36.
[30] M. Meldal, *Macromol. Rapid Commun.* **2008**, *29*, 1016-1051.
[31] C. R. Becer, R. Hoogenboom, U. S. Schubert, *Angew. Chem. Int. Ed.* **2009**, *48*, 4900-4908.
[32] M. Meldal, C. W. Tornoe, *Chem. Rev.* **2008**, *108*, 2952-3015.
[33] W. H. Binder, R. Sachsenhofer, *Macromol. Rapid Commun.* **2008**, *29*, 952-981.
[34] H. Nandivada, X. W. Jiang, J. Lahann, *Adv. Mater.* **2007**, *19*, 2197-2208.
[35] J. E. Moses, A. D. Moorhouse, *Chem. Soc. Rev.* **2007**, *36*, 1249-1262.
[36] K. Kempe, A. Krieg, C. R. Becer, U. S. Schubert, *Chem. Soc. Rev.* **2012**, *41*, 176-191.
[37] H. C. Kolb, K. B. Sharpless, *Drug Discov. Today* **2003**, *8*, 1128-1137.
[38] B. Sandmann, B. Happ, M. D. Hager, J. Vitz, E. Rettler, P. Burtscher, N. Moszner, U. S. Schubert, *J. Polym. Sci., Part A: Polym. Chem.* **2014**, *52*, 239-247.
[39] L. Q. Wan, J. J. Tian, J. Z. Huang, Y. H. Hu, F. R. Huang, L. Du, *J. Appl. Polym. Sci.* **2007**, *106*, 2111-2116.
[40] Q. Wei, H. Q. Deng, Y. B. Cai, J. W. Y. Lam, J. Li, J. Z. Sun, M. Gao, A. J. Qin, B. Z. Tang, *Macromol. Rapid Commun.* **2012**, *33*, 1356-1361.
[41] H. K. Li, J. Mei, J. A. Wang, S. A. Zhang, Q. L. Zhao, Q. A. Wei, A. J. Qin, J. Z. Sun, B. Z. Tang, *Sci. China Chem.* **2011**, *54*, 611-616.
[42] J. J. Tian, X. F. Wang, L. Q. Wan, Y. H. Hu, F. R. Huang, *High Perform. Polym.* **2010**, *22*, 198-212.
[43] A. J. Qin, L. Tang, J. W. Y. Lam, C. K. W. Jim, Y. Yu, H. Zhao, J. Z. Sun, B. Z. Tang, *Adv. Funct. Mater.* **2009**, *19*, 1891-1900.
[44] A. R. Katritzky, N. K. Meher, S. Hanci, R. Gyanda, S. R. Tala, S. Mathai, R. S. Duran, S. Bernard, F. Sabri, S. K. Singh, J. Doskocz, D. A. Ciaramitaro, *J. Polym. Sci., Part A: Polym. Chem.* **2008**, *46*, 238-256.
[45] L. Wang, Y. M. Song, R. Gyanda, R. Sakhuja, N. K. Meher, S. Hanci, K. Gyanda, S. Mathai, F. Sabri, D. A. Ciaramitaro, C. D. Bedford, A. R. Katritzky, R. S. Duran, *J. Appl. Polym. Sci.* **2010**, *117*, 2612-2621.
[46] J. J. Tian, L. Q. Wan, J. Z. Huang, Y. H. Hu, F. R. Huang, L. Du, *Polym. Bull.* **2008**, *60*, 457-465.
[47] L. Q. Wan, Y. H. Luo, L. Xue, J. J. Tian, Y. H. Hu, H. M. Qi, X. N. Shen, F. R. Huang, L. Du, X. B. Chen, *J. Appl. Polym. Sci.* **2007**, *104*, 1038-1042.
[48] Q. Wei, J. Wang, X. Y. Shen, X. A. Zhang, J. Z. Sun, A. J. Qin, B. Z. Tang, *Sci. Rep.-Uk* **2013**, *3*.
[49] Y. J. Li, H. Zhou, Y. P. E, L. Q. Wan, F. R. Huang, L. Du, *Des. Monomers Polym.* **2013**, *16*, 556-563.
[50] L. W. Wan, J. J. Tian, J. H. Huang, Y. H. Hu, F. R. Huang, L. Du, *J. Macromol. Sci., Part A: Pure Appl. Chem.* **2007**, *44*, 175-181.
[51] J. Tian, L. Wan, J. Huang, Y. Hu, F. Huang, L. Du, *Polym. Adv. Technol.* **2007**, *18*, 556-561.
[52] A. R. Katritzky, R. Sakhuja, L. C. Huang, R. Gyanda, L. Wang, D. C. Jackson, D. A. Ciaramitaro, C. D. Bedford, R. S. Duran, *J. Appl. Polym. Sci.* **2010**, *118*, 121-127.
[53] Q. Wei, H. Deng, Y. Cai, J. W. Lam, J. Li, J. Sun, M. Gao, A. Qin, B. Z. Tang, *Macromol. Rapid Commun.* **2012**, *33*, 1356-1361.
[54] S. T. Abu-Orabi, R. Al-Hamdany, A. Atfah, A. A. S. Ali, K. Abu-Shandi, *Asian J. Chem.* **1999**, *11*, 774-783.
[55] H. C. Kolb, M. G. Finn, K. B. Sharpless, *Angew. Chem. Int. Ed.* **2001**, *40*, 2004-2021.

[56] W. A. Hanna, F. E. Gharib, I. I. Marhoon, *JMMCE* **2011**, 1167-1178.
[57] L. Boogh, B. Pettersson, J. A. E. Manson, *Polymer* **1999**, *40*, 2249-2261.
[58] J. Verrey, Y. Winkler, V. Michaud, J. A. E. Manson, *Compos. Sci. Technol.* **2005**, *65*, 1527-1536.
[59] D. M. Laura, H. Keskkula, J. W. Barlow, D. R. Paul, *Polymer* **2000**, *41*, 7165-7174.
[60] A. Gutierrez-Mejia, W. Herrera-Kao, S. Duarte-Aranda, M. I. Loria-Bastarrachea, G. Canche-Escamilla, F. J. Moscoso-Sanchez, J. V. Cauich-Rodriguez, J. M. Cervantes-Uc, *Mater. Sci. Eng. C Mater. Biol. Appl.* **2013**, *33*, 1737-1743.
[61] S. K. Siddhamalli, T. Kyu, *J. Appl. Polym. Sci.* **2000**, *77*, 1257-1268.
[62] Y. F. Yu, M. H. Wang, W. J. Gan, Q. S. Tao, S. J. Li, *J. Phys. Chem. B* **2004**, *108*, 6208-6215.
[63] M. H. Wang, Y. F. Yu, X. G. Wu, S. J. Li, *Polymer* **2004**, *45*, 1253-1259.
[64] R. J. Williams, B. Rozenberg, J.-P. Pascault, in *Polymer Analysis Polymer Physics*, *Vol. 128*, Springer Berlin Heidelberg, **1997**, pp. 95-156.
[65] C. S. Pfeifer, Z. R. Shelton, C. R. Szczpanski, M. D. Barros, N. D. Wilson, J. W. Stansbury, *J. Polym. Sci., Part A: Polym. Chem.* **2014**, *52*, 1796-1806.
[66] J. Stansbury, C. S. Pfeifer, *Abstr. Pap. Am. Chem. S.* **2009**, *237*.
[67] C. R. Szczepanski, J. W. Stansbury, *J. Appl. Polym. Sci.* **2014**, *131*.
[68] C. R. Szczepanski, C. S. Pfeifer, J. W. Stansbury, *Polymer* **2012**, *53*, 4694-4701.
[69] E. Vaccaro, J. H. Waite, *Biomacromolecules* **2001**, *2*, 906-911.
[70] M. J. Harrington, A. Masic, N. Holten-Andersen, J. H. Waite, P. Fratzl, *Science* **2010**, *328*, 216-220.
[71] N. Holten-Andersen, M. J. Harrington, H. Birkedal, B. P. Lee, P. B. Messersmith, K. Y. C. Lee, J. H. Waite, *Proc. Natl. Acad. Sci. U. S. A.* **2011**, *108*, 2651-2655.
[72] D. G. Barrett, D. E. Fullenkamp, L. H. He, N. Holten-Andersen, K. Y. C. Lee, P. B. Messersmith, *Adv. Funct. Mater.* **2013**, *23*, 1111-1119.
[73] M. J. Harrington, J. H. Waite, *Biomacromolecules* **2008**, *9*, 1480-1486.
[74] M. J. Harrington, H. S. Gupta, P. Fratzl, J. H. Waite, *J. Struct. Biol.* **2009**, *167*, 47-54.
[75] M. J. Harrington, J. H. Waite, *Adv. Mater.* **2009**, *21*, 440-444.
[76] H. Ceylan, M. Urel, T. S. Erkal, A. B. Tekinay, A. Dana, M. O. Guler, *Adv. Funct. Mater.* **2013**, *23*, 2081-2090.
[77] M. Krogsgaard, M. A. Behrens, J. S. Pedersen, H. Birkedal, *Biomacromolecules* **2013**, *14*, 297-301.
[78] J. H. Waite, X. X. Qin, K. J. Coyne, *Matrix Biol.* **1998**, *17*, 93-106.
[79] E. Carrington, J. M. Gosline, *Am. Malacol. Bull.* **2004**, *18*, 135-142.
[80] J. H. Waite, H. C. Lichtenegger, G. D. Stucky, P. Hansma, *Biochemistry* **2004**, *43*, 7653-7662.
[81] J. H. Waite, C. C. Broomell, *J. Exp. Biol.* **2012**, *215*, 873-883.
[82] S. Krauss, T. H. Metzger, P. Fratzl, M. J. Harrington, *Biomacromolecules* **2013**, *14*, 1520-1528.
[83] D. E. Fullenkamp, L. H. He, D. G. Barrett, W. R. Burghardt, P. B. Messersmith, *Macromolecules* **2013**, *46*, 1167-1174.
[84] S. Varghese, A. Lele, R. Mashelkar, *J. Polym. Sci., Part A: Polym. Chem.* **2006**, *44*, 666-670.
[85] P. Terech, M. H. Yan, M. Marechal, G. Royal, J. Galvez, S. K. P. Velu, *Phys. Chem. Chem. Phys.* **2013**, *15*, 7338-7344.

[86] M. Burnworth, L. M. Tang, J. R. Kumpfer, A. J. Duncan, F. L. Beyer, G. L. Fiore, S. J. Rowan, C. Weder, *Nature* **2011**, *472*, 334-337.
[87] S. Bode, L. Zedler, F. H. Schacher, B. Dietzek, M. Schmitt, J. Popp, M. D. Hager, U. S. Schubert, *Adv. Mater.* **2013**, *25*, 1634-1638.
[88] B. G. G. Lohmeijer, U. S. Schubert, *Macromol. Chem. Phys.* **2003**, *204*, 1072-1078.
[89] J. F. Gohy, B. G. G. Lohmeijer, U. S. Schubert, *Macromolecules* **2002**, *35*, 4560-4563.
[90] J. F. Gohy, B. G. G. Lohmeijer, U. S. Schubert, *Macromol. Rapid Commun.* **2002**, *23*, 555-560.
[91] J. F. Gohy, B. G. G. Lohmeijer, S. K. Varshney, B. Decamps, E. Leroy, S. Boileau, U. S. Schubert, *Macromolecules* **2002**, *35*, 9748-9755.
[92] B. Happ, G. M. Pavlov, I. Perevyazko, M. D. Hager, A. Winter, U. S. Schubert, *Macromol. Chem. Phys.* **2012**, *213*, 1339-1348.
[93] S. Bode, R. K. Bose, S. Matthes, M. Ehrhardt, A. Seifert, F. H. Schacher, R. M. Paulus, S. Stumpf, B. Sandmann, J. Vitz, A. Winter, S. Hoeppener, S. J. Garcia, S. Spange, S. van der Zwaag, M. D. Hager, U. S. Schubert, *Polym. Chem.* **2013**, *4*, 4966-4973.
[94] B. Sandmann, B. Happ, S. Kupfer, F. H. Schacher, M. D. Hager, U. S. Schubert, *Macromol. Rapid Commun.* **2014**, *36*, 604-609.
[95] X. Sheng, T. C. Mauldin, M. R. Kessler, *J. Polym. Sci., Part A: Polym. Chem.* **2010**, *48*, 4093-4102.
[96] Y. L. Chow, G. E. Buonocore, *Can. J. Chem.* **1983**, *61*, 795-800.
[97] Y. L. Chow, G. E. Buonocore, B. Marciniak, C. Beddard, *Can. J. Chem.* **1983**, *61*, 801-808.
[98] G. E. BuonoCore, A. H. Klahn, C. Bahamondes, F. Aros, M. Tejos, V. Astorga, *Inorg. Chim. Acta* **1997**, *257*, 241-245.
[99] B. Sandmann, B. Happ, J. Vitz, R. M. Paulus, M. D. Hager, P. Burtscher, N. Moszner, U. S. Schubert, *Macromol. Chem. Phys.* **2014**, *215*, 1603-1608.
[100] T. Ishikawa, B.-L. Zhu, H. Maeda, *Toxicol. Ind. Health* **2006**, *22*, 337-341.
[101] L. Tauhardt, K. Kempe, M. Gottschaldt, U. S. Schubert, *Chem. Soc. Rev.* **2013**, *42*, 7998-8011.
[102] J. Mahesh Kumar, M. M. Idris, G. Srinivas, P. Vinay Kumar, V. Meghah, M. Kavitha, C. R. Reddy, P. S. Mainkar, B. Pal, S. Chandrasekar, N. Nagesh, *PLoS One* **2013**, *8*, e70798.
[103] C. Hein, X.-M. Liu, D. Wang, *Pharm. Res.* **2008**, *25*, 2216-2230.
[104] N. Kaval, D. Ermolat'ev, P. Appukkuttan, W. Dehaen, C. O. Kappe, E. Van der Eycken, *J. Com. Chem.* **2005**, *7*, 490-502.
[105] V. D. Bock, H. Hiemstra, J. H. van Maarseveen, *Eur. J. Org. Chem.* **2006**, *2006*, 51-68.
[106] Y. C. Chen, V. Dimonie, M. S. Elasser, *Macromolecules* **1991**, *24*, 3779-3787.
[107] T. Matsumoto, M. Okubo, S. Shibao, *Kobunshi Ronbunshu* **1976**, *33*, 575-583.
[108] C. S. Chern, *Prog. Polym. Sci.* **2006**, *31*, 443-486.
[109] K. Yamanaka, Y. Takagi, T. Inoue, *Polymer* **1989**, *30*, 1839-1884.
[110] M. Rico, J. Lopez, B. Montero, R. Bouza, F. J. Diez, *Eur. Polym. J.* **2014**, *58*, 125-134.
[111] J. Lopez, C. Ramirez, M. J. Abad, L. Barral, J. Cano, F. J. Diez, *J. Appl. Polym. Sci.* **2002**, *85*, 1277-1286.
[112] I. A. Zucchi, M. J. Galante, R. J. J. Williams, *Polymer* **2005**, *46*, 2603-2609.

[113] M. G. Prolongo, C. Arribas, C. Salom, R. M. Masegosa, *J. Therm. Anal. Calorim.* **2007**, *87*, 33-39.
[114] W. F. Schroeder, J. Borrajo, M. I. Aranguren, *J. Appl. Polym. Sci.* **2007**, *106*, 4007-4017.
[115] H. E. Romeo, A. Vilchez, J. Esquena, C. E. Hoppe, R. J. J. Williams, *Eur. Polym. J.* **2012**, *48*, 1101-1109.
[116] Y. H. Liu, *J. Appl. Polym. Sci.* **2013**, *127*, 3279-3292.
[117] Z. N. Hu, J. Zhang, H. P. Wang, T. Li, Z. Y. Liu, Y. F. Yu, *Rsc Adv.* **2014**, *4*, 34927-34937.
[118] C. S. Pfeifer, J. W. Stansbury, in *Polym. Prepr. (Am. Chem. Soc., Div. Polym. Chem.), Vol. 50*, **2009**, pp. 393-394.

List of abbreviations

A6ACA	Acryloyl-6-amino caproic acid
AIBN	Azo-*bis*-(*iso*-butyronitril)
ATR-IR	Attenuated total reflection infrared
ATR-FT-IR	Attenuated total reflection Fourier transform infrared
AUC	Analytical ultracentrifugation
BisGMA	Bisphenol A glycidyl methacrylate
BMA	Butyl methacrylate
Cryo-TEM	Cryogenic-transmission electron microscopy
CTA	Chain transfer agent
CuAAC	Copper(I)-catalyzed azide–alkyne cycloaddition
d	Diameter
Đ	Dispersity
DFT	Density functional theory
Dopa	3,4-Dihydroxyphenylalanine
DLS	Dynamic light scattering
DMF	Dimethyl formamide
DMSO	Dimethyl sulfoxide
DP	Degree of polymerization
DSC	Differential scanning calorimetry
DSI	Depth sensing indentation
EGDMA	Ethylene glycol dimethacrylate
FDA	Fluorescein diacetate
K_{1c}	Stress intensity factor
LMA	Lauryl methacrylate
MMA	Methyl methacrylate
M_n	Number average molar mass
NMR	Nuclear magnetic resonance
PBA	Poly(butyl acrylate)
PEG	Poly(ethylene glycol)

PI	Propidium iodide
PIPS	Polymerization-induced phase separation
PLMA	Poly(lauryl methacrylate)
PMMA	Poly(methyl methacrylate)
RAFT	Reversible addition-fragmentation chain transfer
SAXS	Small-angle X-ray scattering
SD	Standard deviation
SEC	Size exclusion chromatography
SH	Self-healing
SWAXS	Small/wide-angle X-ray scattering
TBTA	*Tris*(benzyl triazolylmethyl)amine
TEG	Triethylene glycol
TEGDMA	Triethylene glycol dimethacrylate
TEM	Transmission electron microscopy
T_g	Glass transition temperature
TGA	Thermogravimetric analysis
THF	Tetrahydrofuran
TMEDA	Tetramethyl ethylene diamine
TRZ-py	Triazole-pyridine
UDMA	Urethane dimethacrylate
UV-vis	Ultra-violet and visible

Curriculum vitae

14.07.1985	Born in Straubing, Germany
1991 – 2005	School education
12/2005 – 02/2006	Practical internship at Thyssen Polymer, Bogen, Germany Department of incoming raw material inspection, and quality control
03/2006 – 09/2007	Study of Chemistry, University of Applied Science Aalen, Germany
02/2008	Practical internship at the Wacker Chemie AG, Burghausen, Germany; Department of Process Analytics
02/2010 – 07/2010	Research internship at Victoria University Wellington, New Zealand **Topic:** "Nanogold-merino scale up"
10/2007 – 07/2011	Study of Applied Chemistry, University of Applied Science Nürnberg, Germany **Scientific degree:** Diplom Chemieingenieur (FH) Diploma thesis at the Siemens AG, Erlangen, Germany **Topic:** "Synthese und Charakterisierung von Dotierstoffen in OLED-Anwendungen"
Since 12/2011	PhD student, Laboratory of Macromolecular and Organic Chemistry (Friedrich Schiller University Jena) in the group of Prof. Dr. Ulrich S. Schubert **Topic:** "Design and application of functional polymers: From self-healing materials via hard tissue composites to methacrylate toughener"

Jena, den

_____

Publication list

Peer-reviewed publications

[1] **B. Sandmann**, S. Bode, M. D. Hager, U. S. Schubert, *Adv. Polym. Sci.*, 262, **2013**, 239-257

[2] **B. Sandmann**, B. Happ, F. H. Schacher, M. D. Hager, U. S. Schubert, *Macromol. Rapid Comm.* **2015**, *36*, 604-609.

[3] S. Bode, R. K. Bose, S. Matthes, M. Ehrhardt, A. Seifert, F. H. Schacher, R. M. Paulus, S. Stumpf, **B. Sandmann**, J. Vitz, A. Winter, S. Hoeppener, S. J. Garcia, S. Spange, S. van der Zwaag, M. D. Hager, U. S. Schubert, *Polym. Chem.* **2013**, *4*, 4966-4973.

[4] **B. Sandmann**, B. Happ, M. D. Hager, J. Vitz, E. Rettler, P. Burtscher, N. Moszner, U. S. Schubert, *J. Polym. Sci., Part A: Polym. Chem.* **2014**, *52*, 239–247.

[5] **B. Sandmann**, B. Happ, J. Vitz, M. D. Hager, P. Burtscher, N. Moszner, U. S. Schubert, *Polym. Chem.* **2013**, *4*, 3938-3942.

[6] **B. Sandmann**, B. Happ, J. Vitz, R. M. Paulus, M. D. Hager, P. Burtscher, N. Moszner, U. S. Schubert, *Macromol. Chem. Phys.* **2014**, *215*, 1603-1608.

[7] D. Pretzel, **B. Sandmann**, M. Hartlieb, J. Vitz, S. Hölzer, N. Fritz, N. Moszner, U. S. Schubert, *J. Polym. Sci., Part A: Polym. Chem.* **2015**, in press (DOI: 10.1002/pola.27676).

[8] **B. Sandmann**, B. Happ, I. Perevyazko, T. Rudolph, F. H. Schacher, S. Hoeppener, U. Mansfeld, M. D. Hager, U. Fischer, P. Burtscher, N. Moszner, U. S. Schubert, *Polym. Chem.* **2015**, in press (DOI: 10.1039/C4PY01544D).

Book chapter

[1] S. Bode, **B. Sandmann**, M. D. Hager and U. S. Schubert, in *Self-Healing Polymers: From Principles to Applications*, ed. W. H. Binder, Wiley-VCH Verlag GmbH & Co. KGaA, 2013, vol. 1, p. 446.

Poster presentation

[1] **B. Sandmann**, B. Happ, M. D. Hager, J. Vitz, E. Rettler, N. Moszner, U. S. Schubert, "Efficient Cu(I) acetate-catalyzed cycloaddition of multifunctional alkynes and azides under solvent-free conditions" (***JCF-Frühjahrssymposium***, March 26 – 29, **2014,** Jena, Germany)

Patents

[1] N. Moszner, P. Burtscher, T. Hirt, B. Happ, **B. Sandmann**, M. D. Hager, U. S. Schubert
" Dentalwerkstoffe auf Basis von polymerisierbaren Aziden und Alkinen."
Europäisches Patentamt (Patent Nr.: 12197372.1 – 1521)

[2] A. Kanitz, R. Kellermann, **B. Sandmann**, G. Schmid, J. H. Wemken
"Organisches elektronisches Bauelement mit Dotierstoff, Verwendung eines Dotierstoffs und Verfahren zur Herstellung des Dotierstoffs."
Deutsches Patent- und Markenamt, Aktenzeichen 10 2011 084 639

Acknowledgements / Danksagung

First of all I would like to thank my doctoral adviser Prof. Dr. Ulrich S. Schubert for giving me the opportunity to prepare my PhD thesis in his group. His continuous support was decisive for the success of this thesis.

I want to thank all the contributing people, since without their support the majority of the achievements in this thesis could not have been accomplished. Many thanks appertain to my supervisor Martin Hager for plenty of decisive hints, fruitful discussions, and having always an open ear during also in difficult times of my work. Furthermore, I would like to pay particular thanks to my friend Bobby Happ not only for his support and productive discussions especially in my familiarization phase of my dissertation that were crucial for the success of this work but also for the nice atmosphere.

I want to thank all staff members of the IOMC and JCSM for doing "hidden" tasks starting with the purchase of chemicals or the maintenance and adjustment of technical instruments. In particular, Wolfgang Günther, Gabrielle Sentis, Nicole Fritz, Uwe Köhn, Simone Burchardt, Sylvia Braunsdorf, Grit Festag, Sandra Köhn, Renzo Paulus, Jürgen Vitz, Igor Perevyazko, Stephanie Höppener, Stephanie Schubert, Steffi Stumpf, Felix H. Schacher, Stephan Kupfer, David Hornig, Tobias Rudolph, Carlos Guerrero-Sanchez, Roberto Yañez, Stefan Hölzer, Matthias Hartlieb, David Pretzel, Christine Weber, Andreas Wild and Esra for service measurements and beneficial scientific discussions. Furthermore, I want to express my gratitude to Prof. Dr. Norbert Moszner, Urs Fischer and the team of Ivoclar Vivadent AG for the nice cooperation and constructive discussion enabling this thesis.

Further gratitude goes to my lab colleges Susi, Marc, Peggy, Christian, Natascha, and Philip for the nice work atmosphere.

At the end I want to thank of course my girlfriend Catalina, my friends Berni, Wastl, Alex and my family, who have always been a great support a great help and enrichment, not only in chemistry but rather in life.

Declaration of authorship / Selbstständigkeitserklärung

Ich erkläre, dass ich die vorliegende Arbeit selbständig und unter Verwendung der angegebenen Hilfsmittel, persönlichen Mitteilungen und Quellen angefertigt habe.

I certify that the work presented here is, to the best of my knowledge and belief, original and the result of my own investigations, except as acknowledged, and has not been submitted, either in part or whole, for a degree at this or any other university.

Jena, den

_____

Benedict Sandmann

Publications P1-P7

P1: B. Sandmann, S. Bode, M. D. Hager, U. S. Schubert, *Adv. Polym. Sci.* **2013**, 239-257 – Reproduced by permission of The Royal Society of Chemistry.

P2: B. Sandmann, B. Happ, F. H. Schacher, M. D. Hager, U. S. Schubert, *Macromol. Rapid Comm.* **2015**, *36*, 604-609 – Reproduced by permission of John Wiley & Sons Ltd., UK. Copyright © 2013 Wiley Periodicals, Inc.

P3: B. Sandmann, B. Happ, M. D. Hager, J. Vitz, E. Rettler, P. Burtscher, N. Moszner, U. S. Schubert, *J. Polym. Sci., Part A: Polym. Chem.* **2014**, *52*, 239-247 – Reproduced by permission of John Wiley & Sons Ltd., UK. Copyright © 2013 Wiley Periodicals, Inc..

P4: B. Sandmann, B. Happ, J. Vitz, M. D. Hager, P. Burtscher, N. Moszner, U. S. Schubert, *Polym. Chem.* **2013**, *4*, 3938-3942 – Reproduced by permission of The Royal Society of Chemistry.

P5: B. Sandmann, B. Happ, J. Vitz, R. M. Paulus, M. D. Hager, P. Burtscher, N. Moszner, U. S. Schubert, *Macromol. Chem. Phys.* **2014**, *215*, 1603-1608 – Reproduced by permission of John Wiley & Sons Ltd., UK. Copyright © 2013 Wiley Periodicals, Inc..

P6: D. Pretzel, B. Sandmann, M. Hartlieb, J. Vitz, S. Hölzer, N. Fritz, N. Moszner, U. S. Schubert, *J. Polym. Sci., Part A: Polym. Chem.* **2015**, in press (DOI: 10.1002/pola.27676) – Reproduced by permission of John Wiley & Sons Ltd., UK. Copyright © 2013 Wiley Periodicals, Inc.

P7: B. Sandmann, B. Happ, I. Perevyazko, T. Rudolph, F. H. Schacher, S. Hoeppener, U. Mansfeld, M. D. Hager, U. Fischer, P. Burtscher, N. Moszner, U. S. Schubert, *Polym. Chem.* **2015**, in press (DOI: 10.1039/C4PY01544D) – Reproduced by permission of The Royal Society of Chemistry.

Publications P1–P7

Publication P1

"Metallopolymers as an emerging class of self-healing materials"

B. Sandmann, S. Bode, M. D. Hager, U. S. Schubert

Adv. Polym. Sci. **2013**, *262*, 239-257.

Adv Polym Sci (2013) 262: 239–258
DOI: 10.1007/12_2013_242

Published online: 6 November 2013

Metallopolymers as an Emerging Class of Self-Healing Materials

Benedict Sandmann, Stefan Bode, Martin D. Hager, and Ulrich S. Schubert

Abstract Metallopolymers are highly interesting materials with properties combining typical polymeric features with the properties of metal–ligand complexes. Thereby, the incorporation of different metal complexes into the polymeric material enables the tuning of the resulting material's properties. In particular, ionic interactions between charged metal complexes and the corresponding counterions as well as reversible (switchable) metal–ligand interactions make these materials potentially interesting as self-healing materials. Compared to other self-healing polymers, the research on these materials is still in its infancy. This review summarizes the latest trends in the research regarding this class of materials.

Keywords Ionomers · Metallopolymers · Self-healing materials · Self-healing polymers · Supramolecular polymers

---

This review represents an extension, refocusing, and update of the chapter "Metal-complex based self-healing polymers" in the book "*Self-healing polymers: From principles to applications*" (Wiley-VCH 2013, edited by Wolfgang Binder). Copyright Wiley-VCH Verlag GmbH & Co. KGaA. Reproduced with permission. The book chapter was tailor-made for the special issue of *Advances in Polymer Science*: *Hierarchical polymer structures: 60 years after the Staudinger Nobel Prize*.

B. Sandmann, S. Bode, and M.D. Hager
Laboratory of Organic and Macromolecular Chemistry (IOMC), Friedrich Schiller University, Humboldtstraße 10, 07743 Jena, Germany

Jena Center for Soft Matter (JCSM), Friedrich Schiller University Jena, Philosophenweg 7, 07743 Jena, Germany
e-mail: martin.hager@uni-jena.de

U.S. Schubert (✉)
Laboratory of Organic and Macromolecular Chemistry (IOMC), Friedrich Schiller University, Humboldtstraße 10, 07743 Jena, Germany

Jena Center for Soft Matter (JCSM), Friedrich Schiller University Jena, Philosophenweg 7, 07743 Jena, Germany

Dutch Polymer Institute (DPI), P.O. Box 902, 5600 AX Eindhoven, The Netherlands
e-mail: ulrich.schubert@uni-jena.de

Contents

1 Introduction

The ground-breaking work of Lehn, Pedersen, and Cram has been honored with the Nobel Prize in chemistry "for their development and use of molecules with structure-specific interactions of high selectivity", namely, for their investigations in the field of crown ethers and host–guest interactions [1]. It was the beginning of supramolecular chemistry as a new important research field in chemistry. Lehn defined supramolecular chemistry as the chemistry "beyond the molecule" [2]. Structures of higher complexity are constructed and hold together by a wide range of interactions, like hydrogen-bonding [3], hydrophobic interactions [4], π–π stacking interactions [5], and metal–ligand interactions [6–8]. Thereby, Nature acts as a role model by providing many inspiring examples of supramolecular structures like the DNA structure (double helix), metallo-proteins, etc. [9]. This field of research on noncovalent systems expands the world of covalent high molar mass materials (i.e., synthetic macromolecules or polymers) discovered by Staudinger, who was honored with the Noble Prize in 1953.

In recent years, an area of special interest has been identified that combines both worlds, i.e., covalent and noncovalent macromolecules, in particular the field of metallo(supramolecular) polymers. These materials combine many polymeric with metal complexes and metallic properties, enabling the design of new materials with outstanding properties, e.g., with self-X properties such as self-repair, self-organization, self-assembly, and self-healing. For instance, metallo-polymers have also been utilized for the fabrication of stimuli-responsive structures, resulting in reversible polymeric materials [10]. Due to this fact, metallopolymers have also been discussed in the context of self-healing materials. Their structural elements can feature reversible interactions similar to those known from hydrogen bonding polymers [11–14] or reversible covalently linked polymers [9, 15–19].

The above-mentioned properties, i.e., reversibility and stimuli-responsiveness, are directly linked to the metal–ligand binding strength. By changing the ligand(s) and the corresponding metal ion, respectively, the intrinsic properties of the final material can be tuned.

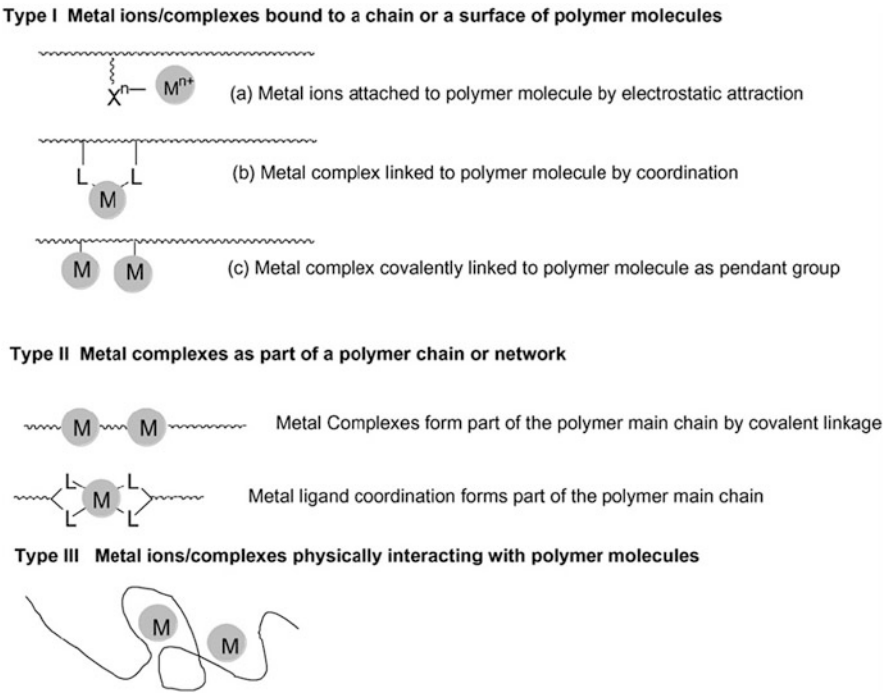

Fig. 1 Various approaches for preparation of metal-containing polymers (the counterions are omitted for clarity) (Copyright 2013 Elsevier) [25]

Ciardelli classified the architecture of metallopolymers into three different types (Fig. 1) [20]. In type I, the metal–ligand pairs are attached to the polymer side chain or as an end group of the backbone by electrostatic interactions, covalent bonds, or metal–ligand coordination (type Ia–Ic, Fig. 1). In type II, the metal ions or complexes are embedded into the main chain by coordinative or covalent associations [21–24]. In type III, the assembly of metal ions into the polymeric arrangement (i.e., the matrix) takes place through physical interactions [25]. In particular, polymers of type I and II are interesting candidates for self-healing polymers. Although conjugated metallopolymers feature very interesting optical properties, non-conjugated polymers have been used nearly exclusively in research on stimuli-responsiveness and self-healing behavior.

The application of metallopolymers as redox-active materials has gained significant importance for creating highly efficient redox conductivity for chemo- and biosensors [26–29], both catalytic and electroluminescent [30–33], magnetic applications [34–37], photovoltaics, and nonlinear optical applications [38–42].

For metal–ligand interactions, the conjunction of both a high binding constant as well as sufficient reversibility represents a challenging task. The stability of a certain complex, a thermodynamic property, is represented by the individual binding constant K. In the case of a very high binding constant between the

ligand(s) and the corresponding metal ion, thermodynamical stable polymers are formed. The physics and properties of these polymers are comparable to classical covalent polymers (Staudinger-like polymers). For a low binding constant, polymeric assemblies only form in the solid state, not in solution (classical inorganic coordination polymers). In contrast, medium binding constants also enable the formation of macromolecular assemblies in solution. The binding constant K depends on several external parameters like pH value, temperature, and solvent polarity as well as on the ligand design and the corresponding metal ion. K can be increased by multiple interacting binding sites, like chelating ligands or multivalent metal ions. Accordingly, for every metal–ligand pair, a detailed investigation of the thermodynamic and kinetic properties is required when a suitable metal–ligand combination is chosen [43].

Kinetically labile metal–ligand interactions open a field for materials with remarkable properties by assembling, disassembling, and reconstructing in a dynamic way. These weak interactions are particularly utilized in materials that have the ability to self-repair [44], self-anneal, and self-correct under certain conditions [45]. Most metallopolymers contain ionic metal complexes. The combination of these positively charged moieties and the corresponding counterions can lead to interesting properties. The melt morphology of diblock copolymers with central metal complexes as linking unit strongly depends on the type and size of the counterions. The groups of Schubert and Gohy investigated the self-assembly of systems having ruthenium ions as the metal, complexed with terpyridine ligands attached to polystyrene (PS) and poly(ethylene oxide) (PEO) [46]. In bulk, the electrostatic interactions between the metal–ligand complex ions and their counterions drive them to form aggregates [47]. This leads to morphologies that are different to their covalent counterpart. Al-Hussein et al. reported highly ordered lamellar structures in the melt of a PS_{20}-[Ru]-PEO_{70} diblock copolymer when bulky counterions were used. Thereby, the metal–ligand complex acting as ionomer is responsible for triggering the microphase separation. This observation can be used to tune the morphology of the metallo(supramolecular) copolymers [48]. The electrostatic interaction between the metal–ligand ions and their associated counterions drives them to form aggregates.

2 Ionomers

The described morphological features for metallopolymers show some parallels with the situation in common ionomers, in which the presence of ionic clusters contributes strongly to the healing process. This has also to be considered for self-healing metallopolymers featuring (ionic) clusters, comparably to ionomers. These latter materials were defined by Tant and Wilkes as a class of ion-containing copolymers. Thereby, the maximum ion group content is about 15 mol% [49]. To distinguish these systems from polyelectrolytes, Eisenberg and Rinaudo further developed the definition, so that ionomer bulk properties are organized by ionic

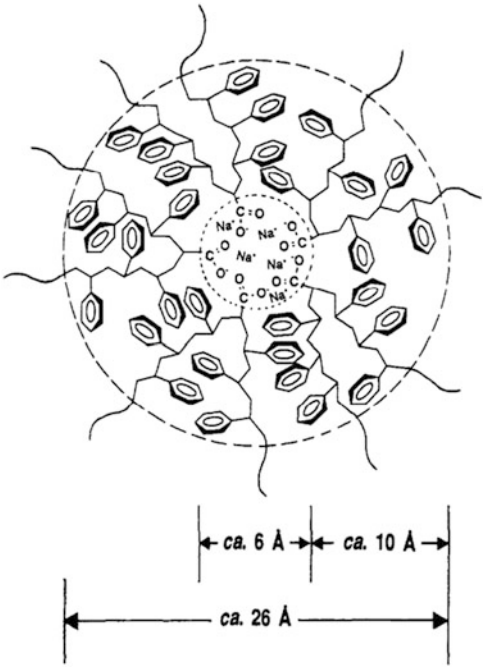

Fig. 2 Region of restricted mobility surrounding a multiplet in a poly(styrene-*co*-sodium methacrylate) ionomer (Reproduced with permission from [52], Copyright 2013 The American Chemical Society)

interactions with respective areas of the polymer structure [50]. Ionomers are generated by a neutralization process. The ionic component (pendant acid groups) is attached to the polymer backbone. After neutralization the ionic groups are part of the polymer structure of the resulting ionomer (or ionic copolymer). The ionic pairs assemble into discrete regions known as multiplets. Eisenberg described in detail the design and constitution of such ionic multiplets (Fig. 2) [51, 52]. In the case of low ionic group contents, the multiplets are isolated. Higher proportions result in an overlapping of the regions with restricted mobility and cluster development (Fig. 3). An increase in the ionic content tremendously influences the mechanical properties of the material [53–56]. Ionic interactions also allow self-healing processes. The reason lies in the reversibility of the cluster formation, so multiple local healing events are possible, e.g., using heat as trigger.

In 2001, Fall investigated the self-healing response by using bullet puncture tests on the commercial poly(ethylene-*co*-methacrylic acid) EMAA materials React-a-Seal®, Surlyn® 8920, and Surlyn® 8940 with varying ionic content [57]. Projectile testing of EMAA copolymers with ionic segments was conducted by Kalista et al. [58–60] and further investigated by Varley [61–65] and van der Zwaag [62, 66]. During the bullet puncture test very high temperatures are generated locally. Due to that, the ionomer was heated above the order–disorder transition and a healing was obtained [58–68]. Furthermore, the heating could also result in melting of the polymer. After the polymer was cooled to room temperature, the aggregates

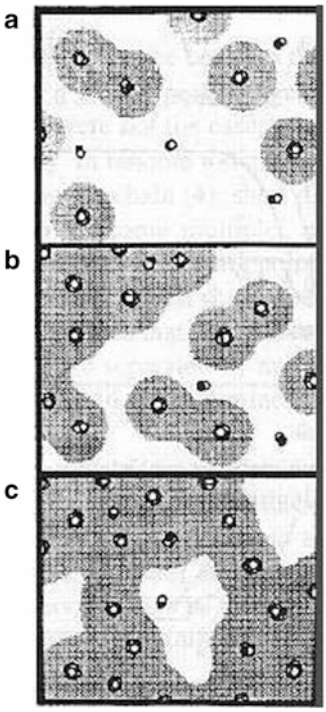

Fig. 3 Morphologies of various ionomers at different ion contents: (**a**) low ion content; (**b**) intermediate ion content; and (**c**) high ion content (Reproduced with permission from [52], Copyright 2013 The American Chemical Society)

(clusters) reformed and the original mechanical properties were recovered. Furthermore, Kalista et al. investigated the self-healing behavior of EMAA materials at temperatures between −50 and 140 °C [60]. The authors could demonstrate that self-healing is possible below the order–disorder temperature due to the reversible formation of hydrogen bonds from the carboxylic acids. Furthermore, they showed that the self-healing efficiency at different temperatures strongly depends on the ionic content. Thus, high ionic contents are better for healing at high temperatures (above the order–disorder transition) and low amounts of cluster are required for healing at low temperatures. Metallopolymers could also feature comparable ionic clusters due to their charged complexes. These could also contribute to the self-healing process.

3 Stimuli-Responsive Metallopolymers

The introduction of metal complexes into polymeric materials can lead to interesting properties and, particularly, the structural properties of these complexes are of importance in self-healing materials [9]. It can be important for the self-healing process that special properties can be changed upon application

of an external stimulus such as light, heat, or change in pH. These stimuli-responsive metallopolymers could be affected in many different ways. As a consequence, the stimuli-responsive metallopolymers are not only interesting candidates for self-healing polymers but also for several other application fields such as sensors [69].

In addition to stimulation by redox processes, the properties of a metallopolymer can also be influenced by other stimuli. An interesting change in metallopolymers was shown by Peng et al. [70]. The authors used the external stimulus light in order to influence the properties of an iron metallopolymer; a redox process from iron(III) to iron(II) could be induced by illumination and this process changed the consistency of the polymer. In this case, a metallopolymer gel, which contains iron(III) ions, was converted into a liquid polymer by simply reducing the iron ions. The subsequent re-oxidation by air led to the original "solid state" system.

Furthermore, the supply of thermal energy could also be used to influence the properties of a metallopolymer and to yield the desired effects. For this purpose, Zhou and coworkers utilized phase-separated ruthenium-containing polymers with two glass transition temperatures [71]. The transitions induced the a kind of mobility that is required for the self-healing process [72].

Beside the mentioned external stimuli, there are also several other possibilities that can influence the polymer properties and structures, leading to changes on the molecular scale and thus, to other changes in the properties of the metallopolymer. For example, Beck and Rowan showed that mechanical energy is adequate (e.g., simple shaking) for generating a change in the properties of the polymer [73]. The authors used an oligo(ethylene gylcol), which was functionalized with two 2,6-*bis*(1'-methylbenzimidazolyl)pyridine units at the termini. In a second step, a metallopolymer was formed by the addition of a lanthanide (lanthanum or europium) and a transition metal ion (cobalt or zinc). In further studies it could be shown that these metallopolymers could also be influenced by other external stimuli [74, 75], e.g., by changes in pH, light, and temperature.

This all-embracing example shows that many different stimuli can affect a metallopolymer to result in the desired properties. In particular, the reversibility of the metal–ligand interaction and the mobility of a metallopolymer are key factors for the implementation of self-healing properties [76, 77]. Additionally, the addressability by other stimuli allows the possibility of triggering healing processes in metallopolymers.

4 Self-Healing Metallopolymers

The above-mentioned properties of metallopolymers are the basic requirements for the generation of self-healing behavior. As a consequence, it is possible to generate a reversible system and to introduce self-healing mechanisms, which is the principle of intrinsic self-healing systems [78–81].

4.1 Biological Archetypes

The self-healing possibilities based on metal–ligand interactions can also be observed in nature. In 2001, Vaccaro and Waite described the ability of mussel byssus threads to heal after an inflicted damage [82]. In the following decade, more detailed insights into the mechanism and the parameters that influence this natural system were collected. Meanwhile, it could be shown that the self-healing behavior is based on an interaction between iron(III) ions and 3,4-dihydroxyphenylalanine (dopa) [83]. The iron center can bind one, two, or three catcheol-based ligands, which are connected with a polymer backbone. The number of bonded ligands depends on the pH value [84–86]. At low pH (below 5), the mono-dopa iron(III) complex is formed, which does not lead to a crosslinking of the polymer chains. The result is an extensible material. By contrast, increasing pH values lead to a more crosslinked polymer network, which provides an increased hardness [83, 87–90]. This principle, which can be found in nature, could also be mimicked by synthetic polymers. For this purpose, poly(ethylene glycol) (PEG) was functionalized with catechol units and Holten-Andersen et al. were able to show the reversibility of the metal–ligand interaction [84, 85].

Beside the iron–dopa interaction, it could be proven that the zinc-histidine system also leads to self-healing behavior of mussel byssus threads, which feature a hierarchical structure [91–93]; a fiber containing a middle block of collagen, which is flanked by histidine-rich parts, in an environment with a high content of zinc ions leads to a reversible crosslinking [93, 94]. The recovery of the mechanical properties of the mussel byssus thread could be demonstrated (Fig. 4) and, furthermore, it was possible to design a model system based on a PEG star functionalized with histidine moieties [95, 96]. These systems were utilized for the generation of metal-containing hydrogels.

4.2 Synthetic Self-Healing Metallopolymers

Several synthetic metallopolymers have been synthesized to obtain self-healing behavior based on metal–ligand interactions. In 2005, Varghese et al. were able to show that a gel based on acryloyl-6-amino caproic acid (A6ACA) can heal scratches if the polymer is dipped into an aqueous copper(II) chloride solution [97]. However, the study did not answer the question of the influence of hydrogen bonds on the self-healing effect, particularly because a medium was selected in which hydrogen bonds exist. Moreover, the mobility of the gel itself could also affect the self-healing behavior; therefore, the particular influence of the metal–ligand interaction on the self-healing process is still unclear.

In addition to the incorporation of the ligand function in the side chain, it is also possible to install the ligand in the main chain of the polymer. Yuan et al. showed that a self-healing behavior can be generated by polymers that feature ligands

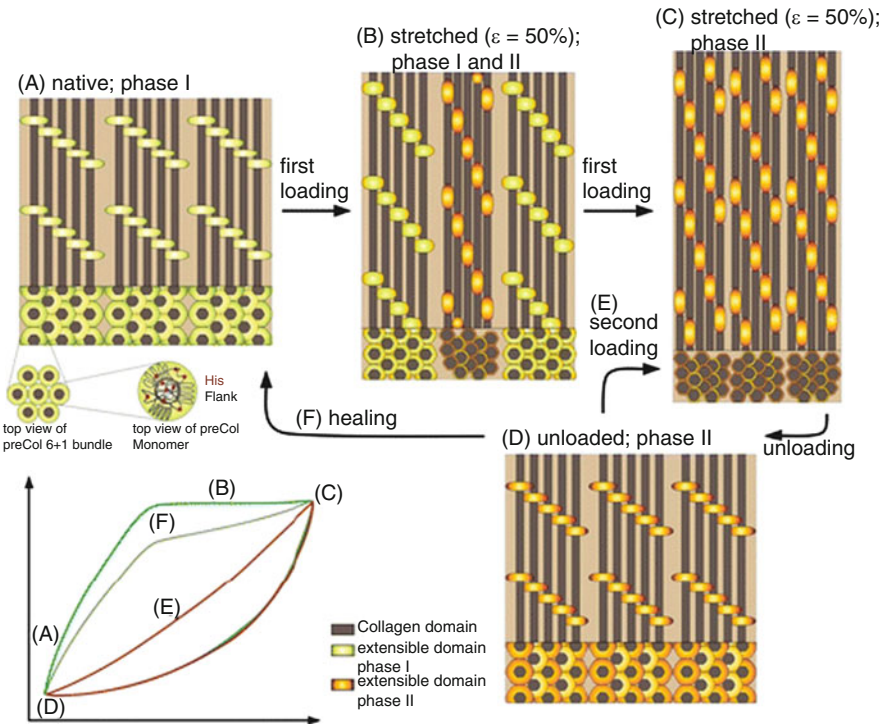

Fig. 4 Molecular model of reversible deformation behavior in mussel byssal threads (Copyright 2013 The American Chemical Society) [95]

within the main chain [98]. The authors used polyurethane analogue polymers as the backbone, in which *bis*(1,2,3-trizol-4-yl) pyridine was incorporated as ligand. Afterwards, these polymers were complexed with zinc(II) and europium(III) ions, respectively, which led to self-healing properties.

In this case, the question also arises as to whether the metal–ligand interaction is the only reason for the self-healing process. There is also the possibility of hydrogen bond formation, which could also contribute to the self-healing properties. In addition, the self-healing efficiency was not quantified.

Furthermore, Terech et al. presented a self-healing metallopolymer gel that was based on the diterpyridyl moiety polymerized by the addition of nickel ions [99]. The resulting linear polymer exhibited very poor mechanical properties and showed a good healing efficiency due to high flexibility of the polymer itself.

In 2011, Rowan and Weder et al. described the self-healing properties of a linear metallopolymer. In order to obtain self-healing behavior, the authors used UV light [44]. For this purpose, poly(ethylene-*co*-butylene) was functionalized with two 2,6-*bis*(1'-methylbenzimidazolyl)pyridine moieties at the termini and the subsequent addition of zinc di[*bis*(trifluoromethylsulfonyl)imide] or lanthanum tri[*bis*(trifluoromethylsulfonyl)imide] led to a linear metallopolymer.

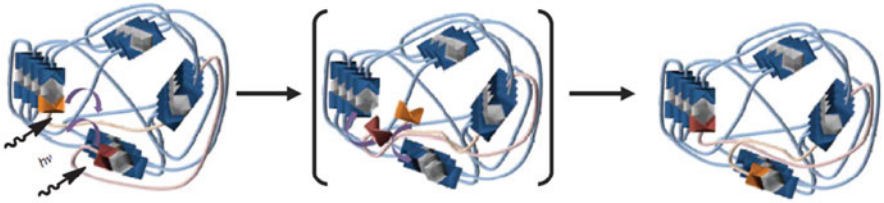

Fig. 5 Proposed self-healing mechanism (Copyright 2013 Nature Publishing Group) [44]

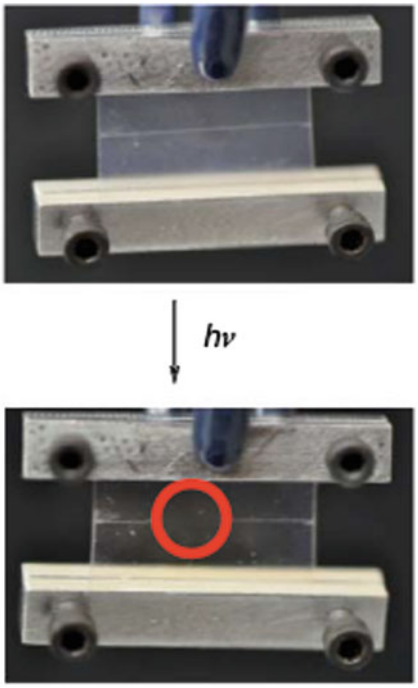

Fig. 6 Demonstration of the self-healing ability of a linear metallopolymer (Copyright 2013 Nature Publishing Group) [44]

This metallopolymer showed self-healing behavior if illuminated by UV light with a wavelength corresponding to the absorption band of the polymer. In this case, energy transfer led to heating of the polymer to 220 °C. The proposed mechanism of the self-healing process is based on the reversibility of the metal–ligand interaction as well as the breakage of metal complex clusters (Fig. 5). The cleavage of the metal complexes increases the mobility of the polymer, which leads to a dynamic motion of the polymers and to the self-healing of inflicted damage. Subsequently, the complexes (and clusters) will be reformed upon cooling,

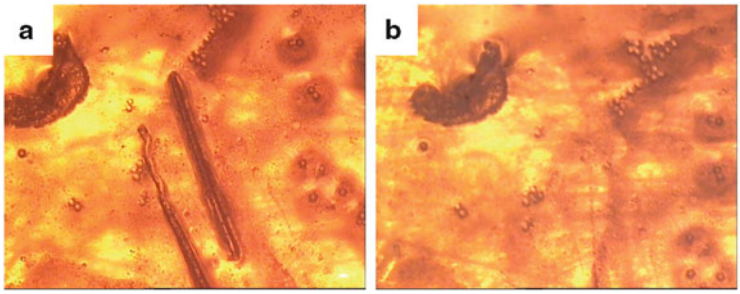

Fig. 7 Self-healing of a metallosupramolecular copolymer network crosslinked by cadmium-terpyridine units: (**a**) scratch and (**b**) healing after 16 h at 80°C (Copyright 2013 The Royal Society of Chemistry) [101]

resulting in an immobilization of the mobile phase and a (complete) healing of the scratch (Fig. 6).

A second example of coatings based on self-healing metallopolymers was recently described by Schubert et al. [100]. A polymer network was synthesized by the crosslinking of terpyridine-functionalized poly(alkyl methacrylates). For this purpose, an iron salt was added, resulting in insoluble and very hard polymer films after drying. Furthermore, it could be shown that decomplexation is not the main process for the self-healing process. In contrast, the ionic interactions between the charged complexes and the counterions (i.e. sulfate) are the basic principle of the self-healing behavior of such crosslinked metallopolymer networks (comparable to ionomers).

Recently, the basic concept of self-healing metallopolymer networks was improved. For this purpose, the Schubert group utilized cadmium(II)-bis-terpyridine complexes [101]. A metallopolymer network based on these complexes was synthesized by the addition of cadmium acetate. The authors could show that these materials behave completely different due to a different coordination of the metal center. Presumably, the acetate moiety also coordinates to the cadmium, but this metal–ligand interaction is much weaker, which results in an improved self-healing behavior (Fig. 7).

4.3 Self-Healing on the Molecular Scale

The above-described examples reveal some basic principles of the self-healing process within metallopolymers. However, a detailed understanding of the process is complicated because different factors play a role (properties of the polymer, binding strength, ionic interactions, etc.). Starting on the macroscopic level, the deformation of the metallopolymer has to be mainly elastic (in particular, when the healing of coatings and thin films is considered). By contrast, plastic deformation will not provide a restoring force. The elastic recovery is important for

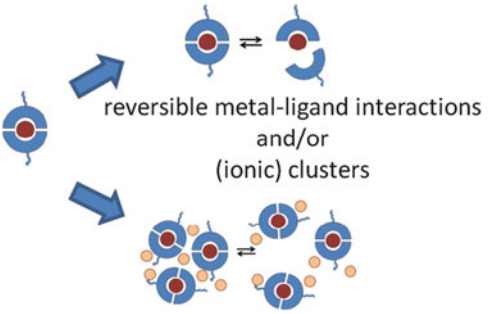

Fig. 8 Metal complexes within the self-healing polymers feature reversibility of the metal–ligand interaction and/or lead to the formation of reversible (ionic) clusters

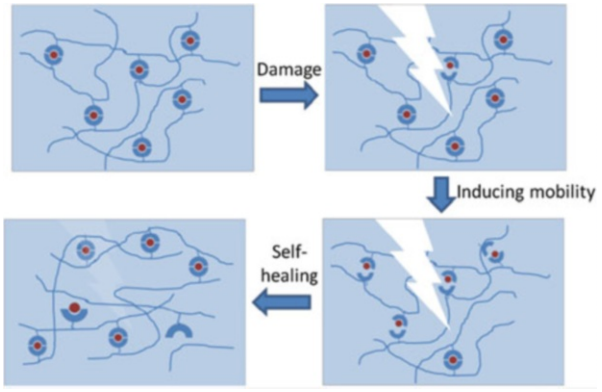

Fig. 9 The self-healing process. The damage can be healed in this case by reversible metal–ligand interactions. The cleavage of these bonds induces mobility, which can lead to closure of the crack. The re-formation of the complexes leads to a new molecular pattern

self-healing because it is the first step of the self-healing process [72]. The healing of bulk materials can also be promoted by bringing the damaged sites into contact.

On the molecular scale (see Fig. 8), the healing of metallopolymers is based on the ionic structure of the complexes and/or on the reversibility of metal complexes, often in combination with an ordered or even hierarchical structure.

Most metal–ligand complexes are positively charged and this could lead to an ionic structure and to a formation of ionic clusters. Comparable to "classic" ionomers, a healing process within metallopolymers could be supported by the ionic interactions of positively charged metal complexes and the corresponding counterions [58, 61]. Moreover, differences in the metal complexes as well as the polymer matrix can also lead to a phase separation, resulting in the formation of clusters [44].

Furthermore, the strength of the metal–ligand bonding can be tuned and, thereby, it is possible to identify a system where the metal–ligand bonding is weak and reversible. As a consequence, the opening and reformation of metal complexes can contribute to the healing process.

After mechanical damage (which will also lead to the cleavage of "normal" covalent bonds) it is possible to induce mobility of the polymer by the cleavage of

metal–ligand interactions and/or the breakage of (ionic) clusters (see Fig. 9). Subsequently, this change leads to healing of the mechanical damage. The original functionality is restored after reformation of complexes and/or clusters (i.e., immobilization). Note that the original structure is not restored, but that a new molecular pattern is created. The phenomena of reversibility and switchability are well known from metal–ligand bonds in solution, but the study of the behavior of the metal–ligand interaction in the solid state is difficult [102–105]. New methods have to be developed in order to investigate these interesting materials in more detail.

5 Conclusion and Outlook

The fascinating material class of metallopolymers combines the world of covalent polymers pioneered by Staudinger with the concepts and systems of supramolecular chemistry and shows interesting properties due to the marriage of polymeric features with the distinct properties of metal complexes. The combination of a wide range of different metal ions with the corresponding ligands allows tuning of the desired properties. In the field of stimuli-responsive polymers, metallopolymers have been frequently applied. Their switchable properties enable the utilization of interesting triggers (e.g., light) for a self-healing process. However, in contrast to other noncovalent interactions (particularly in comparison to the prime example, hydrogen bonds), metal complexes have been applied less frequently in self-healing materials. First examples confirm the great potential of these materials and significant improvements can be expected in the coming years in this field. Nature, which successfully utilizes noncovalent interactions (e.g., in mussel byssus threads), reveals another important issue: the order and spatial arrangement of the metal complexes.

The healing of some synthetic materials has been described on the molecular as well as macroscopic level in recent years.

Metallopolymers, as one of the youngest members of the self-healing polymer family, are a rather new research field. Many possibilities for the design of self-healing polymers are imaginable. Moreover, further intense research is required to clarify the detailed mechanisms of the healing within these materials. A deeper understanding of the behavior of the metal–ligand bonds in the solid state is required. This knowledge can only be gained with the use of new characterization techniques that can reveal the molecular processes within polymeric materials. The utilization of self-healing metallopolymers for potential applications will be the main focus of future research. Due to their fascinating properties (e.g., light absorption or emission), metallopolymers offer the possibility to design new functional coatings [9, 106–109]. For this purpose, the combination of optical and self-healing properties is necessary. This combination could result in a new class of functional coatings. In that context, an improved processability of the self-healing metallopolymer is required and known methods must be applied for these materials [9, 110–112].

Acknowledgements The authors thank the Deutsche Forschungsgemeinschaft (DFG, SPP 1568), the Dutch Polymer Institute (DPI, technolgy area HTE) and the Fonds der chemischen Industrie (FCI) (scholarship for S.B.) for financial support.

References

1. Brunsveld L, Folmer BJB, Meijer EW, Sijbesma RP (2001) Supramolecular polymers. Chem Rev 101:4071–4097
2. Lehn JM (1994) Supramolecular chemistry. Proc Natl Sci Acad USA 106:915–922
3. ten Cate AT, Sijbesma RP (2003) Coils, rods and rings in hydrogen-bonded supramolecular polymers. Macromol Rapid Commun 23:1094–1112
4. Kastner U (2001) The impact of rheological modifiers on water-borne coatings. Coll Surf 183:805–821
5. Lehn JM, Meric R, Vigneron JP, Cesario M, Guilhem J, Pascard C, Asfari Z, Vicens J (1995) Binding of acetylcholine and other quaternary ammonium cations by sulfonated calixarenes. Crystal structure of a [choline-tetrasulfonated calix[4]arene] complex. Supramol Chem 5:97–103
6. Hinderberger D, Schmelz O, Rehahn M, Jeschke G (2004) Electrostatic site attachment of divalent counterions to rodlike ruthenium(II) coordination polymers characterized by EPR spectroscopy. Angew Chem Int Ed 43:4616–4621
7. Schmatloch S, van den Berg AMJ, Alexeev AS, Hofmeier H, Schubert US (2003) Soluble high-molecular-mass poly(ethylene oxide)s via self-organization. Macromolecules 36:9943–9949
8. South CR, Burd C, Weck M (2007) Modular and dynamic functionalization of polymeric scaffolds. Acc Chem Res 40:63–74
9. Whittell GR, Hager MD, Schubert US (2011) Functional soft materials from metallopolymers and metallosupramolecular polymers. Manners I. Nat Mater 10:176–188
10. Weng WG, Beck JB, Jamieson AM, Rowan SJ (2006) Understanding the mechanism of gelation and stimuli-responsive nature of a class of metallo-supramolecular gels. J Am Chem Soc 128:11663–11672
11. Cordier P, Tournilhac F, Soulié-Ziakovic C, Leibler L (2008) Self-healing and thermoreversible rubber from supramolecular assembly. Nature 451:977–980
12. Kitagawa S, Uemura K (2005) Dynamic porous properties of coordination polymers inspired by hydrogen bonds. Chem Soc Rev 34:109–119
13. Montarnal D, Cordier P, Soulié-Ziakovic C, Tournilhac F, Leibler L (2008) Synthesis of self-healing supramolecular rubbers from fatty acid derivates, diethylene triamine, and urea. J Polym Sci A Polym Chem 46:7925–7936
14. Montarnal D, Tournilhac F, Hidalgo M, Couturier J-L, Leibler L (2009) Versatile one-pot synthesis of supramolecular plastics and self-healing rubbers. J Am Chem Soc 131:7966–7967
15. Yuan YC, Yin T, Rong MZ, Zhang MQ (2008) Self healing in polymers and polymer composites. Concepts, realization and outlook: a review. Express Polym Lett 2:238–250
16. Zhang Y, Broekhuis AA, Picchioni F (2009) Thermally self-healing polymeric materials: the next step to recycling thermoset polymers? Macromolecules 42:1906–1912
17. Chen X, Dam MA, Ono K, Mal A, Shen H, Nutt SR, Sheran K, Wudl F (2002) A thermally re-mendable cross-linked polymeric material. Science 295:1698–1702
18. Chen X, Wudl F, Mal AK, Shen H, Nutt SR (2003) New thermally remendable highly cross-linked polymeric materials. Macromolecules 36:1802–1807

19. Kötterizsch J, Stumpf S, Hoeppener S, Vitz J, Hager MD, Schubert US (2013) One-component intrinsic self-healing coatings based on reversible crosslinking by Diels–Alder cycloadditions. Macromol Chem Phys 214:1636–1649
20. Ciardelli F, Tsuchida E, Wöhrle DE (eds) (1996) Macromolecule-metal complexes. Springer, Heidelberg
21. Wong WY, Ho CL (2006) Di-, oligo- and polymetallaynes: syntheses, photophysics, structures and applications. Coord Chem Rev 250:2627–2690
22. Wong WY, Ho CL (2010) Organometallic photovoltaics: a new and versatile approach for harvesting solar energy using conjugated polymetallaynes. Acc Chem Res 43:1246–1256
23. Wong WY, Harvey PD (2010) Recent progress on the photonic properties of conjugated organometallic polymers built upon the *trans-bis*(*para*-ethynylbenzene)*bis*(phosphine)platinum(II) chromophore and related derivatives. Macromol Rapid Commun 31:671–713
24. Ho CL, Wong WY (2011) Metal-containing polymers: facile tuning of photophysical traits and emerging applications in organic electronics and photonics. Coord Chem Rev 255:2469–2502
25. Chan WK (2007) Metal containing polymers with heterocyclic rigid main chains. Coord Chem Rev 251:2104–2118
26. McQuade DT, Pullen AE, Swager TM (2000) Conjugated polymer-based chemical sensors. Chem Rev 100:2537–2574
27. Wild A, Winter A, Hager MD, Schubert US (2012) Fluorometric, water-based sensors for the detection of nerve gas G mimics DMMP, DCP and DCNP. Chem Commun 48:964–966
28. Wild A, Winter A, Hager MD, Schubert US (2012) Fluorometric sensor based on bisterpyridine metallopolymer: detection of cyanide and phosphates in water. Analyst 137:2333–2337
29. Chow C-F (2012) Supramolecular polymeric chemosensor for biomedical applications: design and synthesis of a luminescent zinc metallopolymer as a chemosensor for adenine detection. J Fluorsec 22:1539–1546
30. Holliday BJ, Swager TM (2005) Conducting metallopolymers: the roles of molecular architecture and redox matching. Chem Commun (1):23–36
31. Chen X-Y, Yang X, Holiday BJ (2008) Photoluminescent europium-containing inner-sphere conducting metallopolymer. J Am Chem Soc 130:1546–1547
32. Dennany L, Hogan CF, Keyes TE, Forster RJ (2006) Effect of surface immobilization on the electrochemiluminescence of ruthenium-containing metallopolymer. Anal Chem 78:1412–1417
33. Forster RJ, Hogan CF (2000) Electrochemiluminescent metallopolymer coatings: combined light and current detection in flow injection analysis. Anal Chem 72:5576–5582
34. Batten SR, Neville SM, Turner DR (eds) (2009) Coordination polymers design, analysis and application. Royal Society of Chemistry, Cambridge
35. Manners I (2002) Synthetic metal-containing polymers. 1st edn. Wiley-VCH, Weinheim
36. Werner R, Falk K, Ostrovsky S, Haase W (2001) Metallopolymer with schiff base side chains. Synthesis and characterization of some nickel(II) containing polymers with unexpected cooperative magnetic properties. Macromol Chem Phys 202:2813–2823
37. Djukic B, Dube PA, Razavi F, Seda T, Jenkins HA, Britten JF, Lemaire MT (2009) Preparation and magnetic properties of iron(3+) spin-crossover complexes bearing a thiophene substiuent: toward multifunctional metallopolymers. Inorg Chem 48:699–707
38. Wong WY, Wang XZ, He Z, Chan KK, Djurisic AB, Cheung KY, Yip CT, Ng AMC, Xi YY, Mak CSK, Chan WK (2007) Tuning the absorption, charge transport properties, and solar cell efficiency with the number of thienyl rings in platinum-containing poly(aryleneethynylene)s. J Am Chem Soc 129:14372–14380
39. Wong WY, Wang XZ, He Z, Djurisic AB, Yip CT, Cheung KY, Wang H, Mak CSK, Chan WK (2007) Metallated conjugated polymers as a new avenue towards high-efficiency polymer solar cells. Nat Mater 6:521–527
40. Zhou GJ, Wong WY (2011) Organometallic acetylides of PtII, AuI and HgII as new generation optical power limiting materials. Chem Soc Rev 40:2541–2566

41. Zhou GJ, Wong WY, Lin ZY, Ye C (2006) White metallopolyynes for optical limiting/transparency trade-off optimization. Angew Chem Int Ed 45:6189–6193
42. Wong W-Y, Wang X, Zhang H-L, Cheung K-Y, Fung M-K, Djurisic AB, Chan W-K (2008) Synthesis, characterization and photovoltaic properties of a low-bandgab platinum(II) polyyne functionalized with a 3,4-ethylenedioxythiophene-benzothiadiazole hybrid spacer. J Organmet Chem 693:3603–3612
43. Happ B, Winter A, Hager MD, Schubert US (2012) Photogenerated avenues in macromolecules containing Re(I), Ru(II), Os(II), and Ir(III) metal complexes of pyridine-based ligands. Chem Soc Rev 41:2222–2255
44. Burnworth M, Tang L, Kumpfer JR, Duncan AJ, Beyer FL, Fiore GL, Rowan SJ, Weder C (2011) Optically healable supramolecular polymers. Nature 472:334–337
45. Kurth DG, Higuchi M (2006) Transition metal ions: weak links for strong polymers. Soft Matter 2:915–927
46. Fustin CA, Guillet P, Schubert US, Gohy JF (2007) Metallo-supramolecular block copolymers. Adv Mater 19:1665–1673
47. Al-Hussein M, Lohmeijer BGG, Schubert US, de Jeu WH (2003) Melt morphology of polystyrene-poly(ethylene oxide) metallo-supramolecular diblock copolymer. Macromolecules 36:9281–9284
48. Al-Hussein M, de Jeu WH, Lohmeijer BGG, Schubert US (2005) Phase behavior of the melt of polystyrene–poly(ethylene oxide) metallo-supramolecular diblock copolymer with bulky counterions. Macromolecules 38:2832–2836
49. Tant MR, Wilkes GL (eds) (1987) Viscoelastic behavior of ionomers in bulk and solution, in structure and properties of ionomers. D Reidel, Dordrecht
50. Eisenberg A, Rinaudo M (1990) Polyelectrolytes and ionomers. Polym Bull 24:671
51. Eisenberg A (1970) Clustering of ions in organic polymers. A theoretical approach. Macromolecules 3:147–154
52. Eisenberg A, Hird B, Moore RB (1990) A new multiplet-cluster model for the morphology of random ionomers. Macromolecules 23:4098–4107
53. Bellinger MA, Sauer JA, Hara M (1994) Tensile fracture properties of rigid-rigid blends made of sulfonated polystyrene ionomer and polystyrene. Macromolecules 27:6147–6155
54. Statz RJ (1985) Ethylene copolymer ionomers. In: FB Seymour, T Cheng (eds) History of polyolefins: the world's most widely used polymers. Chemistry and chemists, vol 7. Springer, Heidelberg, pp 177–192
55. Rees R (ed) (1987) Ionomeric thermoplastic elastomers early research – Surlyn and related polymers, in thermoplastic elastomers: a comprehensive review. Carl Hanser Verlag, Munich
56. Hara M, Sauer JA (1994) Mechanical properties of ionomers. J Macromol Sci Polym Rev C34:325–373
57. Fall R (2001) Masters Thesis, Virginia Polytechnic Institute and State University
58. Kalista SJ, Ward TC, Oyetunji Z (2007) Self-healing of poly(ethylene-co-methacrylic acid) copolymers following projectile puncture. Mech Adv Mater Struct 14:391–397
59. Ward TC, Kalista SJ (2007) Thermal characteristics of the self-healing response in poly (ethylene-co-methacrylic acid) copolymers. J R Soc Interface 4:405–411
60. Kalista SJ, Pflug JR, Varley RJ (2013) Effect of ionic content on ballistic self-healing in EMAA copolymers and ionomers. Polym Chem 4:4910–4926
61. Varley RJ, Shen S, van der Zwaag S (2010) The effect of cluster plasticisation on the self healing behaviour of ionomers. Polymer 51:679–686
62. Varley RJ, van der Zwaag S (2008) Towards an understanding of thermally activated self-healing of an ionomer system during ballistic penetration. Acta Mater 56:5737–5750
63. Pingkarawat K, Wang CH, Varley RJ, Mouritz AP (2012) Self-healing of delamination cracks in mendable epoxy matrix laminates using poly[ethylene-*co*-(methacrylic acid)] thermoplastic. Compos A Appl S 43:1301–1307

64. Pingkarawat K, Wang CH, Varley RJ, Mouritz AP (2012) Self-healing of delamination fatigue cracks in carbon fibre-epoxy laminate using mendable thermoplastics. J Mater Sci 47:4449–4456
65. Hughes AE, Cole IS, Muster TH, Varley RJ (2010) Designing green, self-healing coatings for metal protection. Npg Asia Mater 2:143–151
66. Varley RJ, van der Zwaag S (2008) Development of a quasi-static test method to investigate the origin of self-healing in ionomers under ballistic conditions. Polym Test 27:11–19
67. Tadano K, Hirasawa E, Yamamoto H, Yano S (1989) Order-disorder transition of ionic clusters in ionomers. Macromolecules 22:226–233
68. Neppel A, Butler IS, Eisenberg A (1979) Vibrational spectra of polymers. 2. Variable-temperature raman spectroscopy as a probe for ion clustering in ionomers. Macromolecules 12:948–952
69. Stuart MAC, Huck WTS, Genzer J, Muller M, Ober C, Stamm M, Sukhorukov GB, Szleifer I, Tsukruk VV, Urban M, Winnik F, Zauscher S, Luzinov I, Minko S (2010) Emerging applications of stimuli-responsive polymer materials. Nat Mater 9:101–113
70. Peng F, Li GZ, Liu XX, Wu SZ, Tong Z (2008) Redox-responsive gel–sol/sol–gel transition in poly(acrylic acid) aqueous solution containing Fe(III) ions switched by light. J Am Chem Soc 130:16166–16167
71. Zhou GC, Harruna II, Ingram CW (2005) Ruthenium-centered thermosensitive polymers. Polymer 46:10672–10677
72. Wool RP (2008) Self-healing materials: a review. Soft Matter 4:400–418
73. Beck JB, Rowan SJ (2003) Multistimuli, multiresponsive metallo-supramolecular polymers. J Am Chem Soc 125:13922–13923
74. Weng WG, Li Z, Jamieson AM, Rowan SJ (2009) Effect of monomer structure on the gelation of a class of metallo-supramolecular polymers. Soft Matter 5:4647–4657
75. Rowan SJ, Beck JB (2005) Metal–ligand induced supramolecular polymerization: a route to responsive materials. Faraday Discuss 128:43–53
76. Murphy EB, Wudl F (2010) The world of smart healable materials. Prog Polym Sci 35:223–251
77. Wang F, Zhang JQ, Ding X, Dong SY, Liu M, Zheng B, Li SJ, Wu L, Yu YH, Gibson HW, Huang FH (2010) Metal coordination mediated reversible conversion between linear and cross-linked supramolecular polymers. Angew Chem Int Ed 49:1090–1094
78. Hager MD, Greil P, Leyens C, van der Zwaag S, Schubert US (2010) Self-healing materials. Adv Mater 22:5424–5430
79. Herbst F, Döhler D, Michael P, Binder WH (2013) Self-healing polymers via supramolecular forces. Macromol Rapid Commun 34:203–220
80. Billiet S, Hillewaere XKD, Teixeira RFA, Du Prez FE (2013) Chemistry of crosslinking processes for self-healing polymers. Macromol Rapid Commun 34:290–309
81. Brassinne J, Fustin C-A, Gohy JF (2013) Polymer gels constructed through metal–ligand coordination. J Inorg Organomet Polym 23:23–40
82. Vaccaro E, Waite JH (2001) Yield and post-yield behavior of mussel byssal thread: a self-healing biomolecular material. Biomacromolecules 2:906–911
83. Harrington MJ, Masic A, Holten-Andersen N, Waite JH, Fratzl P (2010) Iron-clad fibers: a metal-based biological strategy for hard flexible coatings. Science 328:216–220
84. Holten-Andersen N, Harrington MJ, Birkedal H, Lee BP, Messersmith PB, Lee KYC, Waite JH (2011) pH-induced metal-ligand cross-links inspired by mussel yield self-healing polymer networks with near-covalent elastic moduli. Proc Natl Acad Sci USA 108:2651–2655
85. Barrett DG, Fullenkamp DE, He L, Holten-Andersen N, Lee KYC, Messersmith PB (2013) pH-Based regulation of hydrogel mechanical properties through mussel-inspired chemistry and processing. Adv Funct Mater 23:1111–1119
86. Harrington MJ, Waite JH (2008) pH-Dependent locking of giant mesogens in fibers drawnfrom mussel byssal collagens. Biomacromolecules 9:1480–1486

87. Harrington MJ, Gupta HS, Fratzl P, Waite JH (2009) Collagen insulated from tensile damage by domains that unfold reversibly: in situ X-ray investigation of mechanical yield and damage repair in the mussel byssus. J Struct Biol 167:47–54
88. Harrington MJ, Waite JH (2009) How nature modulates a fiber's mechanical properties: mechanically distinct fibers drawn from natural mesogenic block copolymer variants. Adv Mater 21:440–444
89. Ceylan H, Urel M, Erkal TS, Tekinay AB, Dana A, Guler MO (2013) Mussel inspired dynamic cross-linking of self-healing peptide nanofiber network. Adv Funct Mater 23:2081–2090
90. Krogsgaard M, Behrens MA, Pedersen JS, Birkedal H (2013) Self-healing mussel-inspired multi-pH-responsive hydrogels. Biomacromolecules 14:297–301
91. Waite JH, Qin XX, Coyne KJ (1998) The peculiar collagens of mussel byssus. Matrix Biol 17:93–106
92. Carrington E, Gosline JM (2004) Mechanical design of mussel byssus: load cycle and strain rate dependence. Am Malacol Bull 18:135–142
93. Waite JH, Lichtenegger HC, Stucky GD, Hansma P (2004) Exploring molecular and mechanical gradients in structural bioscaffolds. Biochemistry 43:7653–7662
94. Waite JH, Broomell CC (2012) Changing environments and structure–property relationships in marine biomaterials. J Exp Biol 215:873–883
95. Krauss S, Metzger TH, Fratzl P, Harrington MJ (2013) Self-repair of a biological fiber guided by an ordered elastic framework. Biomacromolecules 14:1520–1528
96. Fullenkamp DE, He L, Barrett DG, Burghardt WR, Messersmith PB (2013) Mussel-inspired histidine-based transient network metal coordination hydrogels. Macromolecules 46:1167–1174
97. Varghese S, Lele A, Mashelkar R (2006) Metal-ion-mediated healing of gels. J Polym Sci A Polym Chem 44:666–670
98. Yuan JC, Fang XL, Zhang LX, Hong GN, Lin YJ, Zheng QF, Xu YZ, Ruan YH, Weng WG, Xia HP, Chen GH (2012) Multi-responsive self-healing metallo-supramolecular gels based on "click" ligand. J Mater Chem 22:11515–11522
99. Terech P, Yan M, Maréchal M, Royal G, Galvez J, Velu SKP (2013) Characterization of strain recovery and "self-healing" in a self-assembled metallo-gel. Phys Chem Chem Phys 15:7338–7344
100. Bode S, Zedler L, Schacher FH, Dietzek B, Schmitt M, Popp J, Hager MD, Schubert US (2013) Self-healing polymer coatings based on crosslinked metallosupramolecular copolymers. Adv Mater 25:1634–1638
101. Bode S, Bose RK, Matthes S, Ehrhardt M, Seifert A, Schacher FH, Paulus RM, Stumpf S, Sandmann B, Vitz J, Winter A, Hoeppener S, Garcia SJ, Spange S, van der Zwaag S, Hager MD, Schubert US (2013) Self-healing metallopolymers based on cadmium *bis*(terpyridine) complex containing polymer networks. Polym Chem 4:4966–4973
102. Lohmeijer BGG, Schubert US (2003) Water-soluble building blocks for terpyridine-containing supramolecular polymers: synthesis, complexation, and pH stability studies of poly(ethylene oxide) moieties. Macromol Chem Phys 204:1072–1078
103. Gohy JF, Lohmeijer BGG, Schubert US (2002) Metallo-supramolecular block copolymer micelles. Macromolecules 35:4560–4563
104. Gohy JF, Lohmeijer BGG, Schubert US (2002) Reversible metallo-supramolecular block copolymer micelles containing a soft core. Macromol Rapid Commun 23:555–560
105. Gohy JF, Lohmeijer BGG, Varshney SK, Decamps B, Leroy E, Boileau S, Schubert US (2002) Stimuli-responsive aqueous micelles from an ABC metallo-supramolecular triblock copolymer. Macromolecules 35:9748–9755
106. Wild A, Winter A, Schlütter F, Schubert US (2011) Advances in the field of π-conjugated 2,2′:6′,2″-Terpyridines. Chem Soc Rev 40:1459–1511
107. Ulbricht C, Beyer B, Friebe C, Winter A, Schubert US (2009) Recent developments in the application of phosphorescent iridium(III) complex systems. Adv Mater 21:4418–4441

108. Wang Q, He Z, Wild A, Wu H, Cao Y, Schubert US, Chui C-H, Wong W-Y (2011) Platinum–acetylide polymers with higher dimensionality for organic solar cells. Chem Asian J 6:1766–1777
109. Schlütter F, Wild A, Winter A, Hager MD, Baumgaertel A, Friebe C, Schubert US (2010) Synthesis and characterization of new self-assembled metallo-polymers containing electron-withdrawing and electron-donating bis(terpyridine) zinc(II) moieties. Macromolecules 43:2759–2771
110. Wild A, Teichler A, von der Ehe C, Winter A, Hager MD, Yao B, Zhang B, Xie Z, Wong W-Y, Schubert US (2013) ZnII bisterpyridine metallopolymers: improved processability by the introduction of polymeric side chains. Macromol Chem Phys 214:1072–1080
111. Wild A, Teichler A, Ho C-L, Wang X-Z, Zhan H, Schlütter F, Winter A, Hager MD, Wong W-Y, Schubert US (2013) Formation of dynamic metallo-copolymers by inkjetprinting: towards white-emitting materials. J Mater Chem C 1:1812–1822
112. Friebe C, Wild A, Perelaer J, Schubert US (2012) Inkjet printing of zinc(II) bis-2,2′:6′,2″-terpyridine metallopolymers: printability and film-forming studies by a combinatorial thin-film library approach. Macromol Rapid Commun 33:503–509

Publication P2

"The self-healing potential of triazole-pyridine-based metallopolymers"

B. Sandmann, B. Happ, F. H. Schacher, M. D. Hager, U. S. Schubert

Macromol. Rapid Comm. **2015**, *36*, 604-609.

The Self-Healing Potential of Triazole-Pyridine-Based Metallopolymers

Benedict Sandmann, Bobby Happ, Stephan Kupfer, Felix H. Schacher, Martin D. Hager,* Ulrich S. Schubert*

The development of artificial self-healing materials represents an emerging and challenging field in material science. Inspired by nature—for instance by the self-healing of mussel byssus threads—metallopolymers gain more and more attention as attractive self-healing materials. These compounds are able to combine the properties of both polymers and metal–ligand interactions. A novel metallopolymer is developed consisting of attached bidentate triazole-pyridine (TRZ-py) ligands and a low glass transition temperature (T_g) lauryl methacrylate backbone. The polymer is cross-linked with different Fe(II) and Co(II) salts. The resulting materials exhibit promising self-healing performance within time intervals of 5.5 to 26.5 h at moderate temperatures of 50 to 100 °C. The materials are characterized by X-ray scattering (SAXS), UV–Vis spectroscopy, and light microscopy.

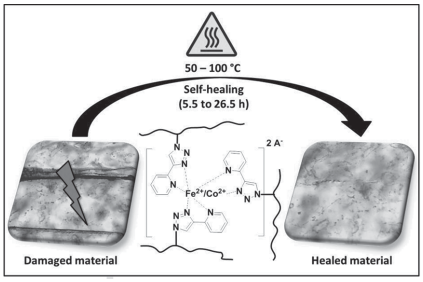

1. Introduction

Self-healing is the ability of a material to heal or repair inflicted damage. Materials with such characteristics represent a strongly emerging field of research. The self-healing ability of a material leads to the (partial) recovery of the mechanical properties and should extend the lifetime, depending on the application. The utilization of polymers for self-healing applications has recently attracted great attention. Different supramolecular interactions[1] in polymers like ionic interactions,[2] π–π stacking,[3] hydrogen-bonding,[4] and metal–ligand interactions[5] have been shown to impart self-healing ability into the respective materials. In recent years, metallopolymers have been identified as an area of special interest.[6] These materials combine the features of polymers and metal complexes, enabling the design of new materials with outstanding properties. A very prominent example of self-healing metallopolymers is mussel byssus threads.[7] This system inspired the design of several artificial self-healing metallopolymers. One way of assembling self-healing metallopolymers is the incorporation of the ligand within the polymer main chain. The first artificial self-healing metallopolymer was reported by the group of Weder. A poly(ethylene-*co*-butylene) backbone carrying 2,6-bis(19-methylbenzimidazolyl)pyridine ligands was cross-linked with $Zn(NTf_2)_2$.[8] The resulting metallopolymer was able to heal-inflicted damage upon exposure to light. The generated heat leads to a disengagement of the metal–ligand bond, a decrease in viscosity, and the healing of scratches. Afterwards, the original material properties were found to

B. Sandmann, Dr. B. Happ, Prof. F. H. Schacher, Dr. M. D. Hager, Prof. U. S. Schubert
Laboratory for Organic and Macromolecular Chemistry (IOMC), Friedrich Schiller University Jena, Humboldtstr. 10, 07743, Jena, Germany
E-mail: martin.hager@uni-jena.de; ulrich.schubert@uni-jena.de
B. Sandmann, Dr. B. Happ, Prof. F. H. Schacher, Dr. M. D. Hager, Prof. U. S. Schubert
Jena Center for Soft Matter (JCSM), Friedrich Schiller University Jena, Philosophenweg 7, 07743, Jena, Germany
B. Sandmann, Dr. B. Happ, Dr. M. D. Hager, Prof. U. S. Schubert
Dutch Polymer Institute (DPI), P.O. Box 902, 5600 AX, Eindhoven, The Netherlands
Dr. S. Kupfer
Institute for Physical Chemistry, Friedrich Schiller University Jena, Helmholtzweg 4, 07743, Jena, Germany

Macromol. Rapid Commun. **2014**, DOI: 10.1002/marc.201400468

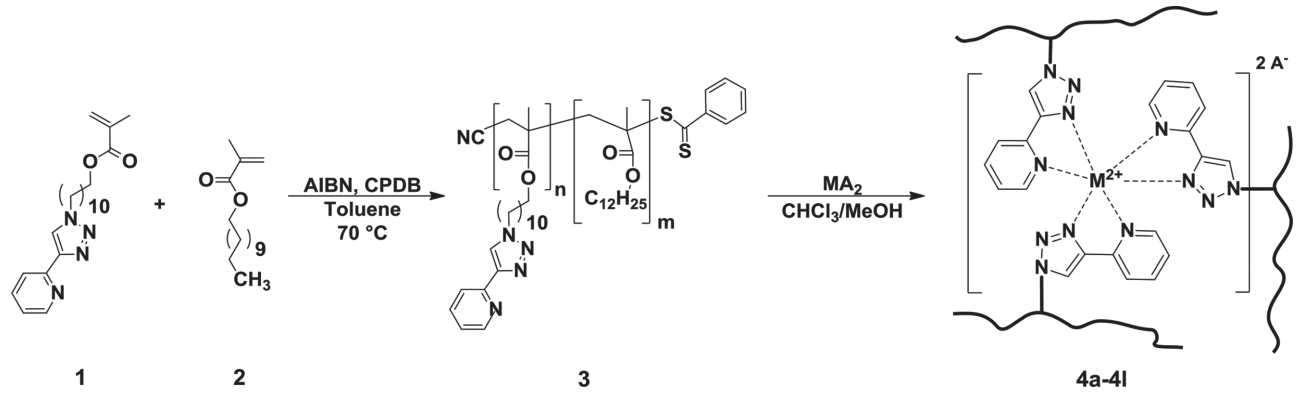

Scheme 1. Schematic representation of the synthesis of copolymer **3** and the subsequent cross-linking using different metal salts into copolymer networks **4a** to **4l**.

be restored. Weder and co-workers[9] continued the development of these switchable self-healing metallopolymers by implementing this complex into cellulose nanocrystals.

One drawback of this system is the rather high energy of 350 mW cm^{-2} and temperatures of 200 °C to 225 °C required for the self-healing process. Recently published polymethacrylates with terpyridine moieties were the first examples for self-healing of side-chain-functionalized metallopolymers.[10] These materials were cross-linked with iron(II) sulfate[10a] and cadmium(II) acetate, respectively.[10b] Self-healing was achieved already at temperatures of 100 °C and within 82 h ($FeSO_4$-based networks) and 60 to 100 °C and 16 to 66 h ($Cd(OAc)_2$-based networks). Nevertheless, such healing conditions are still quite demanding for potential applications.

All these examples have in common that kinetic- and thermodynamic properties of the metal–ligand bond are the key factors for the self-healing process. We hypothesized that the bidentate triazole-pyridines (TRZ-py) exhibit comparable complex properties and, therefore, represents a potential system for the application in self-healing materials. Happ et al.[11] already investigated the complexation properties of 4-(pyridin-2-yl)-1H-1,2,3-triazole with iron(II) chloride tetrahydrate and cobalt(II) tetrafluoroborate hexahydrate.

This contribution reports the synthesis and characterization of a novel triazole-pyridine-based polymer (**3**) and its successful utilization for a self-healing polymer coating. For this purpose, the polymer was cross-linked with several divalent metal salts. The self-healing efficiency of the metallopolymer films at different temperatures was investigated by light microscopy. For mechanistic studies, SAXS, UV–Vis spectroscopic investigations, and quantum chemical calculations at the density functional theory (DFT) level of theory were performed (see Supporting Information). The glass transition temperature (T_g) of the polymers was determined by differential scanning calorimetry (DSC).

2. Results and Discussion

Monomers **1** and **2** were polymerized using the reversible addition–fragmentation chain transfer (RAFT) polymerization procedure (Scheme 1). Effective self-healing systems in general feature a low glass transition temperature, a high flexibility, and network mobility.[10] Therefore, lauryl methacrylate was utilized as comonomer. The aliphatic environment of the alkyl chain decreases the glass transition temperature and enhances the flexibility of the polymer backbone and the network mobility.

For copolymer **3**, a molar mass (M_n) of 39 600 g mol^{-1} and a polydispersity index (PDI) of 1.26 were obtained. Sufficient network mobility in the metallopolymer was ensured by a ligand content of 9% confirmed by ^{1}H-NMR spectroscopy (Figure S1, Supporting Information). The thermoplastic copolymer **3** showed a glass transition at a temperature of –85 °C (determined by DSC, Figure S2, Supporting Information). The DSC traces for all applied copolymers are provided in the Figure S3 and S4 (Supporting Information).

The influence of different divalent cations and anions on the glass transition temperature and the self-healing behavior of the cross-linked copolymers were investigated (Table 1). By cross-linking copolymer **3** with several transition metal salts, the material properties change from thermoplastic features for polymer **3** to at least polymeric networks with elastomeric properties. This network formation resulted in an increase of the T_g for all copolymers **4a** to **4l** to –40 °C (Table 1). An increase of the glass transition temperature was also reported for other metallopolymer systems, e.g., cross-linked poly(vinylamines)[12] or the self-healing metallopolymers described by Rowan and Weder. These systems, showed an increase from –51 °C to –23 °C. However the self-healing itself occurred at far more elevated temperatures of 200 °C to 225 °C.[8] In contrast to a simple T_g-triggered reflow, these temperatures are required to trigger the reversible supramolecular

Table 1. Overview of the investigated copolymers, cross-linking agents, self-healing temperatures, reflections observed in X-ray investigations, and crack dimensions (^{S}= data shown in Supporting Information; *= data not shown).

Polymer	Cross-linking agent	Glass transition temperature [°C]	Self-healing temperature [°C]	Healed crack dimensions (length/width) [µm]	2Θ [°] (SAXS)	*d* [nm] (SAXS)
3	–	– 85^S	–	–	–^{S}	–
4a	$FeCl_2$	– 40^S	50 to 100	1880/34 and 55	1.51^S	5.8
4b	$FeBr_2$	– 40^S	75	1660/18	1.52^S	5.8
4c	$Fe(OAc)_2$	– 40*	no SH	–	–^{S}	–
4d	$Fe(OTf)_2$	– 40^S	75 to 100	2170/42	1.51^S	5.8
4e	$FeSO_4$	– 40*	no SH	–	1.13*	7.8
4f	$CoCl_2$	– 40^S	75 to 100	1370/20	1.51*	5.8
4g	$CoBr_2$	– 40^S	75 to 100	627/18	1.53^S	5.8
4h	$Co(BF_4)_2$	– 40^S	100	1470/23	1.58*	5.6
4i	$Co(OAc)_2$	– 40^S	no SH	–	1.12*	7.9
4k	$MnCl_2$	– 40^S	no SH	–	1.47*	6.0
4l	$CuCl_2$	– 40^S	no SH	–	1.41*	6.3

interaction, i.e., the metal complexes. Without this reversibility (in combination with a temperature above T_g), the healing will not be possible. The thermogravimetric analysis (TGA) showed decomposition of copolymers **3** and **4a–k** at 200 °C. Due to the relative strong complex bond of Fe(II) and Co(II) triazole pyridine complexes, we mainly focused on the investigation of metallocopolymers formed by these salts. Both metals feature comparable binding strengths. For this purpose, copolymer **3** was dissolved in chloroform and the copolymer solution was dropped on top of a notched glass slide with a glass pipette. The metal ion solution was prepared separately by dissolving the salt in methanol. An excess of salt solution was dropped with a pipette on top of the copolymer. The solvents were slowly evaporated in air. The excess of salt and uncross-linked copolymer was removed by washing the surface of the glass slide several times with methanol and chloroform. After drying at elevated temperatures, small scratches were generated on the resulting metallocopolymer films using a scalpel. For subsequent healing studies, the copolymer films were placed on a preheated heating plate at different temperatures.

Subsequently self-healing ability of differently cross-linked copolymers was studied (Table 1). The self-healing process was followed by optical microscopy, as it represents a common method for the characterization of the self-healing process for scratches, scars, and defects.[13] The cross-linking of copolymer films **4a** and **4h** was confirmed by means of UV–vis spectroscopy via the increase of the absorption feature of the $[FeL_3]^{2+}$ species at 433 nm and the $[CoL_3]^{2+}$ species at 320 nm (Figure S10 and S11, Supporting Information). Quantum chemical calculations (time-dependent DFT) performed for $[Fe(TRZ\text{-}py)_3]Cl_2$ (and TRZ-py) unraveled this absorption band to be mainly of MLCT (metal-to-ligand charge-transfer) character, while no bright intraligand states have been observed at this spectral region (detailed information concerning the performed quantum chemical calculations are provided in the Supporting Information). Hence, UV–Vis spectroscopy represents an appropriate tool to monitor the cross-linking of the copolymers.

Two scratches with different widths and the same length (Table 1) were induced on a film with a scalpel (Figure 1). Preliminary assessments of copolymer **4a** showed already a certain self-healing tendency at 50 °C, however, not below that temperature. Though only small scratches of 96 µm length and 10 µm width were healed at 50 °C to 65 °C (Figure S5, Supporting Information). Due to the higher healing performance, the temperature was increased to 75 °C. After 5.5 h of annealing, the smaller scratch was healed completely. By increasing the healing time to 26.5 h, the larger scratch (length: 1880 µm; width: 55 µm) was also completely healed. The relatively low healing temperature and high healing efficiency can be explained by the high mobility and flexibility within the copolymer network **4a** ensured by a low T_g (Table 1) and a high metal–ligand dynamics. By using $FeBr_2$ as cross-linking agent, copolymer **4b** showed a favorable self-healing behavior (Figure 2), although the effective healing temperature of 100 °C is higher in comparison to copolymer **4a** (75 °C). There is only a small effect of the bromine anion to the self-healing efficiency. In the case of $Fe(OTf)_2$-crosslinked copolymer **4d**, efficient self-healing occurred at 75 °C to 100 °C already within 12 h (Figure 3).

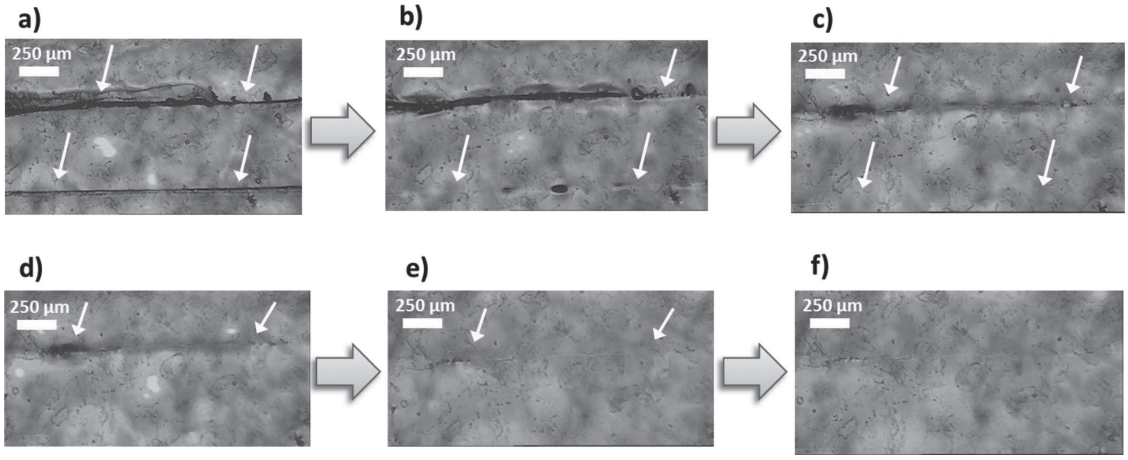

Figure 1. Self-healing of the $FeCl_2$-cross-linked copolymer **4a** at 75 °C; a) t = 0, b) t = 2 h, c) t = 5.5 h, d) t = 8.5 h, e) t = 26.5 h, and f) t = 50.5 h (white arrows indicate the scratch).

The optimal healing temperature of 100 °C is higher in comparison to copolymer **4a**. The ability of the triflate to act as additional ligand during complex rearrangement is in general lower than in the case of chloride, resulting in a less flexible and more rigid network. Due to the higher rigidity of the copolymer network **4e**, the material was not able to self-heal even at elevated temperatures of 130 °C, which we attribute to the presence of the sulphate anion—another nonco-ordinating counter ion on account of the fact that the T_g of (–40 °C) is equal to all other cross-linked polymers (**4a** to **4k**).

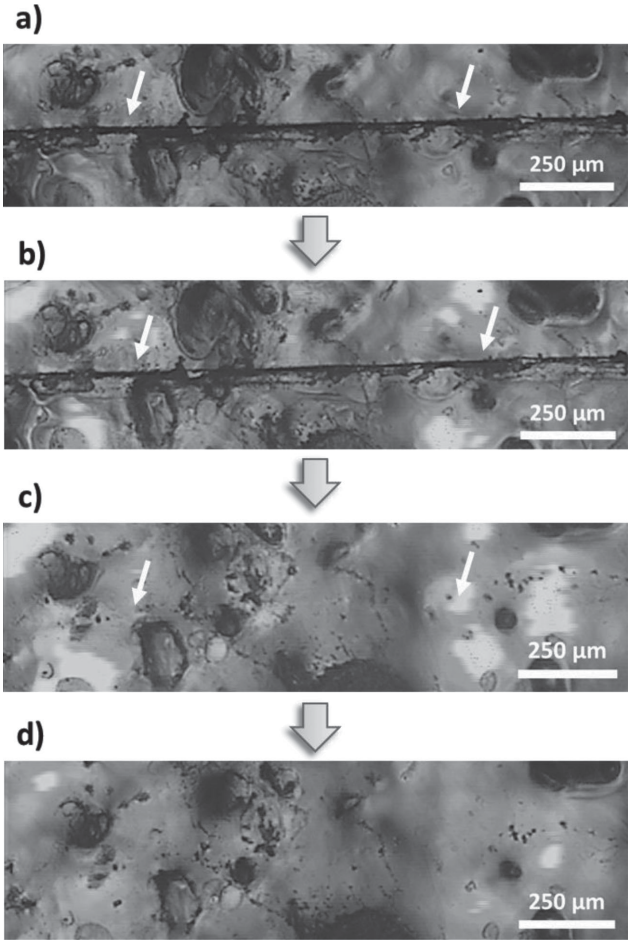

Figure 2. Self-healing of the $FeBr_2$-crosslinked copolymer **4b**; a) t = 0, b) t = after 7 d (room temperature), c) t = 3.5 h (75 °C), and d) t = 21.5 h (75 °C) (white arrows indicate the scratch).

Besides Fe(II)-salts, four different Co(II)-salts, i.e., $CoCl_2$, $CoBr_2$, $Co(BF_4)_2$, and $Co(OAc)_2$, were chosen as cross-linker to investigate the influence of the cation on the healing behavior in comparison to Fe(II) salts. Due to the analogy to $FeCl_2$ and $FeBr_2$, we started with $CoCl_2$ and $CoBr_2$. Both copolymers **4f** and **4g** showed a self-healing behavior, however not below 100 °C (Figures S6 and S7, Supporting Information). Besides, $Co(BF_4)_2$ cross-linked copolymer **4h** was able to self-heal at 100 °C (Figure 4). Copolymers **4i** to **4l** revealed rather weak cross-linking, resulting in a rubbery material like the pristine copolymer **3**. In the case of the $Co(OAc)_2$ cross-linked copolymer **4i**, the presence of the acetate counter ions led to weaker network formation, probably caused by the presence of competing ligands, triazole as well as acetate and, consequently, to inappropriate material properties. As cations with different complex formation properties compared to Co(II) and Fe(II), Cu(II), and Mn(II) were chosen. In both cases, chloride was chosen as anion, as most promising self-healing results were found for the respective Fe(II) and Co(II) cross-linked networks. Copolymer **4l** did not reveal any healing behavior below 75 °C. In addition, it seems that the metallocopolymer irreversibly decomplexes at 100 °C (Figure S8, Supporting Information). Also copolymer **4k** did not show any significant self-healing properties within a temperature range of 75 °C to 100 °C (Figure S9, Supporting Information). Generally, polymer networks based on complexes with counter ions, which potentially can interact with the corresponding metal ion (e.g., chloride) show a better healing behavior.[10b]

Macromol. Rapid Commun. **2014**, DOI: 10.1002/marc.201400468

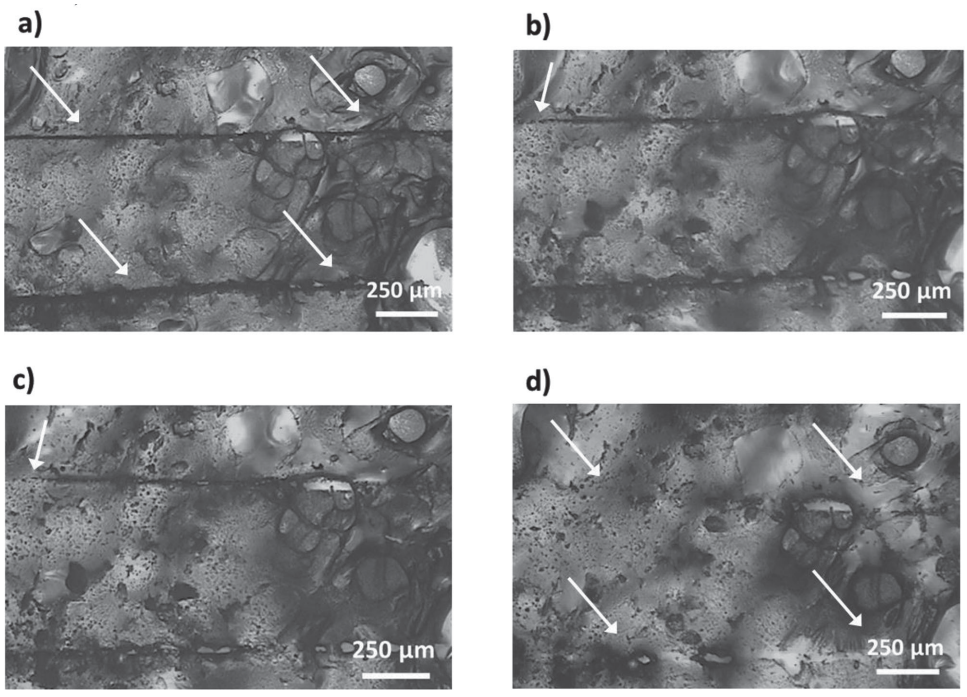

Figure 3. Self-healing of the $Fe(OTf)_2$-cross-linked copolymer **4d** (annealing temperature 75 °C to 100 °C), a) t = 0, b) t = 3.5 h (75 °C), c) t = 9 h (75 °C), and d) t = 12 h (100 °C) (white arrows indicate the scratch).

For structural investigations of the copolymers **3** and **4a** to **4l**, SAXS investigations were performed (Figure S12 to S17). Binder et al. already reported about the formation of clusters as a necessary prerequisite for an efficient self-healing behavior of supramolecular materials based on hydrogen bonding.[1] Bode et al. described characteristic domain sizes of 6.3 nm (2Θ = 1.44) of presumably ionic clusters, consisting of iron(II)-terpyridine units as well as the corresponding counter ions. In the case of $CdCl_2$ cross-linked terpyridine copolymers, 2Θ values of 1.40° and a corresponding domain size of 6.3 nm had been reported.[10b]

Regarding the triazole-pyridine metallocopolymers **4a** to **4l**, domain sizes from 5.8 to 7.9 nm were observed (Table 1). All materials showing self-healing behavior (**4a**, **4b**, **4d**, **4f**, **4g**, **4h**) exhibited distinct broad reflections at 2Θ values of 1.51 to 1.58°. These signals correspond to domain sizes of 5.6 to 5.8 nm. For 2Θ < 1.51°, no self-healing behavior was observed. Exemplary diffractograms of copolymers **4**, **4a**, **4b**, and **4g** are shown in the Supporting Information. These findings are in accordance with the previously investigated terpyridine polymers. The presence of ionic clusters as revealed via SAXS investigations seems to be a prerequisite for successful self-healing.

3. Conclusion

A statistical copolymer of triazole-pyridine methacrylate and lauryl methacrylate was synthesized by RAFT polymerization. The copolymer was cross-linked with several transition metal salts. Fe(II) and Co(II) cross-linked metallocopolymers could be utilized for self-healing studies.

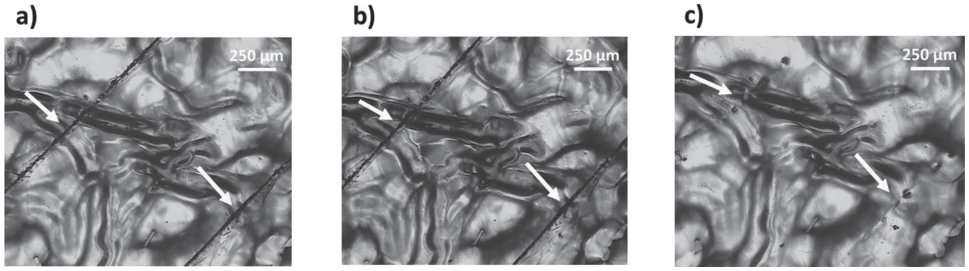

Figure 4. Self-healing of the $Co(BF_4)_2$-crosslinked copolymer **4h**; a) t = 0, b) t = 48 h (room temperature), and c) t = 16.5 h (100 °C) (white arrows indicate the scratch).

Macromol. Rapid Commun. **2014**, DOI: 10.1002/marc.201400468

UV–Vis spectroscopy was applied as a straightforward method for the confirmation of successful cross-linking within the $FeCl_2$- and $Co(BF_4)_2$-metallocopolymer films. X-ray investigations revealed characteristic domain sizes of 5.8 to 7.9 nm. A relation between the presence of presumably ionic clusters and a self-healing tendency of the respective materials could be established. Moreover the influence of the anion on the self-healing behavior was evaluated. For Fe(II) and Co(II) cross-linked polymers, chloride salts revealed the most efficient self-healing behavior. The required healing temperature depends on the salt used for cross-linking and was found to be between 50 °C and 100 °C (with healing times between 5.5 and 26.5 h). The facile and efficient monomer and polymer synthesis enables this class of metallopolymers for a wide field of applications in the area of self-healing materials. To gain more detailed insights into the healing mechanism of this metallopolymer system, the scope of research will focus on detailed investigations about mechanical properties and mechanistic studies effecting the self-healing.

Supporting Information

Supporting Information is available from the Wiley Online Library or from the author.

Acknowledgements: The authors thank the Deutsche Forschungsgemeinschaft (DFG, SPP 1568) for financial support.

Received: August 20, 2014; Revised: November 20, 2014; Published online: ; DOI: 10.1002/marc.201400468

Keywords: metallopolymers; self-healing; triazole-pyridine; X-ray scattering; UV–vis spectroscopy

[1] F. Herbst, D. Dohler, P. Michael, W. H. Binder, *Macromol. Rapid Commun.* **2013**, *34*, 203.
[2] S. J. Kalista, *Mech. Adv. Mater. Struc.* **2007**, *14*, 391.
[3] S. Burattini, H. M. Colquhoun, J. D. Fox, D. Friedmann, B. W. Greenland, P. J. F. Harris, W. Hayes, M. E. Mackay, S. J. Rowan, *Chem. Commun.* **2009**, 6717.
[4] a) G. M. L. van Gemert, J. W. Peeters, S. H. M. Sontjens, H. M. Janssen, A. W. Bosman, *Macromol. Chem. Phys.* **2012**, *213*, 234; b) P. Cordier, F. Tournilhac, C. Soulie-Ziakovic, L. Leibler, *Nature* **2008**, *451*, 977.
[5] a) Z. H. Wang, M. W. Urban, *Polym. Chem.* **2013**, *4*, 4897; b) J. C. Yuan, X. L. Fang, L. X. Zhang, G. N. Hong, Y. J. Lin, Q. F. Zheng, Y. Z. Xu, Y. H. Ruan, W. G. Weng, H. P. Xia, G. H. Chen, *J. Mater. Chem.* **2012**, *22*, 11515; c) B. Sandmann, S. Bode, M. D. Hager, U. S. Schubert, *Adv. Polym. Sci.* **2013**, *262*, 239.
[6] G. R. Whittell, M. D. Hager, U. S. Schubert, I. Manners, *Nat. Mater.* **2011**, *10*, 176.
[7] E. Vaccaro, J. H. Waite, *Biomacromolecules* **2001**, *2*, 906.
[8] M. Burnworth, L. M. Tang, J. R. Kumpfer, A. J. Duncan, F. L. Beyer, G. L. Fiore, S. J. Rowan, C. Weder, *Nature* **2011**, *472*, 334.
[9] S. Coulibaly, A. Roulin, S. Balog, M. V. Biyani, E. J. Foster, S. J. Rowan, G. L. Fiore, C. Weder, *Macromolecules* **2014**, *47*, 152.
[10] a) S. Bode, L. Zedler, F. H. Schacher, B. Dietzek, M. Schmitt, J. Popp, M. D. Hager, U. S. Schubert, *Adv. Mater.* **2013**, *25*, 1634; b) S. Bode, R. K. Bose, S. Matthes, M. Ehrhardt, A. Seifert, F. H. Schacher, R. M. Paulus, S. Stumpf, B. Sandmann, J. Vitz, A. Winter, S. Hoeppener, S. J. Garcia, S. Spange, S. van der Zwaag, M. D. Hager, U. S. Schubert, *Polym. Chem.* **2013**, *4*, 4966.
[11] B. Happ, G. M. Pavlov, I. Perevyazko, M. D. Hager, A. Winter, U. S. Schubert, *Macromol. Chem. Phys.* **2012**, *213*, 1339.
[12] L. A. Belfiore, E. Indra, P. Das, *Macromol. Symp.* **1997**, *114*, 35.
[13] a) R. K. Bose, U. Lafont, J. M. Vega, S. J. Garcia, S. Van der Zwaag, in *Self-Healing Polymers: From Principles to Applications* (Eds: W. H. Binder), Wiley-VCH, Weinheim, Germany **2013**; b) Y. K. Song, C. M. Chung, *Polym. Chem.* **2013**, *4*, 4940; c) C. Suryanarayana, K. C. Rao, D. Kumar, *Prog. Org. Coat.* **2008**, *63*, 72; d) R. S. Trask, G. J. Williams, I. P. Bond, *J. R. Soc. Interface* **2007**, *4*, 363.

Publication P3

"Efficient Cu(I) acetate-catalyzed cycloaddition of multifunctional alkynes and azides: From solution to bulk polymerization"

B. Sandmann, B. Happ, M. D. Hager, J. Vitz, E. Rettler, P. Burtscher, N. Moszner, U. S. Schubert

J. Polym. Sci., Part A: Polym. Chem. **2014**, *52*, 239–247.

Efficient Cu(I) Acetate-Catalyzed Cycloaddition of Multifunctional Alkynes and Azides: From Solution to Bulk Polymerization

Benedict Sandmann,[1,2] Bobby Happ,[1,2,3] Martin D. Hager,[1,2] Jürgen Vitz,[1,2,3] Erik Rettler,[1,2] Peter Burtscher,[4] Norbert Moszner,[4] Ulrich S. Schubert[1,2,3]

[1]Laboratory of Organic and Macromolecular Chemistry (IOMC), Friedrich Schiller University Jena, Humboldtstraße 10, 07743, Jena, Germany
[2]Jena Center for Soft Matter (JCSM), Friedrich Schiller University Jena, Philosophenweg 7, 07743, Jena, Germany
[3]Dutch Polymer Institute (DPI), P.O. Box 902, 5600, AX Eindhoven, The Netherlands
[4]Ivoclar Vivadent AG, Bendererstrasse 2, FL-9494, Schaan, Liechtenstein
Correspondence to: U. S. Schubert (E-mail: ulrich.schubert@uni-jena.de) or
N. Moszner (E-mail: norbert.moszner@ivoclarvivadent.com)

Received 15 August 2013; accepted 19 October 2013; published online 17 November 2013
DOI: 10.1002/pola.26996

ABSTRACT: "Click" chemistry is an effective and commonly used technique in polymer chemistry for the synthesis and modification of polymers. In this study, the bulk polymerization of multifunctional alkynes and azides was achieved by the copper(I)-catalyzed alkyne–azide 1,3-dipolar cycloaddition. The influence of different catalyst systems on the polymerization kinetics of the "click"reaction were evaluated by differential scanning calorimetry. Surprisingly, Cu(I) acetate showed the most efficient catalytic behavior among the applied Cu(I) salts. The polymerization kinetics in solution were investigated by 1H NMR spectroscopy and size exclusion chromatography. According to the 1H NMR investigation the copper(I)-catalyzed cycloaddition follows a second-order kinetics with external catalysis. Additionally, the mechanical properties of the resulting polymers were investigated by depth sensing indentation. Thereby the polymerizations of the alkyne tripropargylamine with the azides 1,3-bis(azidomethyl)benzene and 1,4-bis(azidomethyl)benzene resulted in mechanical hard materials. Furthermore, the combination of the alkynes tripropargylamine and di(prop-2-yn-1-yl) isophorone dicarbamate and polymerization with 1,2-bis(2-azidoethoxy)-ethane resulted in high indentation moduli. © 2013 Wiley Periodicals, Inc. J. Polym. Sci., Part A: Polym. Chem. **2014**, *52*, 239–247

KEYWORDS: bulk polymerization; catalyst screening; click chemistry; crosslinking; cycloaddition; differential scanning calorimetry (DSC); kinetics; nanoindentation; step-growth polymerization

INTRODUCTION The copper(I)-catalyzed azide–alkyne cycloaddition (CuAAC), also known in literature as "click" reaction, was developed independently by Sharpless[1] and Meldal[2] in 2002. This cycloaddition of terminal alkynes and organic azides is inert to a wide range of reactive moieties and functional groups. Among the "click"-type reactions (e.g., Diels−Alder[3], thiole-ene reaction[4]), the CuAAC is the most appealing since it proceeds in most cases in high yields, regioselectively and without undesirable side reactions.[5,6] Even though a lot of effort has recently focused on the development of new catalyst-free click processes,[7–9] it retained the most studied and reliable reaction and has found numerous applications in the field of polymer chemistry and material science.[10–17] In particular, polymer chemistry has benefited from the CuAAC, since it often suffers from inefficient chemical conversion because of the sterical inaccessibleness of reactive species. Consequently, macromolecular architectures arose, such as block copolymers,[18,19] star-like copolymers,[18,20,21] brush architectures,[18,22,23] and dendrimers.[18,24–26] The CuAAC was mostly applied in solutions of the corresponding alkynes and azides.[27] Recently, the photoinduced click-reaction by *in situ* reduction of copper(II) acetate of multifunctional alkynes and azides was described.[28] This approach still requires the presence of a small amount of solvent (i.e., methanol or ethanol). However, totally solvent-free click reactions[9] of polymeric compounds and polymerizations by CuAAC, respectively, were only scarcely studied. Binder et al. could successfully encapsulate a poly(isobutylene)-based azido-telechelic three-arm star and trivalent alkynes into a high-molar mass poly(isobutylene) matrix ($M_n = 250{,}000$ g mol^{-1}). A significant increase of the tensile storage modulus upon shear-induced crosslinking by CuAAC was observed and facilitates the generation of materials with self-healing properties.[29–31]

Additional Supporting Information may be found in the online version of this article.

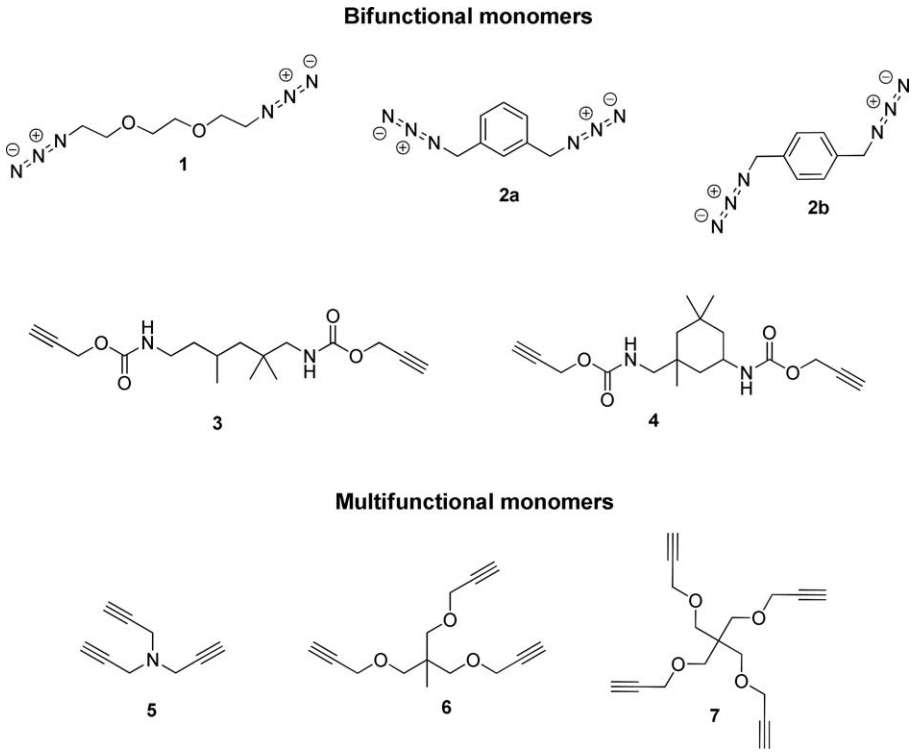

FIGURE 1 Schematic representation of the monomers used for the click-reactions.

Besides, understanding the reaction kinetics of the CuAAC is important as well in order to gain insight into the reaction mechanism and, hence, to determine crucial processing parameters for the design of new polymeric materials. In principle, any copper molecule in the +1 oxidation state catalyzes the CuAAC reaction,[12] in which the catalyst efficiency and reaction kinetics are predominantly influenced by the ligands attached to the copper ion.[32] Bromo-tris(triphenylphosphine)copper(I) bromide [$Cu(PPh_3)_3Br$] is a commonly used catalyst for the polymerization in solution.[33] For the solvent-free CuAAC, [$Cu(PPh_3)_3Br$] is also used due to its good solubility in organic monomers, high catalytic efficiency, and low cost.[34,35] Kessler et al. studied the bulk step-growth polymerization of multifunctional azides and alkynes with [$Cu(PPh_3)_3Br$] as copper(I) source using differential scanning calorimetry and found a reaction order between one and two.[31,36]

This contribution deals with the neat bulk CuAAC polymerization of multifunctional azides and alkynes (Fig. 1). Different copper(I) salts were tested as potential catalyst systems. Thereby the "simple" copper(I) acetate showed surprisingly the highest reactivity. The kinetics of the CuAAC polymerization was investigated by ^{1}H NMR spectroscopy and size exclusion chromatography (SEC) in solution. Moreover, the click-polymerization was also investigated in bulk. The mechanical properties of the resulting polymers were studied by nanoindentation.

EXPERIMENTAL

Materials

Triethylene glycol (Fluka), copper(I) acetate, bromotris (triphenylphosphine)copper(I) bromide ($Cu^IBr(PPh_3)_3$), copper(I) bromide, copper(I)iodide, tetra*kis*(acetonitrile)copper(I) tetrafluoroborate ($Cu^I(CH_3CN)_4BF_4$), and tripropargylamine were purchased from Sigma-Aldrich. The solvents were dried and distilled according to standard procedures. Triethylene glycol bis(4-toluenesulfonate),[37] tris([(1-benzyl-1H-1,2,3-triazole-4-yl)methyl]amine)copper(I) tetrafluoroborate[38] ($Cu^I(TBTA)BF_4$), 1,3-bis(azidomethyl)benzene,[39] and 1,4-bis(azidomethyl)benzene[39] were synthesized and purified following previously described literature procedures.

Safety note: All azides were synthesized with extreme care and tested for their thermal and mechanical stability (hammer test).

Instruments

One-dimensional (^{1}H, ^{13}C) and two-dimensional (HSQC) NMR spectra were recorded on a Bruker AC 300 (300 MHz) at 298 K. Chemical shifts are reported in parts per million (ppm, d scale) relative to the residual signal of the deuterated solvent. Standard abbreviations are used for denoting the signal multiplicity. Elemental analysis was carried out on a CHN-932 Automat Leco instrument. Differential scanning calorimetry (DSC) was measured on a Netzsch DSC 204 F1 Phoenix instrument under a nitrogen atmosphere in a temperature range from −20 to 250 °C with a heating rate of 10 K min^{-1}. Size exclusion chromatograms were recorded using a SEC Shimadzu SCL-10A system controller, a LC-10AD pump, a RID-10A refractive index detector, and a PSS SDV pre/lin S column at 50 °C (eluent: chloroform:triethylamine:iso-propanol 94:4:2; flow rate of 1 mL min^{-1}) using linear PS standards for the molar mass calculation.

Synthesis of the Monomers

Synthesis of 1,2-Bis(2-azidoethoxy)ethane (1)

To a solution of triethylene glycol bis(4-toluenesulfonate) (21.8 mmol, 10.00 g) in DMSO (130 mL), sodium azide (65.0 mmol, 4.25 g) was added in a round bottom flask. The reaction mixture was stirred at room temperature for 48 h. The reaction was quenched with water (100 mL). The product was extracted with diethyl ether and the organic phase was washed with water (3 × 50 mL). After drying over $MgSO_4$ and evaporation of the solvent, the product was obtained as a yellow oil (4.32 g, 98%).

^{1}H NMR (300 MHz, $CDCl_3$, δ): 3.70−3.66 (m, 8H), 3.38 (t, $J = 5$ Hz, 4H); ^{13}C NMR (75 MHz, $CDCl_3$, δ): 70.7, 70.1, 50.7. Anal. calcd for $C_6H_{12}N_6O_2$: C, 36.00%; H, 6.04%; N, 41.98%. Found: C, 36.25%; H, 5.79%; N, 42.08%

Synthesis of Di(prop-2-yn-1-yl) (2,2,4-trimethylhexane-1, 6-diyl)dicarbamate (3)

To a solution of 1,6-diisocyanato-2,2,4-trimethylhexane (23.8 mmol, 5.00 g, diastereomeric mixture) and dibutyltin(II)-dilaurate (0.0004 eq.) in toluene (10 mL) was added prop-2-yn-1-ol (47.6 mmol, 2.61 g) dropwise within 15 min. The reaction mixture was stirred at 60 °C for 48 h. After evaporation of the solvent and running through a short pad of silica the product was obtained as a viscous yellow oil (7.51 g, 98%).

^{1}H NMR (300 MHz, $CDCl_3$, δ): 5.14−4.91 (br, 2H; N−H), 4.65 (br, 4H; C(O)O—CH_2), 3.20−2.88 (m, 4H; NH−C**H**$_2$), 2.46 (d, $J = 1.8$ Hz, 2H; C≡CH), 1.70−1.22 (br, 3H), 1.05−0.86 (m, 11H; CH_2, CH_3); ^{13}C NMR (75 MHz, $CDCl_3$, δ): 155.8, 155.7, 155.4, 129.0, 128.2, 125.3, 78.4, 74.6, 74.5, 52.5, 52.3, 51.4, 48.6, 46.4, 45.9, 41.9, 39.2, 39.1, 37.4, 35.0, 32.9, 29.4, 27.4, 26.1, 25.5, 25.1, 22.3, 21.4, 20.5; EIMS (m/z (%)): 345.18 (100) [$M^+ + Na$]; Anal. calcd for $C_{17}H_{26}N_2O_4$: C, 63.33%; H, 8.13%; N, 8.69%; found: C, 63.07%; H, 7.91%; N, 8.83%.

Synthesis of Di(prop-2-yn-1-yl) isophorone dicarbamate(4)

To a solution of 5-isocyanato-1-isocyanatomethyl-1,3,3-trimethylcyclohexane (13.5 mmol, 3.00 g, diastereomeric mixture) and dibutyltin(II)-dilaurate (0.27 mmol, 0.017 g) in toluene (40 mL) was added prop-2-yn-1-ol (27 mmol, 1.51 g) dropwise within 15 min. The reaction mixture was stirred at 60 °C for 48 h. After evaporation of the solvent and running through a short pad of silica, the product was obtained as a white precipitate (4.15 g, 92%).

^{1}H NMR (250 MHz, $CDCl_3$, δ): 4.67 (s, 4H), 3.78 (m, 2H), 3.26 (m, 1H), 2.92 (d, 1H), 2.47 (d, 1H), 0.76–1.43 (m, 15H); ^{13}C NMR (75 MHz, $CDCl_3$, δ): 155.8, 154.6, 74.7, 74.5, 54.9, 52.5, 52.2, 46.9, 46.2, 44.9, 41.7, 36.4, 35.0, 31.8, 27.6, 23.1; EIMS (m/z (%)): 357.18 (100) [$M^+ + Na$]

Synthesis of 3-(2-Methyl-3-(prop-2-yn-1-yloxy)−2-((prop-2-yn-1-yloxy)methyl)propoxy)prop-1-yne (6)

Potassium hydroxide (1 mol, 65.24 g) was suspended in DMSO (300 mL) for 2 h at 50 °C. 1,1,1-Tris(hydroxymethyl) ethan (12.02 g, 0.1 mol) was added to the solution. Afterward, propargylbromide (56 mL, 0.5 mol) was added within 3 h while the reaction temperature was kept below 22 °C. The reaction mixture was diluted with water (4 L) and subsequently extracted with *tert*-butylmethylether (3 × 400 mL). The organic phase was washed with water (2 × 300 mL) and dried over Na_2SO_4. The solvent was evaporated *in vacuo*. The raw product was purified by column chromatography on silica gel (hexane/EtOAc, 4:1) to afford compound **7** (31.9 g, 37% yield) as an orange solid, m.p. 56–57 °C).

^{1}H NMR (400 MHz, $CDCl_3$, δ): 4.12 (d, $J = 2.4$ Hz, 8H, OCH_2—C≡), 3.53 (s, 8H, OCH2), 2.41 (t, $J = 2.4$ Hz, 4H, ≡CH); ^{13}C NMR (100 MHz, $CDCl_3$, δ): 80.0 (C≡CH), 74.1 (C≡CH), 69.0 (OCH_2), 58.7 (OCH_2—C≡), 44.8 (C).

Synthesis of 3-(3-(Prop-2-yn-1-yloxy)−2,2-bis((prop-2-yn-1-yloxy)methyl)propoxy)prop-1-yne (7)

Potassium hydroxide (3 mol, 195.72 g) was suspended in DMSO (900 mL) for 2 h at 50 °C. Pentaerythriol (40.86 g, 0.3 mol) was added to the solution. Afterward, propargylbromide (168 mL, 1.5 mol) was added within 3 h while the reaction temperature was kept below 24 °C. The reaction mixture was diluted with water (8 L) and subsequently extracted with *tert*-butylmethylether (3 × 800 mL). The organic phase was washed with water (2 × 400 mL) and dried over Na_2SO_4. The solvent was evaporated in *vacuo*. The raw product was purified by column chromatography on silica gel (hexane/EtOAc, 4:1) to afford compound **7** (6.71 g, 29% yield) as an orange liquid.

^{1}H NMR (400 MHz, $CDCl_3$, δ): 4.12 (d, $J = 2.4$ Hz, 8H, OCH_2—C≡), 3.53 (s, 8H, OCH_2), 2.41 (t, $J = 2.4$ Hz, 4H, ≡CH);^{13}C NMR (100 MHz, $CDCl_3$, δ): 74.1 (C≡CH), 80.0 (C≡CH), 69.0 (OCH_2), 58.7 (OCH_2—C≡), 44.8 (C).

General Procedure for the Cu(I)-Catalyzed Polyaddition

Safety note: In the case of copper(I) acetate as catalyst source, spontaneous inflammation has been observed at a catalyst concentration above 4 mol % and at a reaction temperature beyond 50–70 °C.

In the case of the step-growth copolymerization of the bis-alkyne and the bis-azide, both components were charged in a small glass vial using an equimolar ratio and stirred for 10 min. After that, the respective copper(I) catalyst was added (0.5–2 mol %) and the neat solution was stirred for another 5 min until the copper salt has been dissolved. The solution was deposited in a metal or Teflon ferrule (0.5–1 mm height, 15-mm inside diameter) placed on a glass slide using a 1-mL syringe. The obtained polymer reference block was suited for nanoindentation measurements.

For the crosslinking polyadditions, the alkynes with a degree of functionalization higher than two were mixed with the copper(I) catalyst (0.25–2 mol %) before the polymerization. Usually after 1 h stirring, the catalyst was dissolved and the solution turned yellow. The bis-azide was added in equimolar amounts (same content of functional groups) and the

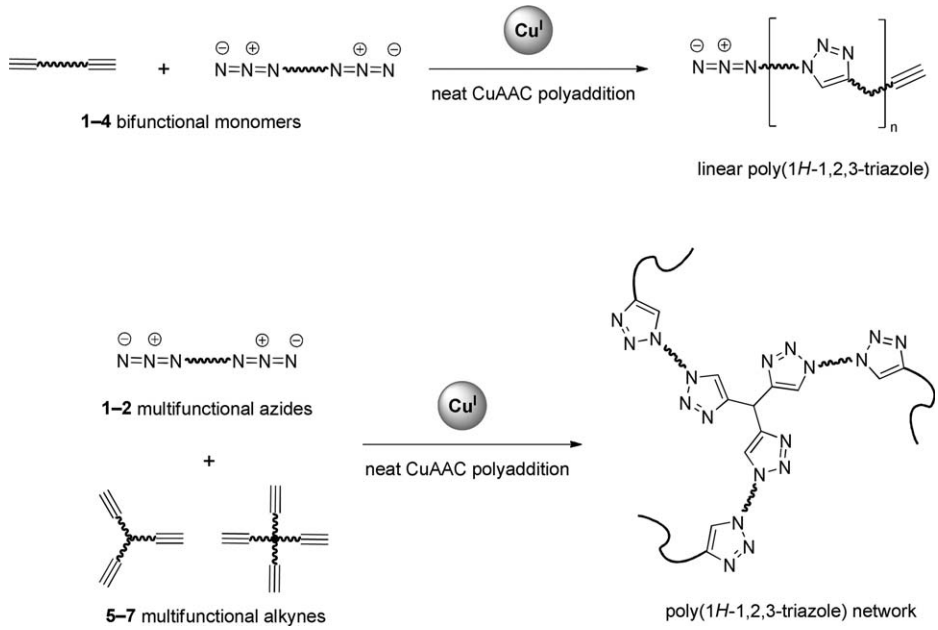

SCHEME 1 Schematic representation of the polyaddition of bifunctional as well as multifunctional monomers by CuAAC.

previously described procedure was repeated for polymerization.

For some polymerization procedures, the ferrule was covered with PET foil and the reaction was carried out under nitrogen using a funnel.

Monitoring of the Step-Growth Copolymerization by ^{1}H NMR Spectroscopy in Solution

First, a solution of 1,2-bis(2-azidoethoxy)ethane (28 mg, 0.14 mmol) and di(prop-2-yn-1-yl) (2,2,4-trimethylhexane-1,6-diyl)dicarbamate (45 mg, 0.14 mmol) was prepared in 0.4 mL of CD_3OD and introduced into a NMR tube. The ^{1}H NMR spectrum was recorded after optimization of the line width at 32 °C without catalyst yielding the spectrum at $t = 0$ min. After that copper(I) acetate (0.5 mg, 4×10^{-3} mmol) was dissolved in 0.1 mL of CD_3OD and added into the NMR tube. After the optimization of acquisition parameters (pulse width, acquisition time, spectral width), a ^{1}H NMR spectrum was recorded every 5 min. The conversion was calculated for the bis-azide monomer by integration of the ^{1}H NMR spectra following the protons adjacent to the two oxygen atoms between 3.70 and 3.66 ppm. The carbamate monomer was not considered for calculation, since most signals were overlaid.

Monitoring of the Step-Growth Copolymerization by SEC in Solution

1,2-Bis(2-azidoethoxy)ethane (80 mg, 0.4 mmol) and di(prop-2-yn-1-yl) (2,2,4-trimethylhexane-1,6-diyl)dicarbamate (129 mg, 0.4 mmol) were dissolved in 1 mL of the respective solvent (MeOH, DMF, DMSO) using a small vial (5 mL). The solution was stirred for 5 min at 32 °C and 20 μL was taken for the SEC measurement at t = 0 min. Subsequently, copper(I) acetate (2 mg, 0.016 mmol) was added and SEC measurements were consecutively carried out.

Mechanical Properties

The mechanical properties of the samples were characterized via depth-sensing indentation (DSI) using a TriboIndenter TI 900 (Hysitron, Minneapolis, MN) and a NanoDMA 06 transducer, equipped with a conospherical diamond indenter tip of ~4.7 μm radius. The measurements were conducted at ambient conditions, at 26.4 °C and 44.8% relative humidity (RH) for polymers **a** and **c**, at 30.0 °C and 38% RH for polymer **b**, measured with a Voltcraft DL-141TH data logger. For the other samples **f** to **h**, the sample compartment of the TriboIndenter was purged with dried air before the measurements to lower the humidity the samples were exposed to. The measurements were started after equilibration of the relative humidity (RH) at $5 \pm 1\%$ and a temperature of 26.4 ± 1.2 °C. For quasi-static testing, an open loop load function with a 1-s loading, 2-s hold at maximum load, and 1-s unloading profile was applied to the polymers **a** to **c** with indent forces between 100 and 2000 μN. For the softer polymers **f** to **h**, a different protocol was used with 10 s loading, 10 s hold at maximum load, and unloading in 1 s with indent forces between 75 and 300 μN.[40] All measurements for each sample were performed in a single automated run in less than 3 h using a 4 × 4 array piezo automation. The reduced modulus E_r was determined from the unloading response utilizing the analysis method proposed by Oliver and Pharr.[41] Values were averaged from at least 10 measurements each. From the reduced modulus E_r, the indentation modulus E_i was calculated using the elastic modulus and Poisson's ratio of the diamond indenter, 1140

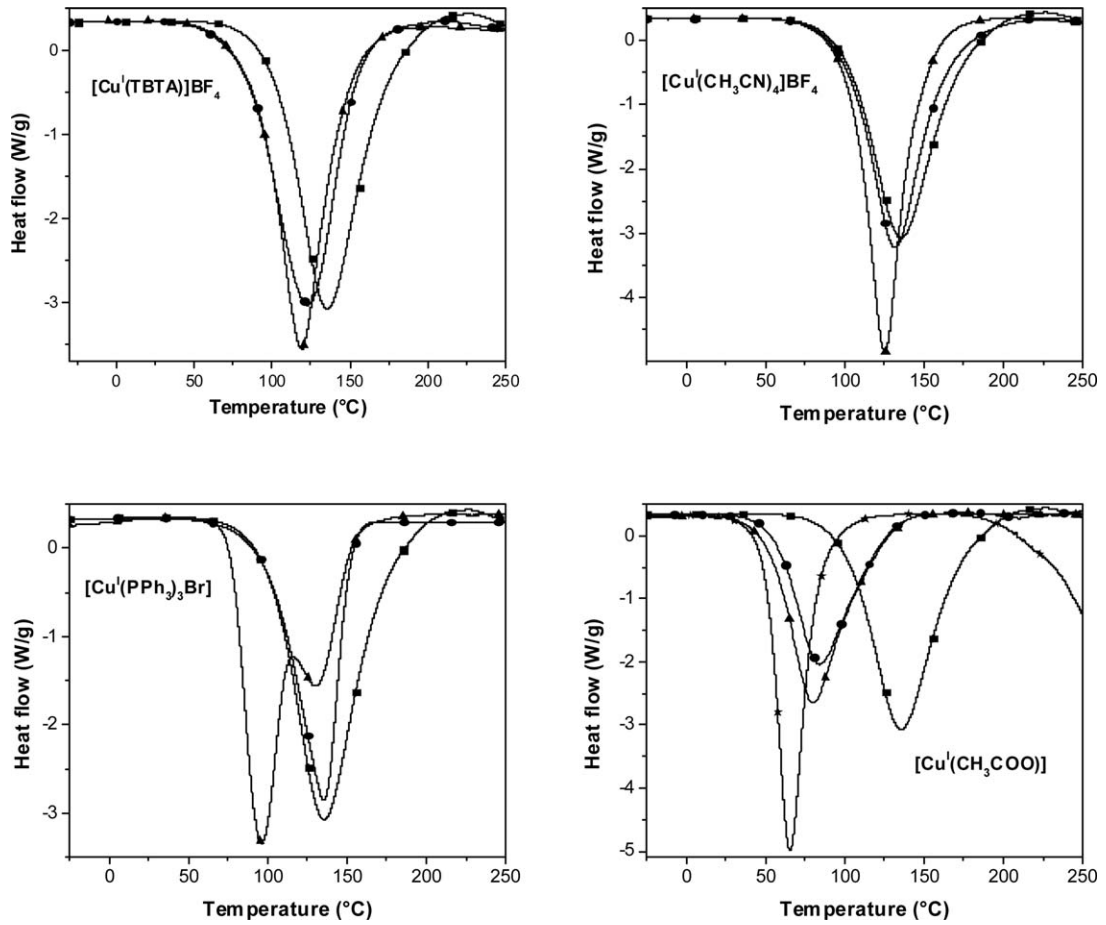

FIGURE 2 DSC traces (exothermic direction: down) for the neat polymerization of **1** and **3** depending on the copper(I) source and its concentration [(■) 0 mol %, (•) 0.5 mol %, (▲) 1 mol % and (⋆) 2 mol % of copper(I)].

GPa and 0.07, respectively, and a Poisson's ratio of 0.4 for the polymeric material, according to

$$E_{i,\text{sample}} = \frac{1-\nu^2_{\text{sample}}}{\frac{1}{E_{r,\text{sample}}} - \frac{1-\nu^2_{\text{indenter}}}{E_{\text{indenter}}}} \quad (1)$$

The hardness has the normal definition:

$$H = \frac{p_{\max}}{A} \quad (2)$$

RESULTS AND DISCUSSION

Catalyst Screening

First, different Cu(I) sources have been studied in order to identify a highly efficient catalyst for the solvent-free

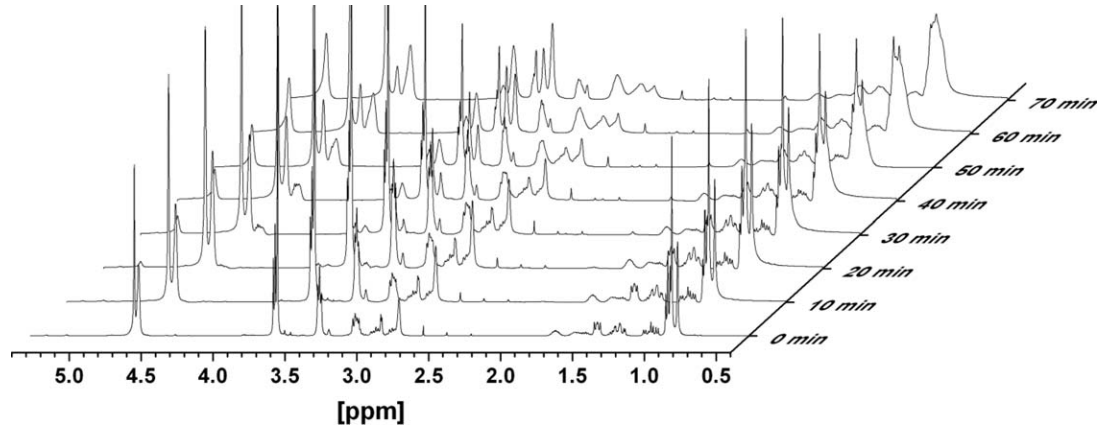

FIGURE 3 ^{1}H NMR spectra ($CDOD_3$, 1.5 mol % CuOAc, 32 °C) of the polymerization of **1** and **3** monomers.

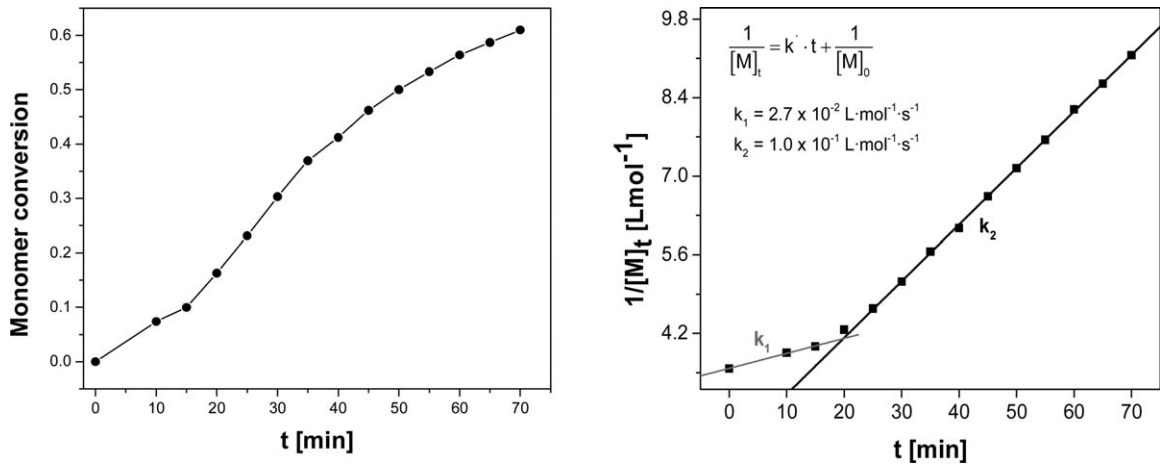

FIGURE 4 Left: Monomer conversion of azide **1** over time. Right: Second-order linearization where [M]t is the monomer concentration at a certain time.

cycloaddition (Scheme 2). For the screening of different copper salts **1** and **3** were chosen as model system (Scheme 1). The amount of catalyst was varied from 0.5 to 2 mol %. DSC measurements were performed in a temperature range of −20 to 250 °C with a constant heating rate of 10 K min^{-1}.

The catalyst efficiency was correlated with the temperature shift of the exothermic click reaction, whereby the noncatalyzed reaction served as a reference (temperature onset at 70 °C). It was assumed that in case of a larger shift (of the DSC curve) to lower temperatures, the catalyst contribution to the reaction is higher. The higher contribution to the

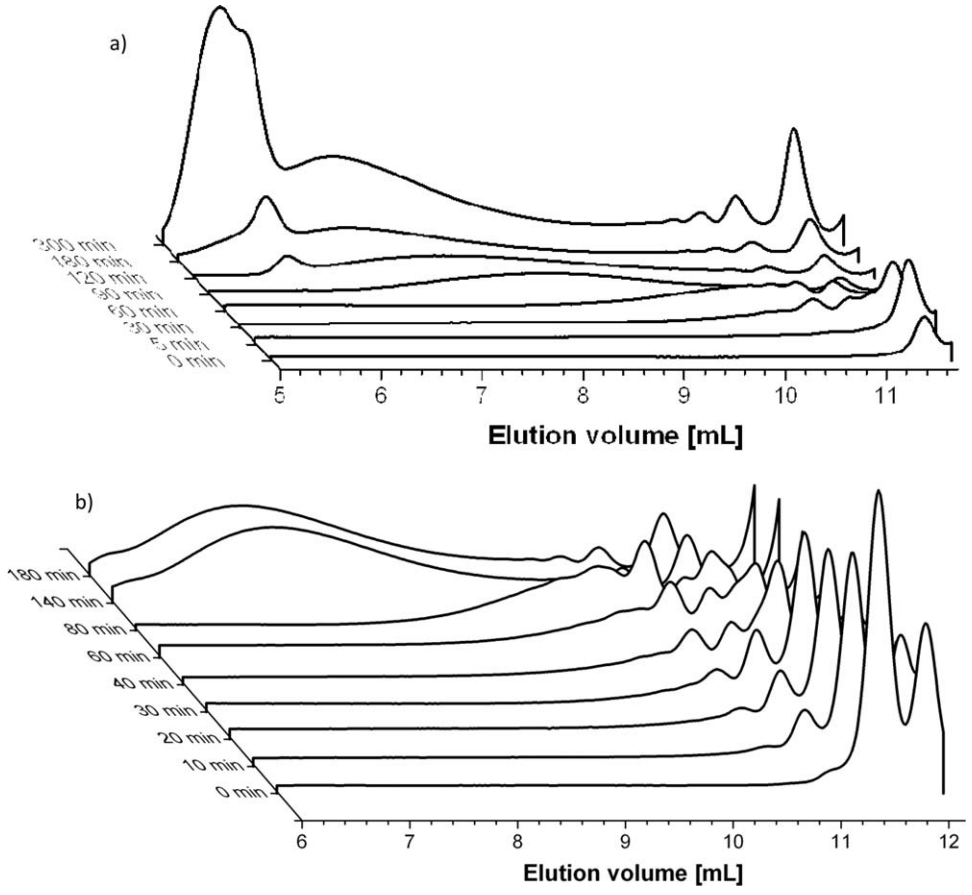

FIGURE 5 SEC analyses of the polymerization processes (DMSO-d_6, DMF-d_7, 1.5 mol % CuOAc, 32 °C) of the TEG-$(N_3)_2$ and the urethane-bisalkyne monomers. (a) Deuterated dimethyl sulfoxide and (b) deuterated DMF as solvents.

TABLE 1 Composition of Polymers, Catalyst Concentrations, and Corresponding *E*-Moduli

Polymer	Monomer I	Monomer II	Monomer III	CuOAc Concentration (mol %)	Indentation Modulus (GPa)
a	**5**	**1**	**4**	0.25	6.25 ± 0.4
b	**5**	**2b**		0.25	5.78 ± 0.14
c	**5**	**2a**		0.25	5.6 ± 0.5
d	**5**	**1**		0.25	0.086 ± 0.028
e	**7**	**1**		0.25	0.038 ± 0.003
f	**6**	**1**		0.25	0.038 ± 0.004

reaction results at least in a higher copper catalyst efficiency. The integration of the individual peaks (Fig. 2) provides the reaction heat ΔH, generated during the reaction. The reaction heat ΔH of the polyaddition was in the range of 560 kJ mol^{-1}. In case of the CuAAC polyaddition of tetraethylene glycol diyne and bisphenol A bisazide as well as tetraethylene glycol diyne/bisphenol E bisazide the reaction heat is in the range of 396–419 kJ mol^{-1} by applying different catalysts.[31] The commonly used copper salts $Cu(TBTA)BF_4$ and $Cu(CH_3CN)_4BF_4$ revealed a relatively low-temperature shift (Fig. 2). Hence, the reaction mainly proceeds uncatalyzed and shows only a minor contribution of the catalyst. In case of $Cu(PPh_3)_3Br$, there is a significant shift of the onset temperature from 95 °C (no catalyst) to 75 °C with a catalyst concentration. of 1.0 mol %. When a concentration of 1.0 mol % is used, the reaction seems to be mainly driven by the catalyst. However, there is still a copper-free contribution to the reaction, which is depicted in a small shoulder next to the main peak (see Fig. 4 bottom left). The largest change in initiation temperature was observed with. The amount of added catalyst has a remarkable effect on the initiation temperature. The uncatalyzed reaction starts at 90 °C and can be lowered to at least 45 °C (2.0 mol % CuOAc). This catalytic system showed by far the highest efficiency and may lead to carbonization at room temperature.

Click Polymerization in Solution

Kinetic Studies by ^1H NMR Spectroscopy

In order to obtain information on the kinetics of the CuAAC step-growth copolymerization in solution ^1H NMR studies were performed using CD_3OD as solvent. The reaction of bifunctional monomers **1** and **3** (Scheme 1) served as a model system, whereby an equimolar monomer ratio was used. The reaction was performed at 32 °C with a CuOAc concentration of 1.5 mol %. The ^1H NMR spectra are depicted in Figure 3 in a time period of 70 min. For the kinetic analysis, only the data below 70 min were taken into account. After 70 min, a signal broadening was observed and, therefore, a reliable interpretation was not possible anymore. The conversion of the copper-catalyzed step-grow polymerization was observed by the change of characteristic signals. The decrease of the azide methylene group ($—CH_2—N_3$) of monomer **1** at 3.38 ppm was correlated with the methyl protons of monomer **3** (0.6–1.7 ppm), in which the methyl protons were used as an internal standard. The conversions of the monomers were calculated by integration of the ^1H NMR spectra. The azide conversion rates versus reaction time are presented in Figure 4.

The plot of the reziproke azide monomer concentration ($1/[M]t$) versus the reaction time (t) is depicted in Figure 4. By linearization it could be proven that the polymerization is

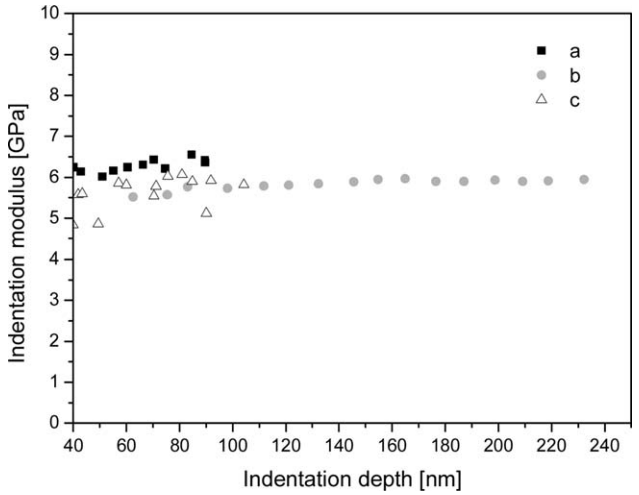

FIGURE 6 Indentation modulus versus indentation depth of the polymers **a**, **b**, and **c.**

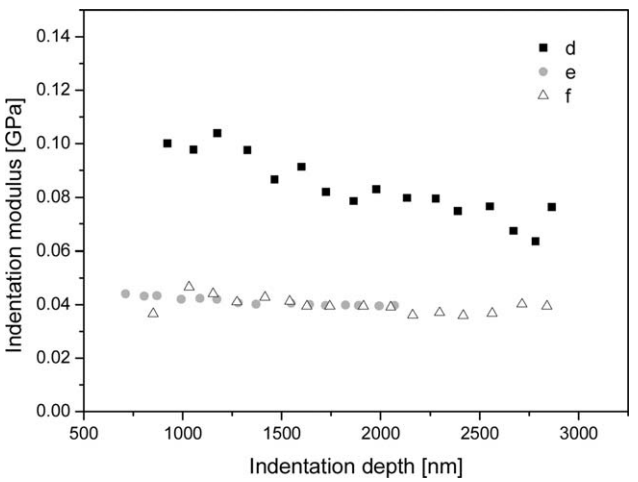

FIGURE 7 Indentation modulus versus indentation depth of the polymers **d**, **e**, and **f.**

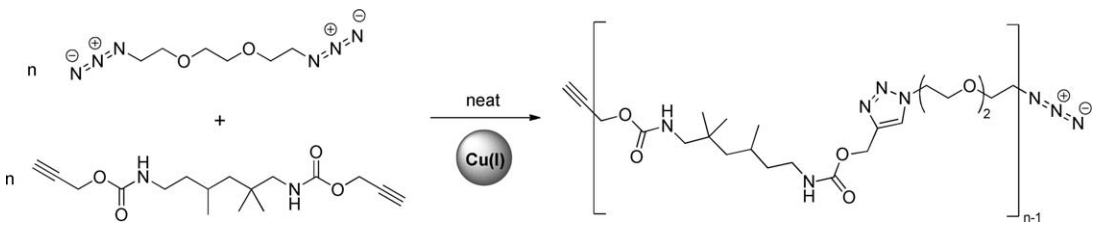

SCHEME 2 Schematic representation of the different copper catalysts for the Huisgen [3+2] cycloaddition reaction under solvent-free conditions.

following a second-order kinetics with external catalysis with an induction period of about 20 min ($k_1 = 2.7 \times 10^{-2}$ L mol^{-1} s^{-1}). The short induction period can be explained by the formation of the active catalyst species. After the active catalyst has been formed, the reaction experiences a rate acceleration of about one order of magnitude ($k_2 = 1.0 \times 10^{-1}$ L mol^{-1} s^{-1}).

Size Exclusion Chromatography

As a second method, SEC was used to investigate the kinetics of the CuAAC reaction shown in Scheme 1. The aim of this characterization strategy was to elucidate the achievable molar masses by the CuAAC reactions. The molar monomer ratio was 1:1. The reactions were performed at 32 °C with a CuOAc concentration of 1.5 mol % using two different solvents. In deuterated dimethylformamide, the reaction progress did not significantly change after 180 min and in deuterated methanol (for the comparability of the ^{1}H NMR kinetics) after 260 min (Fig. 5), respectively.

After 10 min reaction time, a slight increase of oligomeric reaction products is noticeable in case of DMF (Fig. 5) correlating with a decrease of monomer concentration (elution volume of 11.4 mL). After a reaction time of 80 min (DMF) polymers are formed. In case of DMSO as solvent, the reaction tends to the formation of oligomers after a reaction time of 5 min. After 300 min, the molar masses did not increase further. In dimethylformamide molar masses (M_n) of 17,000 g mol^{-1} (PDI = 1.76) can be observed corresponding to a degree of polymerization (DP) of 33. In contrast to DMF molar masses of 166,000 g mol^{-1} (PDI = 2.40) were obtained with a DP of 318 in dimethyl sulfoxide. The relative high molar masses achieved in DMSO in comparison to DMF can be explained by the higher solubility of the polymer and catalyst in DMSO.

Bulk Polymerization

For the polymerization, the alkyne **5** was activated by stirring with the CuOAc for several hours. Thereby, the catalyst concentration could be reduced to 0.25 mol % of CuOAc (Table1). A concentration above 0.25 mol % copper(I) acetate led to carbonization in most cases. Afterward, the azide was added to the monomer/catalyst mixture. The CuAAC reactions were performed under nitrogen for 24 h at room temperature. Afterward, the samples were heated up to 50 °C on a heating plate to maximize the conversion rate. For comparison, a commercial polycarbonate standard sample from Hysitron was used as a reference system (for additional information see the Supporting Information). The mechanical properties of the polymers were correlated with the azide conversion of the monomer by ATR-IR. The reaction progress was followed by the change of the azide absorption band at 2100 cm^{-1} and azide conversions rates of >95% could be achieved in all cases (Table 1). With a quantitative azide conversion polymer **b** exhibited an *E*-modulus of 5.78 ± 0.14 GPa (Table 1). Surprisingly, choosing a more flexible monomer **2a** lead to the indentation modulus of 5.6 ± 0.5 GPa (polymer **c**). Although the azide conversions of polymers **d**, **e**, and **f** have been quantitatively, the *E*-moduli were extremely low. The TEG-bisazide monomer decreases the network density as well as rigidity, which leads to a flexible soft material. With polymer **a**, the network density is believed to be increased and a maximum of 6.25 ±0.4 GPa could be achieved.

Figures 6 and 7 show the indentation moduli, separated into two series for polymers **a–c** and polymers **d–f**, which were used to calculate the averaged indentation moduli for (Table 1). The polymers **a–c, e**, and **f** are nearly independent from the indentation depth, whereas polymer **d** shows a decrease with increasing indentation depth because of inhomogeneity of the polymerized material. The load-displacement responses are shown in the Supporting Information.

CONCLUSIONS

By applying different Cu(I)-salts for the solvent-free click-polyaddition, CuOAc was identified as the most efficient catalyst. It could be shown that the copper(I)-catalyzed cycloaddition follows the trend of a second-order step–growth polymerization with external catalysis after an indication period of 20 min. The achievable molar masses by using the CuAAC strongly depended on the solvents and the solubility of the polymers. For DMSO-d_6, molar masses (M_n) of 166,000 g mol^{-1} could be achieved in comparison to DMF-d_7 where only molar masses of 17,000 g mol^{-1} were obtained. The obtained indentation modulus of 6.25 GPa ± 0.4 make these polymers interesting for a variety of applications.

ACKNOWLEDGMENT

The authors thank Ivoclar Vivadent and the Dutch Polymer Institute (DPI, technology area HTE) for financial support.

REFERENCES AND NOTES

1 V. V. Rostovtsev, L. G. Green, V. V. Fokin, K. B. Sharpless, *Angew. Chem. Int. Ed.* **2002**, *41*, 2596–2599.

2 C. W. Tornoe, C. Christensen, M. Meldal, *J. Org. Chem.* **2002**, *67*, 3057–3064.

3 M. A. Tasdelen, *Polym. Chem.-UK* **2011**, *2*, 2133–2145.

4 A. B. Lowe, *Polym. Chem.-UK* **2010**, *1*, 17–36.

5 M. Meldal, *Macromol. Rapid Commun.* **2008**, *29*, 1016–1051.

6 C. R. Becer, R. Hoogenboom, U. S. Schubert, *Angew. Chem. Int. Ed.* **2009**, *48*, 4900–4908.

7 F. Kloss, U. Kohn, B. O. Jahn, M. D. Hager, H. Goerls, U. S. Schubert, *Chem. Asian J.* **2011**, *6*, 2816–2824.

8 K. Kempe, R. Hoogenboom, M. Jaeger, U. S. Schubert, *Macromolecules* **2011**, *44*, 6424–6432.

9 A. R. Katritzky, N. K. Meher, S. Hanci, R. Gyanda, S. R. Tala, S. Mathai, R. S. Duran, S. Bernard, F. Sabri, S. K. Singh, J. Doskocz, D. A. Ciaramitaro, *J. Polym. Sci. Part A: Polym. Chem.* **2008**, *46*, 238–256.

10 U. Mansfeld, C. Pietsch, R. Hoogenboom, C. R. Becer, U. S. Schubert, *Polym. Chem.* **2010**, *1*, 1560–1598.

11 K. Kempe, A. Krieg, C. R. Becer, U. S. Schubert, *Chem. Soc. Rev.* **2012**, *41*, 176–191.

12 M. Meldal, C. W. Tornøe, *Chem. Rev.* **2008**, *108*, 2952–3015.

13 H. Nandivada, X. Jiang, J. Lahann, *Adv. Mater.* **2007**, *19*, 2197–2208.

14 J. E. Moses, A. D. Moorhouse, *Chem. Soc. Rev.* **2007**, *36*, 1249–1262.

15 W. H. Binder, R. Sachsenhofer, *Macromol. Rapid Commun.* **2007**, *28*, 15–54.

16 W. H. Binder, R. Sachsenhofer, *Macromol. Rapid Commun.* **2008**, *29*, 952–981.

17 H. Struthers, T. L. Mindt, R. Schibli, *Dalton Trans.* **2010**, *39*, 675–696.

18 P. L. Golas, K. Matyjaszewski, *Chem. Soc. Rev.* **2010**, *39*, 1338–1354.

19 J. A. Opsteen, J. C. M. van Hest, *J. Polym. Sci. Part A: Polym. Chem.* **2007**, *45*, 2913–2924.

20 H. Gao, K. Matyjaszewski, *Macromolecules* **2006**, *39*, 4960–4965.

21 H. Durmaz, A. Dag, E. Erdogan, A. L. Demirel, G. Hizal, U. Tunca, *J. Polym. Sci. Part A: Polym. Chem.* **2010**, *48*, 99–108.

22 D. Wu, X. Song, T. Tang, H. Zhao, *J. Polym. Sci. Part A: Polym. Chem.* **2010**, *48*, 443–453.

23 J. Yin, Z. Ge, H. Liu, S. Liu, *J. Polym. Sci. Part A: Polym. Chem.* **2009**, *47*, 2608–2619.

24 J. L. Mynar, T.-L. Choi, M. Yoshida, V. Kim, C. J. Hawker, J. M. J. Frechet, *Chem. Commun.* **2005**, 5169–5171.

25 P. Wu, M. Malkoch, J. N. Hunt, R. Vestberg, E. Kaltgrad, M. G. Finn, V. V. Fokin, K. B. Sharpless, C. J. Hawker, *Chem. Commun.* **2005**, 5775–5777.

26 C. Ornelas, J. Ruiz Aranzaes, E. Cloutet, S. Alves, D. Astruc, *Angew. Chem. Int. Ed.* **2007**, *46*, 872–877.

27 S. Binauld, D. Damiron, T. Hamaide, J. P. Pascault, E. Fleury, E. Drockenmuller, *Chem. Commun.* **2008**, 4138–4140.

28 B. Sandmann, B. Happ, J. Vitz, M. D. Hager, P. Burtscher, N. Moszner, U. S. Schubert, *Polym. Chem.-UK* **2013**, *4*, 3938–3942.

29 M. Gragert, M. Schunack, W. H. Binder, *Macromol. Rapid Commun.* **2011**, *32*, 419–425.

30 M. Schunack, M. Gragert, D. Dohler, P. Michael, W. H. Binder, *Macromol. Chem. Phys.* **2012**, *213*, 205–214.

31 X. Sheng, T. C. Mauldin, M. R. Kessler, *J. Polym. Sci. Part A: Polym. Chem.* **2010**, *48*, 4093–4102.

32 F. Himo, T. Lovell, R. Hilgraf, V. V. Rostovtsev, L. Noodleman, K. B. Sharpless, V. V. Fokin, *J. Am. Chem. Soc.* **2005**, *127*, 210–216.

33 S. Binauld, F. Boisson, T. Hamaide, J. P. Pascault, E. Drockenmuller, E. Fleury, *J. Polym. Sci. Part A: Polym. Chem.* **2008**, *46*, 5506–5517.

34 D. Wang, N. Li, M. M. Zhao, W. L. Shi, C. W. Ma, B. H. Chen, *Green Chem.* **2010**, *12*, 2120–2123.

35 S. Lal, S. Diez-Gonzalez, *J. Org. Chem.* **2011**, *76*, 2367–2373.

36 X. Sheng, D. M. Rock, T. C. Mauldin, M. R. Kessler, *Polymer* **2011**, *52*, 4435–4441.

37 J. Rey, F. C. García, J. M. García, *React. Funct. Polym.* **2011**, *71*, 948–957.

38 P. S. Donnelly, S. D. Zanatta, S. C. Zammit, J. M. White, S. J. Williams, *Chem. Commun.* **2008**, 2459–2461.

39 S. T. Abu-Orabi, R. E. Harmon, *J. Chem. Eng. Data* **1986**, *31*, 379–380.

40 E. F. J. Rettler, J. M. Kranenburg, H. M. L. Lambermont-Thijs, R. Hoogenboom, U. S. Schubert, *Macromol. Chem. Phys.* **2010**, *211*, 2443–2448.

41 W. C. Oliver, G. M. Pharr, *J. Mater. Res.* **1992**, *7*, 1564–1583.

Publication P4

"Photoinduced polyaddition of multifunctional azides and alkynes"

B. Sandmann, B. Happ, J. Vitz, M. D. Hager, P. Burtscher, N. Moszner, U. S. Schubert

Polym. Chem. **2013**, *4*, 3938-3942.

Polymer Chemistry

RSC Publishing

PAPER

View Article Online
View Journal | View Issue

Cite this: *Polym. Chem.*, 2013, **4**, 3938

Photoinduced polyaddition of multifunctional azides and alkynes

Benedict Sandmann,[ab] Bobby Happ,[abc] Jürgen Vitz,[abc] Martin D. Hager,[ab] Peter Burtscher,[d] Norbert Moszner*[d] and Ulrich S. Schubert*[abc]

Received 17th March 2013
Accepted 23rd April 2013

DOI: 10.1039/c3py00356f

www.rsc.org/polymers

The photoinduced copper(I)-catalyzed polymerization of multifunctional azides and alkynes is facilitated by the photoreduction of copper(II) acetate generating copper(I) ions without using any additional photoinitiator. The polymerization can only be carried out in solution using at least 15 wt% of methanol. Depending on the catalyst concentration quantitative monomer conversions can be achieved allowing the determination of the mechanical properties. The bifunctional system consisting of a di-azide and di-alkyne exhibited the highest Young's modulus value of 1600 MPa.

Introduction

In the 1960s, 1,3-dipolar cycloaddition was extensively studied by Rolf Huisgen, among others in particular the non-catalyzed reaction of organic alkynes and organic azides. The discovery of the Cu^{I}-catalyzed azide–alkyne cycloaddition (CuAAC) by the groups of Meldal and Sharpless in 2002 has accelerated the application of this chemical transformation and represents nowadays the most prominent example of click chemistry. Due to its high tolerance to a large range of building blocks and, generally, with the generation of minor (or conveniently separable) by-products it has found a wide range of applications ranging from drug discovery over polymer chemistry to materials science.[1–7]

The required Cu^{I} catalyst can be generated by several approaches in which the most common methods include (i) *in situ* reduction of Cu^{II} to Cu^{I} by various reducing agents or *via* photoreduction, (ii) direct addition of Cu^{I} salts or as Cu^{I}-based triazolylidene carbene complexes, (iii) addition of ligand-stabilized Cu^{I} salts [*tris*(1-benzyl-1*H*-1,2,3-triazol-4-yl)methylamine) (TBTA), *N*,*N*-diisopropylethylamine (DIPEA)], or (iv) using metallic copper (generation by comproportionation of Cu^{0} and Cu^{II}).[1]

Photoinduced reduction of copper(II) complexes can be performed by either direct or indirect photolysis. For the indirect approach, the reduction of the Cu(II) ion results from a reaction with a photoactivator. The photoactivator absorbs light in the ultraviolet or visible region of the electromagnetic spectrum, where the copper complex is light-transmissive and forms reactive intermediates (usually radicals) which provoke the photoreduction of Cu(II) into Cu(I). This method often suffers from undesired side-reactions and the production of undesired byproducts.[8–10]

Direct photolysis generates the desired metal ion upon irradiation of its higher oxidation state species at appropriate wavelengths. In particular copper(II) complexes are able to undergo an intramolecular electron transfer from the π-system of the ligand to the metal ion (ligand-to-metal charge transfer character) resulting in the photoreduction of Cu(II) into Cu(I) species.[11–13] The photoinduced copper(II) catalysis has been used to achieve spatial and temporal control of the CuAAC.[14]

For applications in materials science the 1*H*-1,2,3-triazole heterocycles proved to be a stable linking unit creating advanced block copolymers and polymer networks.[15–17] Recently, the group of Bowman could manage the first CuAAC bulk photopolymerization of multifunctional alkyne and azide monomers using a radical-generating photoinitiator, which was carried out from low molar mass, non-viscous monomer resins. This approach readily provided high glass transition temperature polymers that contained 1*H*-1,2,3-triazole linkages throughout the polymer network.[18]

In our approach several copper(II) salts were tested towards facilitating a photoinduced polymerization of multifunctional azides and alkynes by CuAAC without using a radical-generating photoinitiator. The Young's modulus of the materials was determined by nano-indentation measurements. Depending on the average functionality of the monomer systems used, significant differences in the indentation modulus values were observed.

Experimental section

Materials

All copper(II) salts were acquired from commercial sources and used without further purification. Copper(II) acetate shows an

[a]*Laboratory of Organic and Macromolecular Chemistry (IOMC), Friedrich Schiller University Jena, Humboldtstraße 10, 07743 Jena, Germany. E-mail: ulrich.schubert@uni-jena.de; Fax: +49(0) 3641 9482 02*

[b]*Jena Center for Soft Matter (JCSM), Friedrich Schiller University Jena, Philosophenweg 7, 07743 Jena, Germany*

[c]*Dutch Polymer Institute (DPI), P.O. Box 902, 5600 AX Eindhoven, The Netherlands*

[d]*Ivoclar Vivadent AG, Bendererstrasse 2, FL-9494 Schaan, Liechtenstein. E-mail: norbert.moszner@ivoclarvivadent.com*

absorption maximum at $\lambda_{max} = 247$ nm ($\varepsilon = 3250\ M^{-1}cm^{-1}$) in methanolic solution. Tripropargylamine was purchased from Aldrich. Tetra-alkyne **4** was synthesized according to a literature procedure.[19] The solvents were dried and distilled according to standard procedures and stored under nitrogen.

All photopolymerizations were carried out on a glass substrate. The solutions were irradiated with a Xenon photoflash lamp (320 to 520 nm) using a Kulzer Dentacolor XS (270 W; flash frequency = 20 Hz).

Instrumentation

1D (^{1}H, ^{13}C) and 2D (HSQC) NMR spectra were recorded on a Bruker AC 300 (300 MHz) at 25 °C. Chemical shifts are reported in parts per million (ppm, δ scale) relative to the residual signal of the deuterated solvent. Standard abbreviations are used for denoting the signal multiplicity.

ESI-Q-TOF-MS measurements were performed using a microTOF (Bruker Daltonics) mass spectrometer equipped with an automatic syringe pump, which is supplied from KD Scientific for sample injection. The mass spectrometer was operated in the positive-ion mode. Elemental analysis was carried out on a CHN-932 Automat Leco instrument.

The mechanical properties of the samples were characterized *via* depth-sensing indentation (DSI) using a TriboIndenter TI 900 (Hysitron Inc.) and a NanoDMA 06 transducer equipped with a conospherical diamond indenter tip of 4.7 μm radius. The measurements were conducted under ambient conditions controlled by a Voltcraft DL-141 TH data logger. The measurements were started after equilibration at a relative humidity of 5 ± 1% and a temperature of ±1.2 °C. For quasi-static testing, an open loop load function with a 1 s loading, a 2 s hold at maximum load, and a 1 s unloading profile was applied to the polymers with indent forces between 75 and 300 μN.[20] All measurements for each sample were performed in a single automated run in less than 3 h using a 4 × 4 array piezo automation. The reduced modulus E_r was determined from the unloading response utilizing the analysis method proposed by Oliver and Pharr.[21] The values were averaged from at least ten measurements each. From the reduced modulus E_r, the indentation modulus E_i was calculated using the elastic modulus and the Poisson's ratio of the diamond indenter (1140 GPa and 0.07, respectively) and the Poisson's ratio of the polymeric material (0.4).

Synthesis of 1,2-bis(2-azidoethoxy)ethane (1)

To a solution of triethylene glycol *bis*(4-toluenesulfonate) (21.8 mmol, 10 g) in DMSO (130 mL), sodium azide (65 mmol, 4.25 g) was added in a round bottom flask. The reaction mixture was stirred at room temperature for 48 h. The reaction was quenched with water (100 mL). The product was extracted with diethyl ether and the organic phase was washed with water (3 × 50 mL). After drying over $MgSO_4$ and evaporation of the solvent, the product was obtained as a yellow oil (4.32 g, 98%). ^{1}H NMR (300 MHz, $CDCl_3$, δ): 3.70–3.66 (m, 8H), 3.38 (t, $J = 5$ Hz, 4H); ^{13}C NMR (75 MHz, $CDCl_3$, δ): 70.7, 70.1, 50.7. Anal. calcd for $C_6H_{12}N_6O_2$: C, 36.00%; H, 6.04%; N, 41.98%; found: C, 36.25%; H, 5.79%; N, 42.08%.

Synthesis of di(prop-2-yn-1-yl) (2,2,4-trimethylhexane-1,6-diyl) dicarbamate (2)

To a solution of 1,6-diisocyanato-2,2,4-trimethylhexane (23.8 mmol, 5 g, positional isomeric mixture) and dibutyltin(II)-dilaurate (0.0004 eq.) in toluene (10 mL) was added prop-2-yn-1-ol (47.6 mmol, 2.61 g) dropwise within 15 min. The reaction mixture was stirred at 60 °C for 48 h. After evaporation of the solvent and running through a short pad of silica the product was obtained as a viscous, yellow oil (7.51 g, 98%). ^{1}H NMR (300 MHz, $CDCl_3$, δ): 5.14–4.91 (br, 2H; N–H), 4.65 (br, 4H; C(O)O–CH_2), 3.20–2.88 (m, 4H; NH–CH_2), 2.46 (d, $J = 1.8$ Hz, 2H; C≡CH), 1.70–1.22 (br, 3H), 1.05–0.86 (m, 11H; CH_2, CH_3); ^{13}C NMR (75 MHz, $CDCl_3$, δ): 155.8, 155.7, 155.4, 129.0, 128.2, 125.3, 78.4, 74.6, 74.5, 52.5, 52.3, 51.4, 48.6, 46.4, 45.9, 41.9, 39.2, 39.1, 37.4, 35.0, 32.9, 29.4, 27.4, 26.1, 25.5, 25.1, 22.3, 21.4, 20.5; EIMS (*m*/*z* (%)): 345.18 (100) [M^+ + Na]; Anal. calcd for $C_{17}H_{26}N_2O_4$: C, 63.33%; H, 8.13%; N, 8.69%; found: C, 63.07%; H, 7.91%; N, 8.83%.

General procedure for the Cu(I)-catalyzed polyaddition

Safety note. The copper(I)-catalyzed polyaddition of multifunctional alkynes (at least three alkyne groups per molecule) with copper(II) acetate as the catalyst source may lead to inflammation upon irradiation at catalyst concentrations above 3 mol%.

The multifunctional alkyne and the bis-azide **1** were charged in a small glass vial using an equimolar ratio and were stirred for 10 min. After that, the respective solvent (MeOH, EtOH, DMF, 15–50 wt%) and, subsequently, the copper(II) catalyst was added (0.5 to 3 mol%) and the solution was stirred for another 5 min until the copper salt had been dissolved. The solution was deposited in a metal or Teflon ferrule (0.5 to 1 mm height, 15 mm inside diameter) placed on a glass slide using a 1 mL syringe. The glass slide was inserted into the Kulzer Dentacolor and irradiated for 180 s. The cured polymer reference block was suitable for nano-indentation measurements.

Results and discussion

The aim of the photoinduced polymerization was to reduce copper(II) to copper(I) ions by light excitation using a Xenon photoflash lamp (spectral range of light emission: 320 to 520 nm) and, consequently, gaining control over the initiation of the polyaddition. The monomers depicted in Fig. 1 were used to engineer different model systems with an average functionality equal or greater than two.

The bifunctional system consisting of 1,2-bis(2-azidoethoxy)-ethane and di(prop-2-yn-1-yl) (2,2,4-trimethylhexane-1,6-diyl)-dicarbamate served as a model system in order to study the solubility of different copper(II) salts in a neat reaction regime.

Di-μ-hydroxo-*bis*[(*N*,*N*,*N*′,*N*′-tetramethylethylenediamine)-copper(II)] chloride (Cu[TMEDA]Cl_2) and copper(II) triflate have emerged to be soluble in the neat bifunctional system (Table 1). However, these salts were unable to launch the copper-catalyzed

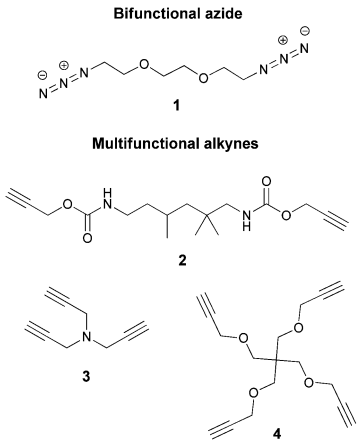

Fig. 1 Schematic representation of the monomers used for the photoinduced CuAAC.

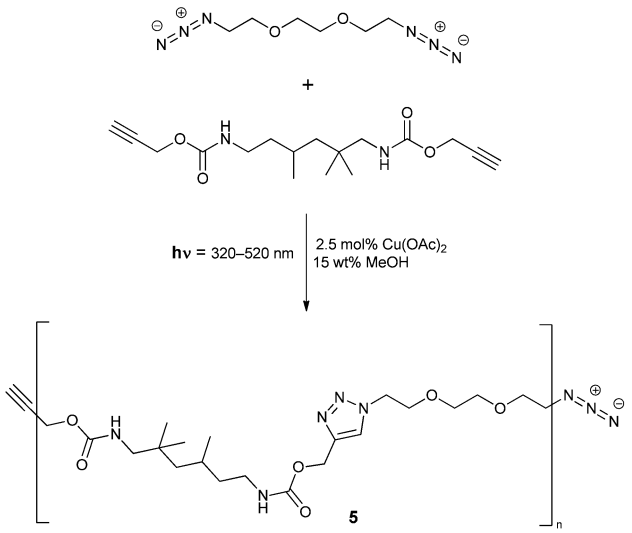

Scheme 1 Schematic representation of the photoinitiated CuAAC polyaddition of monomers **1** and **2**.

polyaddition when irradiating with light. The only copper(II) salt being photocatalytically active without additional photoinitiator was copper(II) acetate in which a solvent (methanol, DMF) has to be present (weight fraction greater than 15%) (Scheme 1). The use of methacrylate-based solvents (2-hydroxyethyl methacrylate), which could have been utilized in a post-polymerization process, failed due to the insolubility of copper(II) acetate.

The curing of the polymer was optimized by an appropriate adjustment of the photocatalysis conditions in the Kulzer device (catalyst and solvent content). A copper(II) acetate content of 2.5 mol% had to be used in order to successfully polymerize at an irradiation time of 180 s. Concentrations exceeding 5 mol% led to carbonization of the reaction mixture. The photopolymerization usually yielded yellow-brownish polymers (see the inset of Fig. 3), which were insoluble in common organic solvents. Hence, the obtained materials could not be studied by NMR spectroscopy or size exclusion chromatography. Attenuated total reflection infrared spectroscopy (ATR-IR) provided an estimation of the monomer conversion by using the asymmetric azide vibration at 2101 cm^{-1}. The monomer conversion exceeded 95% at a catalyst concentration of 2.5 mol% (Fig. 2).

The photopolymerized specimens of the bifunctional system were further suitable for the investigation of the mechanical properties by nano-indentation experiments. The addition of a silicon dioxide-based filler material (Aerosil® OX-50, Evonik) resulted in a general inhibition of the photopolymerization process and the generation of sticky surfaces whereby nano-indentation experiments were inapplicable.

The mechanical properties of the photopolymerized specimens with the monomers **1** and **2** were correlated with the monomer conversions obtained by ATR-IR spectroscopy. If the monomer conversion fell below 90% (catalyst concentration <2.5 mol%) the specimens were too soft and not useful for indentation measurements. The indentation modulus for 95%

Table 1 Solubilty of Cu(II) salts in a neat reaction mixture of monomers **1** and **2**

Structure	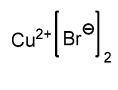	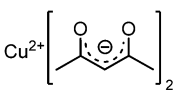	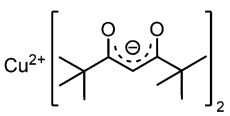	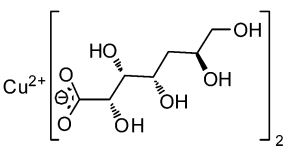
	$CuBr_2$	$Cu(acac)_2$	$Cu(TMHD)_2$	Cu(*D*-gluconate)$_2$
Solubility[a]	0	1	1	1
Structure	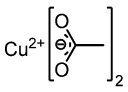	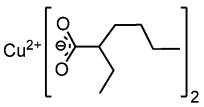	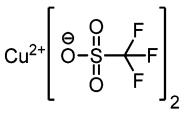	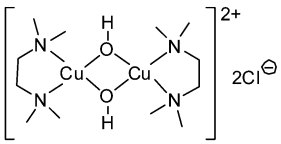
	$Cu(OAc)_2$	Cu(2-ethylhexanoate)$_2$	$Cu(triflate)_2$	$Cu(TMEDA)Cl_2$
Solubility[a]	1	1	5	4

[a] Scale 0 to 5, insoluble to highly soluble (relative scale).

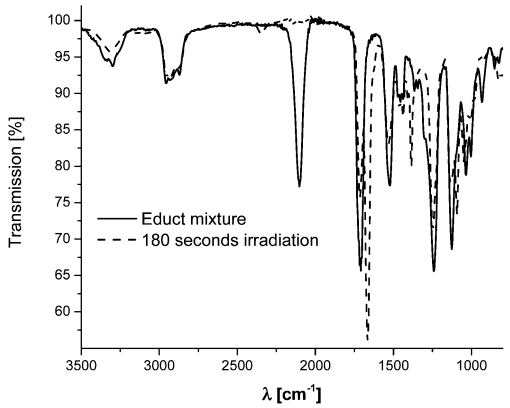

Fig. 2 ATR-IR spectra of monomer mixture **1** and **2** (solid line) and polymer **5** (dashed line).

monomer conversion of polymer **5** is depicted in Fig. 3 in dependence of the depth of indentation. The modulus stayed relatively constant over a depth of 1000 nm and, consequently, confirms the homogeneity of the material. A remarkably high average indentation modulus of 1.6 ± 0.1 GPa was obtained in spite of using flexible monomers as well as small amounts of a solvent. A commercial polycarbonate polymer (Hysitron PC standard 5-218, $E_r = 2.95$ GPa) was used as the reference system and an average indentation modulus of 3.1 ± 0.2 GPa was determined.

The photoinduced polymerization of the difunctional azide **1** and tripropargylamine (Scheme 2) can only be carried out in solution using at least 15 wt% of methanol; otherwise precipitation of the catalyst occurred. Similar observations for the catalyst behavior solubility (solubility and catalytic activity) were retrieved as for the bifunctional system. However, the threshold limit value of the catalyst concentration for almost quantitative monomer conversion dropped to 0.7 mol%; the trifunctional alkyne turned out to be more reactive than the bifunctional one. Uncontrollable reaction rates and carbonization has been already observed at copper(II) acetate concentrations of 2.5 mol%. When stirring a methanolic solution of the monomer mixture **1** and **3** with $Cu(OAc)_2$ (0.7 to 2.5 mol%) a color change from turquoise to

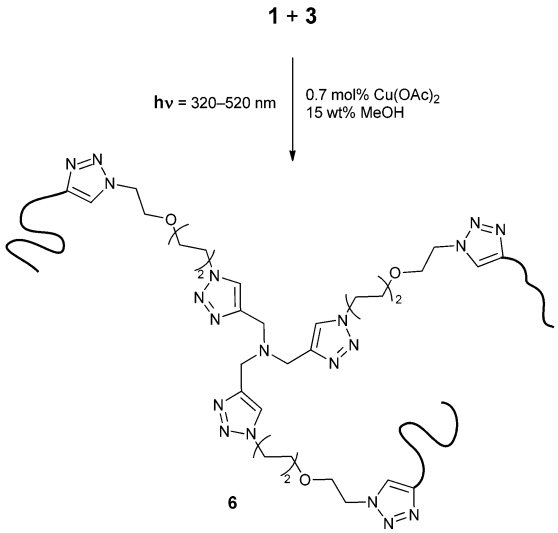

Scheme 2 Schematic representation of the photoinitiated crosslinking by CuAAC of monomers **1** and **3**.

colorless takes place within five minutes (Fig. 4). The catalyst activity highly depends on the color status and reaches its maximum at the colorless state. Thereby the reaction proceeds quantitatively and the colorless polymer **6** was obtained (see inset Fig. 5).

The average indentation modulus of **6** decreased by almost one order of magnitude compared to polymer **5** to 0.17 ± 0.03 GPa. Consequently, the depth of indentation of the tip is twice as much as for polymer **5** (constant applied force) (Fig. 5).

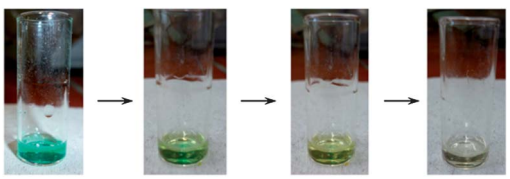

Fig. 4 Color change (at intervals of one minute) of the stock solution of **1** and **3** in MeOH (15 wt%) as well as $Cu^{II}(OAc)_2$ (1 mol%).

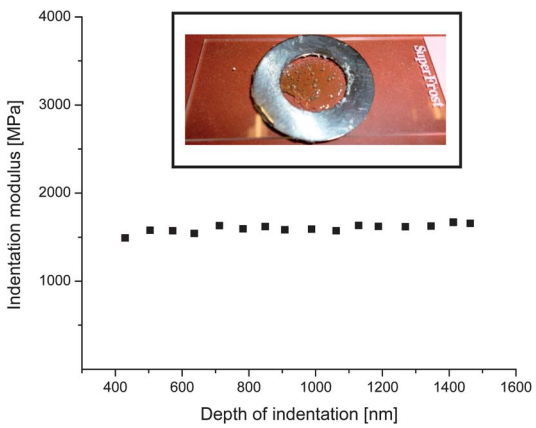

Fig. 3 Dependence of the indentation modulus on the depth of indentation of polymer **5** (monomer conversion >95%).

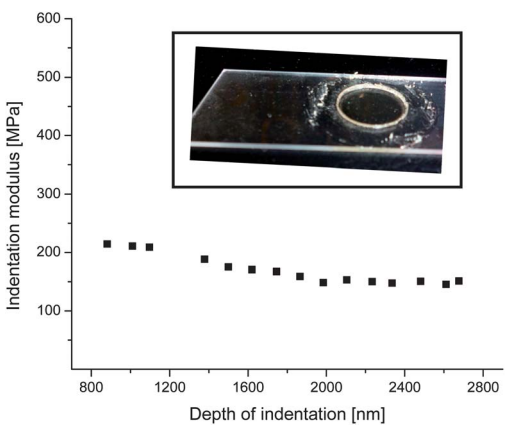

Fig. 5 Dependence of the indentation modulus on the depth of indentation of polymer **6** (monomer conversion >95%).

Furthermore, an overall decrease of the indentation modulus with the increasing depth of indentation was observed revealing an increase in softness of the material.

The reaction of monomers **1** and **4** showed an uncontrollable behavior. If the photopolymerization was carried out with a catalyst fraction below 0.5 mol% no conversion of the monomers could be observed. Using 0.5 mol% or larger amounts of catalyst led to combustion of the reaction mixture.

Conclusions

Among several copper(II) salts only copper(II) acetate is capable of facilitating the photoinduced copper(I)-catalyzed polymerization of multifunctional azides and alkynes by the photoreduction of copper(II) to copper(I) ions without any additional photoinitiator. The copper(I)-catalyzed azide–alkyne polyaddition can only be carried out in solution using at least 15 wt% of a solvent. Depending on the catalyst concentration in the different reaction regimes (bifunctional azide/bifunctional alkyne, bifunctional azide/trifunctional alkyne, bifunctional azide/tetrafunctional alkyne) quantitative monomer conversions can be achieved in which the controllability of the polymerization decreases with higher functionality. A quantitative conversion allowed the determination of the Young's modulus by nano-indentation experiments. The bifunctional system consisting of a di-azide and di-alkyne revealed the highest value of 1600 MPa. In future the development of hybrid-systems including a polymerizable solvent and the azide–alkyne photosystems will be in focus.

Acknowledgements

The authors thank Ivoclar Vivadent as well as the Dutch Polymer Institute (DPI, technology area HTE) for financial support.

Notes and references

1 M. Meldal and C. W. Tornøe, *Chem. Rev.*, 2008, **108**, 2952–3015.
2 W. H. Binder and R. Sachsenhofer, *Macromol. Rapid Commun.*, 2008, **29**, 952–981.
3 H. Nandivada, X. Jiang and J. Lahann, *Adv. Mater.*, 2007, **19**, 2197–2208.
4 J. E. Moses and A. D. Moorhouse, *Chem. Soc. Rev.*, 2007, **36**, 1249–1262.
5 K. Kempe, A. Krieg, C. R. Becer and U. S. Schubert, *Chem. Soc. Rev.*, 2012, **41**, 176–191.
6 H. C. Kolb and K. B. Sharpless, *Drug Discovery Today*, 2003, **8**, 1128–1137.
7 C. R. Becer, R. Hoogenboom and U. S. Schubert, *Angew. Chem., Int. Ed.*, 2009, **48**, 4900–4908.
8 Y. L. Chow and G. E. Buono-Core, *Can. J. Chem.*, 1983, **61**, 795–800.
9 Y. L. Chow, G. E. Buono-Core, B. Marciniak and C. Beddard, *Can. J. Chem.*, 1983, **61**, 801–808.
10 G. E. Buono-Core, A. H. Klahn, C. Bahamondes, F. Aros, M. Tejos and V. Astorga, *Inorg. Chim. Acta*, 1997, **257**, 241–245.
11 G. P. David and P. A. C. D. Silva, *Bull. Chem. Soc. Jpn.*, 1985, **58**, 3566–3569.
12 E. M. Glebov, V. F. Plyusnin, V. P. Grivin, S. A. Krupoder, T. I. Liskovskaya and V. S. Danilovich, *J. Photochem. Photobiol., A*, 2000, **133**, 177–183.
13 L. Harmand, S. Cadet, B. Kauffmann, L. Scarpantonio, P. Batat, G. Jonusauskas, N. D. McClenaghan, D. Lastécouères and J.-M. Vincent, *Angew. Chem., Int. Ed.*, 2012, **51**, 7137–7141.
14 M. A. Tasdelen and Y. Yagci, *Tetrahedron Lett.*, 2010, **51**, 6945–6947.
15 R. T. Chen, S. Marchesan, R. A. Evans, K. E. Styan, G. K. Such, A. Postma, K. M. McLean, B. W. Muir and F. Caruso, *Biomacromolecules*, 2012, **13**, 889–895.
16 M. A. Tasdelen, G. Yilmaz, B. Iskin and Y. Yagci, *Macromolecules*, 2011, **45**, 56–61.
17 B. J. Adzima, Y. Tao, C. J. Kloxin, C. A. DeForest, K. S. Anseth and C. N. Bowman, *Nat. Chem.*, 2011, **3**, 256–259.
18 T. Gong, B. J. Adzima, N. H. Baker and C. N. Bowman, *Adv. Mater.*, 2013, DOI: 10.1002/adma.201203815.
19 A. Natarajan, W. Du, C.-Y. Xiong, G. L. DeNardo, S. J. DeNardo and J. Gervay-Hague, *Chem. Commun.*, 2007, 695–697.
20 E. F. J. Rettler, J. M. Kranenburg, H. M. L. Lambermont-Thijs, R. Hoogenboom and U. S. Schubert, *Macromol. Chem. Phys.*, 2010, **211**, 2443–2448.
21 W. C. Oliver and G. M. Pharr, *J. Mater. Res.*, 1992, **7**, 1564–1583.

Publication P5

"Metal-free cycloaddition of internal alkynes and multifunctional azides under solvent-free conditions"

B. Sandmann, B. Happ, J. Vitz, R. M. Paulus, M. D. Hager, P. Burtscher, N. Moszner, U. S. Schubert

Macromol. Chem. Phys. **2014**, *215*, 1603-1608.

Metal-Free Cycloaddition of Internal Alkynes and Multifunctional Azides Under Solvent-Free Conditions

Benedict Sandmann, Bobby Happ, Jürgen Vitz, Renzo M. Paulus, Martin D. Hager, Peter Burtscher, Norbert Moszner,* U. S. Schubert*

The synthesis of three different electron-deficient internal alkynes for the metal-free 1,3-dipolar azide–alkyne cycloaddition is shown. The alkynes are polymerized with several multifunctional azides and the reaction enthalpy (ΔH) is investigated by differential scanning calorimetry (DSC). The mechanical properties of the resulting polymers are analyzed using nanoindentation. The polymerization results in hard materials with an *E*-modulus of maximum 2.5 GPa, which make them interesting in particular for biomedical applications.

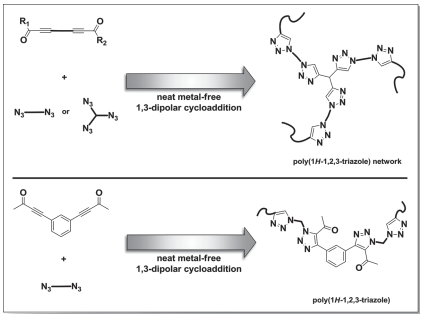

1. Introduction

The conventional 1,3-dipolar cycloaddition of azides and alkynes, which was mainly developed by Rolf Huisgen,[1] did not gain considerable interest due to its low regioselectivity and slow reaction rate, which limits the broad applicability of this reaction in organic syntheses. In 2002, Sharpless[2] and Meldal[3] described the catalyzed reaction (copper(I) species), which pushed the development of the azide–alkyne cycloaddition forward. The Cu(I)-catalyzed azide–alkyne reaction, also known in the literature as a type of "click reaction," represents an important and powerful synthetic tool in organic chemistry due to its remarkable features such as high regioselectivity and strong tolerance to functional groups, mild reaction conditions, and a simple product isolation. This powerful reaction has found a variety of applications in many fields of chemistry.[4–9]

One main part of the copper(I)-catalyzed alkyne–azide cycloaddition (CuAAC) is the catalyst. Due to its cytotoxic properties, it is important to remove the copper residues from the resulting polymer, in particular for biomedical applications.[10] Moreover, highly efficient catalysts, which are used for the CuAAC, often generate very high reaction enthalpies in a short time period, which can result in a spontaneous release of reaction heat and an uncontrolled reaction progress.[11]

Therefore, the development of metal-free click-polymerization procedures is of high interest. In the

B. Sandmann, Dr. B. Happ, Dr. J. Vitz, R. M. Paulus, Dr. M. D. Hager, Prof. U. S. Schubert
Laboratory of Organic and Macromolecular Chemistry (IOMC), Friedrich Schiller University Jena, Humboldtstraße 10, 07743 Jena, Germany
E-mail: ulrich.schubert@uni-jena.de
B. Sandmann, Dr. B. Happ, Dr. J. Vitz, R. M. Paulus, Dr. M. D. Hager, Prof. U. S. Schubert
Jena Center for Soft Matter (JCSM), Friedrich Schiller University Jena, Philosophenweg 7, 07743 Jena, Germany
Dr. B. Happ, Dr. J. Vitz, Prof. U. S. Schubert
Dutch Polymer Institute (DPI) P.O. Box 902, 5600, AX Eindhoven, The Netherlands
Dr. P. Burtscher, Prof. N. Moszner
Ivoclar Vivadent AG, Bendererstrasse 2, FL-9494 Schaan, Liechtenstein
E-mail: norbert.moszner@ivoclarvivadent.com

DOI: 10.1002/macp.201400149

recent years, a significant effort has been devoted to the development of metal-free click reactions.[12–26] The classical (thermal) 1,3-dipolar cycloaddition can be performed between azides and terminal alkynes as well as internal triple bonds. Generally, the reactivity of alkynes for the click reaction is rather low due to its high electron density at the alkyne functionality. One pathway to increase the reactivity of internal alkynes is to reduce its electron density by implementing vicinal electron-withdrawing groups, e.g., carbonyl moieties.[13,27,28]

Tang et al. presented the first example of the efficient 1,3-dipolar polycycloaddition using azides and activated internal alkynes. The polymerizations of 1,4-*bis*(6-azidohexyloxy)benzene, *bis*(benzoylethynyl)-benzenes, and -butane were performed in DMF at elevated temperatures (150 °C).[13]

Katritzky et al.[18] studied the neat polymerization of different internal alkynes and organic azides under mild conditions and found reaction temperatures between room temperature and 80 °C depending on the substitution pattern of the used alkyne.

This work deals with the synthesis of electron-poor internal alkynes (alkynes with adjacent electron-withdrawing carbonyl moieties) and their polymerization with multifunctional azides under solvent-free and metal-free conditions. The reaction heat and the reaction temperature of the polyaddition reaction were monitored by DSC. The increase of reactivity of the alkynes for the metal-free click reaction was achieved by attaching electron-withdrawing carbonyl moieties adjacent to the alkyne functional groups. The mechanical properties of the resulting polymers were investigated by nanoindentation.

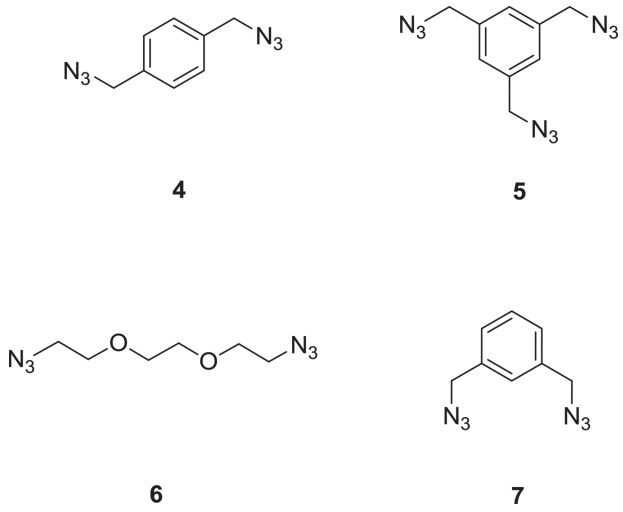

Figure 1. Schematic representation of the used multifunctional azides.

2. Experimental Section

2.1. General Procedure for the Metal-Free Polyaddition

For the crosslinking polyadditions of the respective alkynes and azides (Figure 1), both components were charged in a small glass vial using an equimolar ratio of both functional moieties (i.e., alkyne and azide) and stirred for 2 min. After that, the mixture was placed on a glass slide using a pipette. The polymerizations were performed at a temperature of 100 °C for 24 h. The obtained polymer could be directly used for the nanoindentation measurements.

2.1.1. Instrumentation

1D NMR spectra (1H, 13C) were recorded on a Bruker AC300 (300 MHz) and on a Bruker AC400 (400MHz) at 298 K. Chemical shifts are reported in parts per million (ppm, δ scale) relative to the residual signal of the solvent. Standard abbreviations are used for denoting the signal multiplicity. DSC was measured on a Netzsch DSC 204 F1 Phoenix instrument under a nitrogen atmosphere in a temperature range from −50 to 250 °C with a heating rate of 10 K min^{-1}. Size exclusion chromatograms (SEC) were recorded using a SEC Shimadzu SCL-10A system controller, an LC-10AD pump, a RID-10A refractive index detector, and a PSS SDV pre/lin S column at 50 °C (eluent: chloroform:triethylamine:isopropyl alcohol 94:4:2; flow rate of 1 mL min^{-1}) using linear PS standards for the molar mass calculation. FTIR spectra were recorded on a Shimadzu IRAffinity-1S equipped with a single-reflection ATR accessory.

The mechanical properties of the samples were characterized via depth-sensing indentation (DSI) using a TriboIndenter TI 900 (Hysitron Inc., Minneapolis, MN) and a NanoDMA 06 transducer, equipped with a conospherical diamond indenter tip of ca. 4.7 μm radius. The measurements were started at ambient conditions, at 29.3 °C and 39.7% relative humidity (RH) for polymer **A**, and at 25.6 °C and 34.4% RH for the polymers **B** and **C**, measured with a Voltcraft DL-141TH data logger. For quasi-static testing, a load control function with a 1 s loading, 2 s hold at maximum load, and 1 s unloading profile was applied to polymer **A** with indent forces between 100 μN and 5000 μN. For the softer polymers **B** and **C**, an open loop protocol was used with the same load, hold, and unload times and indent force range as mentioned above.[29] All measurements for each sample were performed in a single automated run in less than 6 h using a 6 × 6 array piezo automation. The reduced modulus E_r was determined from the unloading response utilizing the analysis method proposed by Oliver and Pharr.[30] Values were averaged from at least 10 measurements each. From the reduced modulus E_r, the indentation modulus E_i was calculated using the elastic modulus and Poisson's ratio of the diamond indenter, 1140 GPa and 0.07, respectively, and a Poisson's ratio of 0.4 for the polymeric material, according to:

$$E_{i,sample} = \frac{1-\nu^2_{sample}}{\frac{1}{E_{r,sample}} - \frac{1-\nu^2_{indenter}}{E_{indenter}}} \quad (1)$$

The hardness has the normal definition:

$$H = \frac{P_{max}}{A} \quad (2)$$

2.1.2. Materials

All the chemicals were purchased from Fluka, Sigma–Aldrich, ABCR chemicals and used without further purification. The solvents were dried and distilled according to standard procedures.

1,4-*Bis*(azidomethyl)benzene (**4**),[31] 1,2-*bis*(2-azidoethoxy)-ethane (**6**),[11] 1,3,5-*tris*(azidomethyl)benzene (**5**),[31] and 1,3-*bis*(azidomethyl)benzene (**7**),[31] were synthesized and purified according to previously described literature procedures.

2.1.3. Monomer Synthesis

*2.1.3.1. Synthesis of Ethylene Glycol Oligoester (**1**)*

Ethylene glycol (11.28 mmol, 0.7 g) was added to a solution of diethyl acetylenedicarboxylate (13.8 mmol, 2.34 g) in toluene (50 mL). Afterward, *p*-toluenesulfonic acid monohydrate (0.79 mmol, 0.15 g) was added to the reaction mixture and stirred for 16 h at 130 °C. The water formed was removed from the reaction system by a dean-stark trap. Subsequently, the reaction mixture was washed with a saturated $NaHCO_3$ solution. The product was isolated by preparative SEC using BioBeads S-X8 (exclusion limit: 1000 g mol^{-1}) with CH_2Cl_2 as eluent.

M_n (SEC) = 950 g mol^{-1}; PDI = 2.95; DP = 7 (SEC); ($DP_{theo.}$ = 10).

^1H NMR (400 MHz, $CDCl_3$, δ): 4.17–3.00 (m, 8H), 1.37–0.65 (m, 6H); ^{13}C NMR (100 MHz, $CDCl_3$, δ): 165.0 (Br), 67.0, 62.1 (Br), 66.0, 15.1.

*2.1.3.2. Synthesis of 1,6-hexandiol-oligoester (**2**)*

1,6-Hexandiol (22.51 mmol, 2.66 g) was added to a solution of diethyl acetylenedicarboxylate (27.5 mmol, 4.68 g) in toluene (50 mL). Subsequently, *p*-toluenesulfonic acid monohydrate (1.58 mmol, 0.30 g) was added to the reaction mixture, which was stirred for 16 h at 130 °C. The water formed was removed by a dean-stark trap. Subsequently, the reaction mixture was washed with a saturated $NaHCO_3$ solution. The product was isolated by preparative SEC (BioBeads S-X8) using CH_2Cl_2 as eluent. M_n (SEC) = 1800 g mol^{-1}; PDI = 4.72.

The degrees of polymerization (DP) of oligomer **2** were determined by ^1H NMR spectroscopy. As a second method, size-exclusion chromatography was chosen.

DP = 9 (SEC); DP = 5 (^1H NMR); ($DP_{theo.}$ = 10).

^1H NMR (400 MHz, $CDCl_3$, δ): 4.41–3.91 (m, 8H), 1.78–1.13 (m, 14H); ^{13}C NMR (100 MHz, $CDCl_3$, δ): 162.5, 74.7, 66.8, 62.9, 28.3, 25.3, 13.9.

*2.1.3.3. Synthesis of 4,4′-(1,3-phenylene)bis(but-3-yn-2-one) (**3**)*

n-BuLi (1.6 M solution in hexane, 30 mL, 48 mmol) was added to a solution of 1,3-diethynylbenzene (21 mmol, 2.65 g) in THF (30 mL) at –78 °C under a nitrogen atmosphere.

Then, a solution of distilled ethyl acetate (4.8 mL, 48 mmol) in THF (45 mL) and boron trifluoride diethyl etherate (6.7 mL, 55 mmol) was successively added. After 30 min, the reaction was quenched with a saturated solution of NH_4Cl at –78 °C and

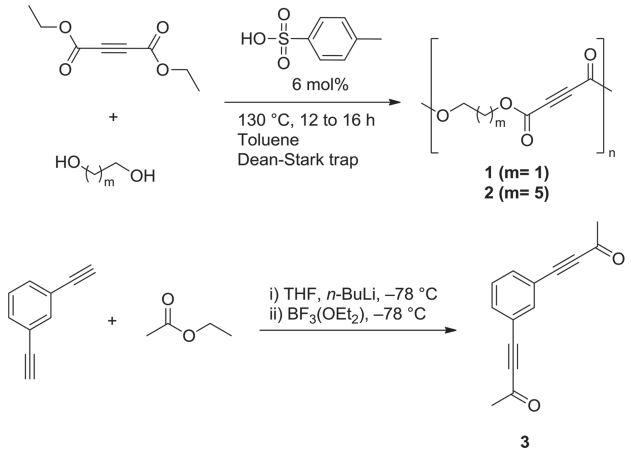

Scheme 1. Schematic representation of the synthesis of the internal alkyne monomers (**1** to **3**) for the metal-free click reaction.

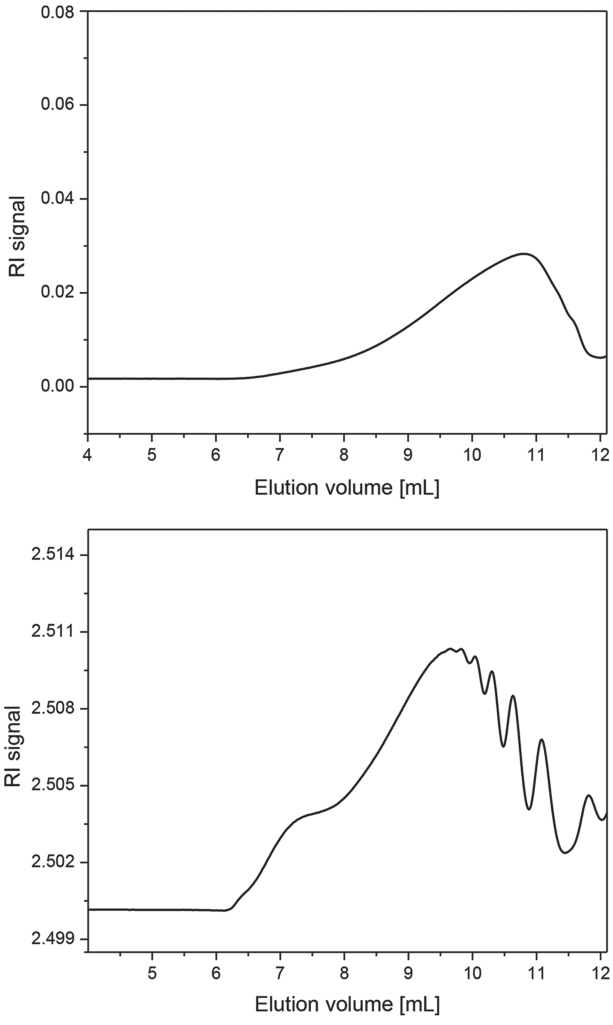

Figure 2. SEC analyses of the ethylene glycol oligoester **1** (top) and 1,6-hexandiol-oligoester **2** (bottom).

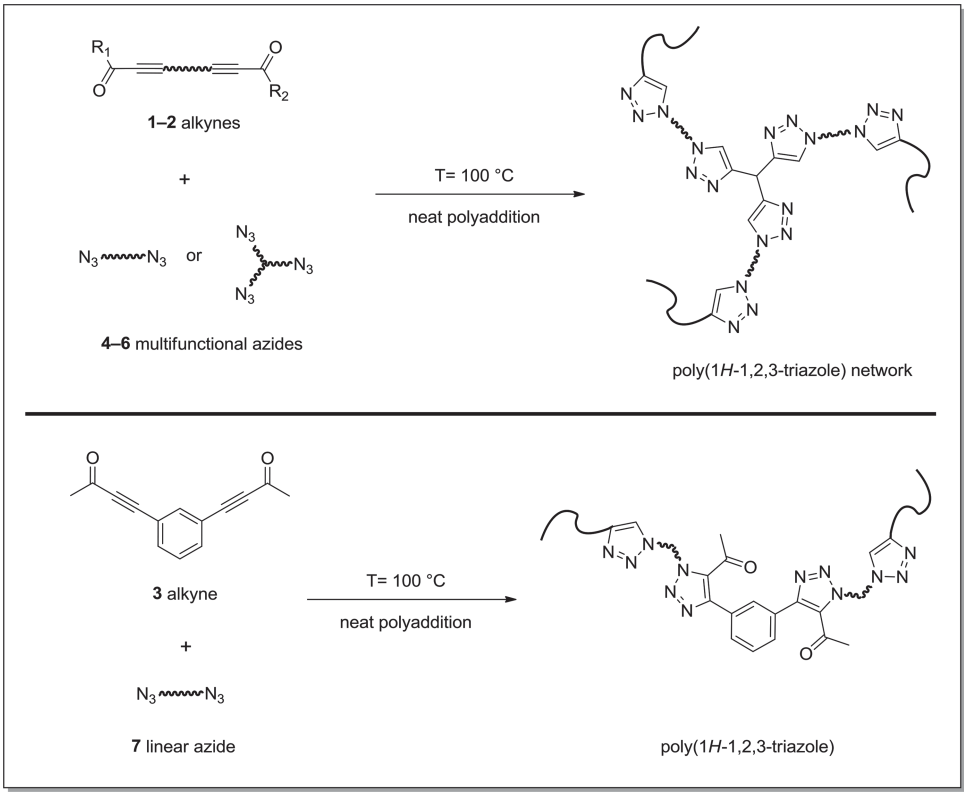

Scheme 2. Schematic representation of the metal-free click reaction of alkynes and multifunctional azides.

allowed to warm to room temperature. The layers were separated and the aqueous layer was further extracted with EtOAc. The combined organic layers were washed with brine dried over Na_2SO_4, filtered, and concentrated in vacuo. The product was isolated as a dark orange liquid by column chromatography on silica gel (hexane: EtOAc, 95:5) with a yield of 5% (0.22 g).

^{1}H NMR (400 MHz, $CDCl_3$, δ): 7.77 (m, 1H, J = 2.8 Hz), 7.64 (dd, J = 7.8 Hz, 1.6, 2H), 7.43 (t, 1H, J = 15.7 Hz), 2.46 (s, 6H); ^{13}C NMR (100 MHz, $CDCl_3$, δ): 184.1, 136.9, 134.7, 129.1, 120.8, 88.8, 87.9, 32.7.

3. Results and Discussion

3.1. Synthesis of the Monomers

Two different classes of electron-deficient internal alkynes have been chosen to study the influence of the substitution pattern of the alkynes, namely acetylene dicarboxylates as well as an alkyne-based ketone. At least bifunctional monomers are required for the polyaddition with the corresponding azides. Therefore, oligoesters based on the acetylene dicarboxylate and glycol and hexanediol have been synthesized. These materials were prepared via a transesterification of diethylene dicarboxylate with the corresponding diol (Scheme 1). The acetylene dicarboxylate was used in a slight excess (1.22:1). As a consequence, only oligomers were obtained and the end-group of the resulting oligoesters were ethylesters. The theoretical DP was 10; the SEC measurements revealed for both oligomers DPs of around 10 (Figure 2). In contrast, the DP of **2** could be determined to be 5 via NMR spectroscopy. Both resulting oligomers were liquids, which could be used for the polyaddition. The alkyne ketone **3** was synthesized via a functionalization of diethynylbenzene. After deprotonation with *n*-BuLi, the alkyne was reacted with ethyl acetate (Scheme 1).

3.2. DSC Study of the Polyaddition

First, the reaction temperature and the reaction enthalpies of the metal-free polyadditions of the internal alkynes **1** to **3** and the corresponding azides (Scheme 2) were investigated via DSC. Both selected polyadditions (**3** and **7** as well as **2** and **6**) revealed an exothermic behavior (Figure 3). The integration of the individual peaks provided the reaction heat ΔH generated during the reaction.

For the polymerization of monomers **2** and **6**, a reaction heat of –278 kJ mol^{-1} was measured and the polymerization already initiated at a temperature of 5 °C. In contrast, the reaction of the aromatic *bis*-alkyne **3** with *bis*(azidomethyl)benzene **7** started at a temperature of 40 °C. An enthalpy of –284 kJ mol^{-1} was generated during polymerization. In comparison to, the reaction heat of the

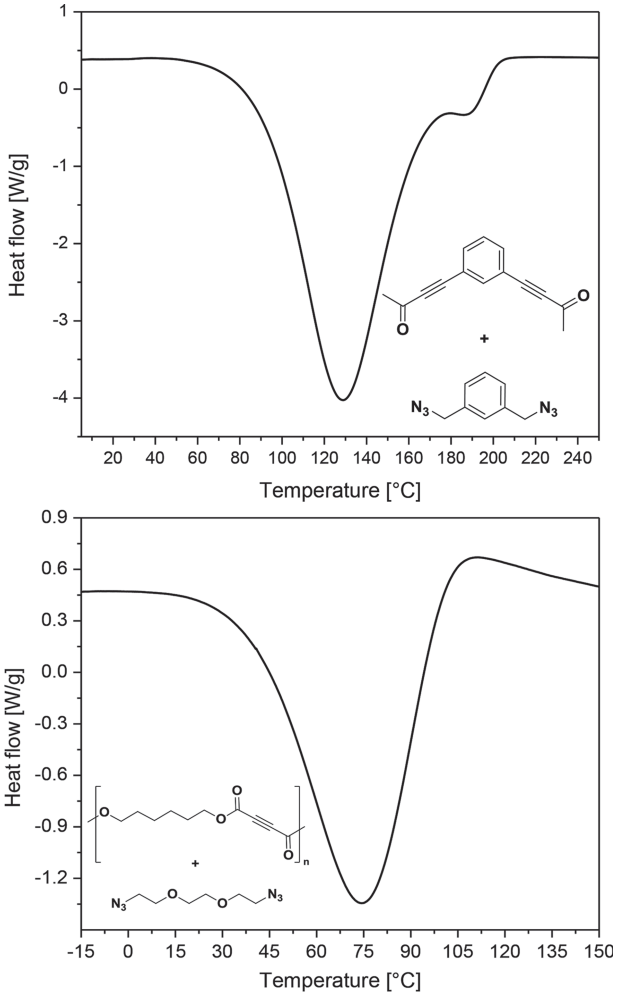

Figure 3. DSC traces (exothermic direction: down) for the neat polymerization of **3** and **7** (top) and for the neat polymerization of **2** and **6** (bottom).

Cu(I)-catalyzed click reaction of 1,2-*bis*(2-azidoethoxy)-ethane and di(prop-2-yn-1-yl) (2,2,4-trimethylhexane-1,6-diyl)dicarbamate with different copper(I) salts is in a range of –315 to –526 kJ mol^{-1}.[11] With increasing polymerization process, a postpolymerization reaction occurred at 180 °C due to sterical effects. Presumably, residual functional groups could only react at higher temperatures, due to the higher mobility at elevated temperatures.

The reactivity and the required reaction temperature of the used monomers can be tuned by the substitution pattern. Reasonable temperatures (75 to 130 °C), particularly for the oligoesters, can be used for the polyaddition in bulk materials in order to harden these materials.

3.3. Polyaddition of Activated Alkynes and Azides

The alkyne monomers **1** to **3** and the corresponding azides **4** to **7** have been utilized for the polyaddition (Scheme 2). The DSC measurements revealed that both alkyne monomers showed sufficient reactivity at 100 °C. Therefore, the click reactions were performed for 24 h at this temperature in order to achieve a quantitative azide conversion. The reaction progress could be followed by ATR-FTIR spectroscopy. The change of the azide absorption band at 2100 cm^{-1} correlates to the monomer conversion. For all of the investigated monomer pairs, a conversion between 80% and 100% of the azide could be achieved under the applied reaction conditions. Under the conditions of a solvent-free and copper-free polymerization of monomers **3** and **7**, most likely a mixture of regioisomers was formed. For the polymerization of monomers **1** and **2**, there are no regiochemical preferences due to the symmetrical structure of the oligoesters. Because of the insolubility of the resulting polymers **A** to **E**, molar masses could not be investigated by SEC.

3.4. Mechanical Properties of the Polymer Networks

The mechanical properties of the synthesized polymer networks were investigated via depth-sensing indentation (DSI). With a quantitatively azide conversion, polymer **A** exhibited an E-modulus of 2.5 ± 0.20 GPa (Table 1). The indentation moduli of the polymers **B** and **C** of 1.54 ± 0.17 GPa for polymer **B** and 1.58 ± 0.24 GPa for polymer **C** were lower than for polymer **A** due to the more flexible monomer **2** and an lower azide conversion of about 80%. The triethyleneglycole-*bis*-azide (TEG-*bis*-azide) monomer **6** decreases the network density as well as rigidity in contrast to the aromatic azides. Consequently, a softer and more flexible material was obtained. Due to the softness of polymer **D** indentation measurements were not possible. Recently, we published the Cu(I)-catalyzed click reaction of tripropargylamine, di(prop-2-yn-1-yl)isophorone dicarbamate, 1,2-*bis*(2-azidoethoxy)ethane, 1,3-*bis*(azidomethyl)benzene, and 1,4-*bis*(azidomethyl)benzene under solvent-free conditions.[11] The E-moduli of the resulting polymers achieved values up to 6.25 ± 0.4 GPa due to the high network density and high monomer conversion. In comparison to these materials, the lower alkyne concentration per molecule of oligomers **1** and **2** resulted in materials with a less

Table 1. Composition and E-modulus of the polymer networks.

Polymer	Monomer 1	Monomer 2	Indentation modulus [GPa]
A	**1**	**7**	2.5 ± 0.20
B	**2**	**4**	1.54 ± 0.17
C	**2**	**5**	1.58 ± 0.24
D	**2**	**6**	Material too soft
E	**3**	**7**	–

crosslinking density and consequently, softer materials (Table 1).

4. Conclusion

By attaching electron-withdrawing carbonyl moieties to the adjacent alkyne functionalities, it was possible to increase the reactivity of the alkyne monomers for the metal-free azide–alkyne cycloaddition under solvent-free conditions. Thereby, the reaction temperature of polymerization of alkynes **2** and **3** with the azides **6** and **7** could be lowered to at least 5 and 40 °C. For the CuAAC, highly efficient catalysts are used which often leads to a release of high reaction enthalpies in a short time period.[11] By performing the click reaction without copper catalysis, the exothermicity was reduced to a value of –278 and –284 kJ mol^{-1}, respectively.

The polyaddition reaction of oligomers **1** and **2** with the *bis*-alkynes **4**, **5**, and **7** results in hard polymer resins with a maximum E-modulus of 2.5 ± 0.20 GPa. These moderate mechanical properties and the absence of catalyst make these polymers interesting especially for biomedical applications.

Acknowledgements: The authors thank the Dutch Polymer Institute (DPI, Technology area HTE) for support.

Received: March 19, 2014; Revised: May 14, 2014; Published online: July 8, 2014; DOI: 10.1002/macp.201400149

Keywords: click chemistry; internal alkynes; metal-free cycloaddition; nanoindentation

[1] R. Huisgen, *1,3-Dipolar Cycloaddition Chemistry*, (Ed: A. Padwa), Wiley, New York **1984**, p. 1.
[2] V. V. Rostovtsev, L. G. Green, V. V. Fokin, K. B. Sharpless, *Angew. Chem Int. Ed.* **2002**, *41*, 2596.
[3] C. W. Tornoe, C. Christensen, M. Meldal, *J. Org. Chem.* **2002**, *67*, 3057.
[4] N. V. Tsarevsky, B. S. Sumerlin, K. Matyjaszewski, *Macromolecules* **2005**, *38*, 3558.
[5] J. A. Opsteen, J. C. M. van Hest, *Chem. Commun.* **2005**, 57.
[6] V. P. Mocharla, B. Colasson, L. V. Lee, S. Roper, K. B. Sharpless, C. H. Wong, H. C. Kolb, *Angew. Chem Int. Ed.* **2005**, *44*, 116.
[7] J.-F. Lutz, *Angew. Chem Int. Ed.* **2007**, *46*, 1018.
[8] M. van Dijk, M. L. Nollet, P. Weijers, A. C. Dechesne, C. F. van Nostrum, W. E. Hennink, D. T. S. Rijkers, R. M. J. Liskamp, *Biomacromolecules* **2008**, *9*, 2834.
[9] H. C. Kolb, K. B. Sharpless, *Drug Discovery Today* **2003**, *8*, 1128.
[10] C. R. Becer, R. Hoogenboom, U. S. Schubert, *Angew. Chem Int. Ed.* **2009**, *48*, 4900.
[11] B. Sandmann, B. Happ, M. D. Hager, J. Vitz, E. Rettler, P. Burtscher, N. Moszner, U. S. Schubert, *J. Polym. Sci., Part A: Polym. Chem.* **2014**, *52*, 239.
[12] L. Q. Wan, J. J. Tian, J. Z. Huang, Y. H. Hu, F. R. Huang, L. Du, *J. Appl. Polym. Sci.* **2007**, *106*, 2111.
[13] Q. Wei, H. Q. Deng, Y. B. Cai, J. W. Y. Lam, J. Li, J. Z. Sun, M. Gao, A. J. Qin, B. Z. Tang, *Macromol. Rapid Commun.* **2012**, *33*, 1356.
[14] H. K. Li, J. Mei, J. A. Wang, S. A. Zhang, Q. L. Zhao, Q. A. Wei, A. J. Qin, J. Z. Sun, B. Z. Tang, *Sci. China Chem.* **2011**, *54*, 611.
[15] J. J. Tian, X. F. Wang, L. Q. Wan, Y. H. Hu, F. R. Huang, *High Perform. Polym.* **2010**, *22*, 198.
[16] H. K. Li, J. Wang, J. Z. Sun, R. R. Hu, A. J. Qin, B. Z. Tang, *Polym. Chem.* **2012**, *3*, 1075.
[17] A. J. Qin, L. Tang, J. W. Y. Lam, C. K. W. Jim, Y. Yu, H. Zhao, J. Z. Sun, B. Z. Tang, *Adv. Funct. Mater.* **2009**, *19*, 1891.
[18] A. R. Katritzky, N. K. Meher, S. Hanci, R. Gyanda, S. R. Tala, S. Mathai, R. S. Duran, S. Bernard, F. Sabri, S. K. Singh, J. Doskocz, D. A. Ciaramitaro, *J. Polym. Sci., Part A: Polym. Chem.* **2008**, *46*, 238.
[19] L. Wang, Y. M. Song, R. Gyanda, R. Sakhuja, N. K. Meher, S. Hanci, K. Gyanda, S. Mathai, F. Sabri, D. A. Ciaramitaro, C. D. Bedford, A. R. Katritzky, R. S. Duran, *J. Appl. Polym. Sci.* **2010**, *117*, 2612.
[20] J. J. Tian, L. Q. Wan, J. Z. Huang, Y. H. Hu, F. R. Huang, L. Du, *Polym. Bull.* **2008**, *60*, 457.
[21] L. Q. Wan, Y. H. Luo, L. Xue, J. J. Tian, Y. H. Hu, H. M. Qi, X. N. Shen, F. R. Huang, L. Du, X. B. Chen, *J. Appl. Polym. Sci.* **2007**, *104*, 1038.
[22] Q. Wei, J. Wang, X. Y. Shen, X. A. Zhang, J. Z. Sun, A. J. Qin, B. Z. Tang, *Sci. Rep. UK* **2013**, *3*, 1.
[23] Y. J. Li, H. Zhou, E. Yanpeng, L. Q. Wan, F. R. Huang, L. Du, *Des. Monomers Polym.* **2013**, *16*, 556.
[24] L. W. Wan, J. J. Tian, J. H. Huang, Y. H. Hu, F. R. Huang, L. Du, *J. Macromol. Sci., Part A: Pure Appl. Chem.* **2007**, *44*, 175.
[25] J. Tian, L. Wan, J. Huang, Y. Hu, F. Huang, L. Du, *Polym. Adv. Technol.* **2007**, *18*, 556.
[26] A. R. Katritzky, R. Sakhuja, L. C. Huang, R. Gyanda, L. Wang, D. C. Jackson, D. A. Ciaramitaro, C. D. Bedford, R. S. Duran, *J. Appl. Polym. Sci.* **2010**, *118*, 121.
[27] S. T. Abu-Orabi, R. Al-Hamdany, A. Atfah, A. A. S. Ali, K. Abu-Shandi, *Asian J. Chem.* **1999**, *11*, 774.
[28] H. C. Kolb, M. G. Finn, K. B. Sharpless, *Angew. Chem Int. Ed.* **2001**, *40*, 2004.
[29] E. F. J. Rettler, J. M. Kranenburg, H. M. L. Lambermont-Thijs, R. Hoogenboom, U. S. Schubert, *Macromol. Chem. Phys.* **2010**, *211*, 2443.
[30] W. C. Oliver, G. M. Pharr, *J. Mater. Res.* **1992**, *7*, 1564.
[31] S. T. Abu-Orabi, R. E. Harmon, *J. Chem. Eng. Data* **1986**, *31*, 379.

Publication P6

"Biological evaluation of 1,2,3-triazole-based polymers for potential applications as hard tissue material"

D. Pretzel, B. Sandmann, M. Hartlieb, J. Vitz, S. Hölzer, N. Fritz, N. Moszner, U. S. Schubert

J. Polym. Sci., Part A: Polym. Chem. **2015***,* in press (DOI: 10.1002/pola.27676).

Biological Evaluation of 1,2,3-Triazole-Based Polymers for Potential Applications as Hard Tissue Material

David Pretzel,[1,2] Benedict Sandmann,[1,2] Matthias Hartlieb,[1,2] Jürgen Vitz,[1,2] Stefan Hölzer,[1,2] Nicole Fritz,[1,2] Norbert Moszner,[3] Ulrich S. Schubert[1,2]

[1]Laboratory for Organic and Macromolecular Chemistry (IOMC), Friedrich Schiller University Jena, Humboldtstr. 10, 07743 Jena, Germany
[2]Jena Center for Soft Matter (JCSM), Friedrich Schiller University Jena, Philosophenweg 7, 07743 Jena, Germany
[3]Ivoclar Vivadent AG, Bendererstrasse 2, FL-9494 Schaan, Liechtenstein
Correspondence to: U. S. Schubert (E-mail: ulrich.schubert@uni-jena.de)

Received 6 January 2015; accepted 26 March 2015; published online 00 Month 2015
DOI: 10.1002/pola.27676

KEYWORDS: biocompatibility; biomaterials; cell viability; click chemistry; crosslinking; cytotoxicity; internal alkynes; metal-free cycloaddition

INTRODUCTION The conventional 1,3-dipolar cycloaddition of azides and alkynes, which was developed by Huisgen[1] in 1961, did not gain considerable attention because of its low regioselectivity and slow reaction rate, which limit the broad applicability of this reaction in organic synthesis. In 2002, Sharpless and coworkers[2] and Meldal and coworkers[3] described the catalyzed reaction [copper(I) species] that pushed the development of the azide–alkyne cycloaddition forward. The Cu(I)-catalyzed azide–alkyne reaction, also known in the literature as a type of "click reaction," represents an important and powerful synthetic tool in organic chemistry because of its remarkable features such as high regioselectivity, strong tolerance to functional groups, mild reaction conditions, and a simple product isolation. This powerful reaction has found a variety of applications in many fields of chemistry.[4–9] One essential element of the copper(I)-catalyzed alkyne–azide cycloaddition (CuAAC) is the catalyst. However, aiming for materials, which can be used in biological systems, the cytotoxicity of copper salts has to be considered. It is important to remove the copper residues from the products, in particular for biomedical applications.[10] Alternatively, the development of metal-free click reaction procedures, for instance, by thermal azide–alkyne cycloaddition (TAAC), for the production of biomedical materials represents a promising way to circumvent this issue. There are various examples of resins produced by TAAC using multifunctional azides and alkynes[11,12] or AB-type monomers.[13] In addition, the crosslinking of polyphenylene[14] and the production of multifunctional polymer films[15] are described. However, to the best of our knowledge, TAAC-based resins were not evaluated as hard biomaterials up to now.

Generally, synthetic polymers play an important role in the production of hard or soft materials in the biomedical context. They potentially possess several advantages like a tunable chemical composition and physical structure enabling a control about mechanical properties. A standardized manufacturing with reasonable costs displays a further advantage. Depending on the scope of use, the synthetic materials can be of a biodegradable (enzymatically, hydrolytic, and pH dependent) or biostable character.

The materials described in this contribution belong to the latter class of polymers. The triazole moiety is stable within biological systems,[16] and even though the ester bond within the backbone of the used polyalkyne is biodegradable, the hydrophobic and stiff nature of the substrates should prevent decomposition within a physiological environment.

In our previous report, we demonstrated the synthesis of crosslinked 1,2,3-triazole-based polymers and their resulting mechanical characteristics, showing excellent properties for the production of hard scaffolds for biomedical applications, including prosthetic materials, scaffolds for tissue engineering, bone cements, as well as parts of medical devices and disposable supplies.[16]

The materials described in this publication consist of oligomeric alkynes, multifunctional azide crosslinkers, and their resulting polymers (Scheme 1). The alkyne components of the presented click scaffolds were synthesized according to literature procedures.[16] To investigate the influence of the length of this building block, two oligoesters with different

Additional Supporting Information may be found in the online version of this article.

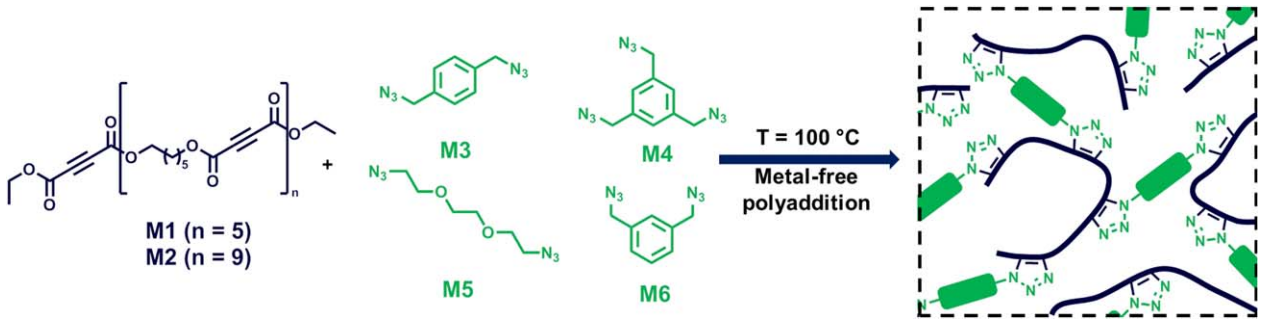

SCHEME 1 Schematic representation of the metal-free click reaction of the alkynes **M1** and **M2** and multifunctional azides **M3–M6**. [Color figure can be viewed in the online issue, which is available at wileyonlinelibrary.com.]

molar masses and dispersities ($Đ$) have been synthesized (**M1**: $M_n = 1058$ g mol^{-1}, $Đ = 2.68$; **M2**: $M_n = 1850$ g mol^{-1}, $Đ = 1.66$). The internal triple bonds should readily react with present azide moieties under elevated temperature. Four different organic azides were used as depicted in Scheme 1. Besides the influence of the substitution pattern (**M3** vs. **M6**) and the number of azides per monomeric unit (**M3** vs. **M4**), the role of the hydrophilicity of the monomer was investigated by using triethylene glycol bis-azide (TEG-N_3; **M5**).

For the production of scaffolds by TAAC, both alkyne and azide were mixed at room temperature using an equimolar ratio of both functional moieties. Subsequently, the mixture was placed on a glass slide and polymerized at a temperature of 100 °C for 24 h.[16] The azide conversion was followed by ATR-IR spectroscopy, monitoring the change of the absorption band at 2100 cm^{-1} as it represents an established technique for following the reaction progress of azide–alkyne cycloaddition reactions.[17–20] Conversions between 60% and 80% were achieved for all of the investigated monomer pairs under the applied reaction conditions. Under the conditions of a solvent-free and copper-free polymerization of the applied monomers **M1–M6**, most likely a mixture of regioisomers was formed.[21,22] Table 1 displays the used component combinations and the resulting analytical data. For all conducted investigations, **P9** [a dimethacrylate composite, consisting of photopolymerized bisphenol A-glycidyl methacrylate 30%, (1,6-bis-(2-methacryloyloxy ethoxycarbonylamino)−2,2,4-trimethylhexane (50%), and triethylene glycol dimethacrylate (20%) provided by Ivoclar Vivadent AG] was used as a reference (details are provided in the Supporting Information). The mechanical properties of the synthesized polymer networks were investigated by depth-sensing indentation.

Unexpectedly, the influence of the length of the alkyne oligomer on the elastic behavior of the resulting polymers is negligible, as expressed by the comparison of **P1–P4** that were polymerized using **M1** with their corresponding **M2** adduct (**P5–P8**). Besides, the substitution pattern has an impact, as scaffolds produced using **M3** have a significantly increased indentation modulus when compared with **M6**. As expected, the utilization of **M5** (TEG-N_3) yields networks with an indentation modulus three orders of magnitude lower than all other substrates because of the flexibility of the used monomer. However, this effect could also be the result of a side reaction which leads to further crosslinking. Azide groups are widely used for photocrosslinking reactions, as they are able to produce nitrenes following UV irradiation.[23,24] A thermal triggering of this process is also reported.[25] Nitrenes can, among others, react with aromatic systems to form covalent connections, which is not possible for **M5** as a comonomer.

TABLE 1 Composition and Analytical Data of the Polymer Networks

Polymer	Alkyne	Azide	Azide Conversion (%)	Indentation Modulus (GPa)	Contact Angle Against Water (°)	Cellular Growth Density (%)	Roughness (Arithmetic, nm)
P1	**M1**	**M3**	78	2.41 ± 0.32	61 ± 2	33	77
P2	**M1**	**M4**	60	3.09 ± 0.27	71 ± 4	84	24
P3	**M1**	**M5**	72	0.008 ± 0.002	72 ± 2	64	56
P4	**M1**	**M6**	71	1.95 ± 0.07	75 ± 2	24	14
P5	**M2**	**M3**	66	2.51 ± 0.09	74 ± 3	50	13
P6	**M2**	**M4**	62	2.58 ± 0.12	58 ± 4	19	42
P7	**M2**	**M5**	67	0.01 ± 0.006	74 ± 1	57	66
P8	**M2**	**M6**	80	1.19 ± 0.10	76 ± 4	79	16
P9	–	–	–	3.74 ± 0.23	73 ± 4	74	77

The cellular growth density was referenced to cells grown on culture plastic (polystyrene, 100%).

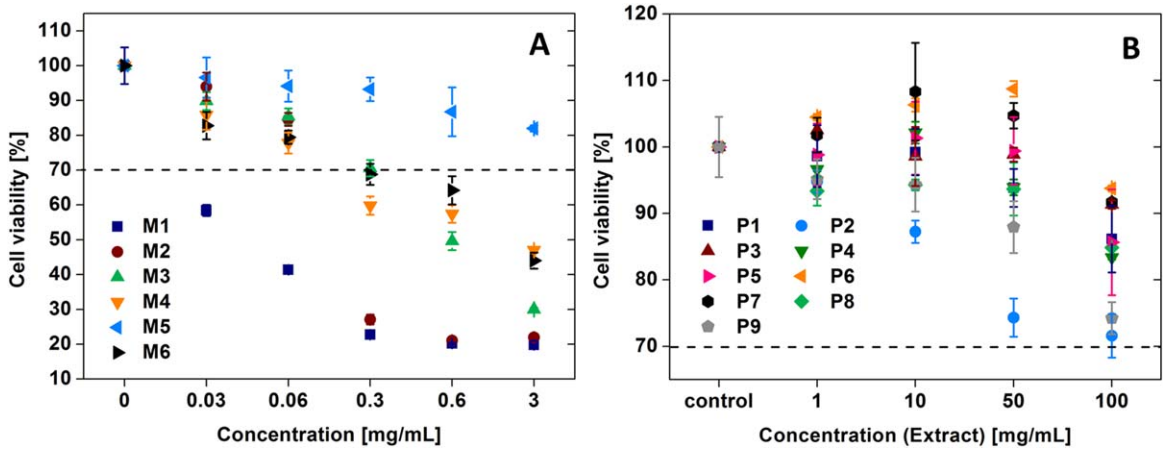

FIGURE 1 Cell viability of L929 mouse fibroblasts after 24h incubation with different concentrations of the educts **M1** to **M6** (A) or extracts of fine-grinded polymer powders **P1–P9** (B). Cells incubated with pure culture medium served as control. The cell viability was determined by XTT assay according to DIN ISO-10993-5. Data are expressed as mean ± SD of six determinations. Dashed line labels the defined border to cytotoxicity at 70%. [Color figure can be viewed in the online issue, which is available at wileyonlinelibrary.com.]

To investigate the surface hydrophilicity, contact angle measurements using water were conducted. All synthesized networks show similar contact angle values under the given conditions (Table 1). Only for **P1** and **P6**, the angle decreased, indicating a more hydrophilic surface. Surprisingly, the use of the polar azide component **M5** did not result in an increase of surface hydrophilicity. The produced films possess a surface roughness in the nanometer range and exhibit no surface-associated porosity (Supporting Information Fig. 3).

In the development of new synthetic hard polymer materials, cell culture-based tests are the first step to determine the biocompatibility. Hence, *in vitro* tests were conducted investigating the toxicity of monomers, polymeric bulk material, and extracts from polymerized samples using L929 mouse fibroblasts, representing a standard cell line for named tests. The *in vitro* cytotoxicity experiments were performed on the basis of the XTT assay, according to the German standard institution guideline DIN ISO-10993-5 as a reference for biomaterial testing. First, the cytotoxic potential of the monomers used for the polymerization was tested to determine a possible undesired biological side effect of residual (nonreacted) monomers remaining in the polymerized samples [Fig. 1(A)].

After 24 h of incubation with different concentrations of the educts (**M1–M6**), the metabolic activity of the cells was found to be significantly reduced in the case of the alkynes **M1** and **M2** as well as for the aromatic azides **M3**, **M4**, and **M6** displaying a concentration-dependent inhibition of the cell metabolism. Alkyne **M2** and azides **M3**, **M4**, and **M6** resulted in a reduction of the cell viability under the defined border to cytotoxicity of 70% in a concentration range from 3 to 0.3 mg mL^{-1}; lower substance concentration around 0.06 mg mL^{-1} was tolerated by the cells. In contrast, alkyne **M1** showed cytotoxic potential at all analyzed concentrations. Exclusively, cells treated with azide **M5** displayed a metabolic activity on the level of untreated controls, which proves the absence of a toxic effect mediated by the TEG bis-azide (**M5**). These results indicate that a significant amount of unbound monomer within the final scaffolds would lead to materials incompatible with biological systems. However, the viability of cells treated with **M5** shows that the presence of azide groups does not necessarily lead to toxicity.

Although salts such as sodium azide display potent toxins via the inhibition of the cytochrome *c* oxidase[26] by the azide anion, covalently bond azides cannot dissociate within a biological environment. It is rather likely that the chemical structure of the azide-containing molecules plays an important role in their cell biological behavior. In particular, the hydrophobic nature of the aromatic hydrocarbons in **M3**, **M4**, and **M6** presumably provoke a harmful interaction with cellular membranes as indicated by the drastic reduction of the cell viability.

A similar reason might be responsible for the cytotoxic effects of the alkynes **M1** and **M2**, which are highly hydrophobic because of their nonpolar character.

Interpreting these results, the precursor materials by themselves (except **M5**) are of potential harmful character and need to be absent in their unreacted form in the final polymeric material. Otherwise, a reduced biocompatibility can be expected. To examine this assumption, the resulting materials **P1–P8**, including the reference material **P9**, were screened for their impact on cellular integrity. First investigations were conducted using aqueous extracts of grinded polymers. The extracts were directly incubated with L929 mouse fibroblasts for 24 h followed by execution of the XTT viability assay. This approach enables the efficient extraction and effect detection of potentially remaining educts within the polymerized samples. As depicted in Figure 1(B), all extracts resulted in an acceptable viability rate above 70% in the case of undiluted extract samples, approaching the level of the untreated control with increasing dilution steps.

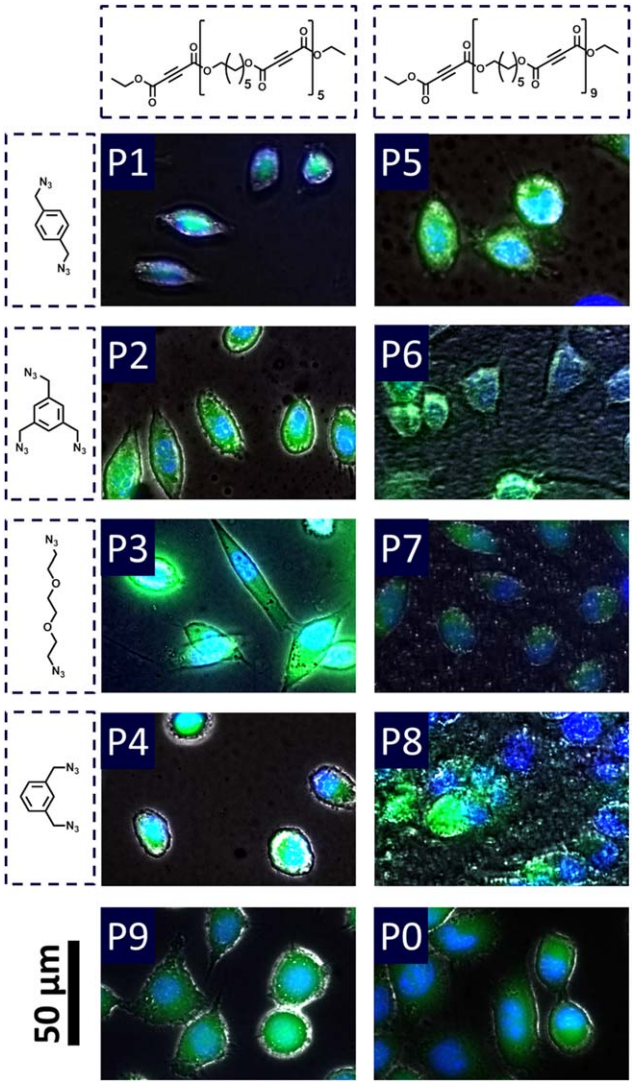

FIGURE 2 The panels display the viability and morphology of L929 cells after incubation on polymer films for 24 h. An overlay of representative bright field and fluorescence microscopy images of cells on the scaffolds **P1–P9** and cell culture plastic (**P0**) is depicted. Blue fluorescent Hoechst dye labels nuclei of all cells present, green fluorescence from FDA tags viable cells, and red fluorescent PI signals originates from nuclei of dead cells. Bright field images also provide an indication about the surface roughness of the click substrates. [Color figure can be viewed in the online issue, which is available at wileyonlinelibrary.com.]

Interestingly, the resulting viability rates after incubation with the polymerized samples **P1–P8** showed a similar profile like the reference material **P9**, thus proving the good biocompatibility of the extracts derived from the synthesized polymeric materials. It has to be noted that the concentrations generated by the extraction method are far above the values which can be expected by simple exposure of substrates to water, rendering the cytotoxicity results highly promising.

The extracts of the polymerized samples, used for the cytotoxicity evaluation, were further subjected to electron spray ionization mass spectrometry to determine a rough concentration value and, if possible, the identity of the components. All extracts revealed distinctly lower signal intensity values (of the most intense signal of the spectrum) when compared with the reference **P9**. **P5** and **P8** show intensities in the range of the control (water) or even below (Supporting Information Fig. 1). Only one set of signals, which appears in the most spectra (**P1**, **P2**, **P4**, **P5**, **P6**, and **P8**), could be identified as a degradation product of the used oligo-alkyne (Supporting Information Fig. 2). However, degradation during pulverization of the networks cannot be excluded, rendering the investigations on intact substrates more valuable.

To confirm the general biocompatibility of the click scaffolds, a live/dead microscopy study of cells that were seeded onto films consisting of the materials **P1–P9** was performed. Twenty-four hours after cell seeding, the materials were washed to remove nonadherent cell bodies and analyzed microscopically. The transparent character of the samples enabled capture of phase contrast micrographs, which showed that L929 mouse fibroblast cells attach onto the polymeric surfaces.

Although the cell-spreading behavior is slightly altered when compared with the cells grown on cell culture plastic, they display morphologies of adherent viable cells.

The cell viability was further investigated using Hoechst/fluorescein diacetate (FDA)/propidium iodide (PI) live/dead staining, which gave information about the cell membrane integrity (exclusion of red fluorescent PI from cell nuclei that were additionally tagged by Hoechst dye) and the viability (strong green fluorescence of FDA in cytoplasm; Fig. 2). The absence of the red fluorescence of PI in all pictures and the successful FDA staining prove the excellent cytocompatibility of the prepared click scaffolds. The bright field images of the background show air inclusions within the films. However, profilometry (Table 1 and Supporting Information Fig. 3) shows no porosity or increased surface roughness for all samples except **P3** which possesses holes.

To assess quantitative information of the cellular growth on distinct materials, representative sections of micrographs were subjected to cell counting. The results were referred to the growth density obtained from cell culture plastic (polystyrene; Table 1). No clear trend is visible comparing the results with the elastic moduli, conversions, or the use of distinct monomer combinations. However, **P1** and **P6**, which show a significantly reduced growth density, also have an increased surface hydrophilicity when compared with the other substrates. Hydrophilic surfaces are known to repel microorganism because of a prevention of attachment.[27] The growth density on the substrates **P2** and **P8** exceeds the value obtained for the reference material **P9**, rendering these substrates particularly suitable for the productions of hard tissue replacements.

The viability of cells grown in the presence of the scaffolds was further assessed by flow cytometry investigations. The average viability of cells consisting of the fraction of nonadherent cells floating in the supernatant and the fraction of

cells adherent to the scaffold surface showed values in the range of the control (grown on cell culture plastic) for all samples (Supporting Information Fig. 4). The observed biocompatibility of the 1,2,3-triazole-based polymers **P1–P8** is in accordance with literature data, stating a nontoxicity of many polytriazole-containing structures, mainly designed in the pharmaceutical field, for example, as a tool for drug discovery for cancer treatment.[28,29] Because of its chemical composition, the triazole units are not subject to metabolic degradation and are stable in typical biological conditions, which are usually of aqueous and mildly reducing nature.[30,31] The ester bonds in the backbone of the oligo-alkyne could be degraded, which is, however, rather unlikely as the hydrophobic nature of the structures prevents the penetration of water, which is required in the process. During our investigations, no sign of degradation under physiological conditions was found.

In summary, the cell study on the educts clearly revealed a cytotoxic potential of the alkynes and aromatic azides used in this contribution, exceptionally the TEG like bis-azide turned out to be cytocompatible at all applied concentrations. Further investigations on the final polymer samples neglected the hazardous character of the educts and presented a polymeric material, which shows highly biocompatible character in its bulk format, as well as in the contact of cells with aqueous polymer extracts. Cells grown on the scaffolds were analyzed regarding their viability and growth density. All polymers revealed good biocompatibility with various growth densities of L929 fibroblasts.

Nevertheless, in view of the development of new synthetic hard matter polymer materials, the *in vitro* assays based on cell culture models described in our contribution display only the first step to determine the biocompatibility of a material. Before a clinical application, additional tests have to be performed, including mainly *in vivo* animal models for the determination of acute and (sub)chronic toxicity, genotoxicity, carcinogenicity, as well as the investigation of reproductive/developmental problems, neurotoxicity, immunotoxicity, and the presence of endotoxins in the final product.

EXPERIMENTAL

Information about Materials and Methods as well as experimental procedures can be found in the Supporting Information.

ACKNOWLEDGEMENTS

The authors thank the Deutsche Forschungsgemeinschaft (DFG, SPP 1568) for financial support.

REFERENCES AND NOTES

1 R. Huisgen, Ed. 1,3-Dipolar Cycloaddition Chemistry; Wiley: New York, **1984**.

2 V. V. Rostovtsev, L. G. Green, V. V. Fokin, K. B. Sharpless, *Angew. Chem. Int. Ed.* **2002**, *41*, 2596–2599.

3 C. W. Tornoe, C. Christensen, M. Meldal, *J. Org. Chem.* **2002**, *67*, 3057–3064.

4 N. V. Tsarevsky, B. S. Sumerlin, K. Matyjaszewski, *Macromolecules* **2005**, *38*, 3558–3561.

5 J. A. Opsteen, J. C. M. van Hest, *Chem. Commun.* **2005**, 57–59.

6 V. P. Mocharla, B. Colasson, L. V. Lee, S. Roper, K. B. Sharpless, C. H. Wong, H. C. Kolb, *Angew. Chem. Int. Ed.* **2005**, *44*, 116–120.

7 J. F. Lutz, *Angew. Chem. Int. Ed.* **2007**, *46*, 1018–1025.

8 M. van Dijk, M. L. Nollet, P. Weijers, A. C. Dechesne, C. F. van Nostrum, W. E. Hennink, D. T. S. Rijkers, R. M. J. Liskamp, *Biomacromolecules* **2008**, *9*, 2834–2843.

9 H. C. Kolb, K. B. Sharpless, *Drug Discov. Today* **2003**, *8*, 1128–1137.

10 C. R. Becer, R. Hoogenboom, U. S. Schubert, *Angew. Chem. Int. Ed.* **2009**, *48*, 4900–4908.

11 J. Tian, L. Wan, J. Huang, Y. Hu, F. Huang, L. Du, *Polym. Bull.* **2008**, *60*, 457–465.

12 J. Tian, L. Wan, J. Huang, Y. Hu, F. Huang, L. Du, *Polym. Adv. Technol.* **2007**, *18*, 556–561.

13 C. Besset, J. Bernard, E. Fleury, J.-P. Pascault, P. Cassagnau, E. Drockenmuller, R. J. J. Williams, *Macromolecules* **2010**, *43*, 5672–5678.

14 R. Pötzsch, B. Voit, *Macromol. Rapid Commun.* **2012**, *33*, 635–639.

15 J. M. Spruell, M. Wolffs, F. A. Leibfarth, B. C. Stahl, J. Heo, L. A. Connal, J. Hu, C. J. Hawker, *J. Am. Chem. Soc.* **2011**, *133*, 16698–16706.

16 B. Sandmann, B. Happ, J. Vitz, R. M. Paulus, M. D. Hager, P. Burtscher, N. Moszner, U. S. Schubert, *Macromol. Chem. Phys.* **2014**, *215*, 1603–1608.

17 S. Saha, M. L. Bruening, G. L. Baker, *Macromolecules* **2012**, *45*, 9063–9069.

18 F. E. Du Prez, M. Lammens, D. Fournier, *Abstr. Pap. Am. Chem. Soc.* **2008**, 236.

19 A. Hasneen, S. J. Kim, H. J. Paik, *Macromol. Res.* **2007**, *15*, 541–546.

20 A. S. Goldmann, D. Quemener, P. E. Millard, T. P. Davis, M. H. Stenzel, C. Barner-Kowollik, A. H. E. Muller, *Polymer* **2008**, *49*, 2274–2281.

21 J. E. Hein, V. V. Fokin, *Chem. Soc. Rev.* **2010**, *39*, 1302–1315.

22 A. J. Scheel, H. Komber, B. I. Voit, *Macromol. Rapid Commun.* **2004**, *25*, 1175–1180.

23 J. Bang, J. Bae, P. Löwenhielm, C. Spiessberger, S. A. Given-Beck, T. P. Russell, C. J. Hawker, *Adv. Mater.* **2007**, *19*, 4552–4557.

24 S. Al Akhrass, D. Damiron, G. Carrot, E. Drockenmuller, *J. Polym. Sci., Part A: Polym. Chem.* **2010**, *48*, 3888–3895.

25 D. Damiron, N. Okhay, S. A. Akhrass, P. Cassagnau, E. Drockenmuller, *J. Polym. Sci., Part A: Polym. Chem.* **2012**, *50*, 98–107.

26 T. Ishikawa, B.-L. Zhu, H. Maeda, *Toxicol. Ind. Health* **2006**, *22*, 337–341.

27 L. Tauhardt, K. Kempe, M. Gottschaldt, U. S. Schubert, *Chem. Soc. Rev.* **2013**, *42*, 7998–8011.

28 J. Mahesh Kumar, M. M. Idris, G. Srinivas, P. Vinay Kumar, V. Meghah, M. Kavitha, C. R. Reddy, P. S. Mainkar, B. Pal, S. Chandrasekar, N. Nagesh, *PLoS One* **2013**, *8*, e70798.

29 C. Hein, X.-M. Liu, D. Wang, *Pharm. Res.* **2008**, *25*, 2216–2230.

30 N. Kaval, D. Ermolat'ev, P. Appukkuttan, W. Dehaen, C. O. Kappe, E. Van der Eycken, *J. Comb. Chem.* **2005**, *7*, 490–502.

31 V. D. Bock, H. Hiemstra, J. H. van Maarseveen, *Eur. J. Org. Chem.* **2006**, *2006*, 51–68.

Publication P7

"Incorporation of core-shell particles in methacrylate based composites for an improvement of the mechanical properties"

B. Sandmann, B. Happ, I. Perevyazko, T. Rudolph, F. H. Schacher, S. Hoeppener, U. Mansfeld, M. D. Hager, U. Fischer, P. Burtscher, N. Moszner, U. S. Schubert

Polym. Chem. **2015***,* in press (DOI: 10.1039/C4PY01544D).

View Article Online
DOI: 10.1039/C4PY01544D

Polymer Chemistry

RSCPublishing

ARTICLE

Cite this: DOI: 10.1039/xoxxoooooox

Incorporation of Core-shell Particles in Methacrylate based Composites for an Improvement of the Mechanical Properties

Benedict Sandmann,[ab] Bobby Happ,[ab] Igor Perevyazko,[ab] Tobias Rudolph,[ab] Felix H. Schacher,[ab] Stephanie Hoeppener,[ab] Ulrich Mansfeld,[ab] Martin D. Hager,[ab] Urs K. Fischer,[c] Peter Burtscher,[c] Norbert Moszner*[c] and Ulrich S. Schubert*[ab]

Received ooth January 2012,
Accepted ooth January 2012

DOI: 10.1039/xoxxoooooox

www.rsc.org/

The fracture toughness of polymeric materials and composites can be enhanced by the incorporation of polymer nanoparticles. The combination of a soft core and a hard shell leads to an improvement of the fracture toughness of the polymeric composites. Thereby, the mechanical resistance of the materials is commonly decreased. In our approach, core–shell nanoparticles consisting of an ethylene glycol dimethacrylate (EGDMA) crosslinked poly(butyl acrylate) (PBA) core and a poly(methyl methacrylate) (PMMA) shell were synthesized. The polymer particles were incorporated in triethylene glycol dimethacrylate (TEGDMA)/urethane dimethacrylate (UDMA) based composites in order to tune the mechanical properties. Different core–shell ratios were applied to study the influence on the fracture toughness and E-modulus. An examination of shell-crosslinking with a TEGDMA content of up to 8% was performed to improve particle stability and dispersability. The particle sizes and morphologies were characterized by dynamic light scattering (DLS), cryogenic transmission electron microscopy (cryo-TEM) and analytical ultracentrifugation (AUC). Latex particle sizes of 70 to 220 nm were obtained. The mechanical properties (flexural strength, E-modulus and K_{1c}) of polymer composites were investigated in three-point bending tests. Core/shell ratios of 50/50 showed a decreasing effect to flexural strength, E-modulus and K_{1c}. Polymer particles with core/shell ratios of 30/70 led to a significant increase of the mechanical properties with maxima of 1.206 MPa·m$^{1/2}$ (K_{1c}) (increase of 65%), E-modulus of 1.90 GPa (increase of 18%) and flexural strength of 79 MPa (increase of 18%). This study represents the first report of a simultaneous improvement of fracture toughness and E-modulus (at the same time) of additive filled polymer composites. The improvement of mechanical properties makes these materials interesting as toughers for hard tissue applications like bone cements or dental replacement materials.

1. Introduction

Polymers and their composites are progressively replacing many structural metallic parts, e.g., in automotive industry,[1] aerospace[2] or dental restoratives.[3] For polymeric materials, the replacement of such materials strongly depends on the mechanical properties like fracture toughness and E-modulus that are decisive for their applications.[1, 2, 4-7] Unfortunately, these properties are limited for polymer materials and need to be improved. There are various ways to increase the fracture toughness of these materials. Thus, glass fibers were incorporated into Nylon 6 as well as maleated ethylene–propylene rubber and achieved an improvement of fracture toughness, though under loss of the resistance (E-modulus).[8] Another attempt towards the enhancement of fracture toughness was the incorporation of hyperbranched polymers as soft domains.[9, 10] A significant increase of the fracture toughness (K_{1c}) from 0.55 MPa·m$^{1/2}$ (unfilled) to 1 MPa·m$^{1/2}$ (7.5% of hyperbranched polymers) was reported, however, accompanied by a loss of the Young's modulus from 2.9 GPa to 2.65 GPa.[10] To overcome the drawback of the loss in young's modulus, latex particles with a soft core and a hard shell have been utilized as an attempt towards toughened and resistance improved materials. For example, core-shell lattices consisting of a poly(butyl acrylate) (PBA) rubbery core and a poly(methyl methacrylate) (PMMA) shell were incorporated into epoxy resins. The obtained fracture toughness (K_{1c}) increase up to 1.74 MPa·m$^{1/2}$ was twice as high as for the unfilled reference material. However, this improvement was accompanied by a decrease of the E-modulus of approximately

View Article Online
DOI: 10.1039/C4PY01544B Polymer Chemistry

10%.[11] Moreover, PBA/PMMA core–shell nanoparticles were used to enhance the fracture toughness of acrylic bone cements.[12] With increasing particle content K_{1c} was enhanced from 1.48 MPa·m$^{1/2}$ (unfilled) to 1.86 MPa·m$^{1/2}$ (10 wt% of latex particles) but the E-modulus decreased from to 2.4 GPa to 2.0 GPa. Up to now there is no report in literature about the incorporation of latex particles into polymer composites that leads to an increase of fracture toughness and mechanical resistance at the same time.

This contribution reports the synthesis of core-shell nanoparticles consisting of an ethylene glycol dimethacrylate (EGDMA) crosslinked soft PBA core and a hard PMMA shell. In some cases the shell was additionally crosslinked with triethylene glycol dimethacrylate (TEGDMA). The particle size and morphology were investigated by DLS, cryo-TEM and AUC measurements. The particles were dispersed in a monomer mixture of TEGDMA and urethane dimethacrylate (UDMA) and were consequently photo-polymerized. The mechanical properties of the resulting polymers were investigated in three-point bending tests.

---

[a]Laboratory of Organic and Macromolecular Chemistry (IOMC), Friedrich Schiller University Jena, Humboldtstraße 10, 07743 Jena, Germany
[b]Jena Center for Soft Matter (JCSM), Friedrich Schiller University Jena, Philosophenweg 7, 07743 Jena, Germany
[c]Ivoclar Vivadent AG, Bendererstrasse 2, FL-9494 Schaan, Liechtenstein
Correspondence to: Ulrich S. Schubert (E-mail: *ulrich.schubert@uni-jena.de*) or Norbert Moszner (E-mail: *norbert.moszner@ivoclarvivadent.com*)

---

2. Experimental section

Materials

Butyl acrylate (BA), methyl methacrylate (MMA), ethylene glycol dimethacrylate (EGDMA), potassium persulfate (KPS), and sodium dodecyl sulfate (SDS), camphorquinone (CQ), ethyl 4-(dimethylamino)-benzoate (EMBO) and hydrochinon-monomethylether (MeHQ) were purchased from Sigma-Aldrich. Triethylene glycol dimethacrylate (TEGDMA) and UDMA ((1,6-bis-(2-methacryloyloxyethoxycarbonylamino)-2,2,4-trimethylhexane, which were synthesized by the addition 2 mol 2-hydroxyethyl methacrylate with 1 mol 2,2,4-trimethylhexamethylenediisocyanate), were provided by Ivoclar Vivadent AG. All chemicals were used without further purification.

Synthesis of core-shell particles

Different crosslinked and non-crosslinked core-shell particles were synthesized in a three step emulsion polymerization. The recipes for the synthesis of the latex particles **1** to **11** are summarized in **Table 1**.

Amounts of PBA seed, PBA and MMA were selected in order to obtain core–shell particles with different core/shell ratios (60/40, 50/50, 40/60, 30/70 and 10/90) with regard to the used monomer masses.

Polymer particles **1**, **2**, **3**, **4** and **10** were synthesized in an emulsion polymerization according to a literature procedure.[12] The particles were isolated by freeze drying and further used for the preparation of the particle dispersions.

General synthesis procedure for the shell-crosslinked latex particles **5**, **6**, **7**, **8**, **9** and **11**:

Crosslinked core–shell particles were synthesized in an emulsion polymerization. A four-necked flask (100 mL) equipped with a mechanical stirrer, a gas inlet tube, a condenser and thermometer was charged with polymer core solution. H_2O and potassium persulfate (KPS, $K_2S_2O_8$) were added to the reactor. The reaction mixture was stirred (stirring rate 260 rpm), purged with nitrogen for 30 min and subsequently heated to 80 °C. When the reactor temperature was stable, a mixture of MMA and TEGDMA was placed in a syringe and added to the reaction mixture (0.5 mL·min^{-1}). The polymerization was performed for 2 h at 80 °C. The emulsion was filtered over a glass frit. The particles were isolated by freeze drying. The isolated particles were directly used for the preparation of particle dispersions.

Preparation of core-shell particle dispersions

Particle dispersions were prepared by redispersing polymer latices **4** to **11** in TEGDMA for 2 d by mechanical stirring. Particles were redispersed in concentrations of 3, 6 and 9 wt% (**Table 2**) and consequently used for the preparation of test specimens. (see preparation of test specimens and measurement of mechanical properties).

Dynamic light scattering

Dynamic light scattering (DLS) was performed at a scattering angle of 90° on an ALV CGS-3 instrument equipped with a He-Ne laser operating at a wavelength of 633 nm at 25 °C. 15 µL of the samples were diluted with 3 mL of MilliQ-water. The CONTIN algorithm was applied to analyze the obtained correlation functions. For temperature control, the DLS is equipped with a Lauda thermostat. Apparent hydrodynamic radii were calculated according to the Stokes-Einstein equation.

Sedimentation velocity experiments

Sedimentation velocity experiments were performed with a ProteomeLab XLI Protein Characterization System analytical ultracentrifuge (Beckman Coulter, Brea, CA), using conventional double-sector Epon centerpieces of 12 mm optical path length and a four hole rotor. Rotor speed was 5,000 to 10,000 rpm, depending on the sample. Cells were filled with 420 µL of nanoparticle suspension and 440 µL of solvent (H_2O or D_2O). The nanoparticle suspensions were used without further purification. Before the run, the rotor was equilibrated for approximately 1 h at 20 °C in the centrifuge. Sedimentation profiles were obtained every 15 s by interference optics. For the analysis of the particle size distribution, the sedimentation velocity data were treated by ls-g*(s) analysis with a Tikhonov–Phillips regularization procedure (confidence level of 0.9 was

View Article Online
DOI: 10.1039/C4PY01544D

used) implemented into the Sedfit program. This method is based on a boundary modeling of a superposition of sedimentation profiles of ideal non-diffusing particles.[13]

The value of the partial specific volume (reciprocal density **υ = 1/ρ**) was determined using the density variation method.[14] Assuming the same size and molar mass of the particles in both solvents, the value of υ can be calculated from the following equation:

$$\upsilon = \frac{s_2\eta_2 - s_1\eta_1}{s_2\eta_2\rho_1 - s_1\eta_1\rho_2}$$

Where s_1, η_1, ρ_1 and s_2, η_2, ρ_2 are the sedimentation coefficients, dynamic viscosity and solvent density measured in H_2O (index 1) and D_2O (index 2), respectively. The determination was made separately for all nanoparticle dispersions.

The hydrodynamic size of the particles was calculated assuming their spherical shape by the modified Svedberg equation:

$$d = 3\sqrt{2}\sqrt{[s]\upsilon}$$

where [s] is the intrinsic sedimentation coefficient $[s] = \frac{s_0\eta_0}{(1-\upsilon\rho_0)}$, υ is the partial specific volume, s_0 is sedimentation coefficient of the particles and η_0, ρ_0 are dynamic viscosity and density of the solvent.

Cryogenic transmission electron microscopy

Cryogenic transmission electron microscopy (cryo-)TEM measurements were performed either on a Philips CM120 (Electron Microscopy Center Jena) or on a FEI Tecnai G2 20 cryo-Transmission Electron Microscope (Jena Center for Soft Matter). Acceleration voltages were set to 120 kV. Samples were prepared on Quantifoil grids (R2/2) after cleaning by argon plasma treatment for 30 s. 7 to 10 µL of the solutions (diluted 1:3 with H_2O) were blotted by a home-build preparation chamber or a Vitrobot Mark IV, respectively. Samples were plunch-frozen in liquid ethane and stored under nitrogen before being transferred to the microscope utilizing a Gatan transfer stage.

Preparation of test specimens and measurement of the mechanical properties

For the preparation of test specimens, the various components were mixed and homogenised using a rolling mill. The formulation of test specimens (**TS**) is displayed in **Table 2**. Test specimens of 2×2×25 mm (specimens for flexural strength and E-modulus experiments) and 2.5×5×25 mm (specimens for K_{1c} experiments) dimension were photo-polymerized (2×3 min) in a Spectramat® (Ivoclar Vivadent AG, Schaan; Hg radiation source, In-doped, 400 W, main emission 400 to 500 nm). Before the polymerization, the samples were covered with a polyester foil. To maximize conversions, test specimens were stored for 24 h at room temperature.

Mechanical measurements were performed on a BZ2.5/TS1S testing machine using the testXpert II V3.3 software (Zwick GmbH Co. KG, Ulm).

Flexural strength and E-modulus experiments were performed in a three-point bending test with a span length of 20 mm and a test speed of 0.8 mm min^{-1} according to EN 24049 (= ISO 4049, Dentistry – Polymer-based filling, restorative and luting materials).

For K_{1c} experiments test specimens were furnished with a 2 mm notch (1.8 mm with diamond saw, 0.2 mm with razor blade). K_{1c} measurements were performed in a three-point bending test with span length of 20 mm and a test speed of 0.25 mm·min^{-1} according to ISO 20795-1 (Dentistry – Base Polymers – Part 1: Denture Base Polymers).

Table 1 Polymer particle composition.

Latex	Particle type	Core/ Shell Ratio	Crosslinker content of polymer shell [%]	Added particle solutions [mL]	Mass BA [g]	Mass MMA [g]	Mass EGDMA [g]	Mass SDS [g]	Mass KPS [g]	Mass TEGDMA [g]	Mass H_2O [g]
1	Seed	–	–	–	175	–	1.75	2	1.75	–	350
2	Core	–	–	29.4 mL of **1**	9.75	–	–	0.38	0.01	–	69
3	Core	–	–	29.4 mL of **1**	9.81	–	–	0.38	0.01	–	69
4	Core-shell	(30/70)	–	7.5 mL of **2**	–	3.78	–	–	0.04	–	15
5	Core-Shell	(30/70)	2	22.5 mL of **3**	–	11.34	–	–	0.12	0.23	45
6	Core-shell	(60/40)	4	7.5 mL of **3**	–	1.08	–	–	0.01	0.04	10
7	Core-shell	(50/50)	4	7.5 mL of **3**	–	1.62	–	–	0.02	0.06	12
8	Core-shell	(40/60)	4	5 mL of **3**	–	1.62	–	–	0.02	0.06	10
9	Core-shell	(30/70)	4	5 mL of **3**	–	2.52	–	–	0.03	0.10	10
10	Core-shell	(30/70)	8	5 mL of **3**	–	2.52	–	–	0.03	0.20	11
11	Core-shell	(10/90)	–	5 mL of **2**	–	9.72	–	–	0.01	–	16

View Article Online
DOI: 10.1039/C4PY01544D

Polymer Chemistry

RSCPublishing

ARTICLE

Table 2 Composition of test specimens (wt% of component of the total mixture).

Latex	Test specimen	Particle concentration [%]	UDMA [g]	TEGDMA [g]	Mass particle dispersion [g]	CQ [g]	EMBO [g]	MeHQ [g]
4	**TS1**	9	4.66 (32%)	1.04 (7.10%)	8.76 (60%)	0.06 (0.40%)	0.06 (0.43%)	0.02 (0.12%)
5	**TS2**	3	6.39 (32%)	7.42 (37.10 %)	6.00 (30%)	0.08 (0.40%)	0.09 (0.45%)	0.02 (0.10%)
5	**TS3**	6	6.39 (32%)	7.42 (37.10 %)	6.00 (30%)	0.08 (0.40%)	0.09 (0.45%)	0.02 (0.10%)
5	**TS4**	9	6.39 (32%)	7.42 (37.10 %)	6.00 (30%)	0.08 (0.40%)	0.09 (0.45%)	0.02 (0.10%)
6	**TS5**	9	6.39 (32%)	4.42 (22.11%)	9.00 (45%)	0.08 (0.40%)	0.09 (0.43%)	0.02 (0.12%)
7	**TS6**	9	6.39 (32%)	4.42 (22.10%)	8.67 (60%)	0.08 (0.40%)	0.09 (0.43%)	0.02 (0.12%)
8	**TS7**	9	6.39 (32%)	4.42 (22.11%)	9.00 (45%)	0.08 (0.40%)	0.09 (0.43%)	0.02 (0.12%)
9	**TS8**	9	5.03 (32 %)	1.12 (7.13%)	9.45 (60 %)	0.06 (0.41%)	0.07 (0.43%)	0.02 (0.12%)
10	**TS9**	9	6.39 (32%)	4.42 (22.10%)	9.00 (45%)	0.08 (0.41%)	0.09 (0.44%)	0.03 (0.13%)
11	**TS10**	9	4.61 (32%)	1.02 (7.10%)	8.67 (60%)	0.06 (0.40%)	0.06 (0.43%)	0.02 (0.12%)
–	**TS11**	0	6.39 (32%)	13.4 (67.1%)	–	0.08 (0.41%)	0.09 (0.45%)	0.02 (0.10%)

3. Results and discussion

Core-shell particles were synthesized in a three step emulsion polymerization. SDS was selected as suitable surfactant as it represents an established detergent for the emulsion polymerization of BA and MMA.[12, 15-17] Thereby, the surfactant concentration was kept above the critical micelle concentration (CMC).[18] The compositions and particle types of lattices are shown in **Table 1**. In the first step, EGDMA crosslinked polymer seeds (latex **1**) with an average particle size of 70 nm (determined by AUC) respectively 86 nm (determined by DLS) were synthesized. The particle size distributions of seed and cores (**1** to **11**) are shown in **Figure SI-1**. Subsequently, the seed particle solution was used for the synthesis of the polymer cores. An additional layer of PBA was polymerized onto the seeds **1**, resulting in polymer cores **2** and **3**, respectively. The sizes of the resulting particles revealed an increase in size up to 114 nm for latex **3**. For latex **2** there is only a minor size increase concluded from DLS (106 nm) and in particular from AUC (89 nm) results. In the last synthesis step, crosslinked (MMA, TEGDMA as crosslinker) and non-crosslinked (MMA) polymer shells were attached to the polymer cores, resulting in lattices **4** to **11**. Thereby, particle sizes of 140 to 234 nm by DLS (respectively 122 to 220 nm determined by AUC) were achieved. The particle size distributions of the core-shell particles **4** to **11** are shown in **Figure SI-2** and **SI-3**.

3.1 Characterization of latex particles

The particle size distribution of the lattices was investigated by DLS and by AUC (**Table 3**). Particle sizes and shapes were investigated by cryo-TEM.

Table 3 Average hydrodynamic diameter of latex particle (determined by DLS (d^{DLS}) and analytical ultracentrifugation (d^{AUC})) and cryogenic transmission electron microscopy ($d^{cryo\text{-}TEM}$) and corresponding densities (ρ^{AUC}).

Latex	$d^{DLS, a}$ [nm]	$d^{AUC, b}$ [nm]	$d^{Cryo\text{-}TEM, c}$ (standard deviation) [nm]	$\rho^{AUC, b}$ [g/cm³]
1	86	70	43 (27)	1.06
2	106	89	95 (6)	1.05
3	114	115	95 (18)	1.07
4	160	180	151 (17)	1.16
5	166	170	157 (31)	1.15
6	140	122	108 (22)	1.12
7	144	140	131 (24)	1.13
8	152	138	133 (21)	1.15
9	166	160	149 (40)	1.16
10	164	160	163 (24)	1.17
11	234	220	222 (32)	1.19

a) Determined by the CONTIN plot in water at 25 °C; intensity weighted
b) Determined via AUC in water at 20 °C.
c) Determined by (manually) measuring the diameters (of approximately 10 to 70 spheres) utilizing ImageJ software.

View Article Online
DOI: 10.1039/C4PY01544D

Polymer Chemistry

RSCPublishing

ARTICLE

3.1.1 Average size and size distributions

For AUC, the size was calculated assuming a spherical shape of the particles using the Svedberg equation.[21] In **Figure 1** the corresponding size distributions of seed, core and core-shell particles are presented. The average values of the sizes and corresponding densities are summarized in **Table 3**. The particle sizes were additionally investigated by cryo-TEM revealing particle sizes of 43 to 222 nm.

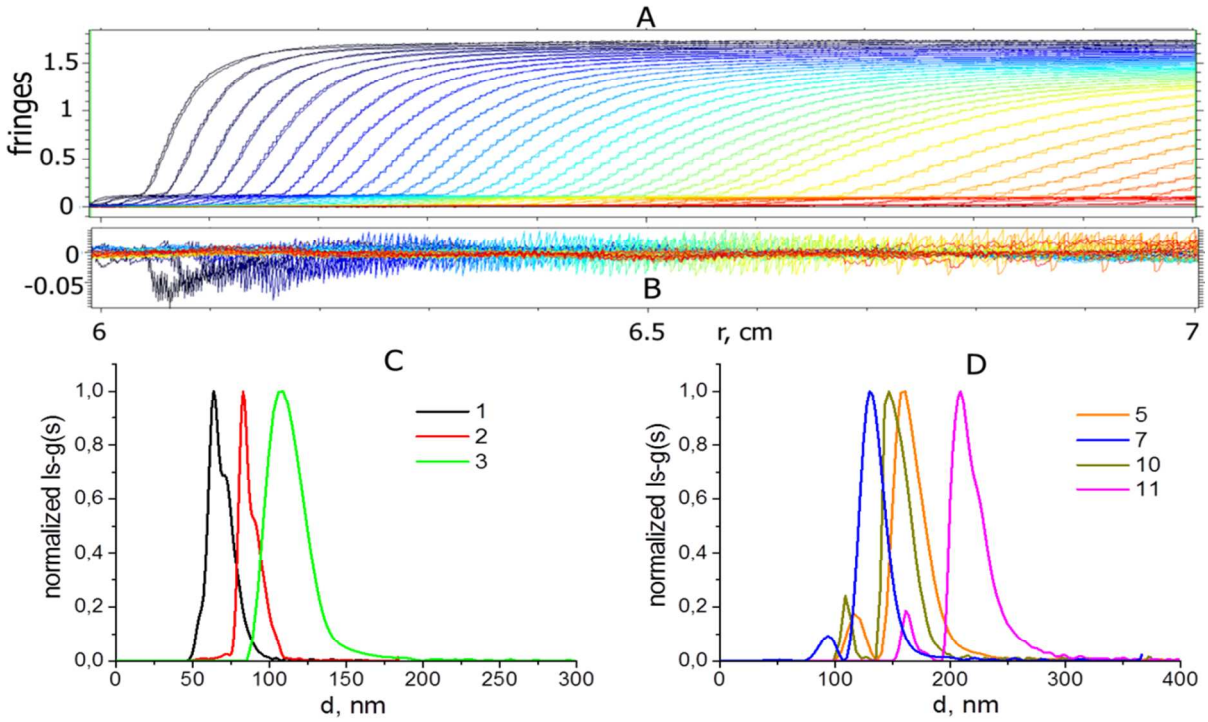

Figure 1. **A** – Sedimentation profiles of sample **11**, obtained at n = 6,000 rpm, Δt = 15 s, **B** – corresponding residual plot, **C** – size distributions of seed (sample **1**) and core particles (samples **2** and **3**) and **D** – selected size distributions of the core-shell particles.

It should be noted that according to AUC all core-shell particle distributions consist of a main peak (90% to 95% of the total mass) and a small fraction of particles with lower size (**Figure 1D**). This fraction could probably be related to unreacted core particles or to particles with a thinner shell. DLS results do not provide such a clear picture about the distribution, which is related to the lower measurement sensitivity in comparison to AUC. Moreover, taking a closer look on the AUC distributions of latex **1** and **2**, a shoulder for larger diameters (**Figure 1C**) that is not observed via DLS (**Figure SI-1**), is present. This could be related to a small amount of aggregation or inhomogenities present in the sample. This effect was not observed for other samples. The average size of the core particles increased by approximately 50 to 90% caused by the shell formation (**Table 3**). The largest particles with a size of 220 nm were observed for sample **11** (core/shell ratio: 10/90). Moreover, the value of the density has as well reached its maximum of 1.19 g cm^{-3} for sample **11**.

As a second method, DLS was used to investigate the different particles concerning their sizes. The apparent hydrodynamic diameter ($<d_{h,app}>$) determined *via* DLS showed a size of 86 nm for the seeds (latex **1**), while for the first core (latex **2**) a size increase up to 106 nm was observed via DLS (**Table 3**). However, AUC showed a smaller increase in diameter up to 89 nm. As the obtained results were not fully conclusive, a new batch for the core was synthesized (latex **3**). Here, the results were in good agreement for both methods (DLS and AUC) and a clear shift to higher hydrodynamic diameter from 70 to 115 nm confirmed the successful formation of an additional PBA layer. In further steps different core-shell compositions of 60/40, 50/50, 40/60, 30/70 and 10/90 were applied to the cores (latex **2** and **3**). The size distributions (determined by DLS) showed an increase of the hydrodynamic diameter, after attaching the polymer shell to core **3** of 52 nm (**5** and **9**), 26 nm (**6**), 30 nm (**7**), 38 nm (**8**), 50 nm (**10**). For core **2** size increases up to 54 nm (**4**) and 128 nm (**11**) were observed. In direct comparison of core-shell lattices **5**, **9** and **10** there is no

View Article Online
DOI: 10.1039/C4PY01544D

significant influence of the TEGDMA crosslinker to the sizes of the resulting core-shell lattices (**Table 3**). The increasing size after shell-attachment can be correlated to the amount of MMA added and at least to the different core/shell ratios for all core-shell particles. The overestimation of particle sizes (**Table 3**), determined by DLS is in accordance with literature reports. Thus, for example, Schubert *et al.* reported on the over assessment of particle sizes for PMMA nanoparticles, determined by DLS.[22]

3.1.2 Cryogenic transmission electron microscopy

The size and morphology of polymer particles were additionally investigated by means of cryo-TEM. cryo-TEM was chosen as a suitable characterization method to study the nanoparticles close to their state in solution and to reduce artefacts from the preparation (e.g., loss of solvent, drying effects, etc.). **Figure 2** depicts representative examples of the synthesized polymer particles **1** to **5** and **9** to **11**. Size distributions were determined by measuring the diameters (of 10 to 70 spheres) and determining the average particle size value. From these values the average particle sizes were calculated (**Table 3**). Seed particles (latex **1**) show a spherical shape with a diameter of 43 nm (standard deviation: 27 nm); however, also few seed particles with smaller diameters were observed. **Figure 2** displays the seed particles after the core formation, resulting in latex **2** and **3**. The diameter of the particles increased by this process to similar sizes of 95 nm (standard deviation: 6 nm) (**2**) and 95 nm (standard deviation: 18 nm) (**3**), while the spherical shape of particles is preserved. Though the same synthesis conditions were applied to obtain **2** and **3**, different seed-core sizes were observed according to DLS and AUC results. For the subsequent studies seed-core nanoparticles **2** and **3** were utilized. In the following synthesis step the uncrosslinked PMMA shell was synthesized on the core particles resulting in lattices **4** and **11**. This step increased the particle diameters to 151 nm (standard deviation: 17 nm) and 222 nm (standard deviation: 32 nm). For all applied size measuring methods, latex **11** exhibited the largest size of all synthesized particles and the highest density value of 1.19 $g \cdot cm^{-3}$. For core-shell particle **4** the cryo-TEM image revealed a contrast distinction. This probably stems from the polymer core with a darker contrast and the attached shell with a weaker contrast. This distinguishing feature was only clearly observable for sample **4**. The particle shapes of **4** and **11** did not remain clearly spherical and became uniform. Gutiérrez-Mejía *et al.* synthesized PBA/PMMA nanoparticles similar to our latex, with a core-shell ratio of 30/70. In their study the clear spherical shape remained after shell formation.[12] This observation is not in accordance with our results as non-uniform particles were observed.

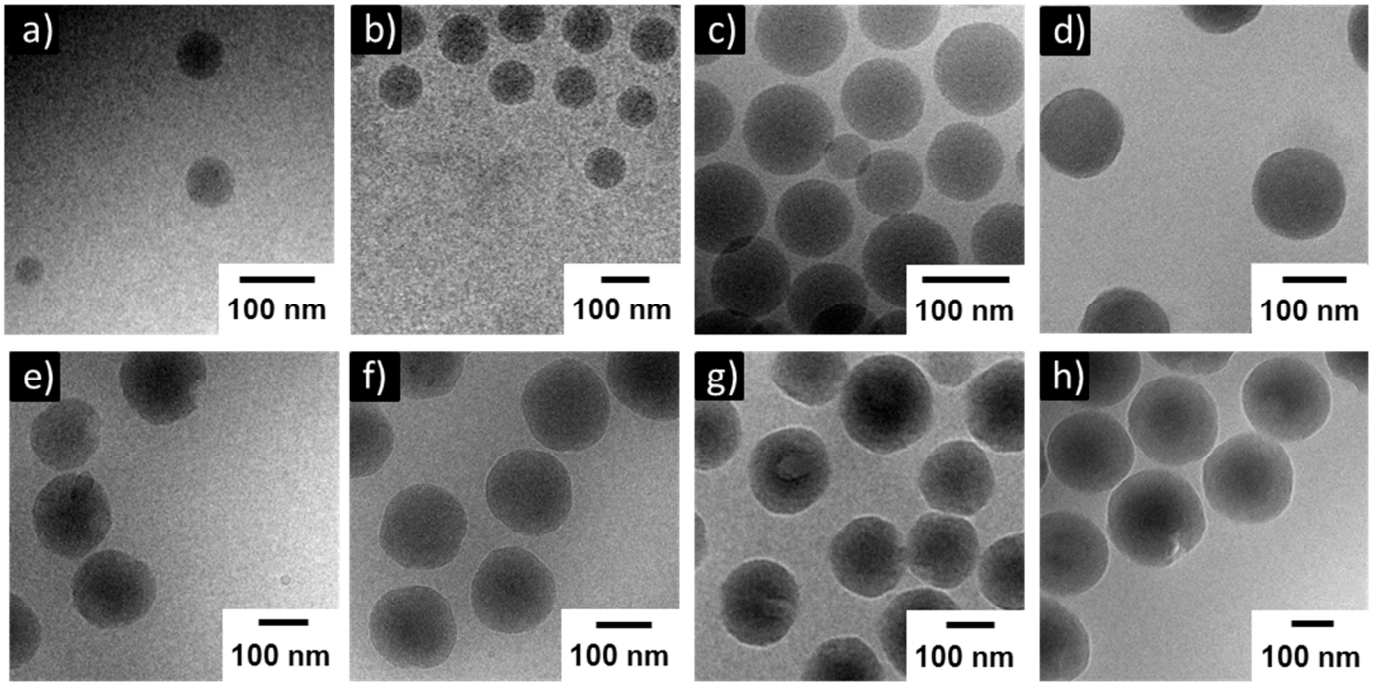

Figure 2. cryo-TEM images of the obtained latex particles **1** to **5**, **9** and **11**; a) **1**, b) **2**, c) **3**, d) **4**, e) **5**, f) **9**, g) **10** and h) **11**.

The polymer shell of lattices **5** to **10** was crosslinked (up to 8%) with TEGDMA in order to improve the particle stability, the dispersability in the TEGDMA monomer and to evaluate the effects on the mechanical properties. This shell formation step led to a significant increase in the particle densities of all shell crosslinked and non-crosslinked samples (**Table 3**). The densities are accompanied with the size growth obtained by cryo-TEM, DLS and AUC. However, as already observed for particles **4** and **11**, a change of the nanoparticle morphology was observed when the PMMA shell was attached. The

View Article Online
DOI: 10.1039/C4PY01544D

resulting core-shell nanoparticles (**5** to **10**) were not homogeneously spherical anymore. We attribute this irregular particle to the incompatibility of both constituting polymers and the polymerization sequence.[20, 23, 24]

During shell-formation, the core latex is swollen with MMA that is different from the monomeric units of the seed polymer, leading to heterogeneous morphologies.[20] Okubo *et al.* reported about uneven "raspberrylike" structures of PBA/polystyrene (PSt) lattices caused by the incompatibility of the corresponding polymers.[25] The group of Sun described the morphologies of PBA/poly(St-*co*-MMA) nanoparticles. It was found that in the second stage of the polymerization, the resulting latex particle structure depends on the added monomer ratio.[26]

The resulting particle sizes of shell-crosslinked lattices (**5** to **10**) determined by cryo-TEM are in good agreement for particle **10** (163 nm) with the sizes obtained by DLS and AUC. In contrast, particle sizes of lattices **5** to **9** showed higher deviations (>5 nm).

cryo-TEM represents an established method for the determination of particle sizes and morphology. For the latex particles investigated within this study, cryo-TEM revealed structural details of particle shapes that would be unrevealed by using only AUC and DLS.

3.2 Mechanical properties

The preparation of test specimens was performed by mixing and homogenising the initial components with the particle dispersions (**Table 2**). Pre-examinations revealed that the dispersability of the non-crosslinked core-shell particles (latex **4** and **11**) in TEGDMA was inferior to the crosslinked ones (lattices **5** to **10**). The monomer formulations were photo-polymerized. The resulting polymer specimens were mechanically pre-treated (see experimental details) and subsequently used for mechanical measurements.

Experimental data of flexural strength, E-modulus and K_{1c} of samples of the test specimens **TS1** to **TS11** are displayed in **Table 4**. Sample **TS11** was used as a reference sample and therefore not enriched with latex particles. The composition of **TS11** was adapted so that there are equal monomer concentrations in all test specimens (**TS1** to **TS11**). Polymer lattices **5** to **10** were crosslinked with TEGDMA to improve the dispersability and to investigate its effect on the mechanical features.

To examine the influence of different core/shell ratios on the mechanical properties, polymer particles were synthesized with core-shell ratios of 60/40, 50/50, 40/60, 30/70 and 10/90 (**TS5** to **TS8** and **TS10**). The implementation of the latex particles with a core-shell ratio of 60/40 (latex **6**) in a composite (**TS5**) led to a rise of flexural strength (80.3 MPa), E-modulus (2.08 GPa) and K_{1c} (1.070 MPa·m$^{1/2}$). By increasing the shell content up to a core-shell ratio of 50/50, (latex **7**, **TS6**) a lower increase of flexural strength (71.8 MPa), K_{1c} (0.763 MPa·m$^{1/2}$) and E-modulus (1.77 GPa) was observed. With a core-shell ratio of 40/60, the effect of incorporated lattices (latex **8**, **TS7**) to the mechanical properties of the polymer matrix revealed a maximum of the E-modulus (2.38 GPa) and flexural strength (81.4) of all applied test samples, accompanied by a small rise of K_{1c} (0.763 MPa·m$^{1/2}$). By applying particles with a core shell ratio of 30/70 (latex **9**), corresponding to test specimen **TS8**, mechanical investigations showed an elevated flexural strength (79.0 MPa), E-modulus (1.89 GPa) and K_{1c} (1.116 MPa·m$^{1/2}$). By increasing the shell content up to maximum of 10/90 (**TS10**), the E-modulus and K_{1c} (1.186 MPa·m$^{1/2}$) reached a value of 1.90 GPa accompanied with a slightly enhanced flexural strength of 78.0 MPa. With regard to the mechanical resistance of test samples **TS6** (50/50) to **TS10** (10/90) (except sample **TS7**), there is a clear rising trend to higher E-moduli with increasing PMMA shell content.

In order to obtain information about the influence of different shell crosslinker ratios in comparison to non-crosslinked (latex **4**, **TS1**) particles on the mechanical properties, the polymer nanoparticles were shell-crosslinked with 2, 4 and 8% TEGDMA and utilized for test specimens (**TS1**, **TS4**, **TS8** and **TS9**). In direct comparison with the specimen containing the non-crosslinked latex particles **TS1** (flexural strength: 78.0 MPa, E-modulus: 1.72 GPa and K_{1c}: 1.139 MPa·m$^{1/2}$), a linker content of 2% (**TS4**) provided the highest K_{1c} value (1.206 MPa·m$^{1/2}$) of all investigated samples as well as an increased E-modulus (1.78 GPa) and a relative low flexural strength (76.4 MPa). With a linker content of 4% (**TS8**) a considerable enhancement of the mechanics (flexural strength: 79.0 MPa; E-modulus: 1.89 GPa, K_{1c}: 1.116 MPa·m$^{1/2}$) was obtained. A further increase of the crosslinker content up to 8% (**TS9**) did not result in an enhancing effect of the mechanical properties. With a flexural strength of 75.1 MPa, E-modulus of 1.87 GPa and K_{1c} of 0.835 MPa·m$^{1/2}$ the TEGDMA linker softens the material.

Additionally, the influence of various particle concentrations within the test specimens and their effect to the mechanical properties was studied. For that purpose a series of samples filled with 3, 6 and 9 wt% of polymer particles (latex **5**) were investigated (**TS2** to **TS4**). With a particle concentration of 3 wt% (**TS2**), there is a slightly decreasing influence to the flexural strength (65.6 MPa), E-modulus (1.55 GPa) and K_{1c} (0.752 MPa·m$^{1/2}$). By increasing the particle concentration to 6 wt%, (**TS3**) an extensive enhancement of flexural strength (78.1 MPa), E-modulus (1.86 GPa) and K_{1c} (0.850 MPa·m$^{1/2}$) was observed. When the particle concentration was further increased up to 9 wt% (**TS4**) the mechanical properties showed a lower flexural strength (76.4 MPa) and E-modulus (1.61 GPa) however with a maximum of K_{1c} (1.206 MPa·m$^{1/2}$).

Table 4 Composition of test specimens and the corresponding mechanical properties.

Test specimen	Particle concentration [%]	Flexural strength [MPa]	E-modulus [GPa]	K_{1c} [MPa·m$^{1/2}$]

View Article Online
DOI: 10.1039/C4PY01544B Polymer Chemistry

TS1	9	78.0 (3.3)	1.72 (0.05)	1.139 (0.059)
TS2	3	65.6 (4.5)	1.55 (0.09)	0.752 (0.065)
TS3	6	78.1 (3.1)	1.86 (0.10)	0.850 (0.038)
TS4	9	76.4 (2.6)	1.78 (0.07)	1.206 (0.055)
TS5	9	80.3 (4.2)	2.08 (0.19)	1.070 (0.060)
TS6	9	71.8 (2.2)	1.77 (0.07)	0.763 (0.062)
TS7	9	81.4 (4.3)	2.38 (0.13)	0.747 (0.045)
TS8	9	79.0 (2.9)	1.89 (0.05)	1.116 (0.056)
TS9	9	75.1 (3.7)	1.87 (0.07)	0.835 (0.273)
TS10	9	78.0 (2.7)	1.90 (0.10)	1.186 (0.070)
TS11	0	68.4 (8.2)	1.61 (0.07)	0.733 (0.071)

Conclusions

By incorporation of core-shell nanoparticles into a TEGDMA / UDMA matrix and subsequent photo-polymerization, it was possible to improve the flexural strength, E-modulus and K_{1c} of the material. To our knowledge, this study represents the first report about an enhancement of fracture properties (K_{1c}) and E-modulus (simultaneous) of additive filled polymer composites at the same time. Particles with diameters of 70 to 220 nm (determined by AUC) were synthesized and cryo-TEM investigations revealed that all core-shell particles (lattices **4** to **11**) showed slightly irregular particle geometries, differing from the clear spherical shape of polymer seed (**1**) and cores (latex **1** and **2**). By crosslinking the polymer shell with a TEGMDA concentration up to 4% it was possible to enhance the dispersability of particles in the monomer (TEGDMA) together with an improvement of the mechanical properties. The best mechanical performance was achieved with the test specimens **TS7** featuring a maximum in flexural strength (81.4 MPa) and E-modulus of 2.38 GPa (see **Table 4**) that refers to lattex **8** (core-shell ratio: 40/60). Particles with a lower shell content (core-shell ratio: 50/50) have less effect to the flexural strength, E-modulus and K_{1c}. In a concentration dependent study of polymer particles within the test specimens, optimal flexural strength and E-modulus values were achieved at a particle concentration of 6% (**TS3**). However, for test sample filled with 9% polymer particles (**TS4**), the highest K_{1c} (1.206 $MPa \cdot m^{1/2}$) value was obtained of all investigated samples. These improvements of mechanical properties of TEGDMA/UDMA composites make them interesting as a toughening additive for hard tissue applications like bone cements or dental replacement materials.

Acknowledgements

The cryo-TEM facilities of the Jena Center for Soft Matter (JCSM) were established by a grant from the German Research Council (DFG) and the European Fonds for Regional Development (EFRE).
We are grateful to Matthias Hartlieb for helpful discussions.

Notes and references

1 R. V. Silva, D. Spinelli, W. W. Bose Filho, S. Claro Neto, G. O. Chierice and J. R. Tarpani, *Compos. Sci. Technol.*, 2006, **66**, 1328-1335.
2 L. M. Butkus, P. D. Mathern and W. S. Johnson, *J. Adhes.*, 1998, **66**, 251-273.
3 K. F. Leinfelder, *J. Am. Dent. Assoc.*, 1997, **128**, 573-581.
4 B. Yu, F. Liu and J. W. He, *J. Mech. Behav. Biomed. Mater.*, 2014, **35**, 1-8.
5 A. Della Bona, P. H. Corazza and Y. Zhang, *Dent. Mater.*, 2014, **30**, 564-569.
6 V. Ravindranath, M. Gosz, E. De Santiago, J. L. Drummond and S. Mostovoy, *J. Biomed. Mater. Res., Part B*, 2007, **80B**, 226-235.
7 J. L. Ferracane and H. X. Berge, *J. Dent. Res.*, 1995, **74**, 1418-1423.
8 D. M. Laura, H. Keskkula, J. W. Barlow and D. R. Paul, *Polymer*, 2000, **41**, 7165-7174.
9 L. Boogh, B. Pettersson and J. A. E. Manson, *Polymer*, 1999, **40**, 2249-2261.
10 J. Verrey, Y. Winkler, V. Michaud and J. A. E. Manson, *Compos. Sci. Technol.*, 2005, **65**, 1527-1536.
11 L. Becu, H. Sautereau, A. Maazouz, J. F. Gerard, M. Pabon and C. Pichot, *Polym. Adv. Technol.*, 1995, **6**, 316-325.
12 A. Gutierrez-Mejia, W. Herrera-Kao, S. Duarte-Aranda, M. I. Loria-Bastarrachea, G. Canche-Escamilla, F. J. Moscoso-Sanchez, J. V. Cauich-Rodriguez and J. M. Cervantes-Uc, *Mater. Sci. Eng. C Mater. Biol. Appl.*, 2013, **33**, 1737-1743.
13 P. Schuck and P. Rossmanith, *Biopolymers*, 2000, **54**, 328-341.
14 W. Maechtle, *Makromol. Chem.*, 1984, **185**, 1025-1039.
15 G. Chang, L. He, W. Zheng, A. Z. Pan, J. Liu, Y. J. Li and R. J. Cao, *J. Colloid Interface Sci.*, 2013, **396**, 129-137.
16 H. T. Zhang, A. L. Wang and J. H. Cao, *Acta Polym Sin*, 2003, 23-29.
17 V. Castelvetro, C. De Vita, G. Giannini and S. Giaiacopi, *J Appl Polym Sci*, 2006, **102**, 3083-3094.
18 A. Rahman and C. W. Brown, *J Appl Polym Sci*, 1983, **28**, 1331-1334.
19 I. Capek, J. Barton and E. Orolinova, *Chem Zvesti*, 1984, **38**, 803-822.
20 C. S. Chern, *Progress in Polymer Science*, 2006, **31**, 443-486.
21 W. Mächtle and L. Börger, eds., *Analytical Ultracentrifugation of Polymers and Nanoparticles*, Springer, Berlin, 2006.
22 I. Perevyazko, A. Vollrath, S. Hornig, G. M. Pavlov and U. S. Schubert, *J. Polym. Sci., Part A: Polym. Chem.*, 2010, **48**, 3924-3931.
23 Y. C. Chen, V. Dimonie and M. S. Elasser, *Macromolecules*, 1991, **24**, 3779-3787.
24 T. Matsumoto, M. Okubo and S. Shibao, *Kobunshi Ronbunshu*, 1976, **33**, 575-583.
25 M. Okubo, Y. Katsuta and T. Matsumoto, *J Polym Sci Pol Lett*, 1980, **18**, 481-486.
26 D. X. Huo, D. Z. Liu and P. Q. Sun, *Polymer International*, 2002, **51**, 1417-1421.

Journal Name

View Article Online
DOI: 10.1039/C4PY01544D ARTICLE

Graphical abstract

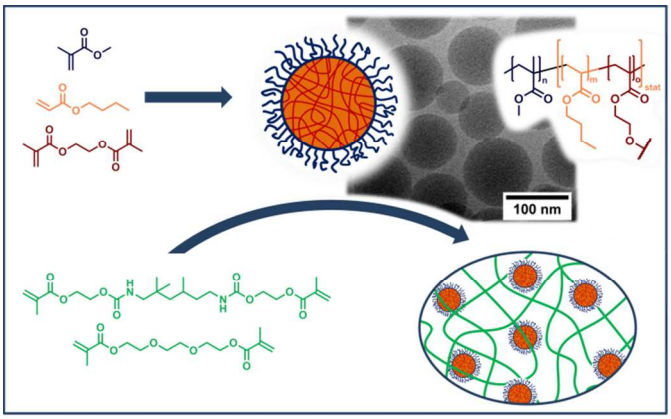

Polymeric core-shell particles consisting of a soft poly(butyl acrylate) core and a hard poly(methyl methacrylate) shell were incorporated into methacrylate based composites. The addition of the lattices leads to an improvement of fracture toughness and E-modulus values. The outstanding improvements of mechanical properties make these polymer lattices interesting as a toughener additive.